The Kirkendall Effect in Solid State Diffusion

PhD Thesis

ALOKE PAUL

Laboratory of Materials and Interface Chemistry
Eindhoven University of Technology
The Netherlands

Advisors:

Prof. G. de With

Prof. F.J.J. van Loo

Dr. A.A. Kodentsov

Examiners:

Prof. Herbert Ipser (Austria)

Prof. Ÿlo Ugaste (Estonia)

To my Parents

Contents

Contents

Chapter 1

Introduction

Before starting, it should be mentioned that the Chapters 1-6 in this thesis are written for scientists and students who have already knowledge about the basic concepts of diffusion in binary solid-state systems. For those readers who want to know more about the concepts, an extensive Appendix is written which will be referred to very often.

1.1 Recent developments in the understanding of the Kirkendall effect

Since the discovery, as far back as 1947 [1], and the following analysis by Darken [2], the Kirkendall effect assumed a prominent role in the diffusion theory, as it is seen as the most explicit evidence for the occurrence of a vacancy mediated mechanism in diffusion processes in solids.

Although this subject is treated in all textbooks on solid-state diffusion and is taught in many universities, the rationalization and description of the Kirkendall effect is by no means as simple as it looks at first sight. Scientists dealing with diffusion phenomena thought that they had a reasonable notion of the Kirkendall effect induced migration of inert inclusions (markers) inside the diffusion zone and the uniqueness of the Kirkendall plane (as marked by inert particles placed at the initial contact surface between the couple halves) has not been questioned for quite a long time.

However, sometimes researchers noticed a peculiar behaviour of markers, when studying solid-state diffusion in different systems. Carter [3] was surprised to find the split up of a molybdenum wire, used as inert marker at the Al_2O_3/MgO-gas interface to study reaction and diffusion in $MgAl_2O_4$-spinel. Bastin and Rieck [4] had the same experience when studying interdiffusion in the Ti-Ni system, as shown in Fig. (1.1-1), where a tungsten wire was split and embedded in two different phases. Shimozaki et al. [5] observed during study of diffusion in the β'-AuZn phase that after interaction the tungsten wire which were placed at the interface of Au/γ-AuZn$_2$ (64 at.% Zn) couple and the "original interface" revealed by traces of the joining plane (presumably because

of the presence of debris at the interface or scratches on the bonding faces) were located at two different planes. If the Kirkendall plane is unique, they should be at the same plane after annealing.

These conspicuous findings were not identified by any of the authors as multiple Kirkendall planes and were not critically examined.

In the mean time, Cornet and Calais [6] published an article in which they described hypothetical diffusion couples of a binary system, where more than one "Kirkendall marker plane" can emerge. Later, van Loo et al. [7] made more explicit predictions on this phenomenon in multiphase diffusion couples. It was only in the last few years, that several systematic studies into the microstructural stability of the Kirkendall plane were undertaken in our laboratory in order to find experimental evidence for the possible occurrence of two Kirkendall planes in a diffusion couple [8-10]. A clear-cut experimental verification of the ideas of Cornet and Calais was found and a number of fundamental concepts related to the Kirkendall effect were reconsidered.

It was shown that in a volume-diffusion controlled interaction the Kirkendall plane can be multiple, stable or unstable. A basic framework, in terms of velocity curve construction was formulated to evaluate these phenomena [8, 9].
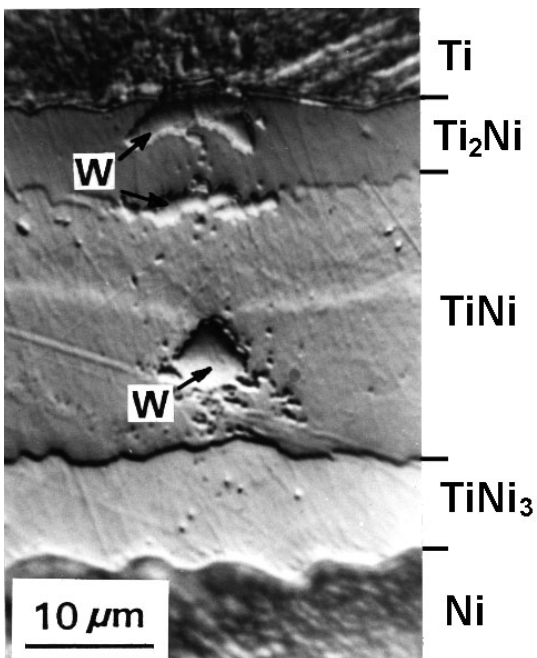
Fig. (1.1-1) Back-scattered electron image of a Ti/Ni diffusion couple annealed at 800 °C for 72 hours. The tungsten wire used as inert markers at the interface before annealing was found to be split and embedded in two different phases [4].

The Kirkendall effect can best be visualized by the motion of inert ("fiducial") markers placed before the diffusion annealing along the anticipated zone of interdiffusion. In the case of a diffusion couple in a binary A-B system, the velocity of these markers is dependent on the difference in intrinsic diffusivities of the species and the concentration gradients developing in the interdiffusion zone [A.17]:

$$v = -(V_B J_B + V_A J_A) = V_B(D_B - D_A)\frac{\partial C_B}{\partial x} \qquad \text{(m.s}^{-1}) \qquad (1.1\text{-}1)$$

where J_i (mole.m^{-2}.s^{-1}) is the intrinsic flux of the species, D_i (m^2.s^{-1}) is the intrinsic diffusion coefficient, C_i (mole.m^{-3}) is the concentration of component i and x (m) is the position parameter. The velocity in a diffusion zone can be determined from the knowledge of intrinsic diffusivities at all compositions over the whole homogeneity range and with the help of the concentration gradient at the position of these markers in a particular diffusion couple.

In a diffusion-controlled interaction, the inert markers positioned at the location of the original interface between the reactants ("Kirkendall plane") are the only markers that stay at a constant composition during the whole diffusion annealing and move parabolically in time with a velocity (A.17)

$$v_K = \frac{dx}{dt} = \frac{x_K - x_0}{2t} = \frac{x_K}{2t} \qquad \text{(m.s}^{-1}) \qquad (1.1\text{-}2)$$

where x_K and x_o (= 0) are the positions of the Kirkendall plane at times $t = t$ and $t = 0$, respectively.

The position(s) of the Kirkendall plane(s) can be found at the point of intersection(s) between the velocity curve *2tv vs. x* (calculated by Eq. (1.1-1)) and the straight-line $2tv_K = x_K$ (determined by Eq. (1.1-2)). It was shown that the *nature* of the Kirkendall plane(s) in a diffusion zone depends on the gradient of the velocity curve at the point of intersection. When the straight line intersects the velocity curve at a point, where $(\partial v / \partial x)_K \leq 0$, one should expect the presence of a stable Kirkendall plane. When the gradient at the point of intersection, $(\partial v / \partial x)_K \rangle 0$, it will result into an unstable Kirkendall plane.

For example, we consider a hypothetical diffusion couple of alloys of A and B (A_yB_{1-y}/A_zB_{1-z}, where y > z), where in the A-rich side of the diffusion zone A is the faster diffusing species, whereas in the B-rich side B is the faster diffusing species. Fig. (1.1-2) shows the schematic presentation of the velocity curves in different
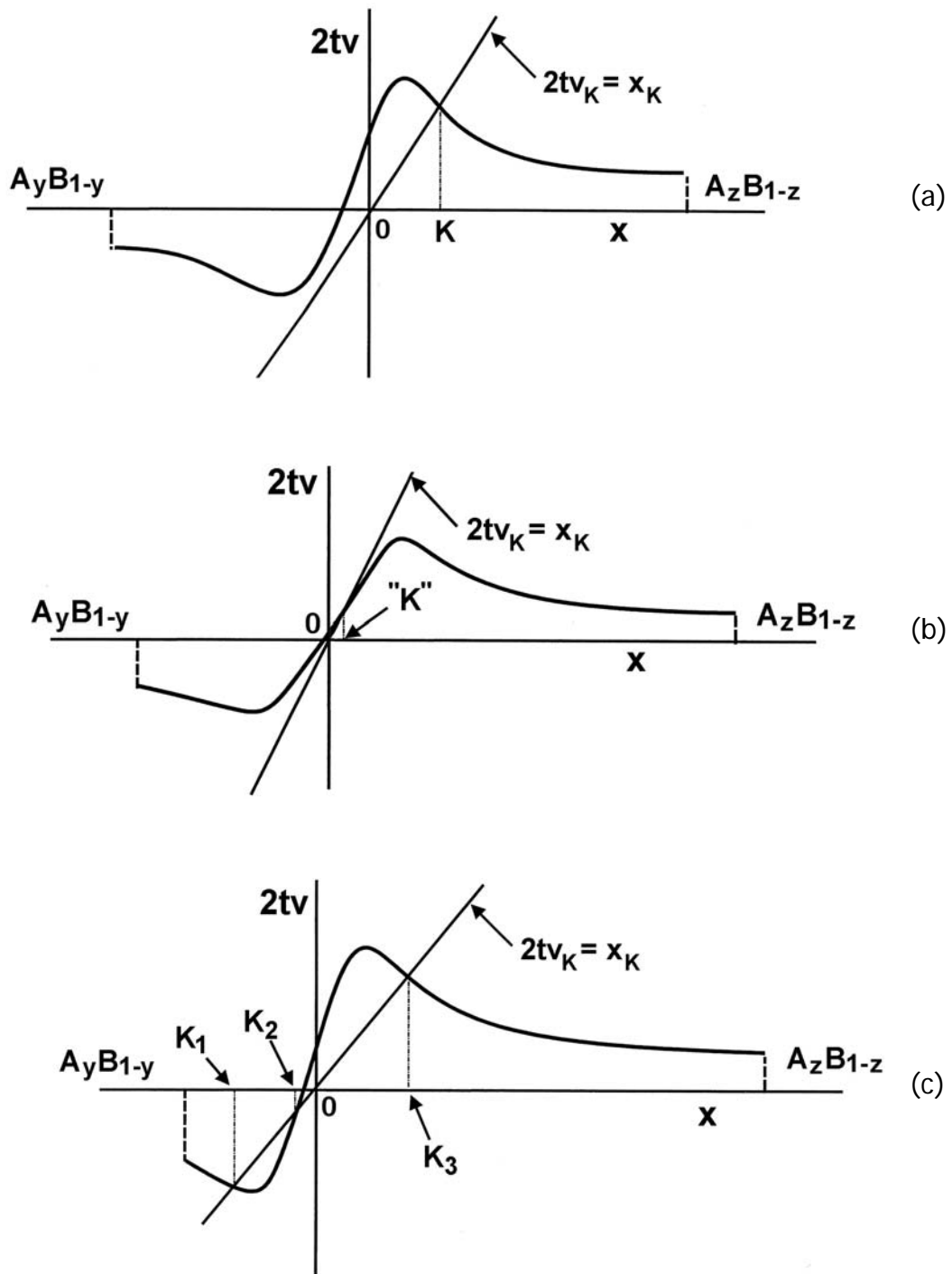
Fig. (1.1-2) Schematic velocity diagrams, pertaining a hypothetical diffusion couple between alloys of A and B, A_yB_{1-y}/A_zB_{1-z} (y>z), where in the A-rich side A diffuses faster than B and in the B-rich side B diffuses faster than A. Different conditions are shown: (a) the straight line $2tv_K = x_K$ intersects the velocity curve $2tv$ vs. x once at a point with a negative gradient, (b) intersects at a point with a positive gradient and (c) intersects at three different positions.

situations. In certain diffusion couples the straight-line $2tv_K = x_K$ may intersect the velocity curve $2tv$ vs. x in the diffusion zone once at a point with a negative gradient (Fig. (1.1-2a)). At the point of intersection one can then expect the presence of one stable Kirkendall plane. Markers, which by some perturbation end up at a position slightly ahead of the Kirkendall plane, will slow down (because of lower velocity) and if these markers are behind this plane, they will move faster (because of higher velocity). In other words, the stable Kirkendall plane acts as attractor to the inert markers. By changing the end-member compositions the straight-line $2tv_K = x_K$ might intersect the velocity curve $2tv$ vs. x at a point with a positive velocity gradient, as shown in Fig. (1.1-2b). In this case one will find an unstable Kirkendall plane. The markers slightly ahead of this plane will move faster, whereas markers slightly behind this plane will move slower. This will result into scatter of the markers and there will be no particular unique plane as the Kirkendall plane. It is also possible to meet a situation as shown in Fig. (1.1-2c), where the straight-line intersects the velocity curve three times at K_1, K_2 and K_3. In this case, one might expect that three Kirkendall planes will be present, but in reality one finds the presence of two stable Kirkendall planes only. The unstable Kirkendall plane is situated between two stable Kirkendall planes and the stable planes will accumulate all the markers during the initial stages of the interdiffusion.

Experimental evidence of the presence of stable and unstable Kirkendall planes were verified in Ni/Pd and Fe/Pd diffusion couples, respectively [10] with the help of the velocity diagram construction, as shown in Fig. (1.1-3). The velocity curve $2tv$ vs. x over the whole homogeneity range was determined by multifoil experiments. It was indeed found that a stable Kirkendall plane is present when the straight-line $2tv_K = x_K$ intersects the velocity curve $2tv$ vs. x at a point with a negative gradient, whereas an unstable Kirkendall plane was found when the gradient is positive at the point of intersection.

In order to verify the experimental findings by shimozaki et al. [5] and in the quest for finding examples as discussed in Fig. (1.1-2) the growth of β′-AuZn phase growing from different Au-Zn end-members were reexamined [9]. With changing end-member compositions, stable and unstable planes as well as the bifurcation of the Kirkendall plane were found in different diffusion couples, as shown in Fig. (1.1-4). Since the intrinsic diffusion coefficients as a function of composition for the β′-AuZn phase are not known, it was not possible to produce quantitative results to construct velocity diagram in these cases.

(a)

(c)

(b)

(d)
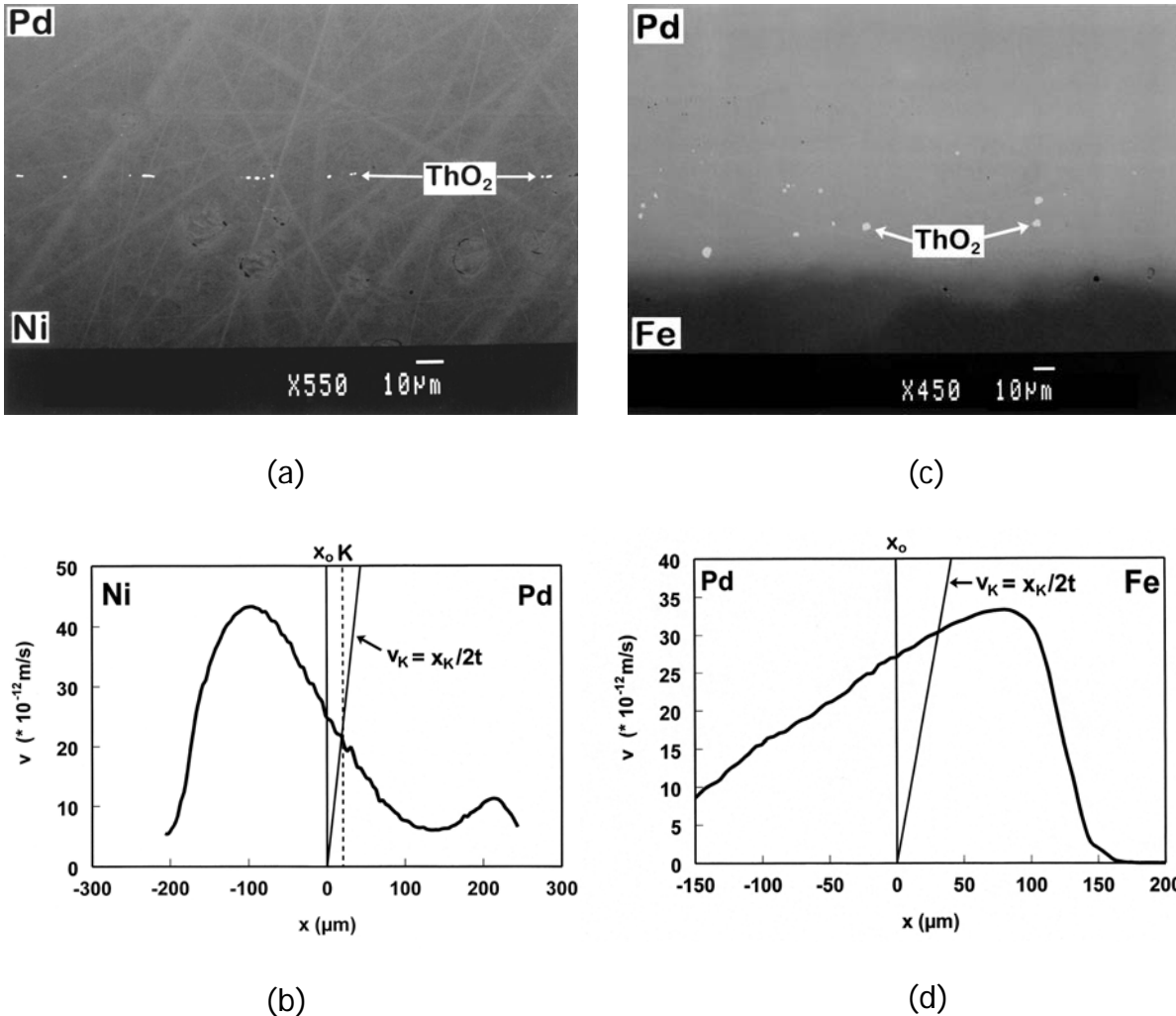
Fig. (1.1-3) (a) Back-scattered electron image of a Ni/Pd couple annealed at 1100 °C for 121 hrs (b) Kirkendall velocity construction pertaining to this Ni/Pd couple (c) Back-scattered electron image of a Fe/Pd couple annealed at 1100 °C for 144 hrs (d) Kirkendall velocity construction pertaining to this Fe/Pd couple.

1.2 Motivation of the work and outline of the thesis

Recent developments in the understanding of the Kirkendall effect in solid-state diffusion were an impetus behind this thesis work. Although bifurcation of the Kirkendall plane in a *single-phased* diffusion zone (β′-AuZn) was explained qualitatively [9], the construction of the velocity curve based on the experimental results was not possible because of the lack of experimental results. There was also the further curiosity whether occurrence of more than two Kirkendall planes is possible in a
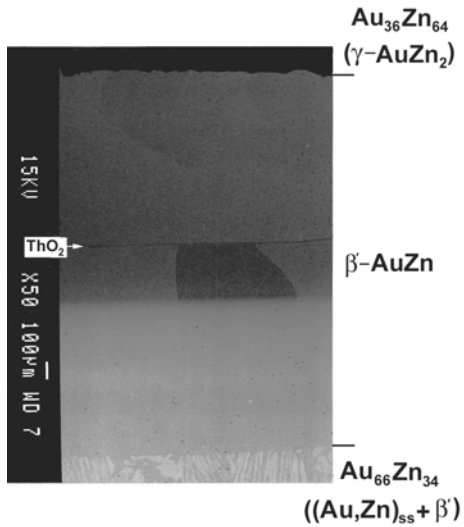
Fig. (1.1-4a) Back-scattered electron image of a diffusion couple grown between the end members $Au_{36}Zn_{64}$ (γ-phase) and $Au_{66}Zn_{34}$ ((Au,Zn)-solid solution + β'-AuZn). Only one Kirkendall plane is present in the diffusion zone.
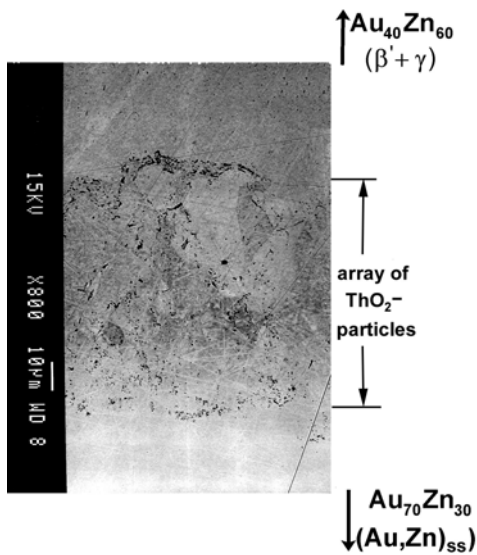
Fig. (1.1-4b) Back-scattered electron image of a diffusion couple grown between the end members $Au_{40}Zn_{60}$ (β' + γ phase) and $Au_{70}Zn_{30}$ ((Au,Zn)-solid solution). The microstructure is shown in the vicinity of the array of ThO_2-particles and the unreacted initial end-members are much further away. The presence of an unstable Kirkendall plane was found in the diffusion zone.
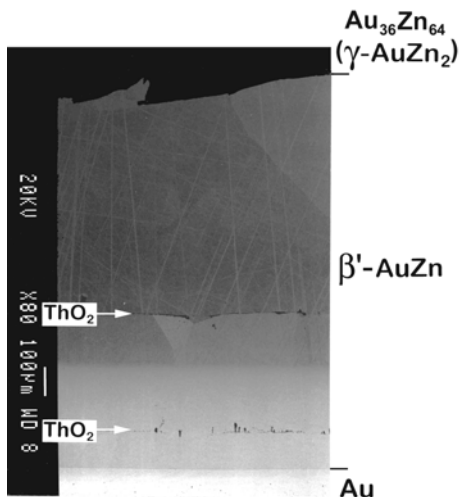
Fig. (1.1-4c) Back-scattered electron image of a diffusion couple grown between the end-members Au and $Au_{36}Zn_{64}$ (γ-AuZn$_2$). Two Kirkendall planes are present in the diffusion zone.

7

diffusion zone. In this work, the bifurcation of the Kirkendall plane was found in a single-phased reaction zone in the β-NiAl system. Systematic studies were carried out to determine the diffusion parameters and the Kirkendall effect was rationalized successfully with the help of the velocity diagram construction as discussed in Chap. 3. The predicted occurrence of the trifurcation of the Kirkendall plane in a diffusion zone of Ti/TiAl$_3$ is also presented in this chapter.

The behaviour of the Kirkendall plane was successfully explained by a diffusion based approach by means of the velocity diagram construction. However, this approach does not shed light on the reactions involved in a multiphase diffusion zone and on the morphological evolution during interdiffusion. A physico-chemical approach, for this purpose, is developed and demonstrated in Chap. 4. This approach has the extra benefit that it explains the morphologies in the diffusion zone.

The Ni-Al system is important both for scientific understandings and for technological applications. In earlier studies the molar volume, one important prerequisite to calculate diffusion parameters, was not taken into consideration or otherwise irregularities in the approach were found. In Chap. 5, results on interdiffusion coefficients calculated with the help of proper molar volume data are presented. Since no suitable Al isotopes are available, the direct measurements of the Al tracer diffusivities are not possible. In this chapter the results on tracer diffusivities in the β-NiAl (of both the species Ni and Al) and γ'-Ni$_3$Al (of Al) phases through an indirect method by the diffusion couple technique are shown.

Research into the interactions between solder and underbump metallization has been triggered after the declaration of the ban to be imposed on lead content solder alloys. With the thrust for miniaturization in modern electronics industry the understanding on the interactions between the materials involved, which controls the overall performance of the structure is even more important. Our knowledge developed during this thesis work has been applied to understand the interactions in Cu(Ni)/Sn and Au/Sn systems important for the electronics industry and the results are presented in Chap. 6.

The theories on the diffusion couple technique and Kirkendall effect developed until now were scattered throughout the literature. In the Appendix A, these theories are presented systematically for binary systems.

References

1. A.D. Smigelkas and E.O. Kirkendall, Zinc diffusion in alpha brass, Trans. AIME **171** (1947) 130-34
2. L.S Darken, Diffusion, mobility and their interrelation through free energy in binary metallic systems, Trans. Met. Soc. AIME **175** (1948) 184-201
3. R.E. Carter, Mechanism of solid-state reaction between magnesium oxide and aluminium oxide and between magnesium oxide and ferric oxide, J. Amer. Cer. Soc. **44** (1961) 116-20
4. G.F. Bastin and G.D. Rieck, Diffusion in the titanium-aluminium system: I. Occurrence and growth of the various intermetallic compounds, Met. Trans. **5** (1974) 1817-26
5. T. Shimozaki, Y. Goda, Y. Wakamatsu and M. Onishi, Interdiffusion and Kirkendall effect in Au-Zn ordered β' phase, Def. Diff. Forum **95-98** (1993) 629
6. J.-F. Cornet and D. Calais, Etude de l'effect Kirkendall d'apres les equations de Darken, J. Phys. Chem. Solids **33** (1972) 1675-84
7. F.J.J. van Loo, B. Pieraggi and R.A. Rapp, Interface migration and the Kirkendall effect in diffusion driven phase transformations, Acta Metall. Mater. **38** (1990) 1769-79
8. M.J.H van Dal, A.M. Gusak, C. Cserháti, A.A. Kodentsov and F.J.J van Loo. Microstructural stability of the Kirkendall plane in solid state diffusion, Phys. Rev. Lett. **86** (2001) 3352-55
9. M.J.H. van Dal, A.M. Gusak, C. Cserháti, A.A. Kodentsov and F.J.J. van Loo, Spatio-temporal instabilities of the Kirkendall-marker planes during Interdiffusion in β'-AuZn, Phil. Mag. A, **82** (2002) 943-54
10. M.J.H. van Dal, M.C.L.P Pleumeekers, A.A. Kodentsov and F.J.J. van Loo, Intrinsic diffusion and Kirkendall effect in Ni-Pd and Fe-Pd solid solutions, Acta Mater. **48** (2000) 385-96

Chapter 2

Experimental Techniques

Throughout this investigation the diffusion couple technique is used. Two dissimilar materials (end-members) are coupled together and annealed at elevated temperature for a certain period of time after applying an external load for good contact. At high temperature interdiffusion takes place and reaction/diffusion products grow with time. The bonded couple is then removed from furnace, cross-sectioned and after metallographic preparation examined by Scanning Electron Microscopy (SEM) and Optical Microscopy (with the help of polarized light). The composition profile of the interaction zone is measured by Electron Probe Microanalysis (EPMA).

2.1 Preparation of the starting materials (end-members)

Many different pure elements and alloys are used in this study. Specifications of the elements are listed in Table 2.1. The required alloys are melted in an arc-melting furnace in argon atmosphere (~0.3 bar). In order to produce good homogenization, the alloys are re-melted at least three times. After collecting the ingot (generally of 10 grams), the weight is measured to check the weight loss; it was found to be within 2 weight percent. Subsequently, they are sealed in a quartz-glass capsule in vacuum ($\sim 10^{-2}$ mbar) or in argon depending on the systems and annealed to equilibrate the phases. After annealing they are quenched in water and the compositions of the phases are then measured by EPMA to verify the phase diagram.

2.2 Preparation of the diffusion couple

Thin slices of one or two millimeters were cut by a slow speed diamond saw from as received pure elements and prepared alloys. Couple halves of two different materials are then ground with 180-grid SiC grinding paper followed by 30 and 10 μm diamond

impregnated discs. After that, final polishing of the surfaces was performed by 0.5 μm alumina slurry.

Prior to annealing, ThO_2-particles (0.5 - 1 μm) or tungsten powder (of ~1 μm in the Au-Sn system) were introduced on the bonding faces as inert markers. A suspension of particles in acetone was dropped onto a bonding face. After a short time the acetone evaporates, keeping more or less evenly distributed particles on the surface.

It is to be mentioned that the markers must be "chemically" inert with respect to the reactants (end-members of the diffusion couple) as well as the reaction products and marker material has to be impervious to a flux of vacancies occurring in the diffusion zone. Secondly, the markers should be identifiable inside the reaction zone by means of optical and/or scanning electron microscopy. In most of our case thorium dioxide (ThO_2) turned out to be the material of choice to use as "fiducial" markers. This thermodynamically very stable oxide is not only chemically inert within the reaction zones studied here, but, what is important, the ThO_2-particles are readily identifiable by scanning electron microscopy as "white contrast" on back-scattered electron images (and as black-particles in the AuZn system). In addition, their presence can be substantiated with EPMA simply by monitoring, for example, the Th-M_α line of the characteristic radiation when the electron probe is positioned in such a way that the volume of X-ray generation includes the anticipated oxide particles. In the Au-Sn system tungsten was used as inert marker. ThO_2-particles were not found back after annealing in this system; probably because of their rather small size and poor embedding in the phases they were removed during standard metallographic preparation.

Another important issue related to this subject is the size of particles used as fiducial markers. Obviously, too large particles may hinder interdiffusion. On the other hand, too small particles can be dragged by the moving grain boundary ("Zener's" drag) [1, 2]. In the cases described in the thesis, the motion of grain boundary of the product phase takes place under a considerable driving force, and we found no experimental evidence that the behaviour of the ThO_2- and W-particles used as Kirkendall markers have been affected by the Zener's drag.

After applying the inert particles, the couple halves are inserted in the vacuum furnace (~10^{-6} mbar). An external pressure of around 5 MPa was applied to ensure a good contact. Once vacuum is reached, the couple is annealed at desired temperature ($\pm$ 2 °C) for the desired period of time.

Table 2.1 Specifications of the pure elements used for the present study

Material	Purity (wt.%)	Supplier
Ni	99.99	Goodfellow (UK)
Al	99.995	Goodfellow (UK)
Co	99.98	Goodfellow (UK)
Si	99.99	Hoboken (Belgium)
Ag	99.99	Drijfhout (Netherlands)
Zn	99.98	Alfa Products (Germany)
Ti	99.995	Alfa Products (Germany)
Au	99.95	Goodfellow (UK)
Sn	99.99	Goodfellow (UK)
Cu	99.999	Alfa Products (Germany)

2.3 Analysis of the diffusion couple

After removing the sample from the furnace, the bonded couple is cross-sectioned by a slow speed diamond saw and ground and polished with final finish by 0.25 μm diamond paste. The interaction zone in the diffusion couple was examined by SEM (JEOL, 840A) and OM (JENAVERT). In some cases, like in Ti-Al and Ni-Al systems, polarized light microscopic techniques were used to examine the grain structure of the reaction layers, which are not visible in SEM. The composition profile of the reaction-diffusion zone was obtained from EPMA (JEOL JXA 8600 Superprobe).

References

1. G.J. van Gurp, W.F. van der Weg and D. Sigurd, Interactions in the Co/Si thin-film system. II. Diffusion-marker experiments, J. Appl. Phys. **49** (1978) 4011-20
2. Ya. E. Geguzin and M.A. Krivoglaz, Migration of macroscopic inclusions in solids, Consultants Bureau, New York-London (1973) 200-06

Chapter 3

Bifurcation and trifurcation of the Kirkendall plane

3.1 Bifurcation of the Kirkendall plane in a single-phased β-NiAl diffusion layer

I. Introduction and Statement of the problem

In recent years, research into the Kirkendall effect accompanying solid-state interdiffusion took a new direction due primarily to the experimental discovery of spatio-temporal instabilities and bifurcation of the Kirkendall marker plane in a multiphase reaction zone [1-4]. In previous publications [2, 4], a basic framework for evaluating these peculiar phenomena was formulated. It was shown that in a volume-diffusion controlled interaction, the Kirkendall plane as marked by inert particles, placed prior to the annealing at the contact surface of a diffusion couple, can be multiple, stable or unstable. However, further developments in this field to *verify the model experimentally* have been hampered by the lack of sufficiently precise information on molar volumes and atomic mobilities of the reacting species in the intermetallic phases where bifurcation of the Kirkendall plane had been observed. This problem has been of concern for few years in our group and has motivated the present study, which has, actually, a simple purpose: to design a model system (where bifurcation occurs in a *single-phased diffusion zone*) and model experiments that allow a direct validation of

---

the concept of the Kirkendall velocity construction.

II. Selection of β-NiAl as a model system and experimental approach

One can envisage an "ideal" material system for this study. Suppose that only one intermetallic compound with a fairly wide homogeneity range is growing in a binary diffusion couple. It is then conceivable that difference in intrinsic diffusivities of the components and, hence, the corresponding Kirkendall velocity may have a "different sign" in different domains of the product layer (see Fig. (1.1-2)). In this case, a straight line $2tv_K = x_K$ and a velocity curve may have more than one intersection. If the Kirkendall planes are fixed by intersections at the locations in the diffusion zone where the gradient of the Kirkendall velocity with respect to the position parameter is negative, they will act as attractors for markers, and the marker planes will be microstructurally stable. This means that under these conditions, a multiple Kirkendall plane can, in principle, emerge [2, 4].

In this respect, a reaction system in which a single-phase diffusion zone of β-NiAl intermetallic growing during interdiffusion from its adjacent phases offers a particular suitable example. Apart from simplicity, a number of aspects have been considered in selecting this material system. The NiAl-phase with B2 (CsCl-type) structure exists over a wide concentration range extended across the stoichiometric (1:1) composition as shown in Fig. (3.1-1) [5]. The unit cell of this intermetallic, as shown in Fig. (3.1-2), consists of two interpenetrating simple cubic sublattices and at the equiatomic composition all Al-atoms occupy the cube corners of one sublattice (lets say α [0;0;0]), and Ni-atoms occupy the corners of the other sublattice (β [1/2;1/2;1/2]). The deviation from stoichiometry is accomplished by essentially two mechanisms [6]. On the Ni-rich side, antisite defects are created, that is Ni-atoms can occupy the Al-sublattice, whereas on the other side of the stoichiometry, structural vacancies are present on the Ni-sublattice. The concentration of these constitutionally generated vacancies can be appreciable.

Such a peculiar defect structure has great influence on the diffusion behaviour of the intermetallic compound, which can change drastically with deviation from the stoichiometric composition [6-11]. Changes in magnitude and sign of the difference $(D_A - D_B)$ can be expected which could lead to a velocity curve (see Fig. (1.1-2)) that makes bifurcation of the Kirkendall plane possible.

It is, however, important to realize that the predicted position(s) of the Kirkendall plane(s) emerging inside the product layer during interdiffusion is determined not only by the shape of the velocity curve, but, also depends on the position of the plane, x_o, in the diffusion zone where the Kirkendall markers were situated before the interaction. In other words, the question whether bifurcation of the Kirkendall plane within a diffusion-grown layer of β-NiAl will occur or not, is highly sensitive to the initial compositions of the end-members of the reaction couple since these define the position $x_o = 0$, through which the line $2tv_K = x_K$ runs.

In our experiments, the simultaneous appearance of two Kirkendall marker planes moving with different velocities was observed inside a β-NiAl diffusion-grown layer during solid-state reaction at 1000 °C between two-phase alloy end-members with nominal compositions $N_{72.24}Al_{27.76}$ and $Ni_{41.7}Al_{58.3}$ (Fig. (3.1-3)).

Thus, the problem is reduced to the construction of the Kirkendall velocity plot pertaining to the β-NiAl product layer formed in this diffusion couple.

There are, in principle, two ways of constructing the Kirkendall velocity curve in a binary A-B system. The first one, from the tracer diffusivities, D_A^* and D_B^* of the species A and B, respectively (A.16):

$$v_K = V_B\left(\frac{V_m}{V_A}D_B^* - \frac{V_m}{V_B}D_A^*\right)\alpha\,\Theta\,\frac{\partial C_B}{\partial x} = \frac{1}{V_m}\left(V_B D_B^* - V_A D_A^*\right)\alpha\,\Theta\,\frac{\partial N_B}{\partial x}$$

$$(3.1\text{-}1)$$

where $\Theta = \dfrac{\partial \ln a_A}{\partial \ln N_A} = \dfrac{\partial \ln a_B}{\partial \ln N_B}$ is the thermodynamic factor, a_A and a_B are the chemical activities of components with pure elements A and B as the reference state, V_m is the molar volume, V_A and V_B are the partial molar volumes of A and B, respectively, α (= $1/f$, f is the correlation factor) is the Manning's correction for the "vacancy wind" effects (see A.16) and C_B and N_B are the concentration and mole fraction, respectively.

The second possibility is to determine intrinsic diffusivities, D_A and D_B following the diffusion couple technique and construct the velocity curve through (A.8):

$$v_K = V_B\left(D_B - D_A\right)\frac{\partial C_B}{\partial x} = \frac{V_A V_B}{V_m^2}\left(D_B - D_A\right)\frac{\partial N_B}{\partial x} \qquad (3.1\text{-}2)$$
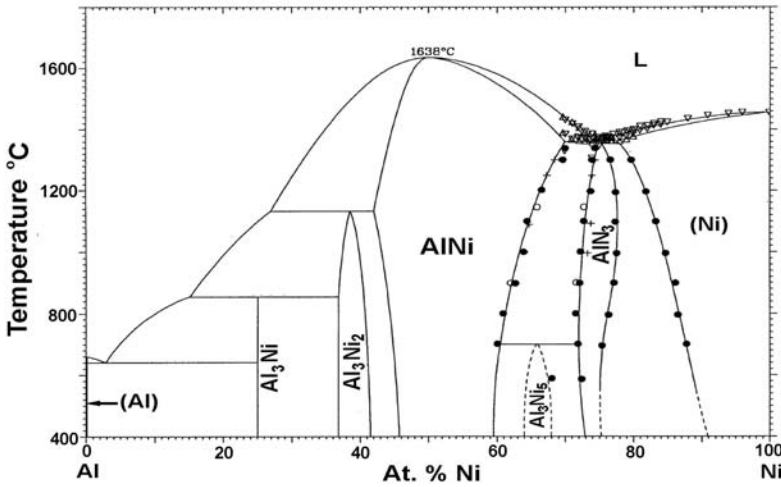
Fig. (3.1-1) Binary Ni-Al phase diagram [5].
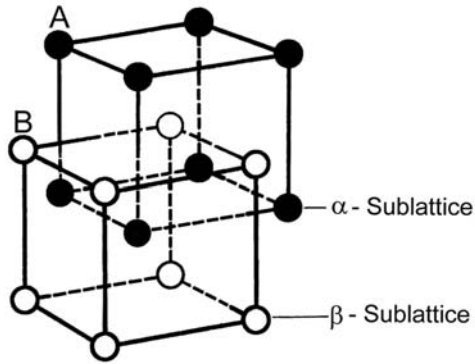
Figure (3.1-2) Pictorial view of the B2-NiAl structure: In completely ordered (eqiatomic) NiAl compounds Ni(Al) atoms occupy the $\alpha(\beta)$ sublattice of full(open) circles.
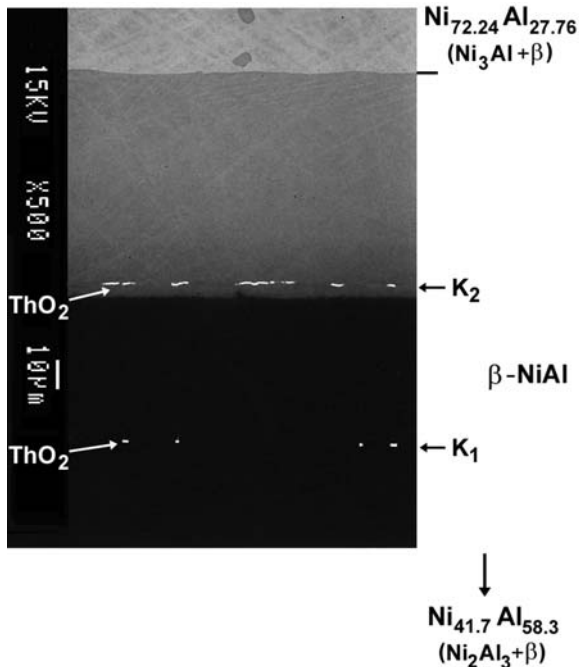
Fig. (3.1-3) Back-scattered electron image of a diffusion zone developed between binary alloys with nominal compositions $Ni_{41.7}Al_{58.3}$ and $Ni_{72.24}Al_{27.76}$ after reaction in vacuum at 1000 °C for 24 hrs. ThO_2-particles were used as inert markers between the initial end-members. Two well-defined "Kirkendall" marker planes emerged upon the interaction.

(The original $Ni_{41.7}Al_{58.3}$-alloy is much further away from the marker plane. Complete diffusion zone of this couple can be seen in see Fig. (3.1-7))

One can make incremental diffusion couples to determine the interdiffusion coefficient, $\tilde{D}$ (see A.9) and the ratio of intrinsic diffusivities, D_A / D_B (see A.10) for each couple. Interdiffusion coefficients and ratio of diffusivities are material constants for a particular composition at certain temperature. Then, the intrinsic diffusivities of the species, D_A and D_B over the homogeneity range can be determined by using the relation $\tilde{D} = V_A C_A D_B + V_B C_B D_A$ (Eq. (A.8-8)).

It turned out that only the second approach could be used because of the absence of suitable radioactive isotopes of Al.

III. Relative mobilities of species and Interdiffusion in the β-NiAl intermetallic

No pores (voids) or changes in the local cross-section of the annealed samples have been observed after annealing and no indication of grain boundary contribution to the overall diffusion transport in the product layer of NiAl-intermetallic was found. Concentration profiles in the annealed couples measured with EPMA were followed by Wagner's approach, which takes into account the volume changes during interaction and enables us to calculate the interdiffusion coefficients (Eq. (A.9-13)) as well as to determine the ratio of intrinsic diffusivities (Eq. (A.10-6)) at the position of the Kirkendall marker plane, following:

$$\tilde{D}(Y) = \frac{1}{2t\dfrac{d(Y/V_m)}{dx}}\left[(1-Y)\int_{-\infty}^{x^*}\frac{Y}{V_m}dx + Y\int_{x^*}^{\infty}\frac{(1-Y)}{V_m}dx\right] \tag{3.1-3}$$

$$\frac{D_B}{D_A} = \frac{V_B}{V_A}\left[\frac{N_B^+\displaystyle\int_{-\infty}^{x_K}\frac{Y}{V_m}dx - N_B^-\displaystyle\int_{x_K}^{\infty}\frac{(1-Y)}{V_m}dx}{-N_A^+\displaystyle\int_{-\infty}^{x_K}\frac{Y}{V_m}dx + N_A^-\displaystyle\int_{x_K}^{\infty}\frac{(1-Y)}{V_m}dx}\right] \tag{3.1-4}$$

where the Sauer-Freise variable $Y = (N_B^- - N_B)/(N_B^+ - N_B^-)$, N_B is the mole fraction of B, N_B^- and N_B^+ are the end-member compositions of B at the unreacted left and right-hand side of the diffusion couple and x^* is the position of interest.

An important prerequisite to find the inter- and intrinsic diffusion coefficients and the Kirkendall velocity values (Eq. (3.1-2)) in the growing intermetallic is the knowledge of the partial molar volume of the species involved in the interaction and the molar volume of the alloys. These data were obtained taking into account the possible presence of constitutional vacancies in the B2 structure and available information on the lattice parameter of NiAl (see A.18).

In Fig. (3.1-4) the values of ratio of intrinsic diffusion coefficients, D_{Ni}/D_{Al}, derived from the examination of the Kirkendall marker shift in the reaction couples listed in Table (3.1-1) are displayed graphically. The lines drawn in this figure represent the result of polynomial interpolation of the sets of the experimental points (pertaining to the Al- and Ni-rich domains of the homogeneous region) and subsequent extrapolation to the equiatomic composition. This result is expected, given the differences in the point defect structure and diffusion mechanisms operative on either side of the stoichiometry in B2 NiAl-phase [6-11].

One sees that indeed a cross-over of the intrinsic diffusivities occurs within the stability range of this intermetallic, which reflects that $(D_{Ni}-D_{Al})$ changes sign near stoichiometric composition.

Another important point is to be mentioned here. Returning to the back-scattered electron image shown in Fig. (3.1-3), one can notice the abrupt change in contrast near the equiatomic composition inside the β-phase layer. This is caused by the steep concentration gradient developed in the reaction product upon interdiffusion. The physical meaning of the existence of this gradient is the slow diffusion in the vicinity of stoichiometric NiAl-intermetallic, which reflects the highest degree of order in the B2 structure of the β-phase in this compositional interval. This also has a profound influence on interdiffusion in this intermetallic compound.

Interdiffusion in β-NiAl has been the subject of intensive investigations [10-17]. It is generally agreed that interdiffusion coefficient in the NiAl-alloys varies several orders of magnitude over the β-field with a minimum near the equiatomic composition. A literature survey has also revealed many conflicting data, which has prompted the additional experimental investigation of the interdiffusion behaviour of this intermetallic.
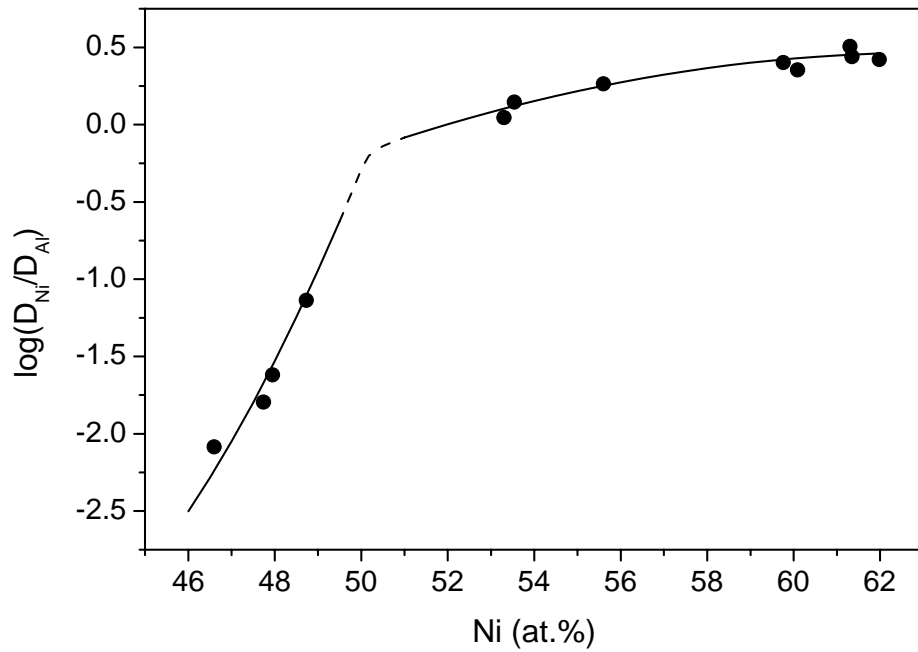
Fig. (3.1-4) Experimentally determined ratio of intrinsic diffusivities of nickel and aluminium, D_{Ni}/D_{Al} in the β-NiAl phase as a function of composition at 1000 °C.

Table (3.1-1) Diffusion couples analysed in the present work

Number of Sample	Diffusion couple	Annealing time (hrs)
1	$Ni_{49.8}Al_{50.2}/Ni_{72.24}Al_{27.76}$	100
2	$Ni_{49.8}Al_{50.2}/Ni_{66.24}Al_{33.76}$	24
3	$Ni_{46}Al_{54}/Ni_{72.24}Al_{27.76}$	24
4	$Ni_{46}Al_{54}/Ni_{66.24}Al_{33.76}$	24
5	$Ni_{46}Al_{54}/Ni_{57.5}Al_{42.5}$	100
6	$Ni_{46}Al_{54}/Ni_{57.5}Al_{42.5}$	24
7	$Ni_{46}Al_{54}/Ni_{49.8}Al_{50.2}$	100
8	$Ni_{49.8}Al_{50.2}/Ni_{57.5}Al_{42.5}$	100
9	$Ni_{46}Al_{54}/Ni_{52.2}Al_{47.8}$	100
10	$Ni_{46}Al_{54}/Ni_{52.2}Al_{47.8}$	24
11	$Ni_{41.7}Al_{58.3}/Ni_{72.24}Al_{27.76}$	24
12	$Ni_{46}Al_{54}/Ni_{54}Al_{46}$	24

In our work, interdiffusion in the NiAl intermetallic phase was studied at 1000 °C. The Sauer-Freise treatment adopted by Wagner (A.9) for diffusional growth of a compound layer was used to evaluate the results of diffusion couple experiments. The values of interdiffusion coefficient, $\tilde{D}$, computed in this manner are plotted in Fig. (3.1-5) shows the concentration dependence of the interdiffusion coefficient in the NiAl-phase at this temperature together with the data reported in the literature (Diffusion studies on the Ni-Al system by Janssen and Rieck [17] are not considered here because in their work no evaluation of the concentration dependence of the interdiffusion in the β-phase has been attempted).

It has to be stressed that direct quantitative comparison between the results of the present investigation and those obtained earlier is difficult. In the work of Shankar and Seigle [2], for example, a "classical" Matano-Boltzmann treatment of the concentration profiles across the reaction zones was used to derive the concentration dependence of interdiffusion coefficient. This is not a suitable treatment for the Ni-Al system, as the molar volume is strongly dependent on the composition and deviates from ideality (A.6, A.18). Therefore, differences (especially, in the Al-rich domain of the homogeneity region) between the interdiffusion data reported presently and those found in Ref. [12], as well as in the work of Helander and Ågren [14], who used in their models data of Shankar and Seigle, are not surprising. From Fig. (3.1-5), one can also notice about an order of magnitude difference between $\tilde{D}$ values for the Ni-rich β-phase reported recently by Nakamura et al. [16] and those of all other investigations.

In contrast, the results of Watanabe *et al.* [13] are very close to the present observations, but unfortunately, from diffusion couples used by these authors, it was not possible to obtain interdiffusion coefficients in the β-NiAl phase with an Al-content beyond 51.5 at.%.

As to the set of interdiffusion data published by Kim and Chang [15], two points are to be addressed. Firstly, in view of the potential existence of rather high concentrations of constitutional vacancies in the B2 structure of NiAl, they suggested to modify the classical treatment of the results obtained in diffusion couple experiments [9, 15] in terms of the so-called "lattice mole fraction", M, and the volume of one mole of lattice sites, V_u. For component i, M and V_u for cubic B2 NiAl phase can be expressed by:

$$M_i = \frac{n_i}{n_a + n_V} = \frac{n_i}{n_s} \; ; \; V_u = a^3 \frac{N_{Avo}}{n_s} \tag{3.1-5}$$

with n_V, n_i, n_a, n_s being the average number of structural vacancies, number of atoms of component i, the total number of atoms and the total number of lattice sites in the unit cell, respectively, N_{Avo} is the Avogadro number and a is the lattice parameter.
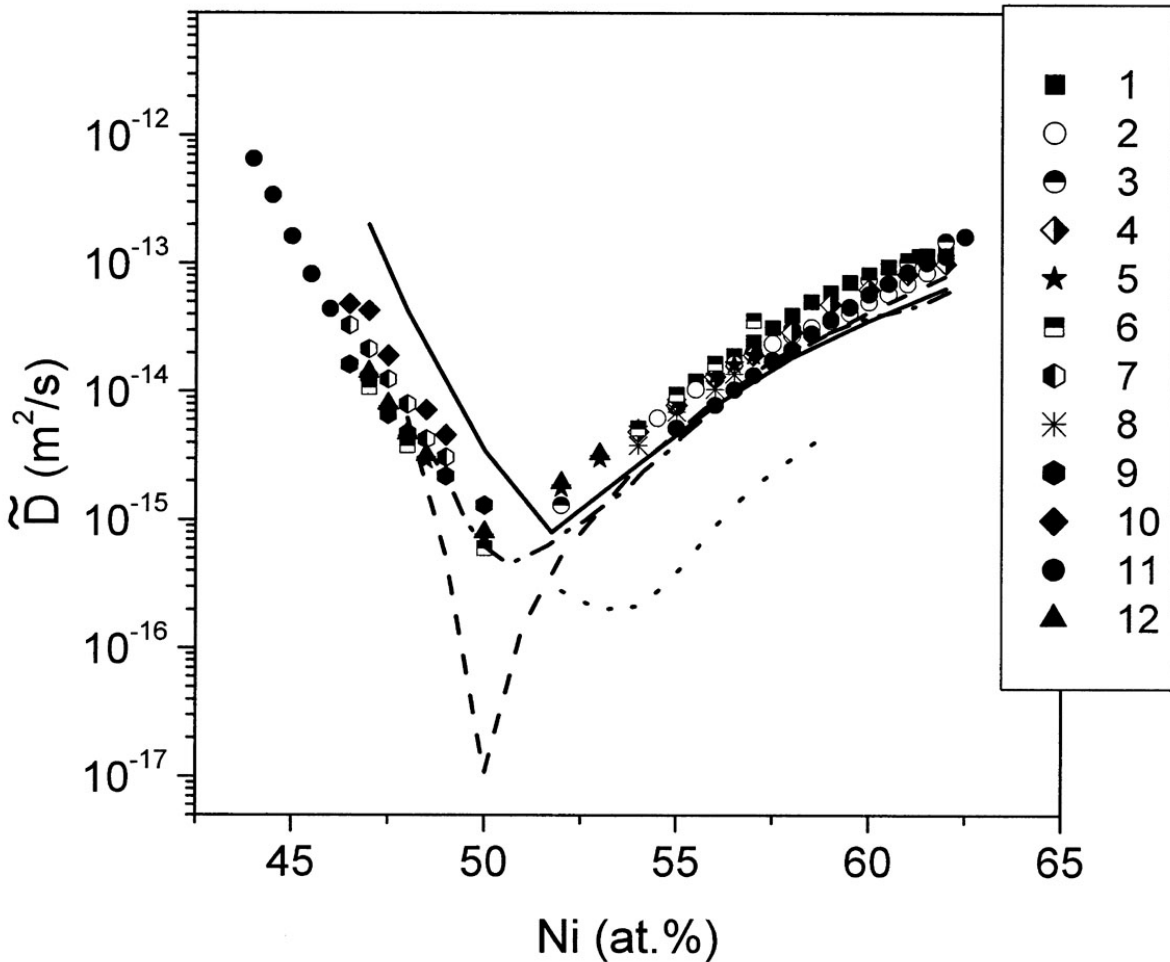
Fig. (3.1-5) Interdiffusion coefficient, $\tilde{D}$, in the NiAl-intermetallic compound at 1000 °C obtained with incremental diffusion couples. (The numbers with the legends corresponding to different samples as listed in Table 3.1-1).
The data reported by Shankar and Siegle [12] (————), by Watanabe *et al.* [13] (- ·· - ·· - ·-), by Kim and Chang [15] (- - - - - - -) and Nakamura *et al.* [16] (......................) are included for comparison.

The authors also claim that this composition variable is physically more reasonable for interdiffusion data analysis in the case of triple-defect B2 phases because of the existence of high concentrations of constitutional vacancies. It is to be remarked, however, that such a claim is somewhat misleading since the proposed treatment is

purely phenomenological and no attempts have been made to elucidate the underlying diffusion mechanisms. Moreover, it can readily be shown that there is no need for such new parameter, because it leads to exactly the same results as when using the classical parameters given in the present paper.

In Wagner's treatment the concentration variable is expressed by N_i/V_m and can be written with the help of Eq. (A.18-1) for molar volume, V_m:

$$\frac{N_i}{V_m} = \frac{n_i}{n_a}\frac{1}{V_m} = \frac{n_i}{a^3 N_{Avo}} \qquad (3.1\text{-}6)$$

Instead of N_i/V_m, Kim and Chang used M_i/V_u for their calculation. However, from Eq. (3.1-5 and -6) we can write,

$$\frac{M_i}{V_u} = \frac{n_i}{n_s}\frac{n_s}{a^3 N_{Avo}} = \frac{N_i}{V_m} \qquad (3.1\text{-}7)$$

which clearly shows the equivalence of the concentration variables.
Note from Fig. (3.1-5) that for off-stoichiometric NiAl, the measurements by Kim and Chang are indeed similar to the present experimental findings with an apparently rapid increase in interdiffusion coefficient for Al-rich alloys.

Secondly, the reported value of interdiffusion coefficient at stoichiometric NiAl is very low, in the order of $10^{-17} \, \text{m}^2/\text{s}$. This low value has nothing to do with the abovementioned introduction of a new concentration parameter. In the cited paper, there seems to be an educated tendency to think of the extremum in the concentration dependence as a "very deep minimum" corresponding to exactly stoichiometric NiAl. As already pointed out, a steep concentration gradient occurs in the proximity of the equiatomic composition, and therefore, the extent of this part of the diffusion zone is small. This thwarts the accurate determination of the interdiffusion coefficient in this compositional interval owing to uncertainties connected with the concentration gradient determination and graphical integration involved in the Wagner's method.

IV. Velocity curve construction in the β-NiAl diffusion layer

Returning to the diffusion couple shown in Fig. (3.1-3), it is now possible to determine the position of the plane within the intermetallic product layer where the Kirkendall markers were situated at time $t = 0$ (i.e. $x_o = 0$). This can be done by subjecting the concentration profile (Fig. (3.1-6a)) measured across the reaction zone to the Sauer-Freise treatment adopted by Wagner (see A.19). Using experimental results on the ratio

of diffusivities of the species (Fig. 3.1-4) and interdiffusion coefficients (Fig. 3.1-5) outlined in the preceding section the intrinsic diffusivities of Ni and Al over the homogeneity range was calculated using $\tilde{D} = V_A C_A D_B + V_B C_B D_A$. From pertinent values of the concentration gradient derived from the concentration-distance plot given in Fig. (3.1-6a), the Kirkendall velocity in the NiAl-intermetallic layer corresponding to the off-stoichiometric domains of the β-phase can be found (as shown in Fig. (3.1-6b)) using Eq. (3.1-2).

From Fig. (3.1-6b), one can see that the straight line $2tv_K = x_K$ intersects the velocity plot twice at locations where the gradient of the Kirkendall velocity with respect to the position parameter is negative. Under these conditions, the appearance of two microstructurally stable Kirkendall planes (i.e. bifurcation) inside the product layer is expected. Apparently, the marker plane locations predicted on the basis of the Kirkendall velocity diagram are in good agreement with the experimental observations, given the accuracy and limitations of the diffusion couple techniques employed.

V. Kirkendall effect and morphological development

An interesting experimental finding related to the presence of Kirkendall planes deserves further attention. It was noticed in the past that a "duplex" grain morphology sometimes develops inside diffusion-grown compound layers [18-20]. The term "duplex" is used here to emphasize that the layer of the same chemical compound looks in the examined reaction zone as if it consists of two sublayers demarcated by a distinct boundary and differing by shape, size or orientation of the grains. This boundary has been proved to coincide with the Kirkendall plane and, therefore, the presence of such a boundary can be considered as a manifestation of the Kirkendall effect [21].

The phenomenon is independent of the presence of any inert markers. The role of the Kirkendall plane in developing a duplex grain morphology in a single-phased product can be (qualitatively) understood from grains developed inside the interdiffusion zone.

When polarized light microscopic techniques were used to examine the diffusion couple shown in Fig. (3.1-1), it appeared possible to discern different grain morphologies ("sublayers") within the product layer (Fig. (3.1-7)). At the interphase interface I, the product NiAl grows by the loss of Ni-atoms from the reactant $Ni_{72.24}Al_{27.76}$ and by the reaction of this end-member with Al-atoms "released" from the other end-member,

25

$Ni_{41.7}Al_{58.3}$. At the interface II, on the other hand, the product phase grows by the reaction of the $Ni_{41.7}Al_{58.3}$ alloy with incoming Ni-atoms (released from the $Ni_{72.24}Al_{27.76}$) and by loss of Al-atoms from the $Ni_{41.7}Al_{58.3}$. As a result, the "sublayers" adjacent to the end-members of the couple exhibit different crystal morphology, possibly related to the morphology of the initial alloy end-members.
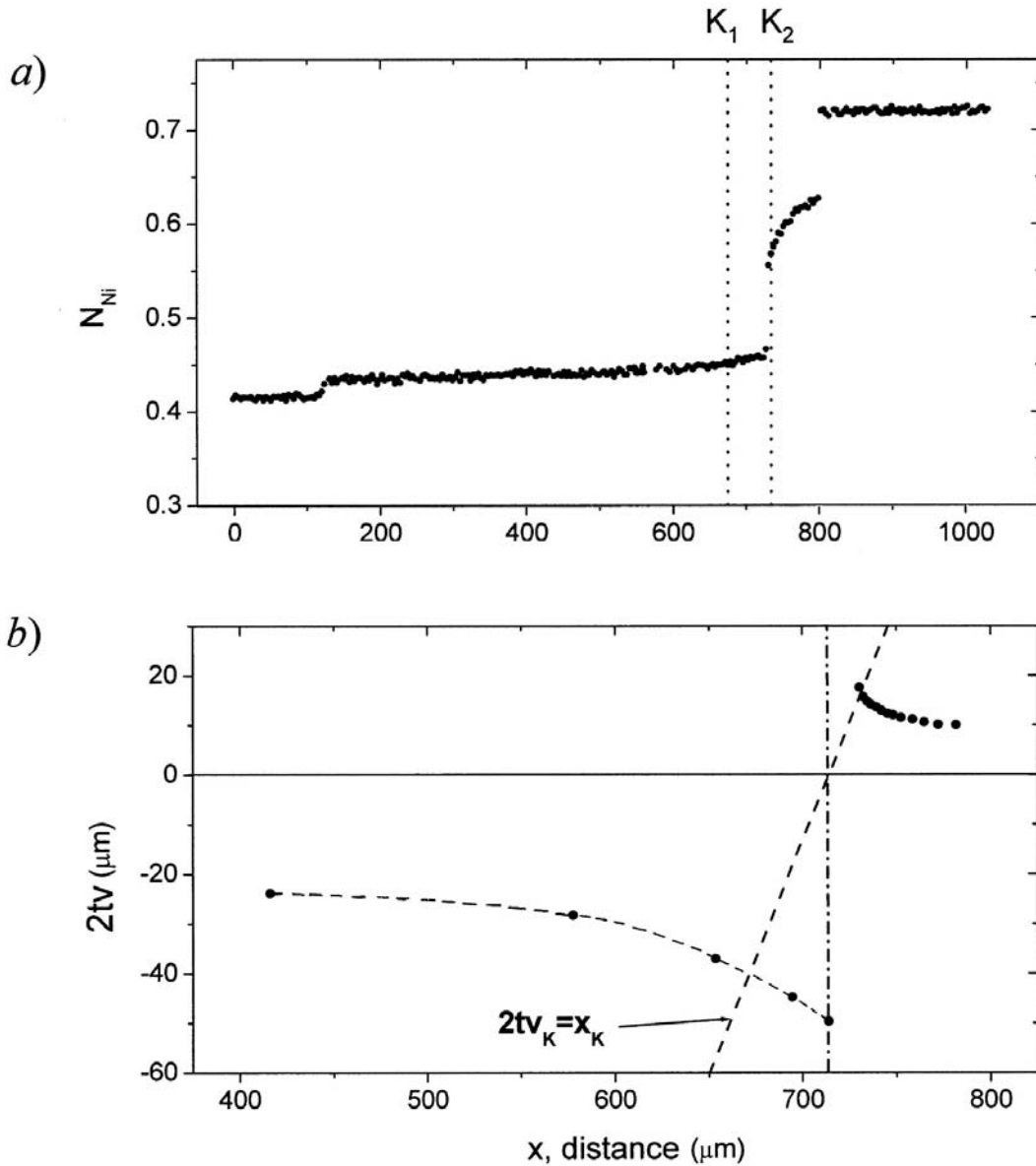
Fig. 3.1-6 (*a*) Distribution of nickel across the reaction zone in the annealed (1000 °C; 24 hrs) $Ni_{41.7}Al_{58.3}/Ni_{72.24}Al_{27.76}$ diffusion couple shown in Fig. (3.1-3). (Letters K_1 and K_2 indicate the observed positions of the Kirkendall marker planes); (b) the Kirkendall velocity diagram of the β-NiAl layer growing in this reaction couple constructed with the experimental data of the present investigation. (Two intersections between the velocity plot and the line $2tv_K = x_K$ are found. The dashed line connecting data points pertaining to the Al-rich part of the product layer is drawn for eye guidance).

26
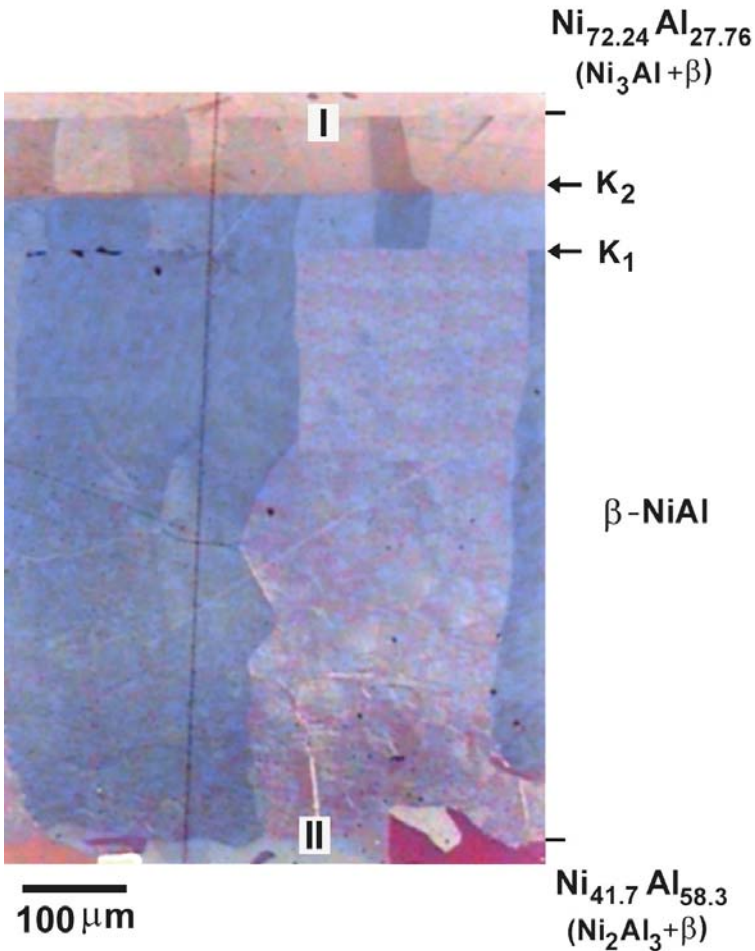
Fig. (3.1-7) Optical image (polarized light) of the reaction zone in the $Ni_{41.7}Al_{58.3}/Ni_{72.24}Al_{27.76}$ diffusion couple after annealing at 1000 °C in vacuum for 24 hrs. (K_1 and K_2 indicate the positions of the stable Kirkendall planes).

The grains in the region between K_1 and K_2 are different from those in the other parts of the couple. This is a general finding, also in other systems where two (or more) Kirkendall planes are found. Sometimes completely new grains are formed, sometimes one sees a kink in existing grain boundaries like in Fig. (3.1-7). This explanation becomes more clear in Chap. 4, where the physico-chemical approach is used for growing line compounds.

3.2 Bifurcation of the Kirkendall plane in a multilayered multiphase reaction zone: Ag-Zn system

I. Interdiffusion and intrinsic diffusion coefficients, and the velocity curve construction

Bifurcation in a multiphase system can be visualized in the Ag-Zn binary system. Pure Ag and Zn slices were coupled at 370 °C for 5 hours. As expected from the phase diagram (Fig. (3.2-1)) [22], three layers of the product intermetallics, β-AgZn, γ-Ag$_5$Zn$_8$ and ε-AgZn$_3$ were formed, as shown in Fig. (3.2-2). Here, the phases are denoted by their binary formulae. However, it is to be pointed out that the intermediate phases in this system exist over wide concentration ranges around the stoichiometric compositions. Prior to annealing ThO$_2$-particles were introduced between the initial couple halves as inert (fiducial) markers. After intersection, a row of ThO$_2$-markers can be seen inside the ε-, as well as in the γ-phase, i.e. two stable Kirkendall planes are present. Such marker behaviour can be rationalized in terms of the Kirkendall velocity construction as is shown below.

The interdiffusion coefficient, $\tilde{D}$, and ratio of intrinsic diffusivities, D_{Zn}/D_{Ag} are calculated at the Kirkendall marker positions (for the ε- and γ-phases) from the measured concentration profile as shown in Fig. (3.2-3) following Wagner's treatment (A.9 and A.10). The average values of molar volumes were calculated from the lattice parameters given in Ref. [23]. The absolute values of the intrinsic diffusivities are determined following the relation $\tilde{D} = V_A C_A D_B + V_B C_B D_A$ (Eq. (A.8-8)) and from the calculated values of interdiffusion and ratio of intrinsic diffusion coefficients. Partial molar volumes of the elements, V_{Ag} and V_{Zn} in the phases were considered as equal to the molar volumes of the pure components Ag, V_m^{Ag} (10.27 cm^3/mole) and Zn, V_m^{Zn} (9.16 cm^3/mole), respectively, considering the ideal case ($V_A \neq V_B$, but constant following Fig. (A.6-1a)). Intrinsic diffusion coefficients for β-phase were calculated, in the same manner, from the incremental couple Ag/(Zn13at.%Ag) in which only one Kirkendall marker plane (in the β-phase) was observed. Interdiffusion coefficients from both couples at the same composition were found to be same within the limit of errors and the values are listed in Table (3.2-1).

The velocity diagram was constructed as shown in Fig. (3.2-4). The position of initial contact plane $x_o = 0$ was found from the Y_{Ag}/V_m vs. x plot. For simplicity, we assumed a

constant marker velocity within the product phase layer, which means that each fiducial marker that might be present inside the product layer will move during the interdiffusion process with the same Kirkendall velocity. Apparently, this leads to a "stepwise" plot of *2tv* vs. *x*. One can see that the line $2tv_K = x_K$ ($x_K = x_K - x_o$ with $x_o = 0$) intersects the velocity plot twice in the domains of the reaction zone corresponding to the product layers of γ-Ag$_5$Zn$_8$ and ε-AgZn$_3$ intermetallics. This means that two microstructurally stable Kirkendall planes will emerge upon interdiffusion, one in the γ- and one in the ε- phase layer, as was found experimentally (Fig. (3.2-2)).
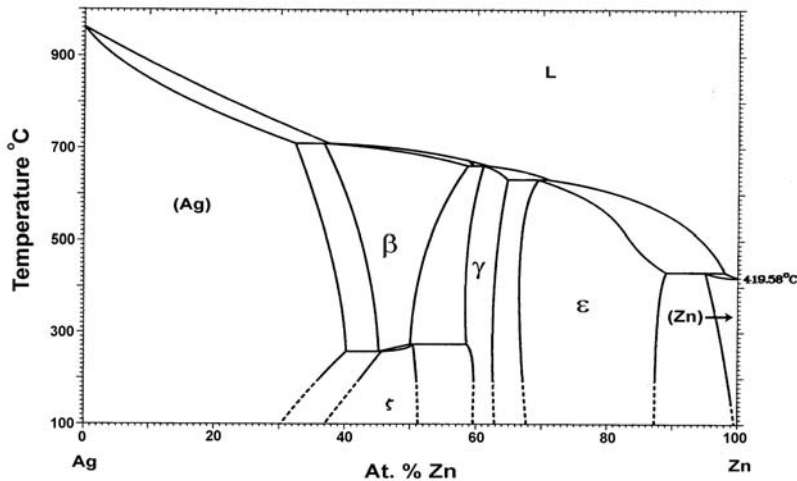
Fig. (3.2-1) Binary phase diagram of Ag-Zn system [22].

II. Kirkendall effect and morphological evolution

The micrographs of different phases grown during interdiffusion in a Zn/Ag diffusion couple (Fig. (3.2-2)) are shown in Fig. (3.2-5), which is a montage of a series of back-scattered electron images taken under different conditions (i.e. with different brightness and contrast).

Following the progression of the micrographs given, the role of the Kirkendall plane in developing of a duplex grain morphology inside the ε - (Fig. (3.2-5a)) and γ - phase (Fig. (3.2-5b)) layers is apparent. The changes in grain structure are seen to be associated with the presence of (stable) marker plane(s) inside the reaction products. On the other hand, no duplex structure has been formed in the β - phase, and no marker plane is present inside this intermetallic layer (Fig. (3.2-5c)). The "uniform" crystal morphology within the product layer is indicative for the absence of a Kirkendall plane.
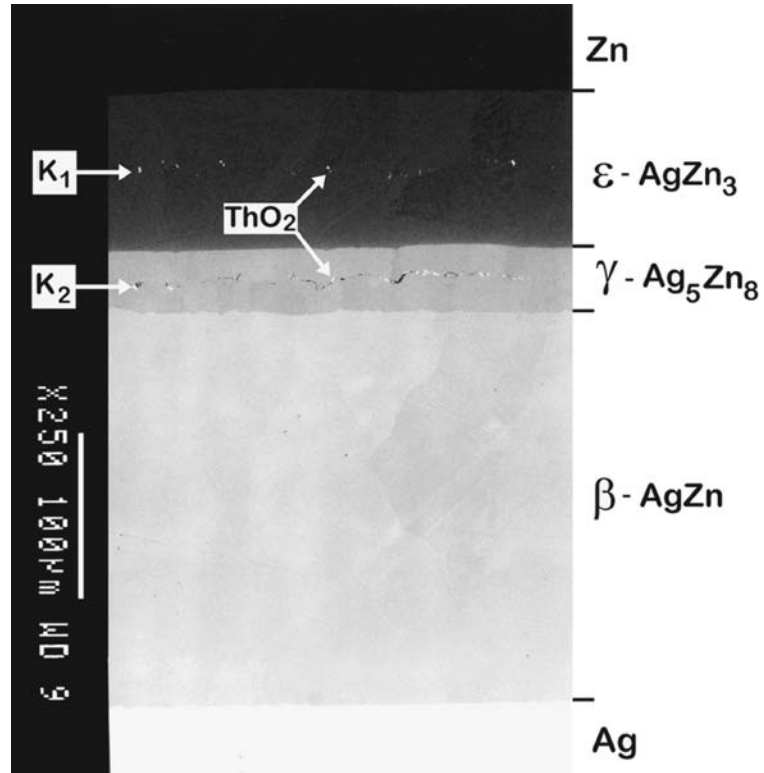
Fig. (3.2-2) Backscattered Electron Image (BEI) of a diffusion zone developed between Zn and Ag after reaction in argon at 370 °C for 5 hrs. ThO_2-particles were used as inert markers between the initial end-members. Two well-defined Kirkendall-marker planes (K_1 and K_2) emerged upon the interaction.
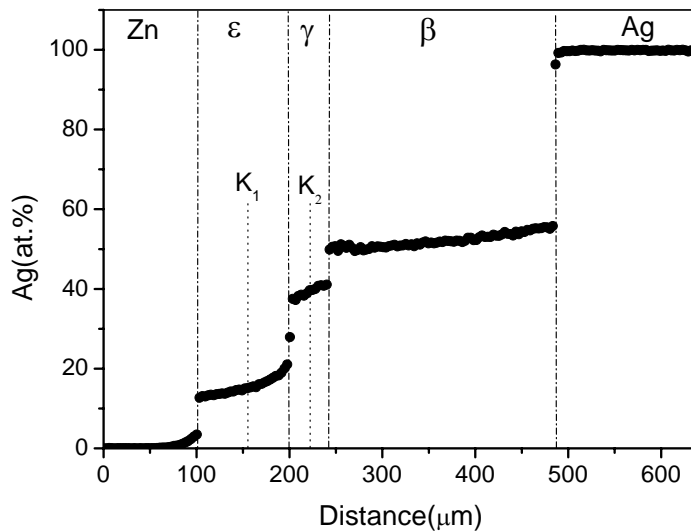
Fig. (3.2-3) Composition profile measured by EPMA of the Ag/Zn couple (as shown in Fig. (3.2-2)) annealed at 370 °C for 5 hrs. K_1 and K_2 correspond to the Kirkendall marker plane positions in the ε- and γ-phase, respectively.

Table 3.2-1 The diffusion coefficients, $\tilde{D}$, average values of molar volume, V_m of the Ag-Zn intermetallics and intrinsic diffusivities, D_{Ag} and D_{Zn} in these phases at 370 $^{\circ}$C for the compositions corresponding to the locations of the Kirkendall planes in the reaction couples studied, along with the calculated marker velocities, v_K.

	Phase (composition, at.%Ag)		
	β - AgZn (49.7)	γ - Ag$_5$Zn$_8$ (38.9)	ε - AgZn$_3$ (14.8)
V_m [m^3/mole]	9.46×10^{-6}	9.44×10^{-6}	9.20×10^{-6}
$\tilde{D}$ [m^2/s]*	1.0×10^{-11}	1.69×10^{-12}	1.67×10^{-12}
D_{Ag} [m^2/s]	2.74×10^{-12}	5.89×10^{-13}	4.1×10^{-13}
D_{Zn} [m^2/s]	1.6×10^{-11}	3.17×10^{-12}	8.0×10^{-12}
v_K [m/s]$^{*)}$	-2.8×10^{-9}	-2.87×10^{-9}	-4.67×10^{-9}

 *) Calculated using the concentration gradient in the product layers in the annealed Zn/Ag couple (370 $^{\circ}$C; 5 hrs).

We assumed partial molar volumes $V_{Ag} = V_m^{Ag} = 10.27 \times 10^{-6}$ and $V_{Zn} = V_m^{Zn} = 9.16 \times 10^{-6}$ m^3/mole.
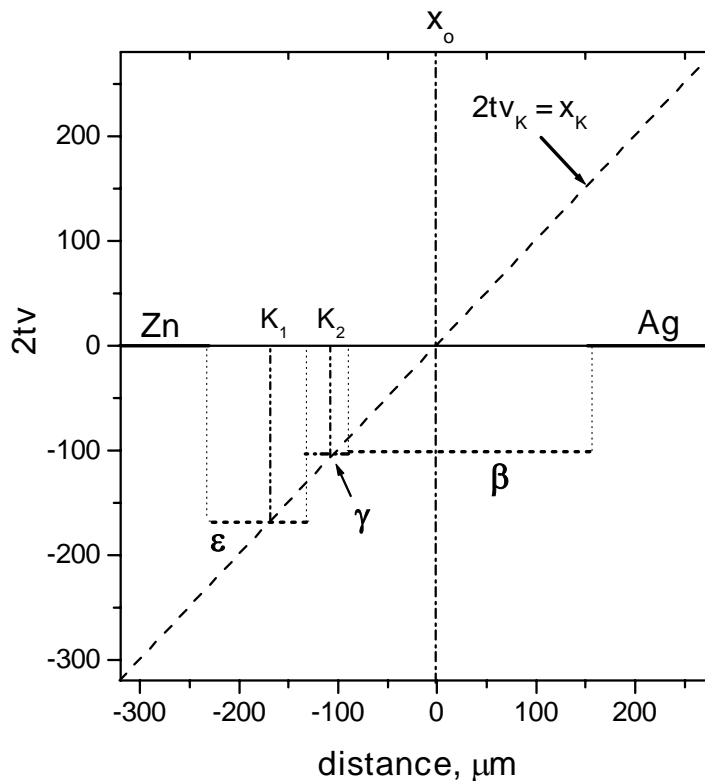
Fig. (3.2-4) The Kirkendall velocity diagram constructed for a Zn/Ag diffusion couple annealed at 370 $^{\circ}$C for 5 hrs. The straight-line $2tv_K = x_K$ intersects the velocity plot twice (at the positions K$_1$ and K$_2$), i.e. two Kirkendall marker planes are present.
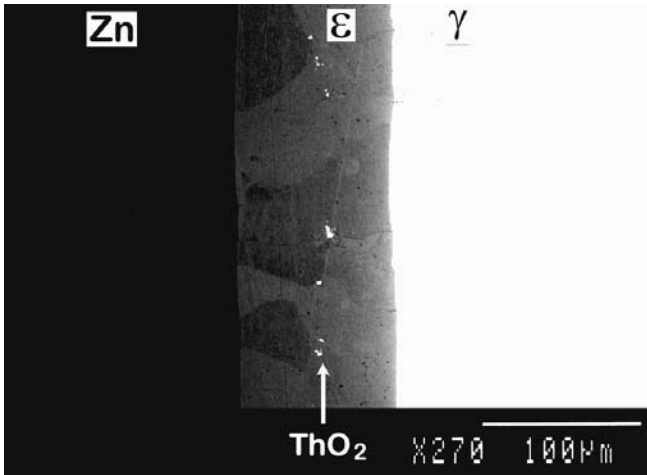
Fig. (3.2-5) Back-scattered electron images of different phases in a multiphase diffusion zone in a Zn/Ag reaction couple annealed at 370° C in argon for 5 hrs:

a) The Kirkendall marker position in ε-phase is clearly evident from the duplex morphology and the presence of ThO_2-particles.
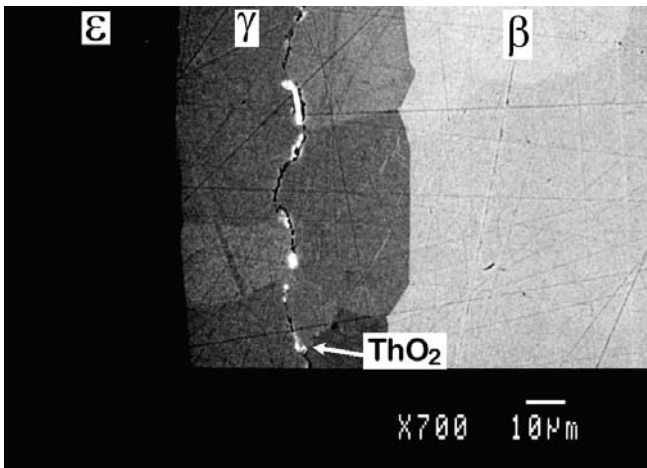
(b) The Kirkendall marker position is demarcated by the grain morphology developed during diffusion in γ-phase.
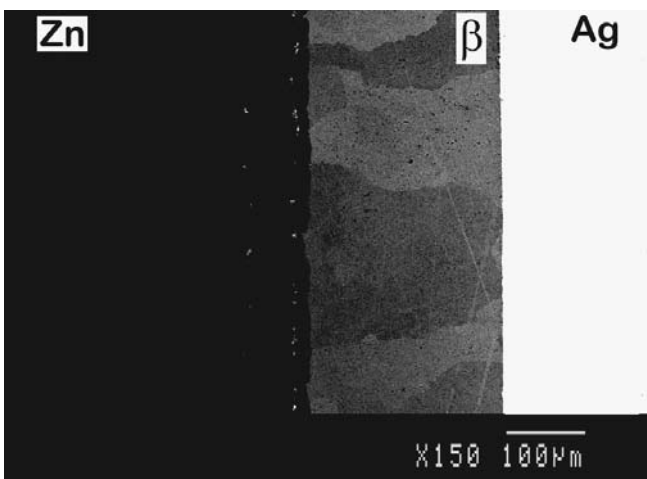
(c) The absence of a duplex nature in the β-phase is evidence for the absence of a Kirkendall marker plane in this layer.

3.3 Trifurcation of the Kirkendall plane: Ti-Al system

I. Interdiffusion and velocity curve construction

Till date there have been many proofs on the bifurcation of the Kirkendall plane: in a single-phased diffusion zone (β-NiAl [chap. 3.1], β′-AuZn [4]), in multiphase diffusion zones in binary systems (Ag-Zn [chap. 3.2], Co-Si [chap. 4.1], Au-Sn [chap. 6.3], Ti-Ni [1, 24] and in ternary system (Ti-Ni-Cr [25]). However, there was no evidence, so far, on the presence of more than two Kirkendall planes. Looking for the possibility for trifurcation of the Kirkendall plane, we found the predicted occurrence in the Ti-Al system, which was subject of earlier investigations in our laboratory [26, 27]. This can be appreciated from Fig. (3.3-1). This micrograph represents a typical diffusion zone morphology developed in a multiphase $TiAl_3$/Ti diffusion couple during reaction at 870 °C after annealing for 1600 hrs. In this experiment ThO_2-particles were used as inert markers between the end members. After interaction, rows of markers can be seen in all three reaction product layers, $TiAl_2$, TiAl and Ti_3Al, which are formed according to the phase diagram Fig. (3.3-2) [22].

The ratio of diffusivities at Kirkendall marker planes and the velocity of the inert markers were calculated with the help of Eq. (A.10-6) and Eq. (A.17-8), respectively from the composition profile (Fig. (3.3-3)) and are listed in Table (3.3-1). The average molar volumes of the phases were calculated at the stoichiometric composition from the crystallographic data available in Ref. [23]. The ratio of diffusivities was found to be in accordance with Ref. [26]. Partial molar volumes of the elements, V_{Ti} *and* V_{Al} in the phases were considered as equal to the molar volumes of the pure components Ti, V_m^{Ti} (10.63 cm^3/mole) and Al, V_m^{Al} (10 cm^3/mole), respectively, considering the ideal case ($V_A{\neq}V_B$, but constant following Fig. (A.6-1a)). The velocity diagram was constructed, as shown in Fig. (3.3-4), from the *2tv vs. x* stepwise plot and the straight line $2tv_K = x_K$ ($x_K = x_K - x_o = x_K$), after finding the x_o position following the procedure given in (A.19). It is clear that the line $2tv_K = x_K$ intersects three times the velocity curve *2tv vs. x*. For simplicity, a constant marker velocity within a product phase layer was assumed.
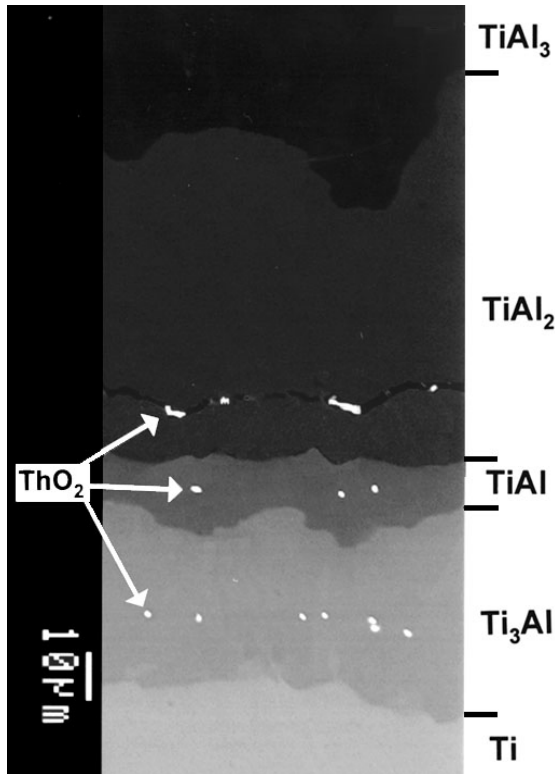
Fig. (3.3-1) Back scattered electron image of a diffusion zone developed between Ti and TiAl₃ after reaction in vacuum at 870 ^{0}C for 1600 hours. The locations of the Kirkendall planes inside the product layers are revealed by rows of ThO₂-particles.
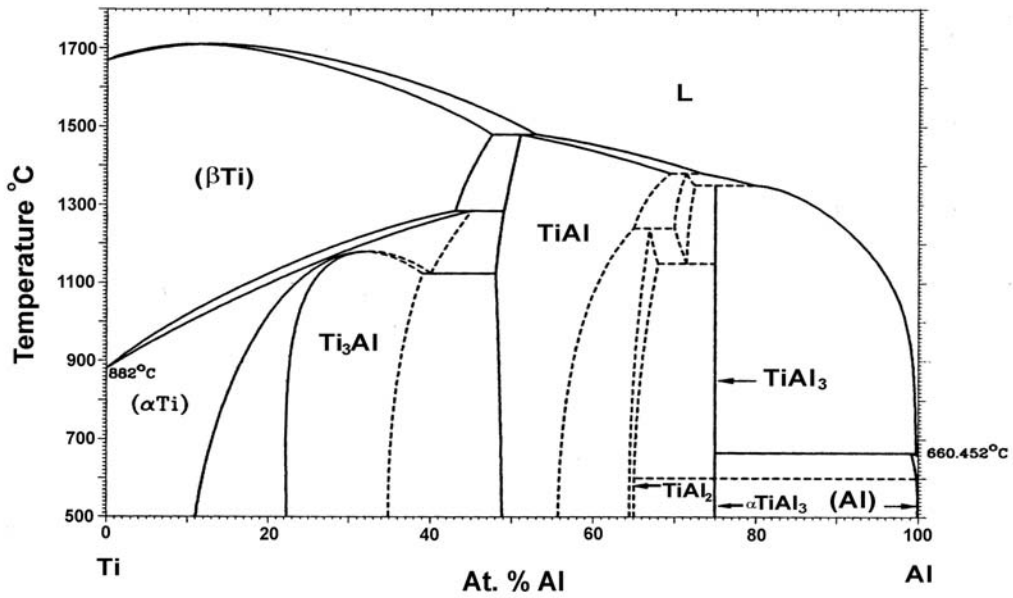
Fig. (3.3-2) Binary phase diagram of the Ti-Al system [22].
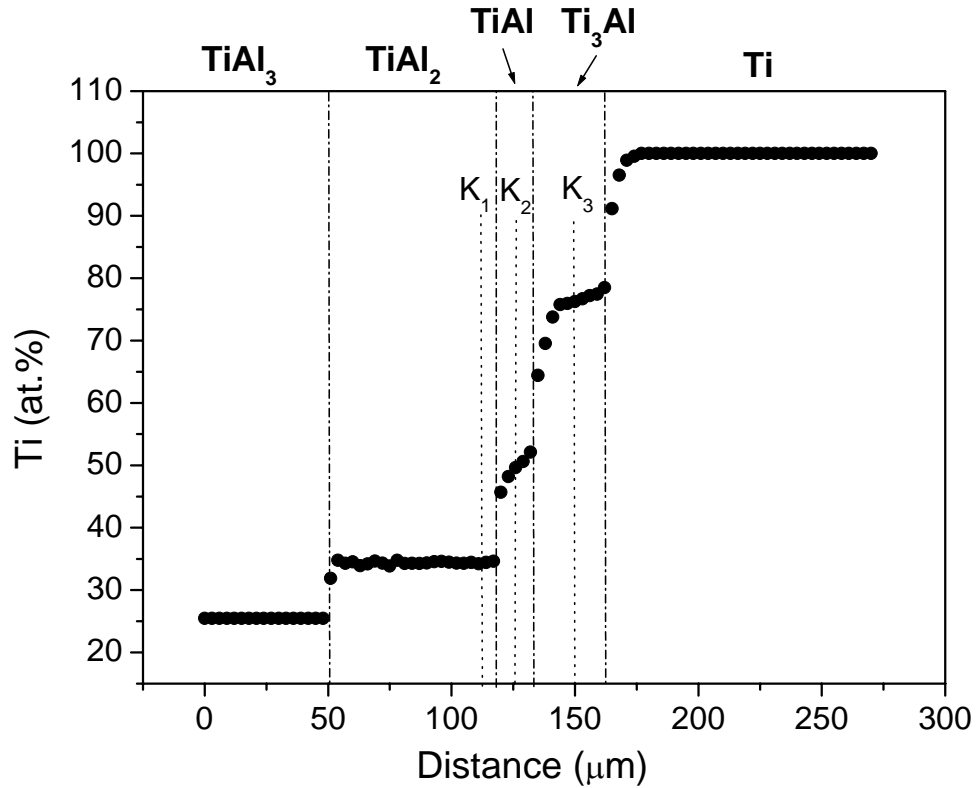
Fig. (3.3-3) Composition profile measured by EPMA of the TiAl$_3$/Ti couple (as shown in Fig. (3.2-1)) annealed at 870 °C for 1600 hrs. K$_1$, K$_2$ and K$_3$ correspond to the Kirkendall marker planes in the TiAl$_2$, TiAl and Ti$_3$Al phase, respectively.

Table 3.3-1 The ratio of diffusivities, average values of molar volume, V_m of the Ti-Al intermetallics at 870 °C for the compositions corresponding to the locations of the Kirkendall planes in the reaction couples studied, and the calculated marker velocities, v_K.

	Phase (composition, at.% Ti)		
	TiAl$_2$ (34.4)	TiAl (49.63)	Ti$_3$Al (76.26)
V_m [m^3/mole]	9.62×10^{-6}	9.81×10^{-6}	10.03×10^{-6}
$\dfrac{V_{Al} D_{Ti}}{V_{Ti} D_{Al}}$	0.0194	0.572	6.537
v_K [m/s]*	-17.74×10^{-13}	-3.99×10^{-13}	17.79×10^{-13}

we assumed $V_{Ti} = V_m^{Ti} = 10.63 \times 10^{-6}$ m^3/mole and $V_{Al} = V_m^{Al} = 10 \times 10^{-6}$ m^3/mole
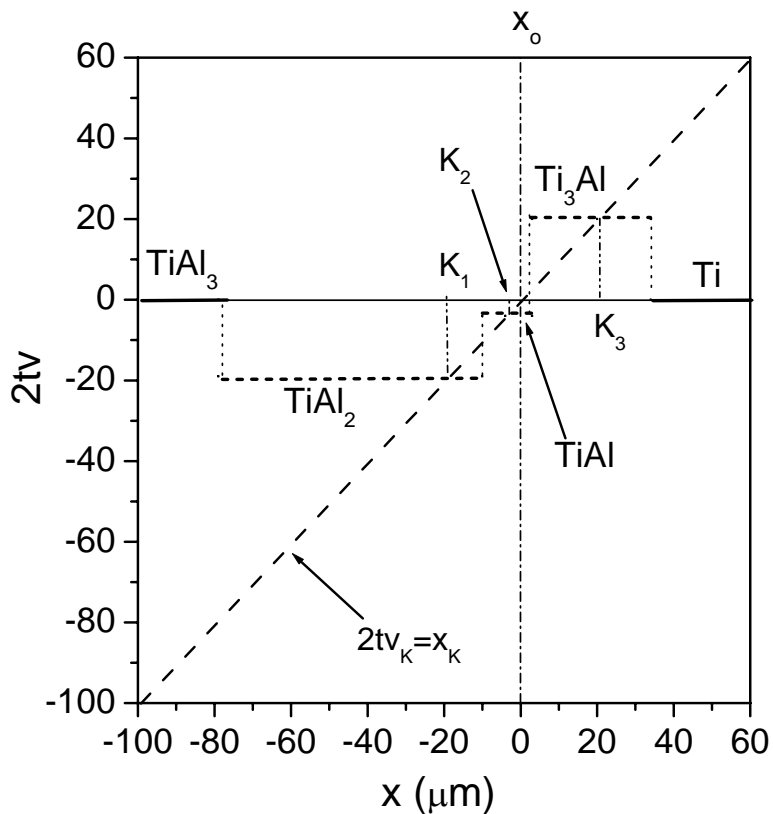
Fig. (3.3-4) The Kirkendall velocity diagram constructed for a TiAl$_3$/Ti diffusion couple annealed at 870 $^{\circ}$C for 1600 hrs. The straight-line $2tv_K = x_K$ intersects the velocity plot thrice (at the positions K$_1$, K$_2$ and K$_3$), i.e. three Kirkendall marker planes are present.

II. The effect of the Kirkendall plane on grain morphology

A duplex microstructure was found in all the three phases, as expected (Fig. (3.3-5a)) because of the presence of Kirkendall planes. This is, in fact, a characteristic morphological feature in the presence of a stable Kirkendall plane. However, it should be mentioned here that in the same couple, in some parts of the diffusion reaction zone, as shown in Fig. (3.3-5b) the Kirkendall plane in the TiAl-phase was missing.

This can be explained from the velocity plot as shown in Fig. (3.3-4). The presence of the Kirkendall plane in a phase layer is critically dependent on the thickness of the other phases. With changing of the thickness of the layers, the position of x_o will move to the right or left hand side (and also the length of the steps in the velocity curve for all the phase(s) will change) and the straight line $2tv_K = x_K$ can easily miss to intersect the velocity curve for one layer, especially if this layer is thin. The difference in the thickness of the total or phase layers can occur because of the grains developed with different

orientations. The lattices of all the three phases (TiAl$_2$ (hexagonal), TiAl (tetragonal), Ti$_3$Al (tetragonal)) are non cubic and can nucleate with different orientations. It is a well-known fact that with the difference in orientation, diffusion rates can be different. In the case of a multiphase diffusion zone, layers grow by the mutual competition between two simultaneous reactions (see Chap. 4). The phase grows by consuming neighbouring phase(s) and at the same time it is consumed because of the growth of other neighbouring phase(s). If the diffusion rate in some grains of the neighbouring phase(s) of TiAl is higher, the growth rate of these grains will be higher, so that they will consume more of the TiAl-phase. This may result into the consumption of one of the sublayers of the TiAl-phase adjacent to the TiAl$_2$ (or Ti$_3$Al) phase and the straight-line $2tv_K = x_K$ does not intersect the velocity curve for the TiAl-phase anymore.

Note that the waviness in the phase layers reflects the difference in the growth rate from grain to grain resulting from the difference in orientation.
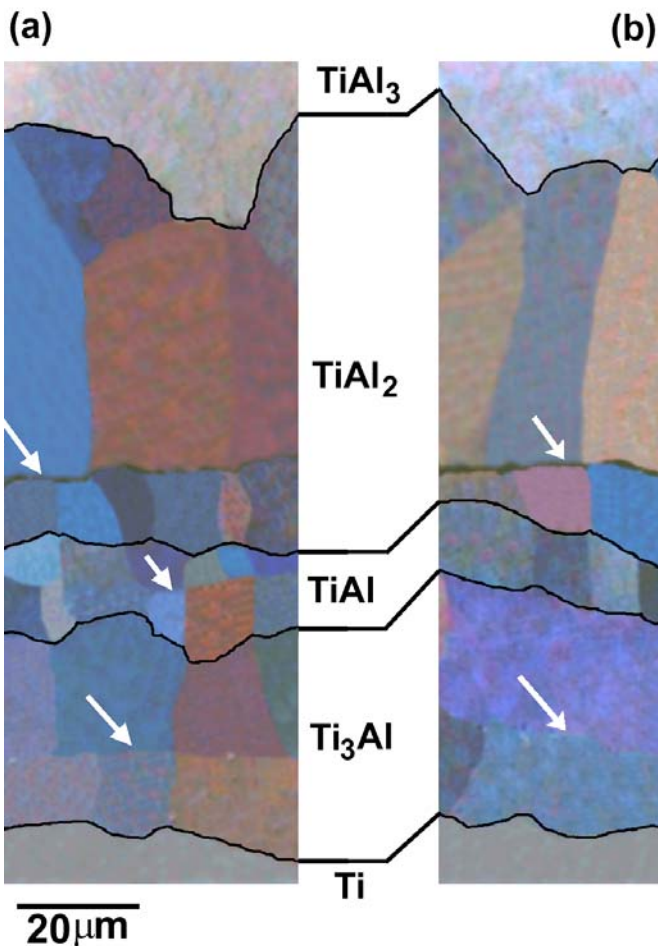
Fig. (3.3-5) Optical micrograph (polarized light) of a diffusion zone developed between Ti and TiAl$_3$ after reaction in vacuum at 870 °C for 1600 hours. Kirkendall marker planes are shown with the help of arrows.
(a) Duplex microstructure is evident in all the phase layers.
(b) One sublayer in TiAl-phase is missing which reflects the absence of a Kirkendall plane in this phase.

3.4 Concluding remarks

Unquestionably, the better understanding of the Kirkendall effect has a great potential for providing insights into the complexities of multiphase diffusion.

We succeeded to demonstrate that the Kirkendall plane bifurcation in a single-phased intermetallic product layer and the bifurcation and trifurcation in a multiphase diffusion zone can be rationalized using the concept of "marker velocity construction". Here, we rely solely on the information deduced from the experiments with incremental diffusion couples, which have proved to be a versatile technique for studying diffusion behaviour in intermetallic compounds.

It is likely that improved models based, for example, on diffusion mechanism considerations will be developed in the future to describe the Kirkendall-effect mediated behaviour of inert inclusions (markers) during growth of an intermetallic layer. Nevertheless, the success of the present phenomenological model in the understanding of bifurcation and trifurcation of the Kirkendall plane is very gratifying.

The results of the present study may also alter some previous notions about the diffusional growth of a compound layer. For instance, it was found that the stable Kirkendall plane(s) can be revealed by the grain morphology changes in the product layer. In other words, in this case, there is no need for any fiducial markers at all to find the positions of the Kirkendall planes!

The bifurcation and trifurcation of the Kirkendall plane was observed, not only because of the grains growing from the interfaces with starting reactants, but also because of the grains developed at a location in between the stable Kirkendall planes. This is more clearly explained in next chapter (Chap. 4) with the help of a physico-chemical approach developed during this thesis work.

References

1. M.J.H. van Dal, M.C.L.P Pleumeekers, A.A. Kodentsov and F.J.J. van Loo, Intrinsic diffusion and Kirkendall effect in Ni-Pd and Fe-Pd solid solutions, Acta Mater. **48** (2000) 385-96
2. M.J.H van Dal, A.M. Gusak, C. Cserháti, A.A. Kodentsov and F.J.J van Loo. Microstructural stability of the Kirkendall plane in solid state diffusion, Phys. Rev. Lett. **86** (2001) 3352-55

3. M.J.H. van Dal, A.A. Kodentsov and F.J.J. van Loo, Formation of Co-Si intermetallics in bulk diffusion couples: Part II - Manifestations of the Kirkendall effect accompanying reactive diffusion, Intermetallics **9** (2001) 451-56
4. M.J.H. van Dal, A.M. Gusak, C. Cserháti, A.A. Kodentsov and F.J.J. van Loo, Spatio-temporal instabilities of the Kirkendall-marker planes during Interdiffusion in β'-AuZn, Phil. Mag. A, **82** (2002) 943-54
5. P. Nash, Phase Diagrams of Binary Nickel Alloys, Materials Park (Ohio): ASM International (1991) 3-11
6. Y.A. Chang and J.P. Neumann, Thermodynamics and defect structure of intermetallic phases with the B2 (CsCl) structure, Prog. Solid State Chem. **14** (1982) 221-301
7. C.R. Kao and Y.A. Chang, On the composition dependencies of self-diffusion coefficients in B2 intermetallic compounds, Intermetallics, **1** (1993) 237-50
8. I.V. Belova and G.E. Murch, The anti-structural bridge mechanism for diffusion in ordered alloys of the B2 type, Intermetallics **6** (1998) 115-19
9. S. Kim and Y.A. Chang, Use of lattice mole fraction to analyze interdiffusion data in strongly ordered triple-defect B2 intermetallic phases, Scripta Mater. **40** (1999) 1277-81
10. St. Frank, S.V. Divinski, U. Södervall and Chr. Herzig, Ni tracer diffusion in the B2-compound NiAl: influence of temperature and composition, Acta Mater. **49** (2001) 1399-1411
11. S.V. Divinski and Chr. Herzig, Ni tracer self-diffusion, interdiffusion and diffusion mechanisms in NiAl, Defect Diffusion Forum **203-205** (2002) 177-92
12. S. Shankar, L.L. and Seigle, Interdiffusion and Intrinsic diffusion in the NiAl phase of the Al-Ni system, Met. Trans. A, **9A** (1978) 1467-76
13. M. Watanabe, Z. Horita and M. Nemoto, Measurements of interdiffusion coefficients in Ni-Al system, Defect Diffusion Forum **143-147** (1997) 345-50
14. T. Helander and J. Ågren, A phenomenological treatment of diffusion in Al-Fe and Al-Ni alloys having B2-B.C.C ordered structure, Acta. Mater **47** (1999) 1141-52
15. S. Kim and Y.A. Chang, An interdiffusion study of a NiAl alloy using single-phase diffusion couples, Metall. Mater. Trans. A, **31A** (2000) 1519-24
16. R. Nakamura, K. Takasawa, Y. Yamazaki and Y. Iijima, Single-phase interdiffusion in the B2 type intermetallic compounds NiAl, CoAl and FeAl, Intermetallics **10** (2002) 195-204
17. M.M.P. Janssen and G.D. Rieck, Reaction diffusion and Kirkendall-effect in the Nickel-Aluminium system, Trans. Met. Soc. AIME, **239** (1967) 1372-85
18. J.H. Gülpen, A.A. Kodentsov and F.J.J. van Loo, Growth of silicides on Ni-Si and Ni-SiC bulk diffusion couples, Z. Metallkunde **86** (1995) 530-39
19. J.A. van Beek, S.A. Stolk and F.J.J. van Loo, Multiphase diffusion in the systems Fe-Sn and Ni-Sn, Z. Metallkunde **73** (1982) 439-44
20. K. Przybylski, W.W. Smeltzer, High temperature oxidation mechanism of CoO to Co_3O_4, J. Electrochem. Soc. **128** (1981) 897
21. A. Paul, M.J.H. van Dal, A.A. Kodentsov and F.J.J. van Loo, The Kirkendall effect in multiphase diffusion, Acta Mater. **52** (2004) 623-30
22. T.B. Massalski, Binary alloy phase diagrams, American society for metals, Metals Park, Ohio (1986)
23. P. Villars and L. Calvert, Pearson's Handbook for crystallographic Data for Intermetallic Phases, American Society for Metals, Metals Park, Ohio (1985)
24. G.F. Bastin and G.D. Rieck, Diffusion in the titanium-aluminium system: I. Occurrence and growth of the various intermetallic compounds, Met. Trans. **5** (1974) 1817-26
25. M.J.H. van Dal, Microstructural stability of the Kirkendall plane, PhD thesis (2001)
26. F.J.J. van Loo, Diffusion in the Titanium-Aluminium system, PhD Thesis, 1971
27. F.J.J. van Loo and G.D. Rieck, Diffusion in the titanium-aluminium system- Interdiffusion in the composition range between 25 and 100 at.% Ti-part II, Acta Metall., **21** (1973) 73-84

Chapter 4

A physico-chemical approach and morphological evolution

4.1 Multiphase diffusion growth and morphological developments in the Co-Si system

Recently, bifurcation and trifurcation of the Kirkendall planes have been discovered in many diffusion couples in our laboratory. This phenomenon can quantitatively be rationalized using classical diffusion theory by means of the Kirkendall velocity diagram. Now, it is understood that the position of the Kirkendall plane is revealed in the reaction zone not only by inert markers, but also by a different crystal morphology developed on either side of the plane.

For applications, it has been a challenge for researchers to develop a predictive capability, which envisage not only the thickness of the layers but also the position of the Kirkendall plane(s) and the morphology developing during interdiffusion. The Kirkendall plane is mechanically the weakest plane in the structure, because foreign inclusions and pores (resulting from a negative surface, i.e. scratch, on the bonding faces) will be accumulated along this plane. This plane has also strong influence on the morphological development, which ultimately controls the overall performance of the structure.

There are two types of treatment, a "diffusion based model" and a "physico-chemical approach" to predict the details of the structure. The diffusion-based model can successfully predict the thickness of the layers and the Kirkendall plane position(s) (as shown in A.20). However, it has the limitation that this approach does not shed light on

_____

This chapter is written based on the articles:

1. A. Paul, M.J.H. van Dal, A.A. Kodentsov and F.J.J. van Loo, The Kirkendall effect in multiphase diffusion, Acta Materialia, **52** (2004) 623-30

2. A. Paul, A.A. Kodentsov and F.J.J. van Loo, Bifurcation and trifurcation of a Kirkendall plane during multiphase interdiffusion, submitted to Def. Diff. Forum, 2004

the *reactions involved* during interdiffusion. For that purpose, a physico-chemical approach is developed during this thesis work, which (with the help of the diffusion based approach) elucidates the role of the Kirkendall effect in the morphogenesis of interdiffusion systems. The models are verified using the experimental results in the Co-Si system. The main advantage to consider this system is that there are numerous experimental results found in our laboratory [1, 2] and all the phases present in the system have a narrow homogeneity range. It is demonstrated that both the approaches, physico-chemical and diffusion based model lead to the same results regarding the predictions of the Kirkendall plane positions, however, the physico-chemical approach has the extra benefit of the prediction of the morphological developments.

I. Diffusion based approach

This approach is illustrated in A.20 by using examples of interaction in the system Co-Si. The pertinent experimental information on Co-silicide growth, which provides the basis for verification of the proposed models are found in our publications [1, 2].

In the Co-Si system three (nearly) stoichiometric compounds, viz. Co_2Si, $CoSi$ and $CoSi_2$ exist, as shown in Fig. (4.1-1). The most important data for the ensuing discussion are listed in Table (4.1-1). The average values of $\widetilde{D}_{int}$ at 1100 °C for intermetallic compounds of the Co-Si system obtained experimentally using different types of diffusion couples are given together with the ratio's of intrinsic diffusion fluxes of Si and Co determined in the product phase layers at the position of the Kirkendall plane and the molar volumes of the Co-silicides.

The thickness of the product layers can be predicted for any type of semi-infinite multiphase diffusion couple of this system if the values of $\widetilde{D}_{int}$ are known for all the compounds formed during reaction. The results of the calculations (see A.20) for three different couples of the Co-Si system are presented in Table (4.1-2). The positions of the Kirkendall planes were calculated from ratio of intrinsic diffusivities. The straight-line $2tv_K = x_K$ and the velocity plot $2tv$ vs. x found by $v = V_B(D_B - D_A)\dfrac{\partial C_B}{\partial x}$, as explained in section A.17, A.20, should intersect at the Kirkendall plane positions(s). In Figs. (A.20-2b, A.21-3a, and -3b) the Kirkendall velocity diagrams experimentally constructed for various diffusion couples of the Co-Si system are shown. In the case of the Co-Si couple

(Fig. (A.20-2b)), it is impossible for a Kirkendall plane to be located in the CoSi$_2$-phase layer since the line $2tv_K = x_K$ does not hit the velocity plot $2tv$ vs. x in the domain of the reaction zone corresponding to that phase. As suggested in Ref. [3], in such situation one can define a virtual Kirkendall plane for this phase layer, whose meaning is more clearly understood from the physico-chemical treatment presented in the next section.

II. A physico-chemical approach

If one considers the couple Co$_2$Si/CoSi$_2$, it is clear from Fig. (4.1-2) that the product phase is growing in two ways, due to a different type of nucleation. At the interface Co$_2$Si/CoSi the CoSi-phase nucleates and grows by the loss of Co atoms from Co$_2$Si and by the reaction of Co$_2$Si with Si atoms, released from CoSi$_2$. At the CoSi/CoSi$_2$ interface the CoSi-phase nucleates and grows by the reaction of CoSi$_2$ with Co atoms (released from Co$_2$Si) and by the loss of Si atoms from CoSi$_2$.

In terms of chemical reaction equations the process can be described a follows:

at the interface Co$_2$Si/CoSi

$$3pCo_{\frac{2}{3}}Si_{\frac{1}{3}} \quad \rightarrow \quad p[Co]_d + 2pCo_{\frac{1}{2}}Si_{\frac{1}{2}}$$

$$3qCo_{\frac{2}{3}}Si_{\frac{1}{3}} + q[Si]_d \quad \rightarrow \quad 4qCo_{\frac{1}{2}}Si_{\frac{1}{2}}$$

at the interface CoSi/CoSi$_2$

$$3pCo_{\frac{1}{3}}Si_{\frac{2}{3}} + p[Co]_d \quad \rightarrow \quad 4pCo_{\frac{1}{2}}Si_{\frac{1}{2}}$$
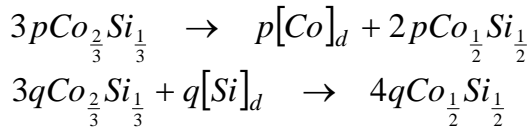
$$3qCo_{\frac{1}{3}}Si_{\frac{2}{3}} \quad \rightarrow \quad q[Si]_d + 2qCo_{\frac{1}{2}}Si_{\frac{1}{2}}$$
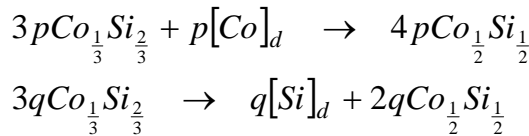
The parameters p and q are the number of moles of Co and Si atoms, respectively, transferred per unit area of the reaction layer during the total diffusion time. The symbols [Co]$_d$ and [Si]$_d$ denote the diffusing atom species in the product layer; they do not represent the phases Co or Si.

For a quasi-steady state growth of the product layer, one can write

$$p = \int_0^t |J_{Co}|dt = \int_0^t \frac{k}{t^{1/2}} dt = 2t|J_{Co}| \; ; \; q = 2t|J_{Si}| \tag{4.1-1}$$

as the intrinsic flux, J_i in a diffusion-controlled interaction is proportional to $t^{-1/2}$. Here k is a constant.
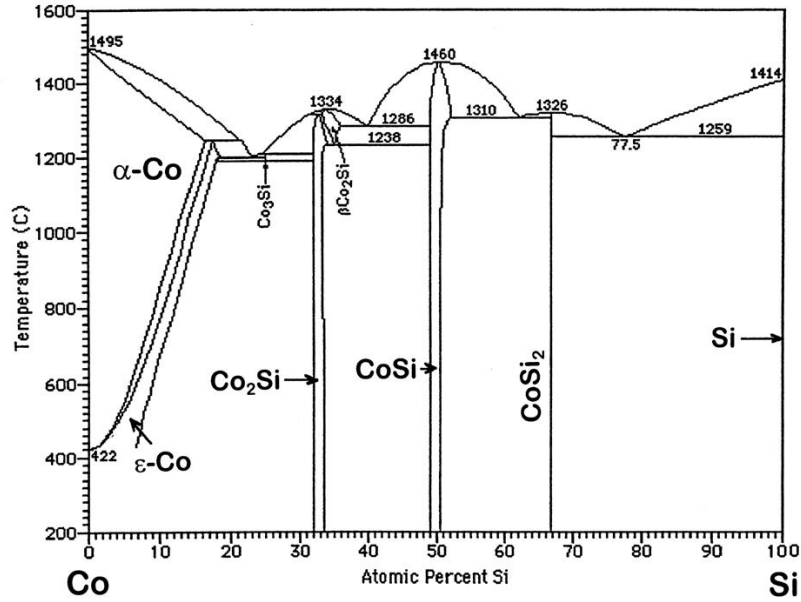
Fig. (4.1-1) Binary phase diagram of Co-Si system. Three line compounds with narrow homogeneity range are present in the system.
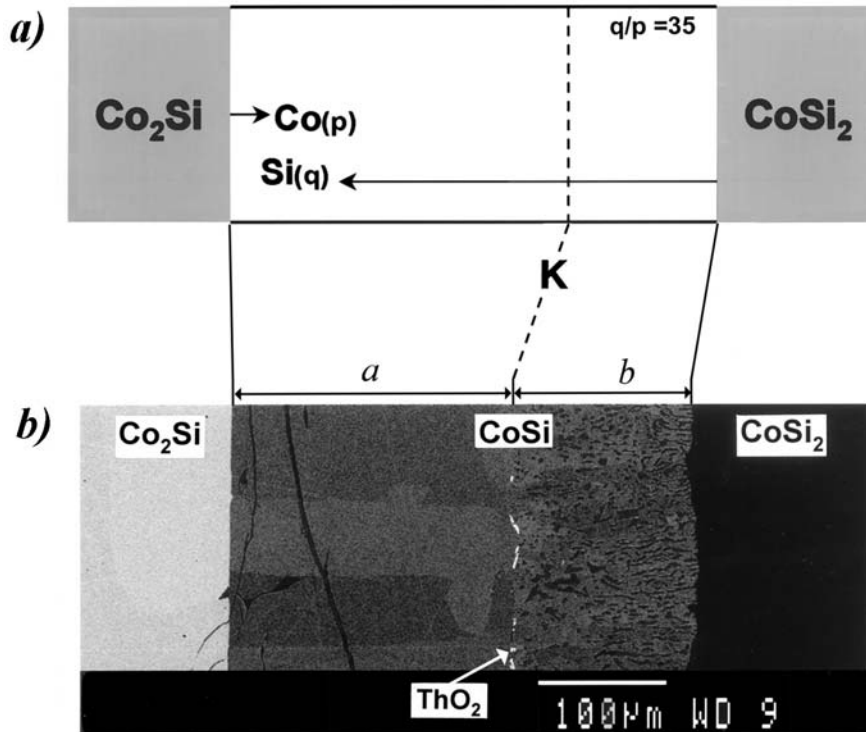
Fig. (4.1-2a) Schematic illustration of the growth of the CoSi-layer between the Co_2Si and $CoSi_2$ compounds and b) backscattered electron image showing the formation of CoSi in an annealed $Co_2Si/CoSi_2$ diffusion couple (1100 °C; 25 hrs). The Kirkendall plane (K) is revealed by the ThO_2-particles exhibiting a white contrast on the micrograph.

Table (4.1-1) The integrated diffusion coefficients, $\tilde{D}_{int}$, molar volumes V_m of the Co-silicides and ratio's of intrinsic fluxes of Si and Co, $V_{Co}D_{Si}/V_{Si}D_{Co}$ in these phases at 1100 °C.

	Phase		
	Co$_2$Si	CoSi	CoSi$_2$
$\tilde{D}_{int}$ [m^2.s^{-1}]*	$(1.5\pm0.5)\times10^{-14}$	$(4.6\pm0.3)\times10^{-14}$	$(7.7\pm1.2)\times10^{-16}$
$\dfrac{V_{Co}D_{Si}}{V_{Si}D_{Co}}$	0.06 ± 0.025	35 ± 15	1.4 ± 0.25
V_m [m^3.mole^{-1}]	6.56×10^{-6}	6.60×10^{-6}	7.75×10^{-6}

*) average values obtained from different diffusion couples

Table (4.1-2) The calculated thicknesses, d and Kirkendall velocities, v_K corresponding to the phase layers growing during interdiffusion in various couples of the Co-Si system at 1100 °C along with the predicted positions, x_K (where coordinate $x_K = x_K - x_o$; $x_o = 0$) of Kirkendall plane(s) in the reaction products (see Figs. (A.20-2b, -3a and -3b)).

Diffusion Couple (annealing time)	Calculated values	Product Phase		
		CoSi	Co$_2$Si	CoSi$_2$
Co$_2$Si/CoSi$_2$ (25 hrs)	d (10^{-6} m)	315		
	v_K (10^{-10} m/s)	2.75		
	x_K (10^{-6} m)	49.5		
Co/CoSi$_2$ (100 hrs)	d (10^{-6} m)	463	164	
	v_K (10^{-10} m/s)	1.86	-2.31	
	x_K (10^{-6} m)	133.8	-166.3	
Co/Si (100 hrs)	d (10^{-6} m)	321	131	6.8
	v_K (10^{-10} m/s)	2.69	-2.92	0.4
	x_K (10^{-6} m)	193.7	-210.5	28.6 (virtual)

Therefore, the ratio q/p equals to the ratio of the momentary diffusion fluxes of the components inside the phase layer at time t, that is (considering Eqs. (A.4-9 and A.8-1))

$$\frac{q}{p} = \frac{\int_0^t |J_{Si}| dt}{\int_0^t |J_{Co}| dt} = \left| \frac{J_{Si}}{J_{Co}} \right|_{CoSi} = \frac{V_{Co} D_{Si}}{V_{Si} D_{Co}} \qquad (4.1\text{-}2)$$

The reaction zone developed in this couple can be considered as if it was composed of two regions separated by the Kirkendall plane and the following relations can be defined:

$$\begin{aligned} (2p + 4q)V_m^{CoSi} &= a \\ (4p + 2q)V_m^{CoSi} &= b \end{aligned} \qquad (4.1\text{-}3)$$

with a and b being the thicknesses of the CoSi-layer nucleated at either side of the Kirkendall plane (Fig. 4.1-2).

We know the total layer thickness of the CoSi-phase that will grow after 25 hours of annealing in the $Co_2Si/CoSi_2$ couple as shown in Table (4.1-2) calculated by the diffusion-based approach (see A.20) and we can write, $a + b = 315$ μm. The ratio of diffusivities q/p is known from Eq. (4.1-2) in this phase as listed in Table (4.1-1). From these information's we can solve the Eq. (4.1-3) and find the values of a and b as 208 and 107 μm, respectively, and p and q as 0.22 and 7.73 mole/m² , respectively.

According to the basic diffusion concepts we earlier found (see Eq. (A.8-7))

$$2tv_K = -2t(V_{Si}J_{Si} + V_{Co}J_{Co}) = -2tV_m(J_{Si} + J_{Co}) \qquad (4.1\text{-}4)$$

considering $V_{Si} = V_{Co} = V_m$ (i.e. we take the partial molar volumes of the species in a phase is equal to the molar volume of the phase). According to the physico-chemical approach we can transform Eq. (4.1-4) into:

$$2tv_K = x_K^{CoSi} = V_m^{CoSi}(q - p) \qquad (4.1\text{-}5)$$

With the values of p and q, the velocity of the marker plane, v_K was calculated from Eq. (4.1-5) as 2.75×10^{-10} m/s which agrees with the value listed in Table (4.1-2) calculated by the diffusion-based approach through Eq. (A.17-9):

$$v = \frac{V_{Co}}{V_m^{CoSi}} \frac{\dfrac{D_{Si}}{D_{Co}} - 1}{\left(\dfrac{V_{Co} D_{Si}}{V_{Si} D_{Co}}\right) N_{Co} + N_{Si}} \frac{\tilde{D}_{\text{int}}^{CoSi}}{\Delta x_{CoSi}}$$

(4.1-6)

where Δx_{CoSi} is the thickness of CoSi diffusion layer developed after interaction.

This shows the equivalence of the diffusion-based and the physico-chemical approaches in describing a product phase growth and by both approaches we get the same results. In fact, the results could not be otherwise, since both models describe the same phenomenological processes in terms of purely phenomenological quantities.

The calculated results calculated are also consistent with the experimentally found location of the Kirkendall plane, x_K (Fig. (4.1-2)). The micrograph presented in Fig. (4.1-2b) indeed shows the completely different crystal morphology developed within the product layer on either side of the Kirkendall plane, originating from the two different nucleation sites.

The fact that the experimentally observed value of b seems to be somewhat higher than the calculated results which stems from the presence of pores in the part of the CoSi-layer adjoining the CoSi$_2$ end-member. The pore formation can be attributed to the release of Si atoms from CoSi$_2$ upon the reaction and the incomplete plastic relaxation inside the diffusion zone associated with the poor mechanical characteristics of the Co-silicides.

A similar analysis can be used to describe the solid-state interaction between Co and CoSi$_2$ when two product layers grow in the diffusion zone (Fig. (4.1-3)). In this case, one can write the following reaction scheme:

at the interface Co/Co$_2$Si on the Co$_2$Si-side

$$2s'Co + s'[Si]_d \quad \rightarrow \quad 3s'Co_{\frac{2}{3}} Si_{\frac{1}{3}}$$
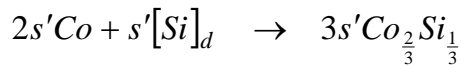
at the interface Co$_2$Si/CoSi on the Co$_2$Si - side

$$4s'Co_{\frac{1}{2}} Si_{\frac{1}{2}} \quad \rightarrow \quad s'[Si]_d + 3s'Co_{\frac{2}{3}} Si_{\frac{1}{3}}$$

$$2r'Co_{\frac{1}{2}} Si_{\frac{1}{2}} + r'[Co]_d \quad \rightarrow \quad 3r'Co_{\frac{2}{3}} Si_{\frac{1}{3}}$$
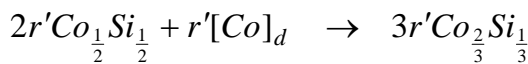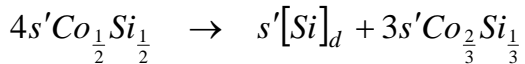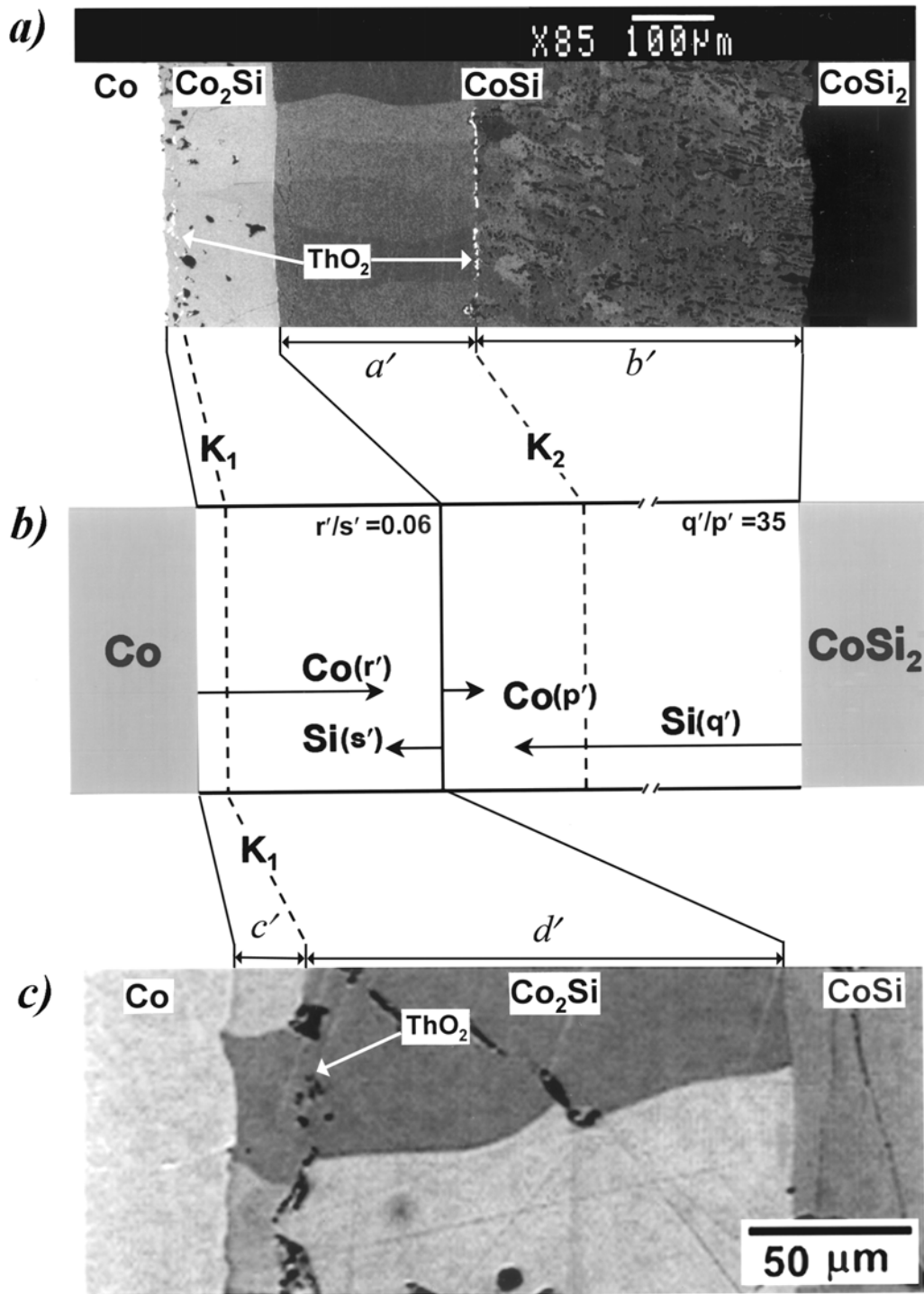
Fig. (4.1-3*a*) Backscattered electron image of the reaction zone between Co and CoSi$_2$ showing the formation of two Kirkendall marker planes (K$_1$ and K$_2$) after interdiffusion at 1100 ^{0}C for 100 hrs (ThO$_2$-particles were used as inert markers between the couple halves), (b) A schematic representation of the diffusion process in the reaction zone of the Co/CoSi$_2$ couple,(c) Magnified area of the diffusion zone in Fig. (4.1-3*a*) close to the reaction product/Co interface (optical micrograph, polarized light).
Different crystal morphology in the product layers on either side of the Kirkendall planes is clearly visible.

at the interface Co₂Si/CoSi on the CoSi - side

$$3p'Co_{\frac{2}{3}}Si_{\frac{1}{3}} \rightarrow p'[Co]_d + 2p'Co_{\frac{1}{2}}Si_{\frac{1}{2}}$$

$$3q'Co_{\frac{2}{3}}Si_{\frac{1}{3}} + q'[Si]_d \rightarrow 4q'Co_{\frac{1}{2}}Si_{\frac{1}{2}}$$

at the interface CoSi/CoSi₂ on the CoSi - side

$$3p'Co_{\frac{1}{3}}Si_{\frac{2}{3}} + p'[Co]_d \rightarrow 4p'Co_{\frac{1}{2}}Si_{\frac{1}{2}}$$

$$3q'Co_{\frac{1}{3}}Si_{\frac{2}{3}} \rightarrow q'[Si]_d + 2q'Co_{\frac{1}{2}}Si_{\frac{1}{2}}$$

Apparently, the resultant thickness of the product layer depends on the growth from, and at the same time, consumption by the neighbouring layers. The total thickness of each product layer, however, always increases with time.

The thicknesses of the phase layers growing on either side of the Kirkendall plane(s) (Fig. (4.1-3)) can be expressed by

$$V_m^{Co_2Si_{\frac{2}{3}\frac{1}{3}}} \times 3s' = c'$$

$$V_m^{Co_2Si_{\frac{2}{3}\frac{1}{3}}} \times (3s' + 3r' - 3p' - 3q') = d'$$

$$V_m^{Co_1Si_{\frac{1}{2}\frac{1}{2}}} \times (2p' + 4q' - 4s' - 2r') = a'$$

$$V_m^{Co_1Si_{\frac{1}{2}\frac{1}{2}}} \times (4p' + 2q') = b'$$

(4.1-7)

In view of Eqs. (A.8-7, 4.1-1 and 4.1-4), the velocity, v_K and the position of the Kirkendall plane, x_K in each product layer of the Co/CoSi₂ couple can be found as following:

for the Co₂Si layer: $V_m^{Co_2Si}(s' - r') = 2tv_K^{Co_2Si} = x_K^{Co_2Si}$

for the CoSi-layer: $V_m^{CoSi}(q' - p') = 2tv_K^{CoSi} = x_K^{CoSi}$

(4.1-8)

Again we assumed $V_A = V_B = V_m$.

To simplify further calculations, we ignored the presence of the solid solution of Si in cobalt next to the intermetallic layer. This means that the value of c' will be slightly overestimated because a small amount of that part of the Co₂Si-layer will actually dissolve in the cobalt end-member. With these assumptions, the parameters a', b', c', d' and p', q', r', s' in Eq. (4.1-7) were computed using values of the thickness of the phases ($a' + b' = 463$ and $c' + d' = 164$ μm) calculated from the integrated diffusion coefficients (Table (4.1-2)) and ratio's of intrinsic diffusion fluxes (q'/p' and s'/r') in the

product phases listed in Table (4.1-1). It was found that $a' = 168.5$ μm, $b' = 294.5$ μm, $c' = 32$ μm, and $d' = 133$ μm and $p' = 0.6$, $q' = 21.0$, $r' = 26.8$ and $s' = 1.6$ mole.m^{-2}, respectively. This leads, through Eq. (4.1-8), to the same values of the Kirkendall velocity in the product layers as deduced from the diffusion-based model (Table (4.1-2)), and they are in fair agreement with the experimental results. The locations of the Kirkendall planes predicted in this manner agree with those determined by means of the Kirkendall velocity construction (Table (4.1-2), Fig. (A.21-3a)) and with those found experimentally (Fig. 4.1-3a).

Again, an important microstructural feature is to be noticed here. In Figs. (4.1-3a and -3c), one clearly sees two different grain morphologies in each product phase layer, corresponding to the two different nucleation sites as follows from the chemical reaction equations.

In order to analyse the diffusion-controlled growth of three product phases between the end-members Co and Si (Fig. (4.1-4)), three more equations are to be added to the previous reaction scheme of the Co/CoSi$_2$ couple. These are:

at the interface CoSi/CoSi$_2$, on the CoSi$_2$-side
$$4m''Co_{\frac{1}{2}}Si_{\frac{1}{2}} \quad \rightarrow \quad m''[Co]_d + 3m''Co_{\frac{1}{3}}Si_{\frac{2}{3}}$$
$$2n''Co_{\frac{1}{2}}Si_{\frac{1}{2}} + n''[Si]_d \quad \rightarrow \quad 3n''Co_{\frac{1}{3}}Si_{\frac{2}{3}}$$
at the interface CoSi$_2$/Si, on the CoSi$_2$-side
$$2m''Si + m''[Co]_d \quad \rightarrow \quad 3m''Co_{\frac{1}{3}}Si_{\frac{2}{3}}$$
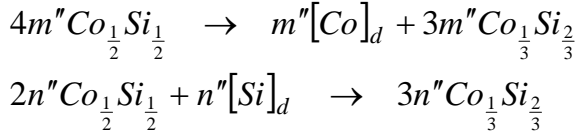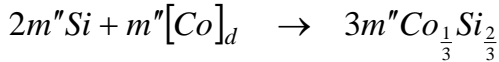
The rest of the treatment follows the line of the previous case, and the problem reduces to solving the system of equations

$$V_m^{Co_{\frac{2}{3}}Si_{\frac{1}{3}}} \times 3s'' = c''$$

$$V_m^{Co_{\frac{2}{3}}Si_{\frac{1}{3}}} \times (3s'' + 3r'' - 3p'' - 3q'') = d''$$

$$V_m^{Co_{\frac{1}{2}}Si_{\frac{1}{2}}} \times (2p'' + 4q'' - 4s'' - 2r'') = a''$$

$$V_m^{Co_{\frac{1}{2}}Si_{\frac{1}{2}}} \times (4p'' + 2q'' - 4m'' - 2n'') = b''$$

$$V_m^{Co_{\frac{1}{3}}Si_{\frac{2}{3}}} \times (3m'' + 3n'' - 3p'' - 3q'') = e''$$

$$V_m^{Co_{\frac{1}{3}}Si_{\frac{2}{3}}} \times 3m'' = f''$$

(4.1-9)
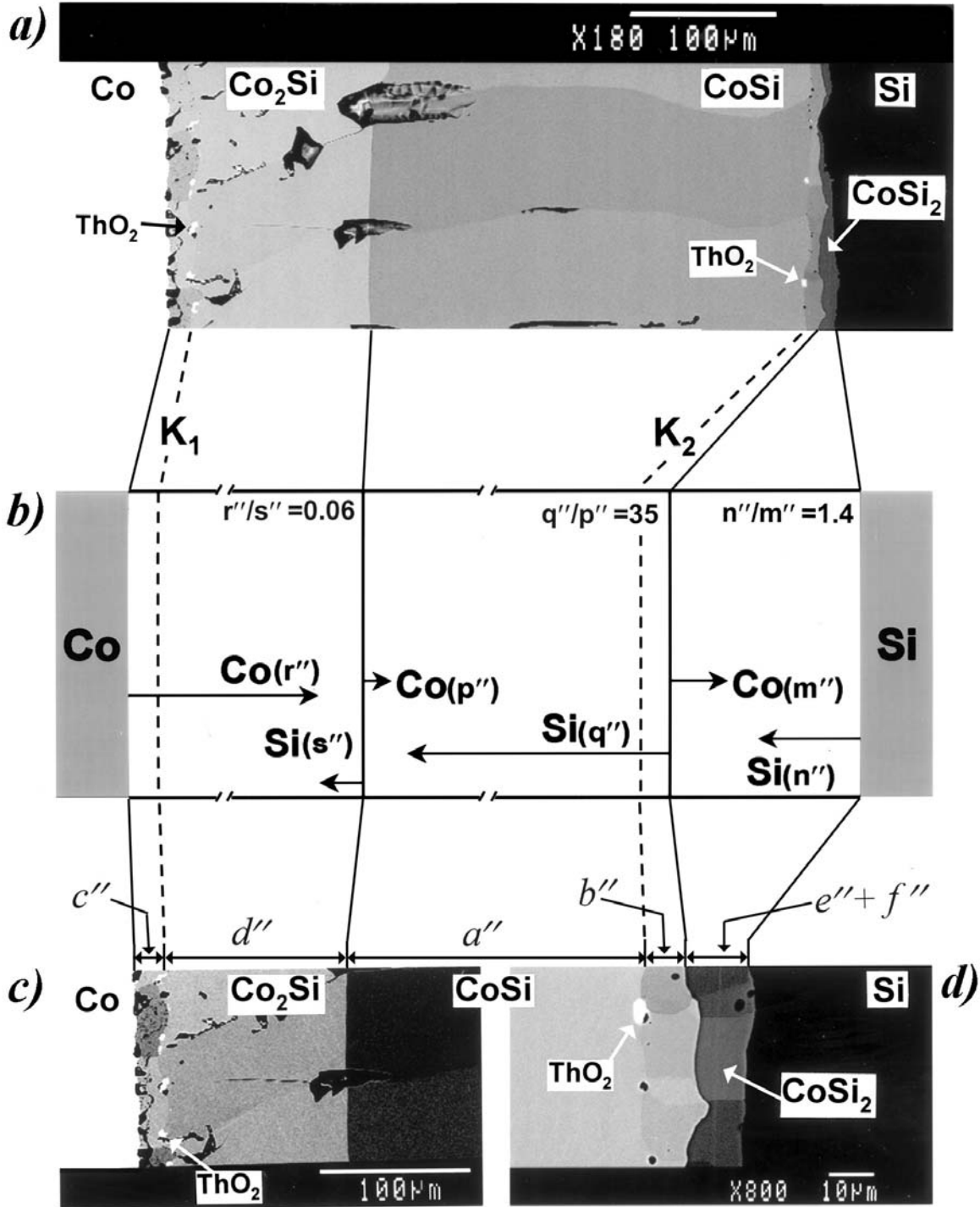
Fig. (4.1-4a) Backscattered electron image of a cross section of a Co/Si diffusion couple after annealing at 1100 °C for 100hrs, b) a schematic representation of the interdiffusion process in the reaction zone between Co and Si; (c) and (d) magnified areas of the reaction zone in the vicinity of the Co/CoSi$_2$ and CoSi$_2$/Si interface, respectively. (Backscattered electron images).

The Kirkendall planes marked by ThO$_2$-particles (K$_1$ and K$_2$) emerged in the Co$_2$Si- and CoSi-phase layers and no Kirkendall plane was found in the CoSi$_2$ product. The "*uniform*" crystal morphology within the CoSi$_2$-layer is indicative for the absence of a Kirkendall plane.

with the $\dfrac{q''}{p''}-$, $\dfrac{s''}{r''}-$ and $\dfrac{n''}{m''}-$ratio's being equal to 35, 0.06 and 1.4, respectively (Table (4.1-1)).

The total thicknesses of the product phase layers are calculated using the integrated diffusion data from Table (4.1-1), and listed in Table (4.1-2). With these informations the values calculated from Eq. (4.1-9) as $a'' = 313.4$, $b'' = 7.6$, $c'' = 40$, $d'' = 91$, $e'' = -209$ and $f'' = 215.8$ μm and the fluxes as $p'' = 0.87$, $q'' = 30.4$, $r'' = 33.8$, $s'' = 2.0$, $m'' = 9.3$ and $n'' = 13.0$ mole.m^{-2}. Again, the actual thickness c'' is slightly less than the calculated one owing to dissolution of a small part of the Co$_2$Si-layer into cobalt (Fig. (4.1-4)). The negative value of e'' stems from the fact that the rate of the CoSi$_2$ formation from CoSi ($3m'' + 3n''$) is lower than its consumption by the reaction at the CoSi/CoSi$_2$ interface ($3p'' + 3q''$).

Further, the Kirkendall velocity and locations of the Kirkendall(s) in each product layer can be found by

$$V_m^{CoSi}\left(q'' - p''\right) = 2tv_K^{CoSi} = x_K^{CoSi}$$

$$V_m^{Co_2Si}\left(s'' - r''\right) = 2tv_K^{Co_2Si} = x_K^{Co_2Si}$$

$$V_m^{CoSi_2}\left(n'' - m''\right) = 2tv_K^{CoSi_2} = x_K^{CoSi_2}$$

The calculated values of the fluxes lead to the same values of the Kirkendall velocity and the location for the Kirkendall plane positions in these product layers as found using the diffusion based model (Fig. (A.20-2b)). They both agree with the experimental results (Fig. (4.1-4)).

In the CoSi$_2$ layer no Kirkendall plane can be present. This is reflected in the negative value of e'' and corresponds with the position of the virtual Kirkendall plane as shown in Fig. (A.20-2b). The "*uniform*" crystal morphology in the CoSi$_2$-phase layer is indicative for the absence of a Kirkendall plane as can be seen in Fig. (4.1-4d) as well.

4.2 Application of the physico-chemical approach in a system consisting of phases with wide homogeneity range

In the previous section (chap. 4.1), we have shown that the physico-chemical approach can be used successfully to analyze/predict the diffusion structure developed in diffusion

couples where line compounds are formed. It was demonstrated that this approach leads to the same results as those calculated by diffusion-based model.

Our next interest is to check if this approach can also be used in a system, where a diffusion zone is developed by phases with a wide homogeneity range. Whether we can use this approach to the phases with wide homogeneity range depends largely on whether we can predict the composition profile, *a priori*, from the data available on the interdiffusion coefficients. The problem is that there are not many systems where one can find the data on interdiffusion coefficients all over the composition range, which are needed to predict the composition profile. However, using some simplifications this approach can be used to rationalize the experimentally found composition profile and to explain the characteristic microstructure developed during interdiffusion. In this section the Ag-Zn and Ti-Al systems are chosen. The specific reason behind selecting these two systems is that we already have used the diffusion-based approach to rationalize the marker positions in these systems (Chap. 3), which will help to understand the applicability of the physico-chemical approach in the case of phases with a wide homogeneity range.

I. A diffusion zone in the Ag-Zn system showing bifurcation of the Kirkendall plane

Let us consider the experimentally found diffusion layer in a Ag/Zn diffusion couple annealed for 5 hours at 370 °C, as shown in Fig. (3.2-2). The composition profile measured by EPMA is shown in Fig. (3.2-3). For the sake of simplicity and application of physico-chemical approach the average composition of the phases are calculated as $Ag_{0.154}Zn_{0.846}$ for the ε-AgZn$_3$ phase, $Ag_{0.394}Zn_{0.606}$ for the γ-Ag$_5$Zn$_8$ and $Ag_{0.521}Zn_{0.479}$ for the β-AgZn phase. The average compositions were calculated, for example, for the ε-phase from

$$N_{Ag}^{\varepsilon}\bigg|_{ave} = \frac{\displaystyle\int_{N_{Ag}^{-\varepsilon}}^{N_{Ag}^{+\varepsilon}} N_{Ag}\, dx}{\Delta x_{\varepsilon}} \tag{4.2-1}$$

where $N_{Ag}^{-\varepsilon}$ and $N_{Ag}^{+\varepsilon}$ are the lower and upper limit of the mole fractions in the ε-phase developed during interdiffusion and Δx_{ε} is the layer thickness of the ε-phase.

The diffusion fluxes are shown in the schematic diagram Fig. (4.2-1b). The layer thickness of the ε- and γ-phase are divided into two sublayers a, b and c, d respectively and can be measured directly from the micrograph presented in Fig. (4.2-1a). We found no Kirkendall plane in the β-AgZn phase, but we can consider a virtual Kirkendall plane in this phase and divide the layer into to sublayers as e and f. We cannot determine these two sublayers from experimental results but we can measure the total thickness of the layer as, $(e + f)$. We can write the reaction scheme at different interfaces as following:

Interface I- Zn/AgZn$_3$ (AgZn$_3$ side)
$$5.49nZn + n[Ag]_d \quad \rightarrow \quad 6.49nAg_{0.154}Zn_{0.846}$$
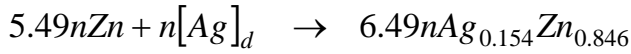
Interface II- AgZn$_3$/Ag$_5$Zn$_8$ (AgZn$_3$ side)
$$0.64mAg_{0.394}Zn_{0.606} + m[Zn]_d \quad \rightarrow \quad 1.64mAg_{0.154}Zn_{0.846}$$
$$3.53nAg_{0.394}Zn_{0.606} \quad \rightarrow \quad n[Ag]_d + 2.53nAg_{0.154}Zn_{0.846}$$
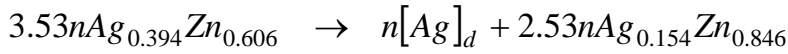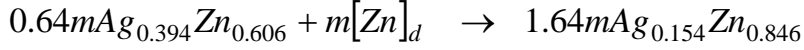
Interface II- AgZn$_3$/Ag$_5$Zn$_8$ (Ag$_5$Zn$_8$ side)
$$1.64pAg_{0.154}Zn_{0.846} \quad \rightarrow \quad p[Zn]_d + 0.64pAg_{0.394}Zn_{0.606}$$
$$2.53qAg_{0.154}Zn_{0.846} + q[Ag]_d \quad \rightarrow \quad 3.53qAg_{0.394}Zn_{0.606}$$
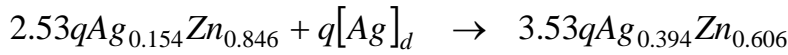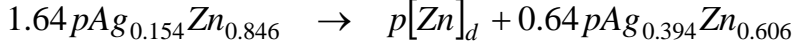
Interface III – Ag$_5$Zn$_8$/AgZn (Ag$_5$Zn$_8$ side)
$$3.10pAg_{0.521}Zn_{0.479} + p[Zn]_d \quad \rightarrow \quad 4.10pAg_{0.394}Zn_{0.606}$$
$$4.77qAg_{0.521}Zn_{0.479} \quad \rightarrow \quad q[Ag]_d + 3.77qAg_{0.394}Zn_{0.606}$$
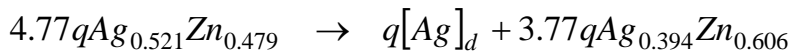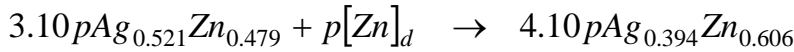
Interface III – Ag$_5$Zn$_8$/AgZn (AgZn side)
$$4.10rAg_{0.394}Zn_{0.606} \quad \rightarrow \quad r[Zn]_d + 3.10rAg_{0.521}Zn_{0.479}$$
$$3.77sAg_{0.394}Zn_{0.606} + s[Ag]_d \quad \rightarrow \quad 4.77sAg_{0.521}Zn_{0.479}$$
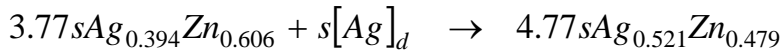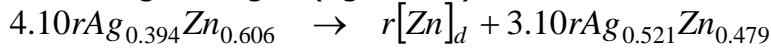
Interface IV - AgZn/Ag (AgZn side)
$$1.09rAg + r[Zn]_d \quad \rightarrow \quad 2.09rAg_{0.521}Zn_{0.479}$$
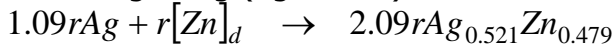
where m, n, p, q, r and s are the flux (moles.m^{-2}) of the species as shown in the Fig. (4.2-1b).

The resultant thickness of the product layers depends on the growth from, and at the same time consumption by the neighbouring phases. The thickness of the phase sublayers can be written as

a)

b)
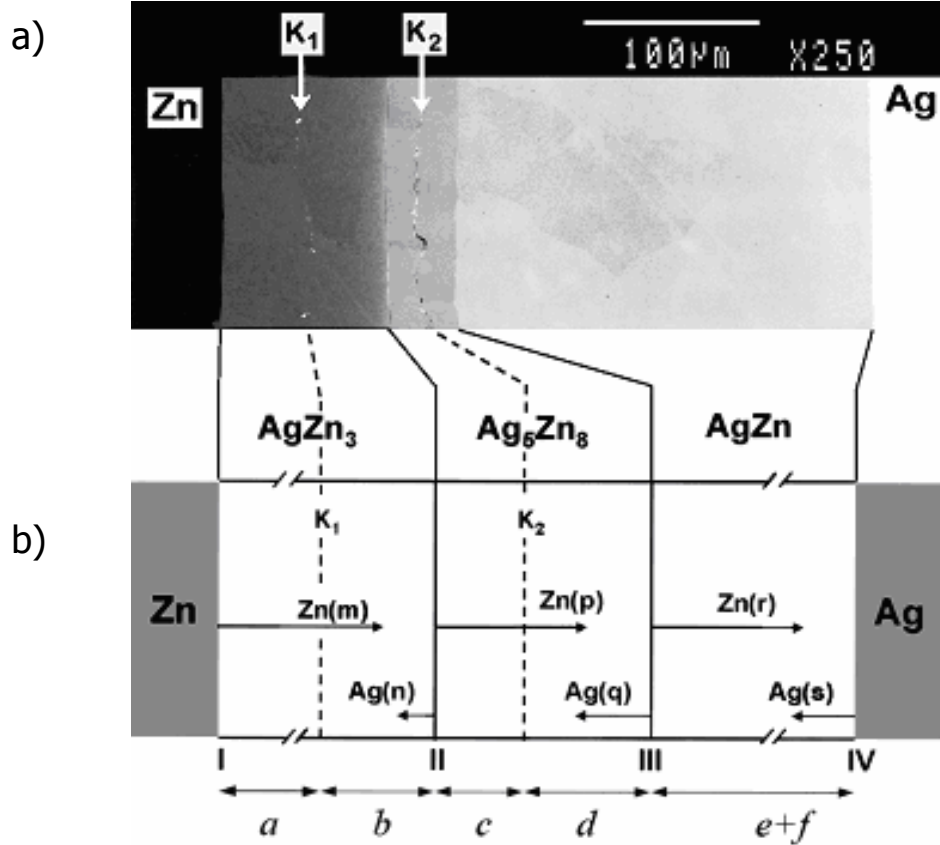
Fig. (4.2-1a) Backscattered electron image of a cross section of a Zn/Ag diffusion couple annealed for 5 hours at 370 °C. K_1 and K_2 are the positions of the Kirkendall plane.
(b) a schematic representation of the interdiffusion process in the reaction zone of the Zn/Ag couple.

$$V_m^{AgZn_3}\left(6.49n\right)=a$$

$$V_m^{AgZn_3}\left(1.64m+2.53n-1.64p-2.53q\right)=b$$

$$V_m^{Ag_5Zn_8}\left(0.64p+3.53q-0.64m-3.53n\right)=c$$

$$V_m^{Ag_5Zn_8}\left(4.10p+3.77q-4.10r-3.77s\right)=d$$

$$V_m^{AgZn}\left(3.10r+4.77s-3.10p-4.77q\right)=e$$

$$V_m^{AgZn}\left(2.09r\right)=f$$

(4.2-2)

The data on molar volumes of the phases are given in Table (3.2-1). The values of the sublayers are measured directly from the micrograph Fig. (4.2-1a) as a = 48.6, b = 50.2, c = 16.65, d = 24.45 and $(e + f)$ = 244 μm. To determine the values for the fluxes in the phases from Eq. (4.2-2) the ratio of diffusivities of Zn and Ag in the β-phase measured from an incremental couple is considered and we can write

$$\frac{r}{s} = \frac{V_{Ag} D_{Zn}}{V_{Zn} D_{Ag}} = 6.5$$. From these informations Eq. (4.2-2) can be solved and we find the

values m = 19.60, n = 0.81, p = 13.91, q = 2.35, r = 13.53, s = 2.06 mole.m^2 and e = -23.72 and f = 267.72 μm. The negative value of e reflects the absence of Kirkendall plane in β-phase, because the formation of the phase by $(3.10r + 4.77s)$ is less than the consumption of the phase by $(3.10p + 4.77q)$.

The velocity of the Kirkendall marker plane in the phases can be calculated by (considering the molar volume of the pure phases as the partial molar volumes of the components in the phase compounds, i.e. $V_{Ag} = V_m^{Ag} = 10.27 \times 10^{-6}$ and $V_{Zn} = V_m^{Zn} = 9.16 \times 10^{-6}$ m^2/s),

$$v_K^{\varepsilon} = -\left(V_{Ag} J_{Ag} + V_{Zn} J_{Zn}\right) = \frac{1}{2t}\left(V_m^{Ag} n - V_m^{Zn} m\right) = -4.75 \times 10^{-9} \, m/s$$

$$v_K^{\gamma} = \frac{1}{2t}\left(V_m^{Ag} q - V_m^{Zn} p\right) = -2.87 \times 10^{-9} \, m/s$$

$$v_K^{\beta} = \frac{1}{2t}\left(V_m^{Ag} s - V_m^{Zn} r\right) = -2.85 \times 10^{-9} \, m/s$$

It is clear that the data calculated by physico-chemical approach are equal to the data calculated by diffusion-based approach (Table 3.2-1). The minor difference in the values resulted from the fact that we neglected dissolution of Ag in the Zn end-member. The physico-chemical approach explains the reactions at the interfaces and the grain morphology developed during interdiffusion.

II. A TiAl$_3$/Ti diffusion couple showing trifurcation of the Kirkendall plane

We consider the experimentally found diffusion couple of TiAl$_3$/Ti annealed for 1600 hours at 870 °C. Kirkendall planes were found in every phases developed during interdiffusion as could be seen in Fig. (3.3-1). The average phase compositions were found to be Ti$_{0.344}$Al$_{0.656}$ for the TiAl$_2$-phase, Ti$_{0.494}$Al$_{0.506}$ for the TiAl-phase and Ti$_{0.749}$Al$_{0.251}$ for the Ti$_3$Al-phase, which can be appreciated from Fig. (3.3-3). We divide each phases into two sublayers by the Kirkendall plane positions as shown in Fig. (4.2-2) and can write the reaction scheme at different interfaces following Fig. (4.2-2b) as,

Interface I - TiAl$_3$/TiAl$_2$ (TiAl$_2$ side)
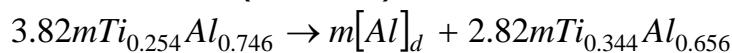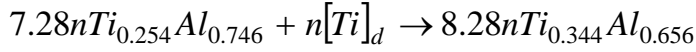
$$3.82mTi_{0.254}Al_{0.746} \rightarrow m[Al]_d + 2.82mTi_{0.344}Al_{0.656}$$

$$7.28nTi_{0.254}Al_{0.746} + n[Ti]_d \rightarrow 8.28nTi_{0.344}Al_{0.656}$$

Interface II - TiAl$_2$/TiAl (TiAl$_2$ side)

$$2.29mTi_{0.494}Al_{0.506} + m[Al]_d \rightarrow 3.29mTi_{0.344}Al_{0.656}$$
$$4.37nTi_{0.494}Al_{0.506} \rightarrow n[Ti]_d + 3.37nTi_{0.344}Al_{0.656}$$

Interface II - TiAl$_2$/TiAl (TiAl side)

$$3.29pTi_{0.344}Al_{0.656} \rightarrow p[Al]_d + 2.29pTi_{0.494}Al_{0.506}$$
$$3.37qTi_{0.344}Al_{0.656} + q[Ti]_d \rightarrow 4.37qTi_{0.494}Al_{0.506}$$
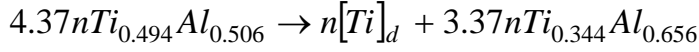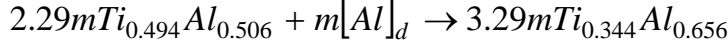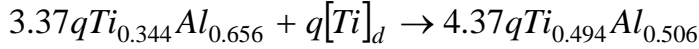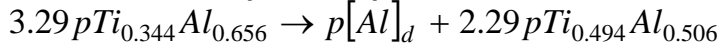
Interface III - TiAl/Ti$_3$Al (TiAl side)

$$1.94pTi_{0.749}Al_{0.251} + p[Al]_d \rightarrow 2.94pTi_{0.494}Al_{0.506}$$
$$1.98qTi_{0.749}Al_{0.251} \rightarrow q[Ti]_d + 0.98qTi_{0.494}Al_{0.506}$$
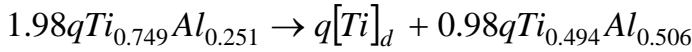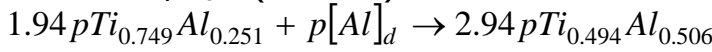
Interface III - TiAl/Ti$_3$Al (Ti$_3$Al side)

$$2.94rTi_{0.494}Al_{0.506} \rightarrow r[Al]_d + 1.94rTi_{0.749}Al_{0.251}$$
$$0.98sTi_{0.494}Al_{0.506} + s[Ti]_d \rightarrow 1.98sTi_{0.749}Al_{0.251}$$
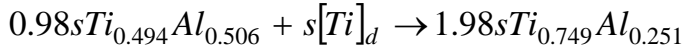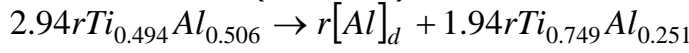
Interface IV Ti$_3$Al/Ti (Ti$_3$Al side)

$$2.98rTi + r[Al]_d \rightarrow 3.98rTi_{0.749}Al_{0.251}$$
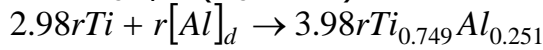
The thickness of the phase sublayers growing either side of the Kirkendall planes can be written as,

$$V_m^{TiAl_2}(2.82m + 8.28n) = a$$
$$V_m^{TiAl_2}(3.29m + 3.37n - 3.29p - 3.37q) = b$$
$$V_m^{TiAl}(2.29p + 4.37q - 2.29m - 4.37n) = c$$
$$V_m^{TiAl}(2.94p + 0.98q - 2.94r - 0.98s) = d$$
$$V_m^{Ti_3Al}(1.94r + 1.98s - 1.94p - 1.98q) = e$$
$$V_m^{Ti_3Al}(3.98r) = f$$

(4.2-3)

The values on molar volumes are listed in Table (3.3-1). The average length of the sublayers are measured directly from the micrograph Fig. (4.2-2a) as a = 60, b = 9, c = 6, d = 7, e = 17 and f = 14 μm and after solving the Eq. (4.2-3) we find, m = 2.06, n = 0.05, p = 1.14, q = 0.68, r = 0.35 and s = 2.3.
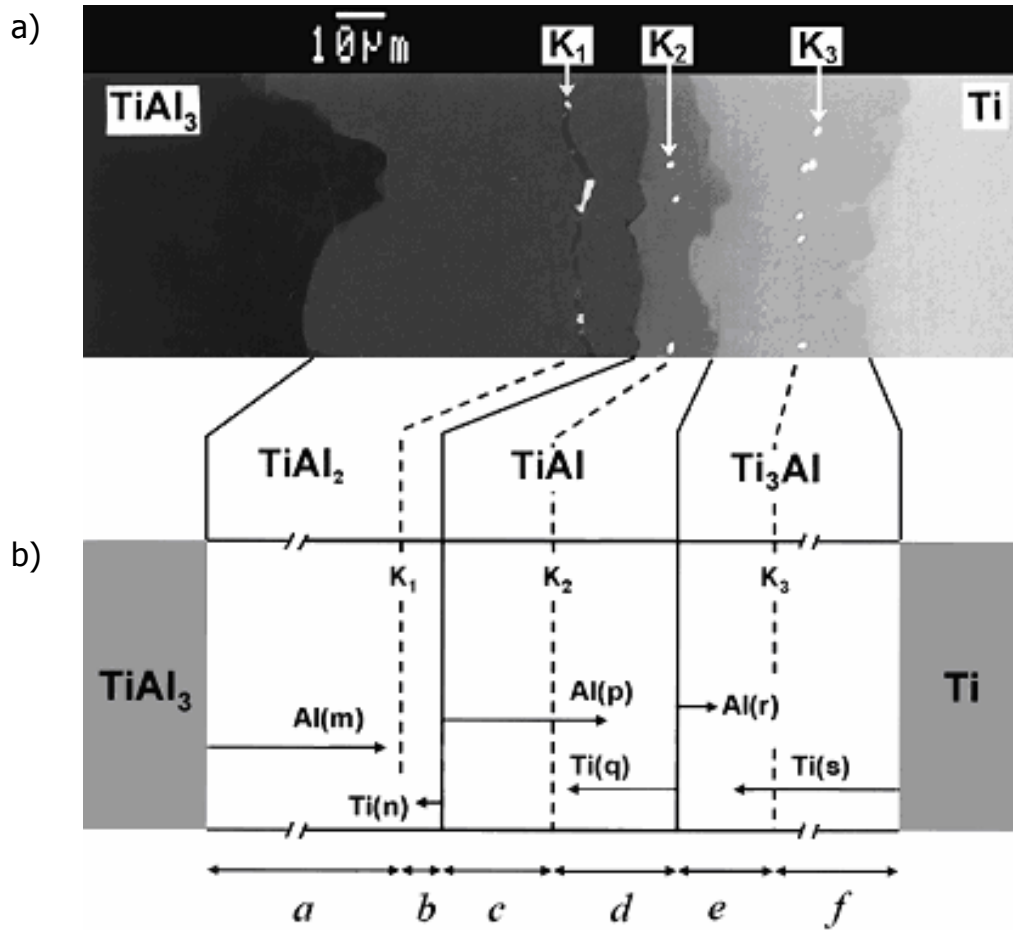
Fig. (4.2-2a) Backscattered electron image of a TiAl$_3$/Ti diffusion couple annealed for 1600 hours at 870 °C. K$_1$, K$_2$ and K$_3$ show the position of the three Kirkendall planes.
(b) a schematic representation of the interdiffusion process in the TiAl$_3$/Ti diffusion couple.

Considering the molar volume of the pure phases as the partial molar volumes of the components in the phases ($V_{Ti} = V_m^{Ti} = 10.63 \times 10^{-6}$ and $V_{Al} = V_m^{Al} = 10 \times 10^{-6}$ m^2/s), the velocity of the Kirkendall marker plane can be found as

$$v_K^{TiAl_2} = -\left(V_{Ti} J_{Ti} + V_{Al} J_{Al}\right) = \frac{1}{2t}\left(V_m^{Ti} n - V_m^{Al} m\right) = -17.42 \times 10^{-13} \, m/s$$

$$v_K^{TiAl} = \frac{1}{2t}\left(V_m^{Ti} q - V_m^{Al} p\right) = -3.62 \times 10^{-13} \, m/s$$

$$v_K^{Ti_3Al} = \frac{1}{2t}\left(V_m^{Ti} s - V_m^{Al} r\right) = 18.18 \times \times 10^{-13} \, m/s$$

Comparison of these data with those in Table (3.3-1) shows the equivalence of the diffusion-based and physico-chemical approach. The minor difference in the data

calculated here from the data by the diffusion-based approach (as shown in Table (3.3-1)) is because we neglected the Al dissolved in the Ti end-member.

4.3 Conclusions

The conclusions of the present analysis lead to a change in view on the formation and growth of product layers during solid-state reactions.

As demonstrated in the preceding sections, all thermodynamically stable phases will grow simultaneously in a purely diffusion-limited process. If n phases will grow between two stoichiometric binary compounds, $2n$ equations can be defined for the interfacial reactions occurring in the diffusion zone. If one calculates the layer thickness from knowledge of the integrated diffusion coefficients for each product phase, and combines this with information on the component mobilities in each growing compound, one can solve this set of equations, resulting in the coordinates (position) of the (possibly virtual) Kirkendall plane(s) belonging to each phase layer. There is no reason whatsoever for a product phase layer to be totally consumed by its neighbours as it is sometimes stated [4]. Sometimes, in a diffusion couple one or more phase layers seem to be missing. It is well possible that the layers are present but difficult to detect when they are present as very thin layers because of the very high difference in the growth rate compared to other layers.

It should be stated that these conclusions are only valid in a diffusion-controlled growth process. Especially during the start of the annealing procedure deviations can occur. It is, therefore, possible to miss equilibrium phases at this stage, which becomes important in thin-film experiments.

The role of the Kirkendall effect in developing a duplex grain morphology inside the product layers is clear by considering the nucleation sites of the growing phases, using the chemical reaction equations as a starting point. The existence of two or more Kirkendall planes in a diffusion zone is the result of nucleation of new crystals away from the interfaces of the initial materials with the reaction product. Now we realize that such an abrupt change in grain morphology was noticed in the past without being recognized as the location of the Kirkendall plane.

An interesting question here is whether the presence of a Kirkendall plane in a diffusion zone should always be accompanied by a sharp change in morphology within a phase

layer as observed in the Co-Si and Ti-Al systems. It seems to be found always in product layers of stoichiometric compounds (e.g. Ni_5Si_2 [5], Ni_3Sn_2 [6], Co_3O_4 [7]). It is also found for compounds with a homogeneity range if the Kirkendall plane is of the stable type. This is the situation when at the point of intersection between the velocity curve (*2tv* vs. *x*) and the straight-line $2tv_K = x_K$, the gradient of the Kirkendall velocity with respect to the position parameter is negative (e.g. β'-AuZn [8], β-NiAl (Chap. 3.1)). If, on the contrary, this gradient at the intersection is positive, the inert particles (markers) at the Kirkendall plane will spread more or less randomly over the product layer. The Kirkendall plane is then microstructurally unstable [8], which will probably not result in a duplex layer.

Generally speaking, it might be expected that the sharp change in grain morphology within the product layer could become more vague with increasing diffusion time because of recrystallization processes, which occur simultaneously with the phase growth. In our experiments, we indeed see sometimes the development of rather wavy boundaries between the "sublayers" of the duplex structure, but the changes remain clearly visible.

Our analysis also provides the experimental possibility to investigate the initial stages of the interaction. Suppose that inert markers of about 0.5 μm are placed in between the end-members prior to annealing. Then, these markers are expected to be situated in the phase layers where they should be according to our analysis, provided that in a diffusion-controlled regime these phases are all present when the total product layer thickness is, say, 1 μm. In the Co/Si diffusion couple, for instance, that thickness is reached after approximately 1 sec of annealing at 1100 ^{0}C, for the $TiAl_3$/Ti couple after about 8 minutes of interaction at 870 ^{0}C. The fact that we found the markers back at all Kirkendall planes proves that after these reaction times, the respective phases were already formed, because once caught by a stable Kirkendall plane, the inert particles cannot escape later on towards other positions.

If in the case of two Kirkendall planes one stable Kirkendall plane (recognizable by an abrupt change in the product layer morphology) is not "marked" by the inert Kirkendall markers, this is an indication that this phase was formed after a certain incubation time. The markers have then already found a stable position in the other Kirkendall plane before the phase in question starts to grow. The experiment should, of course, be carried out carefully. Misinterpretation might occur when, for instance, during preparation of the couple, markers (particles) are pressed into the softer end-member.

Then, they do not represent the position of the original contact interface, which might create a situation where the markers are biased towards the phase layers adjacent to this "soft" end-member.

We believe that it is certainly worthwhile to investigate in this direction the reaction phenomena in "thin-film" structures, since often a sequential phase growth is reported before simultaneous growth sets in [9-12]. The critical thickness (or, equivalently, reaction time) after which all phases start to grow, might, however, be very small, which asks for very small inert particles (markers) to verify this statement experimentally. The size of particles should, on the other hand, not be too small because then they can be dragged by, for example, grain boundaries, which renders them unsuitable to mark the Kirkendall plane.

It is important to note that both the diffusion-based and physico-chemical models are purely phenomenological and do not require any assumptions on the operative diffusion mechanisms. The widely used notion that the occurrence of the Kirkendall effect (in the sense of marker displacement with respect to the laboratory-fixed frame of reference) proves a vacancy-mediated diffusion mechanism is incomplete. In this respect, additional information about the variation of the number of lattice sites on either side of the Kirkendall plane during interdiffusion, or microstructural evidence (like, the presence of pores), is needed to make the statement valid.

Reference

1. M.J.H. van Dal, D.G.G.M. Huibers, A.A. Kodentsov, F.J.J. van Loo, Formation of Co–Si intermetallics in bulk diffusion couples. Part I. Growth kinetics and mobilities of species in the silicide phases, Intermetallics **9** (2001) 409-21
2. M.J.H. van Dal, A.A. Kodentsov and F.J.J. van Loo, Formation of Co-Si intermetallics in bulk diffusion couples: Part II - Manifestations of the Kirkendall effect accompanying reactive diffusion, Intermetallics **9** (2001) 451-56
3. F.J.J. van Loo, B. Pieraggi and R.A. Rapp, Interface migration and the Kirkendall effect in diffusion driven phase transformations, Acta Metall. Mater. **38** (1990) 1769-79
4. V.I. Dybkov, Growth kinetics of chemical compound layers, Cambridge International science publishing (UK),1998
5. J.H. Gülpen, A.A. Kodentsov and F.J.J. van Loo, Growth of silicides on Ni-Si and Ni-SiC bulk diffusion couples, Z. Metallkd. **86** (1995) 530
6. J.A. van Beek, S.A. Stolk and F.J.J. van Loo, Multiphase diffusion in the systems Fe-Sn and Ni-Sn, Z. Metallkd. **73** (1982) 439
7. K. Przybylski, W.W. Smeltzer, High temperature oxidation mechanism of CoO to Co_3O_4, J Electrochem. Soc. **128** (1981) 897-902

8. M.J.H. van Dal, A.M. Gusak, C. Cserháti, A.A. Kodentsov and F.J.J. van Loo, Spatio-temporal instabilities of the Kirkendall-marker planes during Interdiffusion in β'-AuZn, Phil. Mag. A **82** (2002) 943-54

9. K.N. Tu, G. Ottaviani, U. Gösele and H. Föll, Intermetallic compound formation in thin-film and in bulk samples of the Ni-Si binary system, J. Appl. Phys. **54** (1983) 758-63

10. J. Philibert, Reactive diffusion in thin films, Appl. Surf. Sci. **53** (1991) 74-81

11. F.M. d' Heurle and P. Gas, Kinetics of formation of silicides: A review, J. Mater. Res. **1** (1986) 205-21

12. R. Pretorius, T.K. Marais and C.C. Theron, Thin film compound phase formation sequence: An effective heat of formation model, Mat. Sci. Eng. R. **10 (**1993) 1-83.

Chapter 5

Diffusion studies in the β-NiAl and γ'-Ni$_3$Al phases

Materials in the Ni-Al system are attractive for a wide range of applications, because of their high strength to density ratio. Good oxidation resistance at high temperature makes them suitable for the use in blades and vanes in gas and aircraft turbine engines. Numerous experiments have been conducted on mechanical properties of the materials in this system, including on diffusion properties but these studies give in some respects conflicting results. Several processes are driven by diffusion like recrystallisation, grain growth, solid-state reactions, and therefore, the knowledge of diffusion is essential.

5.1 Studies in the β-NiAl phase
I. Interdiffusion Coefficients

The β-NiAl phase draws special attention because of its complex defect structure, where on the Ni-rich side antisite defects are present (i.e. Ni atoms occupy the Al sublattice) and on the Al-rich side vacancies are present in the Ni sublattice as explained in Chap. 3.1.II. Different atomistic diffusion mechanisms are believed to be operative on either side of the stoichiometry.

After going through available literature [1-5] on this phase, it was found that the variation in molar volume with composition was not taken into consideration [1-3] or irregularities were observed in the treatment [4].

In this study interdiffusion coefficients are calculated by Wagner's approach (A.9) in the
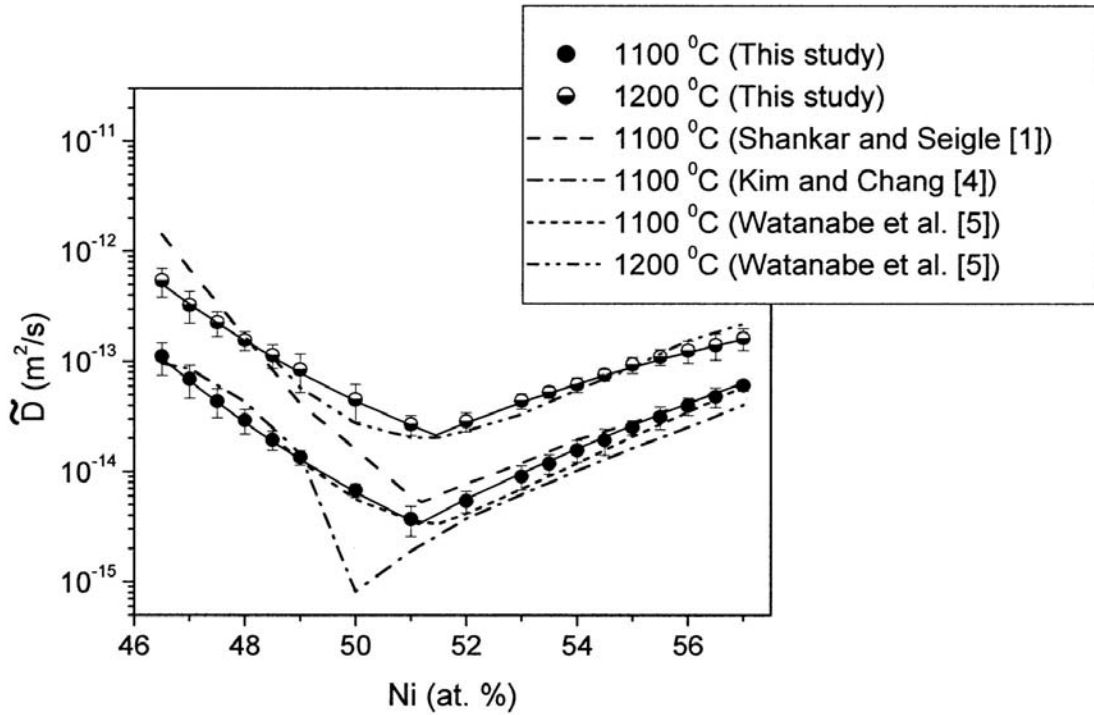
Fig. (5.1-1) Interdiffusion coefficient, $\tilde{D}$ in the β-NiAl phase at 1100 and 1200 °C obtained from incremental couples. The data reported by Shankar and Seigle [1] and Kim and Chang [4] and Watanabe et al. [5] are shown for comparison.
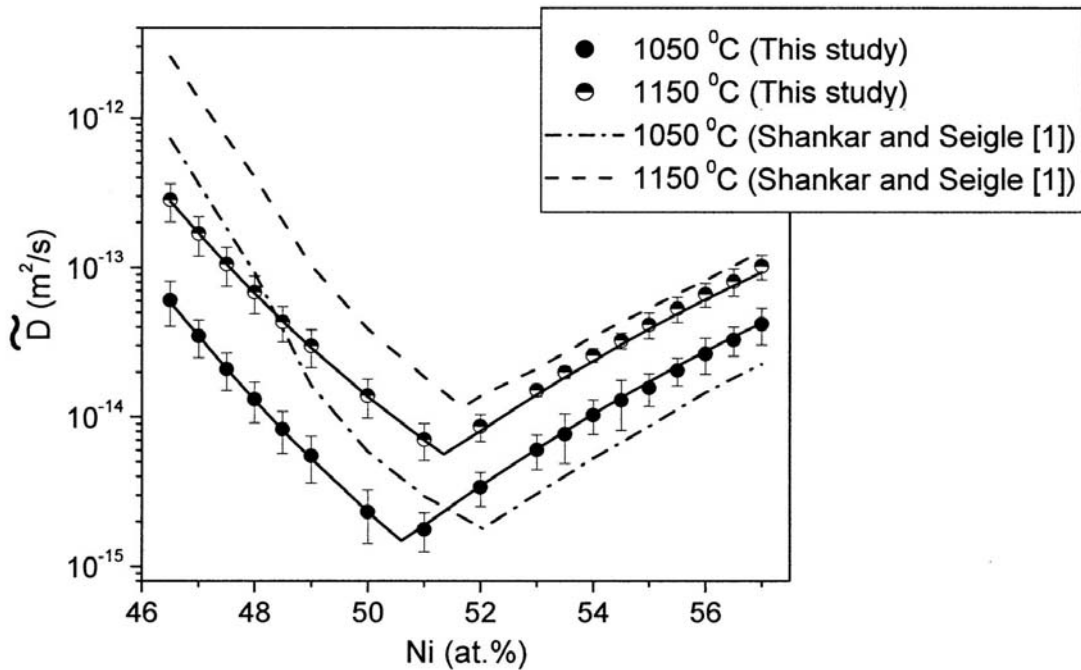
Fig. (5.1-2) Interdiffusion coefficient, $\tilde{D}$ in the β-NiAl phase at 1050 and 1150 °C obtained from incremental couples. The data reported by Shankar and Seigle [1] are incorporated for comparison.
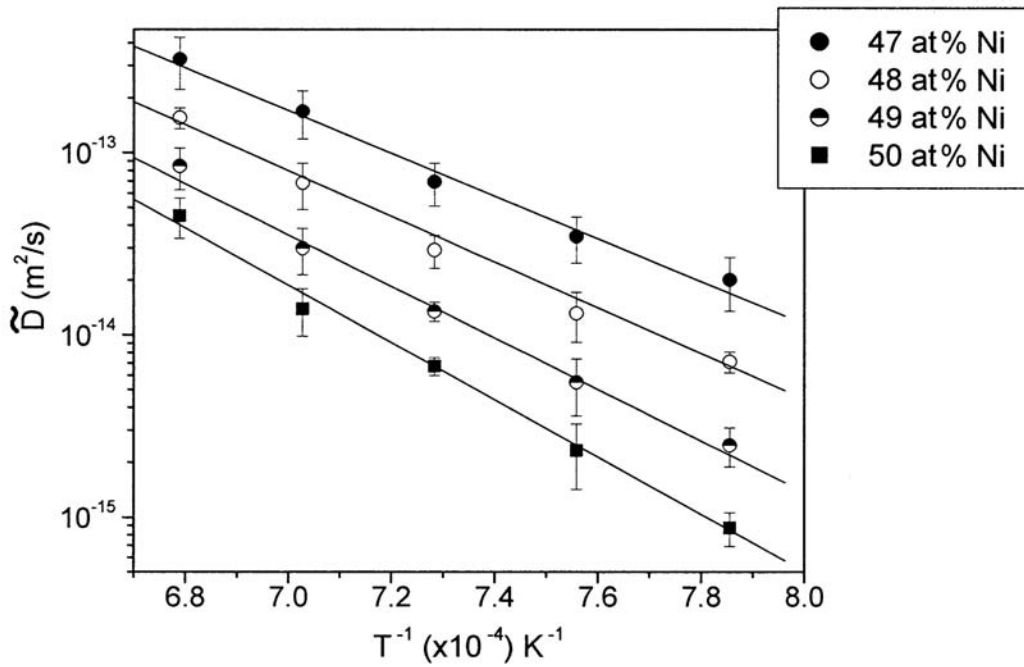
Fig. (5.1-3) The interdiffusion coefficients, D at the compositions in the Al-rich domain of the β-NiAl phase are shown as a function of reciprocal temperature.
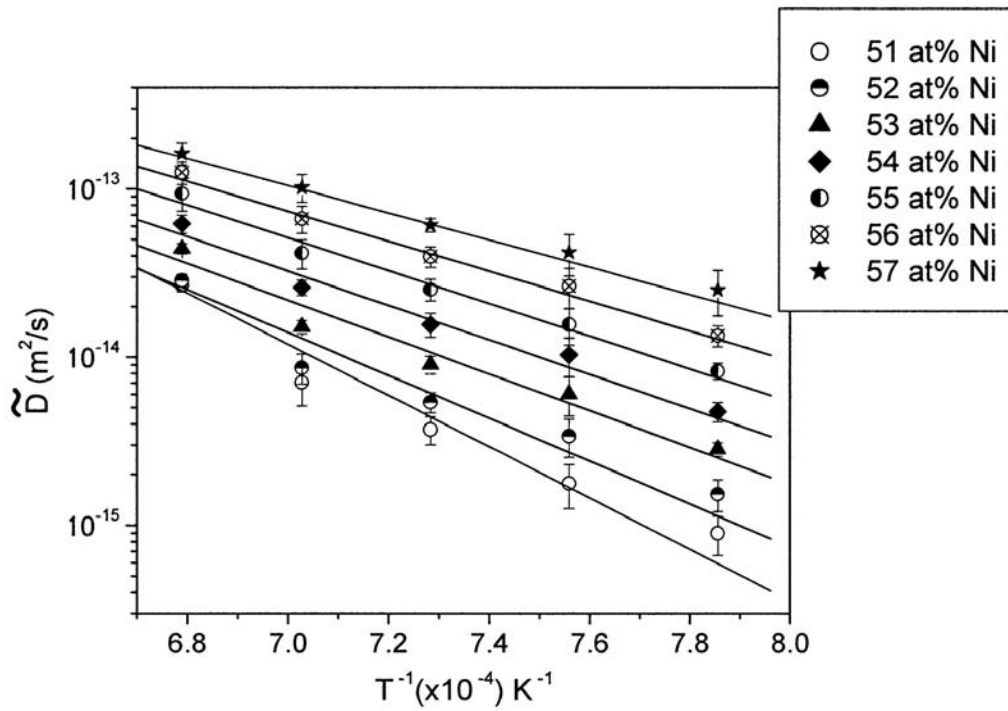
Fig. (5.1-4) The interdiffusion coefficients, $\tilde{D}$ at the compositions in the Ni-rich domain of the β-NiAl phase are shown as a function of reciprocal temperature.

temperature range of 1000 - 1200 °C. Molar volumes across the homogeneity range were determined from the data available on the lattice parameter and constitutional vacancies present in the structure (see A.18). Results obtained on interdiffusion coefficients are shown in Figs. (3.1-5 (see Chapter 3.1), 5.1-1 and 5.1-2) and compared with the results available in literature [1, 4, 5]. Shankar and Seigle [1] did not consider the variation in molar volume with composition in their calculations and this could be the reason behind the significant differences in the interdiffusion coefficients from the results determined in this study, especially in the Al-rich part, as the molar volume changes dramatically in this domain (see Fig. (A.19-3)). Kim and Chang [4] and Watanabe et al. [5] considered the data on molar volume in their calculations and good agreement between the results from them and those in the present study is found (except the results in the off-stoichiometric region by Kim and Chang). The deep minimum found by Kim and Chang at stoichiometric composition should be questioned and might have been caused the uncertainties in determination of the composition gradient required for calculation of interdiffusion coefficients. For further discussion see Chap. (3.1-III).

The temperature dependent interdiffusion coefficient can, according to our results, be expressed in terms of Arrhenius equation:

$$\tilde{D} = D_o \exp\left(-\frac{Q}{RT}\right) \qquad (5.1\text{-}1)$$

where $\tilde{D}$ is the interdiffusion coefficient, D_o is the pre-exponential factor, Q is the activation energy, R is the gas constant and T is the temperature in Kelvin. The changes in interdiffusion coefficients with temperature at different Ni compositions are shown in Fig. (5.1-3 and -4). It should be mentioned that the interdiffusion coefficients sometimes do not follow the Arrhenius law especially in the range of 50-53 at.% Ni. This is clearly seen from the Figs. (5.1-3 and -4). Obviously, the defect structure changes in this region with temperature and, therefore, the diffusion mechanism changes with temperature. So, the intrinsic diffusivities may vary with temperature in a non-Arrhenius way, which leads to a nonlinear variation for interdiffusion coefficients with temperature. The values of D_o and Q calculated with the help of Eq. (5.1-1) are shown in Fig. (5.1-5). The results obtained by Shankar and Siegle [1] and Kim and Chang [4] are given for comparison. Good agreement exists between D_o and Q values found in this study and the data determined by Kim and Chang.

II. Intrinsic Diffusion coefficients

Series of incremental diffusion couples are studied to measure the intrinsic diffusivities of the species over the homogeneity range at 1000 °C. The ratios of diffusivities, D_{Ni}/D_{Al} at Kirkendall plane positions in different couples were calculated following Eq. (A.10-6) and are shown in Fig. (3.1-4) (see Chap. 3.1). Partial molar volumes of the species required for the calculations were obtained from the data as plotted in Fig. (A.18-3). Intrinsic diffusivities of the species were then calculated over the homogeneity range from the data on the ratio of the intrinsic diffusivities and from the interdiffusivities (see Fig. (3.1-5)) after solving $\tilde{D} = \left(C_A V_A D_B + C_B V_B D_A \right)$ as shown in Fig. (5.1-6). The molar volume at the vicinity of 50 at.% changes dramatically and determination of the intrinsic diffusivities at that composition was not possible, because it is difficult to calculate the partial molar volumes of the species at that composition.

III. Tracer diffusion coefficients

The atomistic diffusion mechanism in β-NiAl is of interest because of the complicated defect structure of this phase. Knowledge on mobilities of the species measured from the data on tracer diffusivities (through Eq. (A.14-6)) is important to understand the diffusion process. Ni tracer diffusivities were measured by Hancock and McDonnel [6] and Frank et al. [7] in the β-NiAl phase. Significant difference is present in the values found in these two studies. Measuring the Al tracer diffusivities is not possible because of a lack of suitable Al isotopes. Minamino et al. [8] and Lutze-Birk and Jacobi [9] measured the In tracer diffusivities in this phase on the belief that In may have more or less the same diffusivity as Al, as they both belong to same group in the periodic table and have similar atomic sizes.

There is also a possibility to determine tracer diffusivities by the classical diffusion couple technique from the knowledge on intrinsic diffusivities, D_i following (Eq. (A.16-1)):

$$D_A = \frac{V_m}{V_B} D_A^* \Theta \left(1 + W_A \right); \quad D_B = \frac{V_m}{V_A} D_B^* \Theta \left(1 - W_B \right) \tag{5.1-2}$$

where the vacancy wind factor $W_i = \dfrac{2 N_i \left(D_A^* - D_B^* \right)}{M_o \left(N_A D_A^* + N_B D_B^* \right)}$, with M_o as a constant

which depends on the crystal structure of the system, N_i is the mole fraction of species i

and Θ is the thermodynamic factor $\partial \ln a_A / \partial \ln N_A = \partial \ln a_B / \partial \ln N_B$.
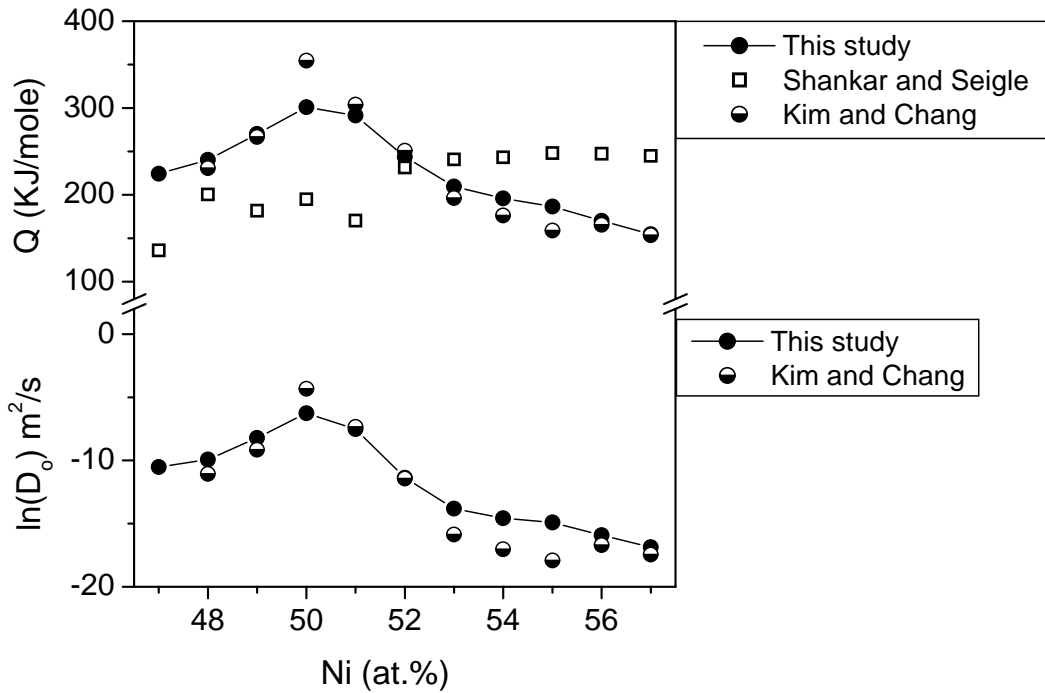
Fig. (5.1-5) The activation energy, Q and pre-exponential factor, D_o over the homogeneity range in the β-NiAl phase. Results found by Shankar and Siegle [1] and Kim and Chang [4] are incorporated for comparison.
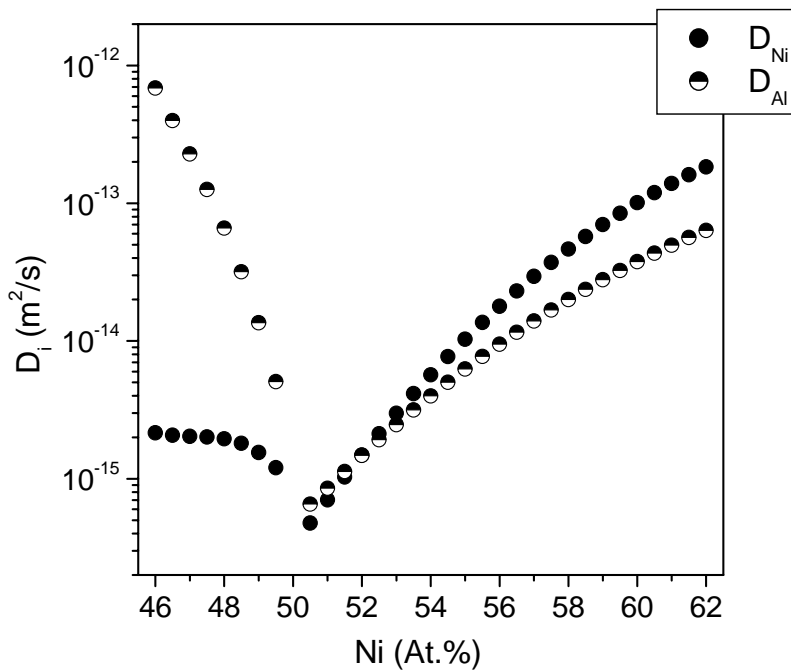
Fig. (5.1-6) Intrinsic diffusivities of Ni and Al in the β-NiAl phase at 1000 °C.
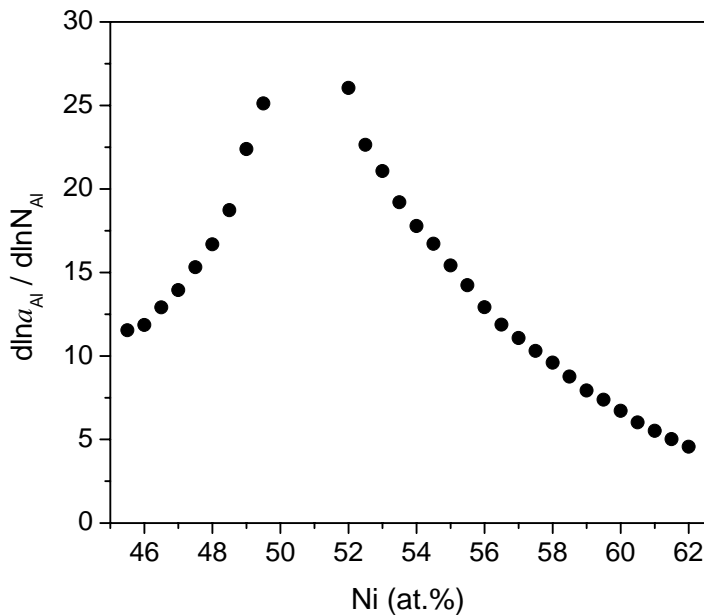
Fig. (5.1-7) Thermodynamic factor, $\mathrm{d}\ln a_{\mathrm{Al}}/\mathrm{d}\ln\mathrm{N}_{\mathrm{Al}}$ calculated from the activity data available in Ref. [10].

The vacancy wind effect can be measured from the knowledge on tracer diffusion coefficients if M_o is known. However, as discussed in A.16, the experimental investigations into the vacancy wind effect are ambiguous. In many cases to simplify the calculation the vacancy wind effects are neglected, considering its value of $W_i = 0$. Now we have an opportunity to check the significance of this effect on the calculated tracer diffusivities from data determined on intrinsic diffusivities. Although this model was developed for random solid solutions it has also been used for stoichiometric compounds (A.16). The values on thermodynamic factor were determined from the activity data available in Ref. [10] and shown in Fig. (5.1-7). Note that the values near stoichiometric composition were not calculated because of the inconvenience in measuring high concentration gradient and large scatter in this regime in the experimental data points. Tracer diffusivities of Ni and Al are calculated through Eq. (5.1-2) from the data on intrinsic diffusivities (Fig. (5.1-6)) found in this study and are shown in Fig. (5.1-8 and -9). Data are shown for both cases when vacancy wind effect was neglected and also when the effect was taken under consideration. The changes in vacancy wind effect for Ni and Al are shown in Fig. (5.1-10). The value of M_o was considered to be 5.33 as given by Manning for a body centered cubic lattice (A.16). It can be seen that the differences on the calculated tracer diffusivities by considering vacancy wind effects are negligible and fall within the limit of experimental errors. Ni and In tracer diffusivities available in the literature are incorporated for the comparison. Tracer diffusivities calculated by this classical diffusion couple technique fall in the range of data found directly from tracer methods.
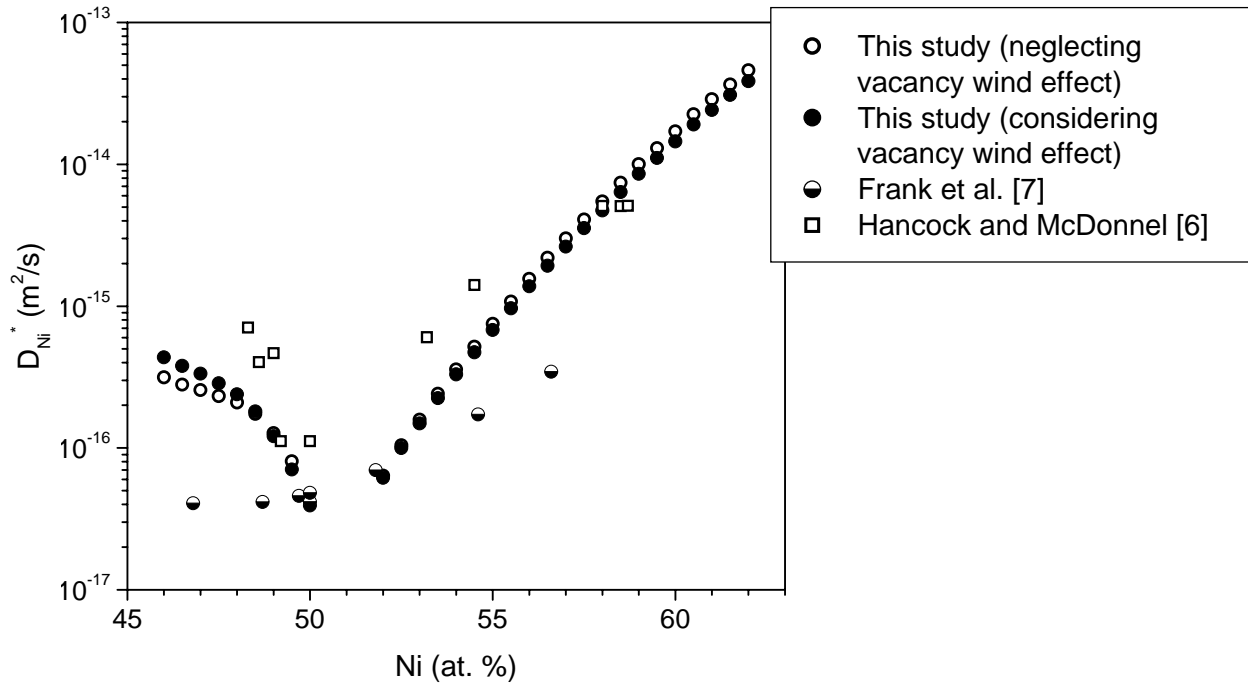
Fig. (5.1-8) Ni tracer diffusivities in the β-NiAl phase calculated by the diffusion couple technique. Data measured by the tracer method are incorporated for comparison.
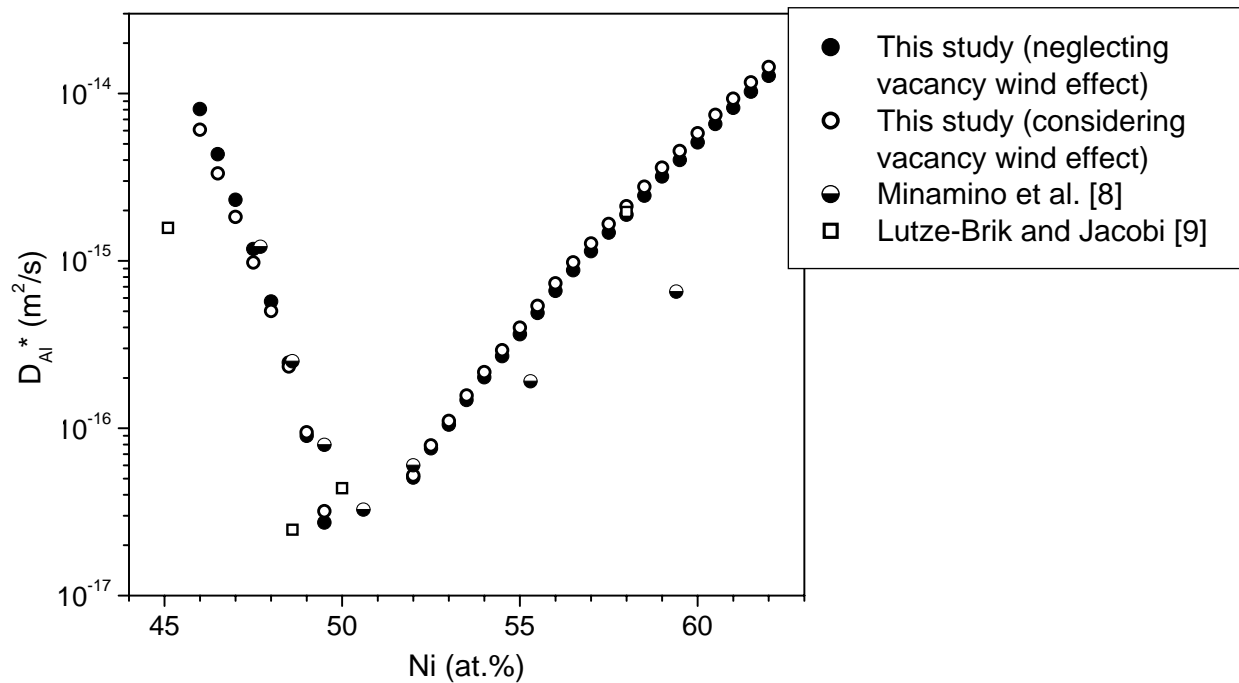
Fig. (5.1-9) Al tracer diffusivities in β-NiAl calculated by the diffusion couple technique. Tracer diffusivities in this phase available in literature are incorporated for comparison.
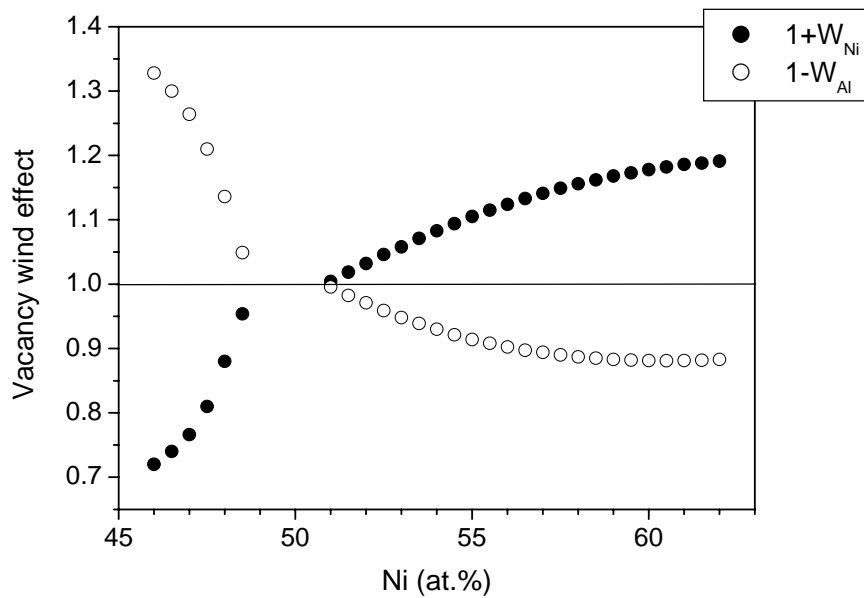
Fig. (5.1-10) The in vacancy wind effect as a function of composition.

5.2 Studies in the γ′-Ni₃Al phase

The goal of this part of our study was to determine the tracer diffusion coefficients of Al in Ni₃Al from the interdiffusion coefficients and Ni-tracer diffusivities available in the literature [11-13]. Tracer measurements concentrated mainly on the determination of Ni diffusivities because of the lack of a proper Al isotope. Larikov [14] is the only one who reported the tracer diffusion coefficients of Al in Ni₃Al and found that the values are almost equal to the Ni tracer diffusivities in this phase. This measurement is, however, doubtful since the Ni tracer diffusion data they measured are significantly larger than in other recent reports. For the purpose of this study, the diffusion couple technique was used to determine the interdiffusion coefficients and the ratio of intrinsic diffusivities.

I. Experimental results and interdiffusion coefficients

Four different binary alloys were prepared for two types of diffusion couples, A: N₆₅Al₃₅/Ni₈₅Al₁₅ and B: Ni₇₂Al₂₈/Ni₇₈Al₂₂. A typical morphology of an annealed diffusion couple can be seen in Fig. (5.2-1). The interface between the end members and the Ni₃Al-phase grown during interdiffusion is wavy which can be explained by the heterogeneous structure of the initial two phase materials. The moving interface of the growing Ni₃Al incorporates the Ni₃Al precipitates on both sides of the new phase and in the course of this process the interface becomes irregular. One clearly sees the different

crystal morphology of Ni_3Al on both sides of the Kirkendall plane because the crystals grow differently at either side of the end-members.

The exact location of the Kirkendall plane can be determined easily from the presence of straight row of ThO_2-particles visible in white contrast in Fig. (5.2-1). The irregular nature of the interface makes it difficult to determine the thickness of the Ni_3Al-layer. In order to calculate the average thickness the SEM images were processed by computer and the contours were fitted with a polinom. The areas of the reaction product on both sides of the original welding plane were calculated. Summing the two areas gives the average thickness of the reaction layer, while by taking the ratio, the position of the Kirkendall plane was determined. On Fig. (5.2-2) a typical concentration profile is shown and the Kirkendall plane position is indicated. In general, the ThO_2 particles in the interdiffusion zone are located at the stoichiometric Ni_3Al composition within the experimental error (~1 at.%). The layer thickness and the position of the Kirkendall plane changes along the sample due to the wavy nature of the interface. To perform the diffusion analysis the concentration profile was scaled to the calculated average phase thickness.

In this way a stepwise linear concentration profile was constructed (see Fig. (5.2-2)). The changes in molar volume in this phase can be calculated from [5]:

$$V_m = 6.60 + 0.823x_{Al} + 0.965x_{Al}^2 \qquad \text{cm}^3/\text{mole} \qquad (5.2-1)$$

where x_{Al} is the mole fraction of Al. Partial molar volumes of Ni and Al were calculated to be 6.54×10^{-6} and 7.85×10^{-6} m^3/mole at 75 at.%Ni.

Time dependence of the phase growth was measured at two different temperatures (900 and 1050 °C). Parabolic growth was found which demonstrates the diffusion control of the process. Interdiffusion coefficients at 75 at.% Ni were calculated applying the Wagner analysis [A.9] and are shown in Fig. (5.2-3). Janssen [15] reported that below 1000 °C grain boundary diffusion becomes the dominant process. However, in our case the average grain size of the product phase was found to be comparable with the thickness of the whole Ni_3Al layer (as can be seen in Fig. (5.2-1)). Moreover, the protruding of the interface does not specifically occur at the grain boundaries. This indicates that the importance of grain boundary diffusion is small compared to volume diffusion.
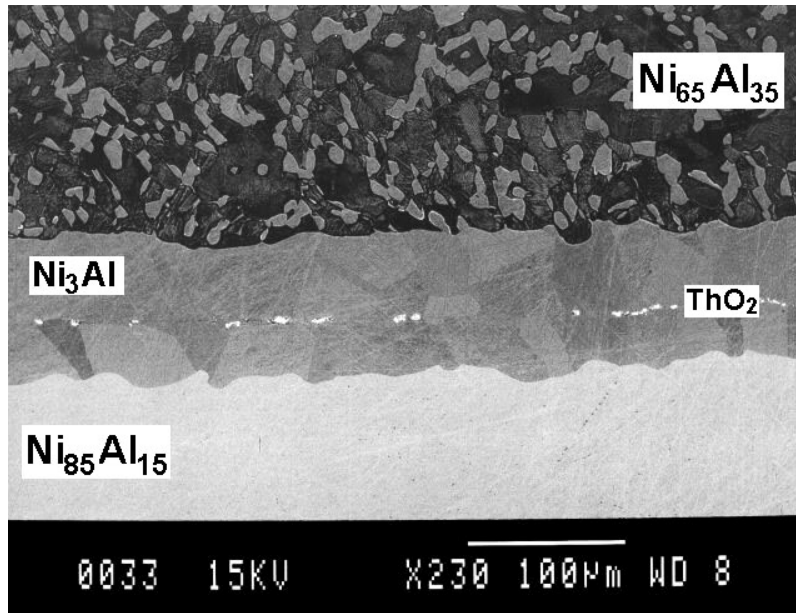
Fig.(5.2-1) Back-scattered electron image of the diffusion zone after annealing for 196 hrs at 1000 °C. The Kirkendall markers (ThO₂-particles) are visible with white contrast.
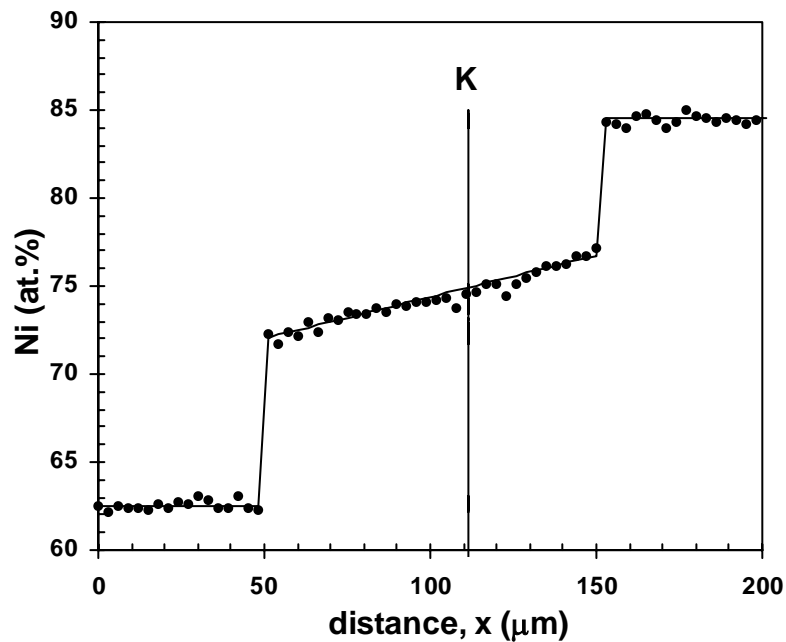
Fig. (5.2-2) A typical composition profile of the couple (shown in Fig. (5.2-1)) annealed for 196 hrs at 1000 °C. The Kirkendall plane position is indicated by "K".

The values of the interdiffusion coefficients calculated near the stoichiometric composition are plotted on Fig. (5.2-3) together with data obtained from the literature [5, 15]. The authors in these references performed multi-phase diffusion measurement, but their starting materials were different. The data found by Watanabe et al. [5] were lower than the results obtained in the present study and the data reported by Janssen [15].

II. Determination of the Al tracer diffusivities

Since inert ThO_2-particles were used to mark the initial welding plane, the ratio of the intrinsic diffusion coefficients at this position after interaction can be calculated through Eq. (A.10-6) (see appendix A.10).

The calculated values of intrinsic diffusivities are listed in Table (5.2-1). The ratio of the intrinsic diffusivities, D_A/D_B can be related to the ratio of tracer diffusivities from Eq. (5.1-2) (see also A.16):

$$\frac{D_A V_B}{D_B V_A} = \frac{D_A^*(1+W_A)}{D_B^*(1-W_B)} \tag{5.2-2}$$

where the vacancy wind factor $W_i = \dfrac{2N_i\left(D_A^* - D_B^*\right)}{M_o\left(N_A D_A^* + N_B D_B^*\right)}$, M_o is a constant, which depends on the crystal structure of the system.

It has been suggested that Manning's theory might be applied for $L1_2$ compounds where the diffusion of the minor element occurs by ordinary vacancy mechanism over the sublattice of the other species [12, 13]. Following the statements of Ikeda et al. [12] and Numakura et al. [13] this assumption seems to be adoptable in our case as well. The value of M_o was considered to be 7.15 for calculations as suggested by Manning (see A.20).

Since the tracer diffusion coefficients of Ni in Ni_3Al are well documented in the literature [17], the tracer diffusivities of Al can be computed using Eq. (5.2-2). From the measured Ni tracer data and ratio of diffusivities as listed in Table (5.2-1), a second order equation was obtained and the tracer diffusion coefficients of Al in Ni_3Al near the position of the Kirkendall plane (i.e. at ~75at. % Ni) were calculated. The values of W_{Ni} and W_{Al} are found to be ~0.18 and ~0.06, respectively. The calculated Al tracer
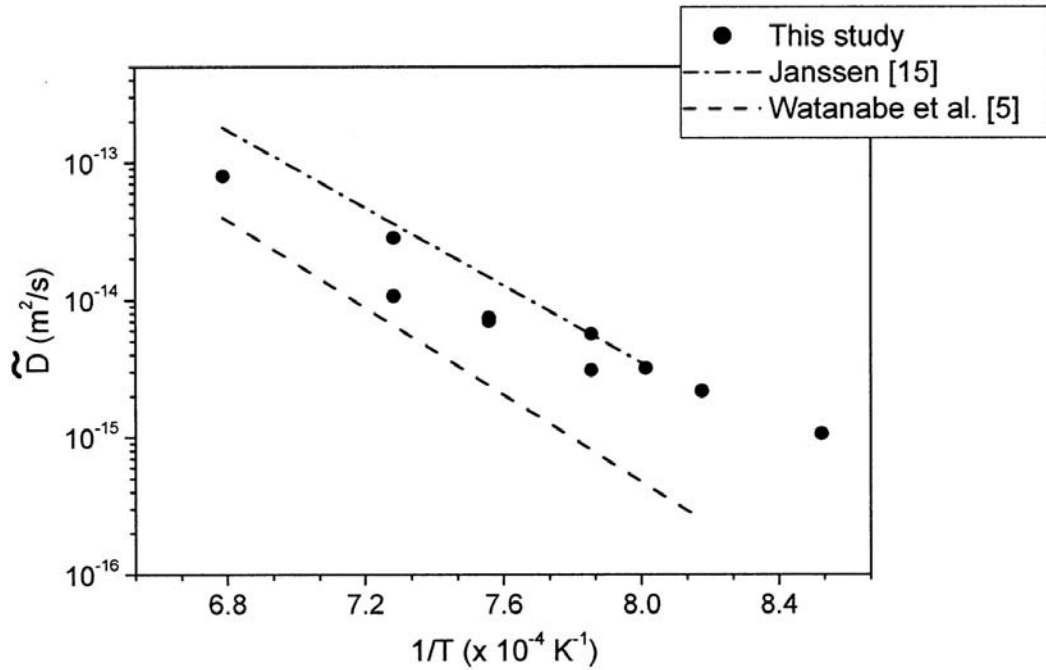
Fig. (5.2-3) Interdiffusion coefficients calculated at the marker plane position are plotted with respected to temperature. Data available in literature is incorporated for comparison.
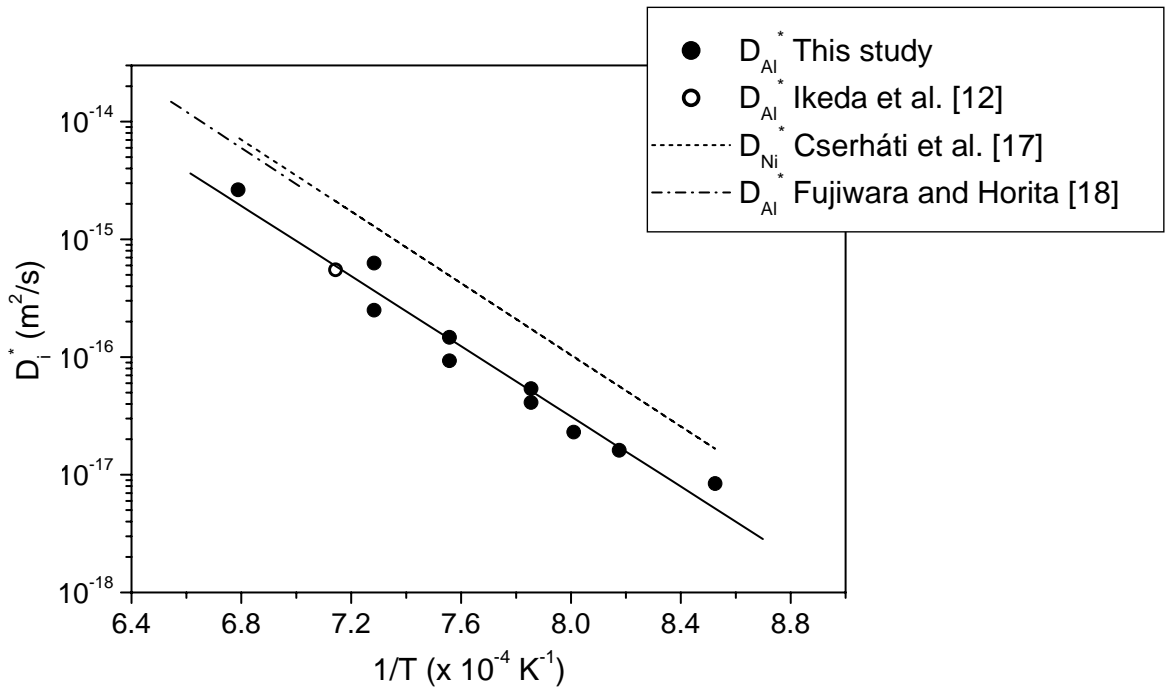
Fig. (5.2-4) The Al tracer diffusion coefficients calculated in this study are plotted together with the data available in literature. Ni tracer diffusion coefficients are incorporated for comparison.

diffusion coefficients are represented by an Arrhenius plot in Fig. (5.2-4) together with data's found by Fujiwara and Horita [18] and Ni tracer diffusion data's found in Ref. [17] are incorporated for comparison.

Table (5.2-1) Details of the couples used in this study: annealing temperature (K), time (hrs), mole fraction of Ni at the Kirkendall plane position (Ni^K) and the ratio of diffusivities calculated in this study (A: $Ni_{65}Al_{35}/Ni_{85}Al_{15}$, B: $Ni_{72}Al_{28}/Ni_{78}Al_{22}$).

Couple	Temperature (°C)	Time (hrs)	Ni^K (at. %)	D_{Ni}/D_{Al}
A	900	400	74.6	1.92
A	950	196	75.0	3.67
A	975	196	75.0	4.58
A	1000	196	74.5	3.33
A	1000	196	74.5	4.50
A	1050	392	74.9	5.75
A	1050	98	74.8	3.50
B	1100	196	74.9	5.50
B	1100	196	75.3	2.00
B	1100	196	73.9	2.00
A	1200	196	76.0	2.83

Our results determined in this study are compared with the data available in literature in Fig. (5.2-4). The result of Ikeda et al. [12] was measured in a *single-phase* interdiffusion experiment and fits well within our results, although in that work besides the slightly different circumstances, the correct value of the thermodynamic factor was also needed. Fujiwara and Horita [18] performed intrinsic diffusion measurement using NiAl(62 at.%)/Ni diffusion couples. They were also able to estimate the tracer diffusion coefficient of Al in Ni_3Al. They found values of the Al tracer diffusion coefficients are more close to the Ni tracer diffusion coefficients. However, their initial materials were different in the sense that a concentration gradient will develop in the NiAl and Ni end members. NiAl exists in a large composition range and Al can dissolve into the Ni solid solution up to about 16 at.% at 1200 °C. Measuring the long tail in composition profile in both the end phases with desired accuracy is technically difficult. The advantage of our study is that we were able to avoid this uncertainty by using saturated two-phase alloys as end-members for the diffusion couple.

5.3 Conclusions

Intrinsic and tracer diffusivities of Al and Ni are measured by the diffusion couple technique in β-NiAl and γ′-Ni₃Al. Tracer diffusivities determined indirectly in this study in the β-NiAl phase are found to be within the range of data of In and Ni tracer diffusivities available in literature measured directly by the tracer method. Al tracer diffusivities in the γ′-Ni₃Al phase are measured using the knowledge on Ni tracer diffusivities in this phase. It was not possible to measure Al tracer diffusivities directly by the tracer method because of the lack of suitable Al isotopes. Vacancy wind effects on the diffusion rates of Al and Ni were considered in both phases. It was found that the vacancy wind effects on the calculated tracer diffusivities fall within the range of experimental errors what one might expect.

References

1. S. Shankar, L.L. and Seigle, Interdiffusion and Intrinsic diffusion in the NiAl phase of the Al-Ni system, Met. Trans. A, **9A** (1978) 1467-76
2. R. Nakamura, K. Takasawa, Y. Yamazaki and Y. Iijima, Single-phase interdiffusion in the B2 type intermetallic compounds NiAl, CoAl and FeAl, Intermetallics **10** (2002) 195-204
3. T. Helander and J. Ågren, A phenomenological treatment of diffusion in Al-Fe and Al-Ni alloys having B2-B.C.C ordered structure, Acta. Mater **47** (1999) 1141-52
4. S. Kim and Y.A. Chang, An interdiffusion study of a NiAl alloy using single-phase diffusion couples, Metall. Mater. Trans. A, **31A** (2000) 1519-24
5. M. Watanabe, Z. Horita and M. Nemoto, Measurements of interdiffusion coefficients in Ni-Al system, Def. Diff. Forum **143-147** (1997) 345-50
6. G.F. Hancock and B.R. McDonnel, Diffusion in the intermetallic compound NiAl, Phys. Stat. Sol. A **4** (1971) 143-50
7. St. Frank, S.V. Divinski, U. Södervall and Chr. Herzig, Ni tracer diffusion in the B2-compound NiAl: influence of temperature and composition, Acta Mater. **49** (2001) 1399-1411
8. Y. Minamino, Y. Koizumi and Y. Inui, In diffusion in B2-type ordered NiAl intermetallic compound, Def. Diff. Forum **194-199** (2001) 517-22
9. A. Lutze-Birk and H. Jacobi, Diffusion of ^{114m}In in NiAl, Scripta Met. **9** (1975) 761-65
10. A. Steiner and K.L. Komarek, Thermodynamic activities of solid nickel-aluminium alloys, Trans. Met. Soc. AIME, **230** (1964) 786-90
11. H. Mehrer, Diffusion in solids metals and alloys, Landolt Börnstein, **III/26**, Springer, (1990)
12. T. Ikeda, A. Almazouzi, H. Numakura, M. Koiwa, W. Sprengel and H. Nakajima, Single-phase interdiffusion in Ni₃Al, Acta Mater. **46** (1998) 5369-76
13. H. Numakura, T. Ikeda, M. Koiwa and A. Almazouzi, Self-diffusion mechanism in Ni-based LI2 type intermetallic compound, Phil. Mag. **A 77** (1998) 887-909
14. L.N. Larikov, V.V. Geichenko and V.M. Falchenko, Diffusion process in ordered alloys (trans. From Russian by NBS and NSF) New Delhi, (1981) p.117
15. M.M.P Janssen, Diffusion in the nickel-rich part of the Ni-Al system at 1000°C to 1300°C; Ni₃Al layer growth, diffusion coefficients and interface concentrations, Met. Trans. **4** (1973) 1623-33
16. M. Koiwa, S. Ishioka, Random walks and correlation factor in diffusion in a three-dimensional lattice with coordination number 8, Phil. Mag. A **48** (1983) 1-9

17. C. Cserháti, I.A. Szabó, G. Erdélyi and Zs. Márton, Tracer diffusion of ^{63}Ni in Ni$_3$(Al,Ge) ternery intermetallic compound, Intermetallics **10** (2002) 887-92

18. K. Fujiwara and Z. Horita, Intrinsic diffusion in Ni$_3$Al, Def. Diff. Forum **194-199** (2001) 565-70.

Chapter 6

Intermetallic growth and Kirkendall effect manifestations in Cu(Ni)/Sn and Au/Sn diffusion couples

The ability to rationalize (and predict) the Kirkendall effect manifestations still remains an elusive problem. During this thesis work, we have developed an alternative theory (see Chap. 4) to explain diffusion controlled growth of line compounds and morphological evolutions of product layers, taking into consideration chemical reactions occurring at the interphase interfaces. This approach was demonstrated to be equivalent to the traditional diffusion-based treatment; both models describe the same phenomenological process in terms of purely phenomenological quantities.

Motivated by the apparently coherent analysis, we turn our attention to study the growth of intermetallics in two other technologically important systems, namely Cu(Ni)/Sn and Au/Sn. The formation of intermetallic phases at the interface between tin-bearing solder alloys and constituents of under-bump metallizations (Cu, Ni, Au, etc.) is an important phenomenon, which controls (to a large extent) the strength of the joint throughout the lifetime of an electronic component. It is necessary to add here that the thrust for miniaturisation and environmentally friendly products, Au-Sn system offers possibility for a fluxless joining [1] in C4 ("Controlled collapse Chip Connection") flip-chip technology.

The Kirkendall effect in these systems deserves further investigation, because its manifestations, like, for example, the development of diffusion porosity, deformation on a macroscopic scale, etc., will noticeably affect the overall performance (reliability) of

---

This chapter is written based on the articles:

1. A. Paul, A.A. Kodentsov and F.J.J. van Loo, Intermetallic growth and Kirkendall effect manifestations in Cu/Sn and Au/Sn diffusion couples, Z. Metallkunde In press, 2004
2. A. Paul, C. Luef, A.A. Kodentsov, H. Flandorfer, H. Ipser and F.J.J. van Loo, Solid-state diffusion controlled interaction in the Cu(Ni)/Sn system, unpublished research

the interconnect, especially when manufacturing advanced Pb-free electronics where dimensions of the solder volumes are decreasing markedly.

The purpose of this chapter is to report on kinetic and morphological aspects of the intermetallic growth in Cu(Ni)/Sn and Au/Sn diffusion couples and to contribute to the understanding of the role of the Kirkendall effect in the solid-state interactions in these systems.

6.1 Solid-state interactions in Cu/Sn binary diffusion couples

As expected from the binary Cu-Sn phase diagram (Fig. (6.1-1)) [2], two intermetallic compounds, viz. ε-Cu_3Sn and η-Cu_6Sn_5 should be formed between Cu and Sn interactions below the liquidus temperature. These phases were indeed found in the Cu/Sn diffusion couple after annealing at 215 °C for 225 hrs (Fig. (6.1-2)). It can be seen that the product layers in the reaction zone are bound by somewhat wavy interfaces. This might be attributed to the influence of short-circuit (mainly grain-boundary) diffusion and diffusion anisotropy on the overall mass transport across the intermetallic layers, although absolute proof is lacking.

The growth of the intermetallic layers obeys the parabolic law underlying a diffusion-controlled process. On the basis of the thickness measurements, the apparent rate constants $k_p = \Delta x^2 / 2t$ (Δx is the reaction layer thickness and t is the annealing time, see A.17) at 215 °C were deduced as 7.55×10^{-17} and 1.58×10^{-16} m^2/s for Cu_3Sn and Cu_6Sn_5, respectively. From the position of the Kirkendall markers (ThO$_2$-particles), the ratio of the volume intrinsic fluxes of the components (see A.10) in the phase layer of η-Cu_6Sn_5 was found to be

$$\frac{|J_{Sn}|}{|J_{Cu}|} = \frac{D_{Sn}V_{Cu}}{D_{Cu}V_{Sn}} = 1.6$$

In order to determine the relative diffusivities of species in the ε-Cu_3Sn phase, an incremental couple based on pure copper and laboratory prepared Cu_6Sn_5-compound was studied. Fig. (6.1-3) shows microstructure of the diffusion zone in this couple after heat-treatment at 215 °C for 225 hrs. The ThO$_2$-markers are clearly visible inside the ε-Cu_3Sn product layer. It was calculated that in Cu_3Sn
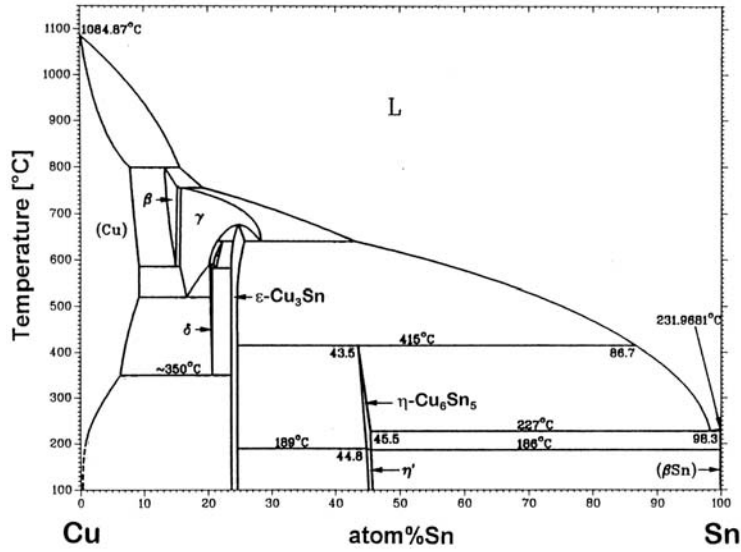
Fig. (6.1-1) Binary phase diagram of Cu-Sn binary system.
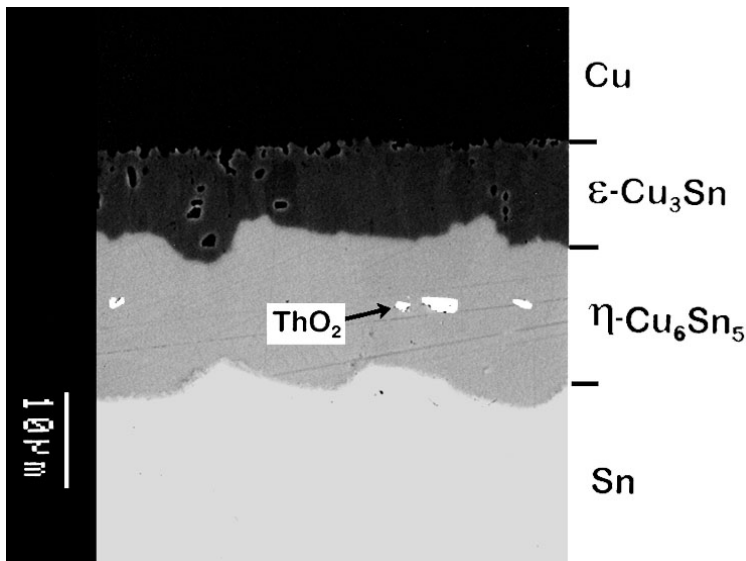
Fig. (6.1-2) Backscattered Electron Image (BEI) of the diffusion zone developed between Cu and Sn after reaction at 215 °C in vacuum for 225 hrs. ThO$_2$-particles ("white contrast") were used as Kirkendall markers.
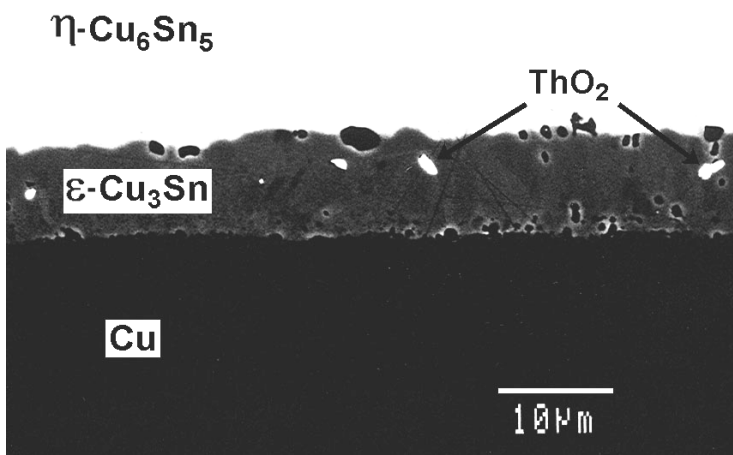
Fig. (6.1-3) BEI of the reaction zone developed in the incremental couple based on Cu and η-Cu$_6$Sn$_5$ after annealing at 215 °C for 225 hrs. ThO$_2$-particles were used as "Kirkendall markers".

$$\frac{|J_{Sn}|}{|J_{Cu}|} = \frac{D_{Sn}V_{Cu}}{D_{Cu}V_{Sn}} = 0.9$$

From a phenomenological viewpoint it is conceivable that at the reaction interfaces, product Cu-Sn intermetallics nucleate and grow by the loss of Cu- or Sn-atoms from or by adding Cu- or Sn-atoms to the adjoining phase layer. In terms of chemical reaction equations it can be re-stated as (see Fig. (6.1-4)):

Interface I - Cu/Cu$_3$Sn on the Cu$_3$Sn-side
$$3qCu + q[Sn]_d \rightarrow 4qCu_{3/4}Sn_{1/4}$$
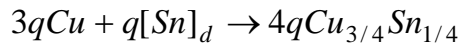
Interface II - Cu$_3$Sn/Cu$_6$Sn$_5$ on the Cu$_3$Sn-side:

$$\frac{11}{9}pCu_{6/11}Sn_{5/11} + p[Cu]_d \rightarrow \frac{20}{9}pCu_{3/4}Sn_{1/4}$$

$$\frac{11}{3}qCu_{6/11}Sn_{5/11} \rightarrow q[Sn]_d + \frac{8}{3}qCu_{3/4}Sn_{1/4}$$
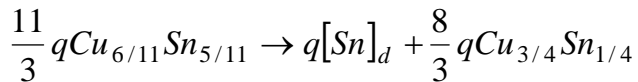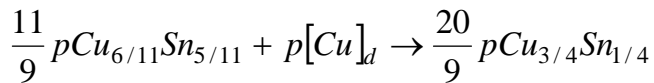
Interface II - Cu$_3$Sn/Cu$_6$Sn$_5$ on the Cu$_6$Sn$_5$-side:

$$\frac{20}{9}rCu_{3/4}Sn_{1/4} \rightarrow r[Cu]_d + \frac{11}{9}rCu_{6/11}Sn_{5/11}$$

$$\frac{8}{3}sCu_{3/4}Sn_{1/4} + s[Sn]_d \rightarrow \frac{11}{3}sCu_{6/11}Sn_{5/11}$$
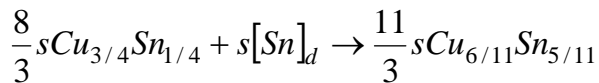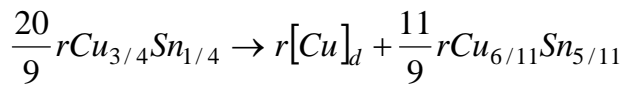
Interface III - Cu$_6$Sn$_5$/Sn on the Cu$_6$Sn$_5$-side:

$$\frac{5}{6}rSn + r[Cu]_d \rightarrow \frac{11}{6}rCu_{6/11}Sn_{5/11}$$
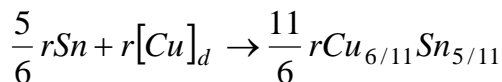
Here, the symbols $[Cu]_d$ and $[Sn]_d$ denote the diffusing atom species in the product layer; they do not represent the phases Cu and Sn.
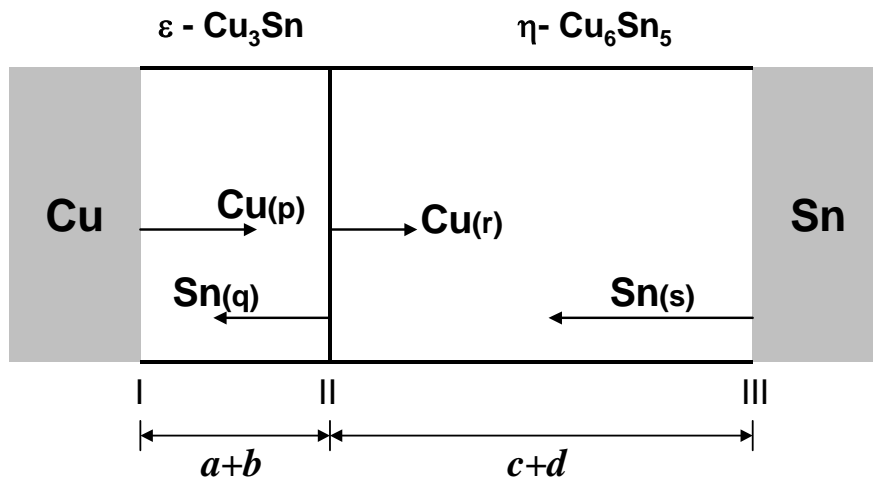
Fig. (6.1-4) Schematic illustration of the growth of Cu$_3$Sn and Cu$_6$Sn$_5$ layers in a binary Cu/Sn couple.

The parameters p and q are the total amount of moles of Cu- and Sn-atoms, respectively, transferred per unit area through the product layer of Cu_3Sn during total diffusion time, t. Analogously, r and s are the number of moles of Cu- and Sn-atoms transported during interaction across unit area through the Cu_6Sn_5-phase layer.

For a volume diffusion-controlled growth of the intermetallic compounds, the magnitude of the intrinsic flux across a phase layer, J_i, is inversely proportional to the square root of the reaction time. In this case, one can write

$$p = \int_0^t |J_{Cu}| dt = \int_0^t \frac{\text{constant}}{\sqrt{t}} dt = 2t |J_{Cu}| \tag{6.1-1}$$

Similarly, $q = 2t |J_{Sn}|$, and therefore, the ratio q/p equals the ratio of the instantaneous fluxes in the Cu_3Sn-product layer, i.e.

$$\frac{q}{p} = \frac{|J_{Sn}|}{|J_{Cu}|} = 0.9 \tag{6.1-2}$$

In the same way, we found for the product layer of Cu_6Sn_5

$$\frac{s}{r} = \frac{|J_{Sn}|}{|J_{Cu}|} = 1.6 \tag{6.1-3}$$

The thickness of the parts of the product phase layers resulting from the interfacial reactions given above (Fig. (6.1-4)) can be expressed by

$$V_m^{Cu_3Sn} \times 4q = a$$
$$V_m^{Cu_3Sn} \times \left(\frac{20}{9} p + \frac{8}{3} q - \frac{20}{9} r - \frac{8}{3} s \right) = b$$
$$V_m^{Cu_6Sn_5} \times \left(\frac{11}{9} r + \frac{11}{3} s - \frac{11}{9} p - \frac{11}{3} q \right) = c \tag{6.1-4}$$
$$V_m^{Cu_6Sn_5} \times \left(\frac{11}{6} r \right) = d$$

Note that to simplify calculations we have ignored the presence of the solid solution of Sn in copper next to the product intermetallic layer. This means that the value of a will be slightly overestimated, because a small amount of that part of the Cu_3Sn-layer will actually dissolved in the copper end-member. For the Cu/Sn diffusion couple annealed at 215 °C for 225 hrs, the average thickness of the intermetallic layers (in μm) was found to be

$$a + b = 8.9$$
$$c + d = 16.5 \tag{6.1-5}$$

83

Thus, we have defined system of eight equations with eight unknowns (Eq. (6.1-2)-(6.1-5)).

Further, we assume that for the partial molar volume of the species in a phase is equal to the molar volume of that phase of interest, i.e. $V_{Sn} = V_{Cu} = V_m$. Using the lattice parameter values given in Ref. [3], the molar volumes were calculated as $V_m^{Cu_3Sn} = 9.49$ cm^3/mole; $V_m^{Cu_6Sn_5} = 11.64$ cm^3/mole

With these assumptions, the marker velocity, v_K and the location of the Kirkendall plane, x_K in each product layer of the Cu/Sn couple can be found (see Chap. 4.1):

$$x_K = 2tv_K = -2t\left(V_{Sn}J_{Sn} + V_{Cu}J_{Cu}\right)$$

Comparing these equations with Eq. (4), one can write

$$V_m^{Cu_3Sn}(q - p) = 2tv_K^{Cu_3Sn} = x_K^{Cu_3Sn}$$
$$V_m^{Cu_6Sn_5}(s - r) = 2tv_K^{Cu_6Sn_5} = x_K^{Cu_6Sn_5}$$

(6.1-6)

By solving set of equations (6.1-2) - (6.1-5), one finds for the case of annealed Cu/Sn couple (215 °C; 225 hrs) that a = 13.6 µm, b = -4.7 µm, c = 8.7 µm and d = 7.8 µm. The negative value of parameter b stems from the fact that rate of the Cu$_3$Sn formation from Cu$_6$Sn$_5$, that is, $\left(\dfrac{20}{9}p + \dfrac{8}{3}q\right)$ is lower than its consumption at the Cu$_3$Sn/Cu$_6$Sn$_5$-interface $\left(\dfrac{20}{9}r + \dfrac{8}{3}s\right)$.

Accordingly, the coefficients p, q, r and s in the equations of the interfacial reactions are 0.4, 0.36, 0.37 and 0.57 mole/m^2, respectively. This leads, through Eq. (6.1-6), to the following values of the Kirkendall velocity: -2.47×10^{-13} m/s in the Cu$_3$Sn- and 1.42×10^{-12} m/s in the Cu$_6$Sn$_5$-phase layer. Co-ordinates of the Kirkendall marker plane(s), x_K (= x_K - x_o) in this diffusion couple obtained through Eq. (6.1-6) are -0.4 µm and 2.3 µm corresponding to the Cu$_3$Sn- and Cu$_6$Sn$_5$-product layers, respectively.

Returning to the diffusion couple shown in Fig. (6.1-2), it is possible to determine the position of the plane within the reaction zone where the Kirkendall markers were situated at time t = 0 (i.e. x_o = 0). This can be done by subjecting the concentration profile measured across the reaction zone with EPMA to the Sauer-Freise treatment (see A.19). Finally, using experimental results discussed in this section, the Kirkendall velocity

diagram for the Cu/Sn diffusion couple annealed at 215 °C for 225 hrs was constructed (Fig. (6.1-5)). From the negative value of b = -4.7 µm, it follows that no Kirkendall plane can be found on the Cu₃Sn-layer. The position for the Kirkendall plane calculated for this product phase (x_K = -0.4 µm) is, therefore, a virtual plane as can be appreciated from Fig. (6.1-5).

Apparently, the location of the marker plane in the Cu₆Sn₅-layer found with Eq. (6.1-6) and that predicted on the basis of the Kirkendall velocity diagram is in good agreement with the experimental observations, given the accuracy of the diffusion couple technique employed.
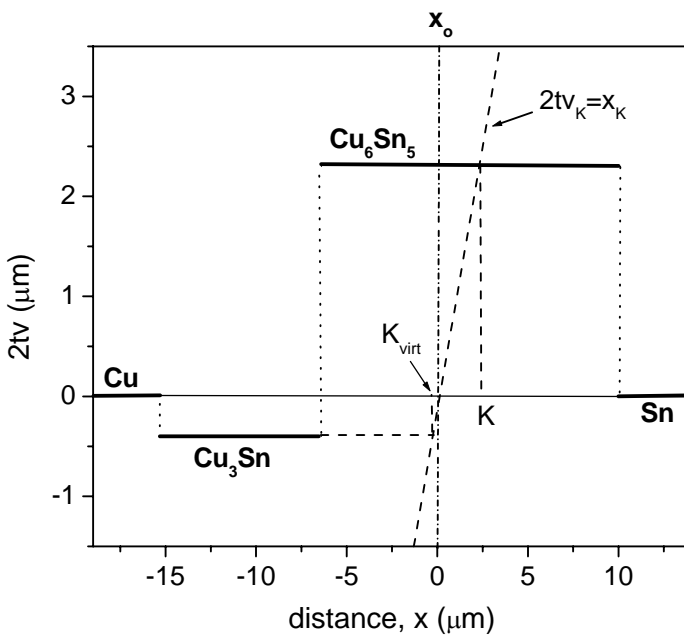
Fig. (6.1-5) The Kirkendall velocity diagram constructed for a Cu/Sn diffusion couple annealed at 215 °C for 225 hrs. The straight-line $2tv_K = x_K$ intersects the velocity plot in the domain of the reaction zone corresponding to the single-phased layer of η-Cu₆Sn₅. The stable Kirkendall plane (K) exists inside this product layer. For the Cu₃Sn one could define a virtual Kirkendall plane (K_{virt}).

6.2 Solid-state interactions in Cu(Ni)/Sn ternary diffusion couples

The ternary Cu-Ni-Sn is one of the most important systems to study in electronics industry. Ni is used on Cu layer as underbump metallization to decrease the reaction rate with Sn-based solder alloys for better reliability of the interconnects.

Before proceeding to study ternary interactions, knowledge on binary interactions is important for comparison. It is already shown in previous section that in a binary Cu/Sn diffusion couple both the equilibrium phases according grow to phase diagram at 215 °C (see Fig. (6.2-1)). ThO₂-particles present in the Cu₆Sn₅-phase are clearly visible. Sometimes the presence of very small ThO₂-particles in the Cu₃Sn-phase was found, which could be incidental and dragged by the grain boundaries. In that case they don't

act as Kirkendall marker to detect the marker plane. On the other hand, when the binary Ni/Sn was coupled at same temperature and for same annealing time, only one phase Ni_3Sn_4 was found to develop in the diffusion zone. According to the Ni-Sn binary phase diagram [2] two other equilibrium phases, Ni_3Sn and Ni_3Sn_2 should also develop in the reaction zone. The absence of these phases could be because of difficulties in nucleation. Sometimes, phases are present in a reaction zone as a very thin layer and difficult to detect with the analytical techniques used in this study (see A.21). The total layer thickness of the diffusion grown layer in a Ni-Sn binary couple at 215 °C after 400 hrs of annealing was found to be around 9.2 μm, which is few times less than the total thickness in the Cu-Sn diffusion couple. In both Ni-Sn and Cu-Sn binary diffusion couples, the boundaries of the phase layers were quite wavy, which could be the result of grain boundary diffusion.
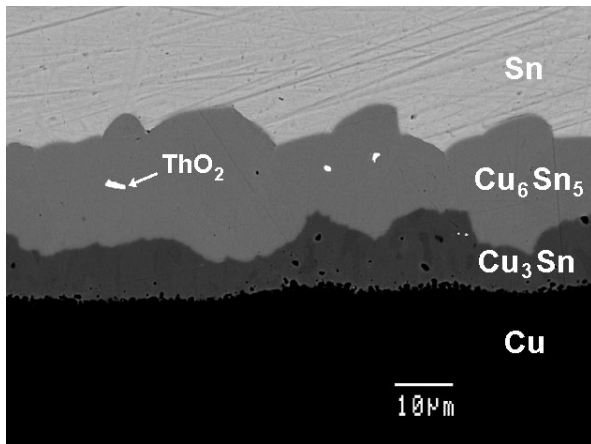
Fig. (6.2-1) BEI image of binary Cu/Sn diffusion couple annealed at 215 °C for 400 hrs.
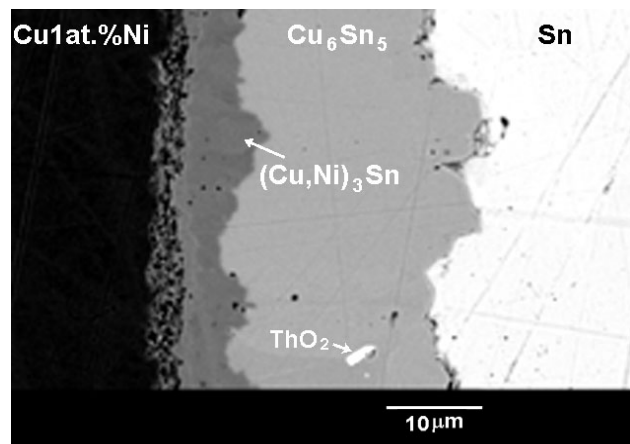
Fig. (6.2-2) BEI image of ternary Cu1at.%Ni/Sn diffusion couple annealed at 215 °C for 400 hrs.

To study ternary interactions, end-member alloys of Cu with increasing amount of Ni are prepared and coupled with pure Sn at 215 °C. When a Cu1at.%Ni/Sn couple was annealed for 400 hrs, Cu_6Sn_5 (presence of Ni was not detected in this phase during EPMA measurements) and $(Cu,Ni)_3Sn$ layers were developed as shown in Fig. (6.2-2). The total thickness of the diffusion zone was comparable with that in a binary Cu/Sn couple   (Fig. (6.2-1). The presence of inert ThO_2-markers in the Cu_6Sn_5 phase is almost at the same place compared to Cu/Sn binary couple, which reflects similar (ratio of) intrinsic diffusivities of Cu and Sn in this phase. However, the amount of pores present in $(Cu,Ni)_3Sn$-phase increased drastically, which is basically the result of unequal intrinsic flux of Cu(Ni) and Sn in this phase and of poor mechanical properties (see A.7).

With increasing amount of Ni in the Cu-Ni alloy end-member, however, a striking difference was found in the diffusion zone. When Cu5at.%Ni/Sn was coupled at same conditions, only the $(Cu,Ni)_6Sn_5$-phase developed with straight boundaries as shown in Fig. (6.2-3). The layer thickness is around 5 times higher than the total thickness of the Cu/Sn binary couple. The inert ThO_2-markers, inserted between the couple halves before annealing, were found at the $(Cu,Ni)_6Sn_5$/Sn interface, which means that Sn is virtually the only mobile species in this phase. The same type of reaction zone was found, when Sn was coupled with end-members of Cu-Ni alloy up to 15 at.% of Ni.
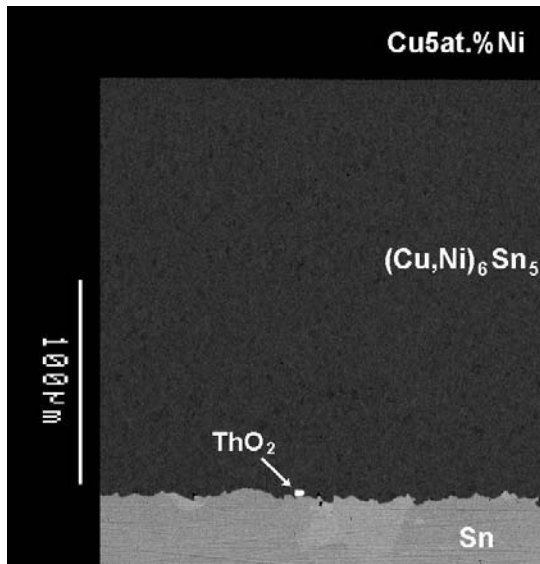
Fig. (6.2-3) BEI image of the Cu5at%.Ni/Sn diffusion couple annealed at 215 °C for 400 hrs. ThO_2-markers were found at the $(Cu,Ni)_6Sn_5$/Sn interface which reflects that Sn is by far the faster moving species in the reaction zone compared to Cu(Ni).
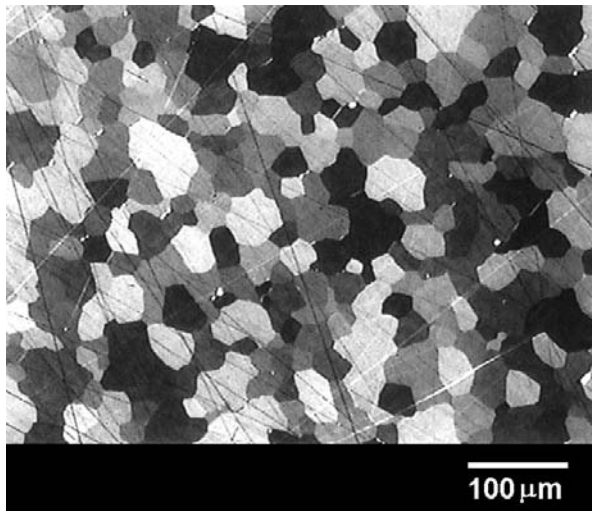
Fig. (6.2-4) Micrograph showing grains of the Cu_6Sn_5-phase in a binary Cu/Sn diffusion couple at 225 °C after annealing for 400 hrs.
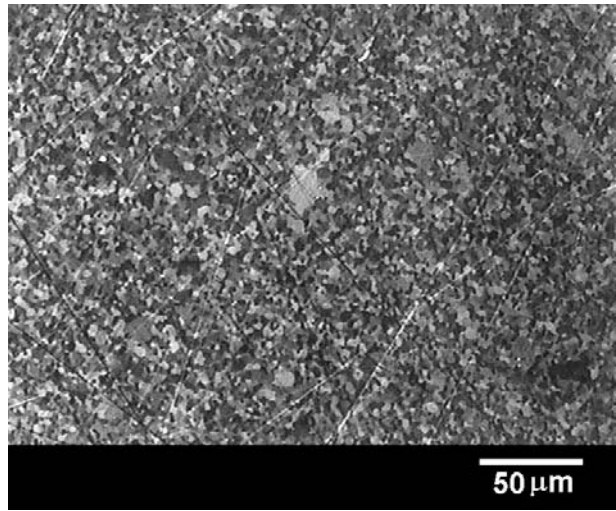
Fig. (6.2-5) Micrograph showing grains of the $(Cu,Ni)_6Sn_5$-phase in a ternary Cu5at.%Ni/Sn diffusion couple at 225 °C annealed for 400 hrs.

An etching agent based on $FeCl_3$ was used to remove Sn to expose the $(Cu,Ni)_6Sn_5$-layer. Then a standard metallographic treatment was followed to examine the microstructure under microscope. A distinct difference was found in the grain size between the layers grown under binary (and end-member with Cu1at.%Ni) couples and those of Cu(5-15)at.%Ni/Sn as shown in Figs. (6.2-4 and -5). The decrease in grain size (by more than an order of magnitude) may have increased the diffusion rate by fast grain boundary diffusion resulting in a much thicker reaction zone for the latter case. It is very well possible that in the grain boundary diffusion process only Sn takes part, which explains the position of the ThO_2-particles at the $Sn/(Cu,Ni)_6Sn_5$-phase. Further research is going to understand the actual reason.

6.3 Reactive phase formation in the binary Au/Sn system

To stress the salient points of the proposed phenomenological treatment, we will confine the following discussion to the interactions at one temperature, viz. 180 °C. Fig. (6.3-1) shows a typical morphology of the diffusion zone developed in the Au/Sn couple after annealing at this temperature. Again, one can notice the rather irregular shape of the interfaces between the product phase layers. As already mentioned, the appearance of such "wavy" interphase interfaces in the reaction zone of a binary couple is often attributed to a grain boundary diffusion in the growing layers. It is, however, unlikely that this mechanism alone can account for the experimental observations, given the rather coarse-grained structure of the reaction product layers. For orthorhombic structures such as those of η-$AuSn_4$ and ε-$AuSn_2$ as well as for hexagonal δ-AuSn, one anticipates that the lattice diffusion will display a strong anisotropy.

It is to be remarked here that when local equilibria are attained in the diffusion zone between Au and Sn, the formation of five intermediate phases, viz. ζ-, ζ'- "Au_5Sn", δ-AuSn, ε-$AuSn_2$ and η-$AuSn_4$, is expected according to phase diagram (see Fig. (6.3-2)) [2] during interaction at 180 °C. However, after standard metallographic preparation of the Au/Sn couples, only three intermetallic phases are visible on backscattered electron images of the reaction zone (Fig. (6.3-1)).

It is well documented that sometimes certain phases seem to be missing in a diffusion couple when investigated by microscopic and microprobe analysis [3]. One of the reasons for the absence of an equilibrium phase might be the presence of a barrier layer at the interface, such as, for example, an oxide film at the contact surface or the presence of impurities in the starting materials. Sometimes, the absence of certain

phases might be due primarily to difficulties in nucleation, however, it is important to point out that the apparent absence of a particular intermediate phase in a diffusion zone cannot automatically be interpreted as the result of nucleation problems. It is possible that the phase is present as such a thin layer that it cannot be detected easily by the experimental techniques used.

The apparent absence of the ζ- and ζ'- "Au_5Sn" phases on the micrograph given in Fig. (Fig. (6.3-1)) turned out to be connected with the procedure used for preparation of the samples, and nucleation of the Au-rich phases appeared not to be a problem. When cross-sections of the Au/Sn - couples annealed under the same conditions were prepared with SiO_2 - polishing suspension (OPS™) as a final finish (instead of 0.25 μm diamond slurry), the "missing" phases became visible (Fig. (6.3-3)).

Growth kinetics of the Au-Sn compounds was studied on a series of diffusion couples. It was found that at 180 °C the growth rate of the product layers of δ-, ϵ- and η-phases follows a square root dependence on the annealing time. This generally indicates that diffusion is the rate-limiting step of the intermetallic growth. The parabolic rate constants derived from the thickness measurements are 1.55×10^{-16} m^2/s, 2.28×10^{-16} m^2/s and 4.18×10^{-15} m^2/s for the δ-AuSn, ϵ-$AuSn_2$ and η-$AuSn_4$ intermetallic compounds, respectively.

Prior to annealing of the diffusion couple shown in Fig. (6.3-1), W-particles were introduced between the initial couple halves as fiducial markers. After interaction, the tungsten markers can be seen inside the δ-AuSn- as well as in the η-$AuSn_4$ - phase layer, i.e. two Kirkendall planes are present. From the Kirkendall plane locations and the composition profile across the reaction zone of this couple, the ratio's of volume intrinsic fluxes of the components $\dfrac{|J_{Au}|}{|J_{Sn}|} = \dfrac{D_{Au}V_{Sn}}{D_{Sn}V_{Au}}$ in the intermetallics δ-AuSn and η-$AuSn_4$ were deduced as ~12.7 and 0.024, respectively.

From Fig (6.3-1), one can also see that no Kirkendall marker plane is present in the ϵ-$AuSn_2$ layer, which makes it impossible to assess component mobilities in this ordered structure by means of the standard procedure. Our attempts to obtain the $\dfrac{|J_{Au}|}{|J_{Sn}|}$ - values for the ϵ- phase using incremental diffusion couples were inconclusive due mainly to the
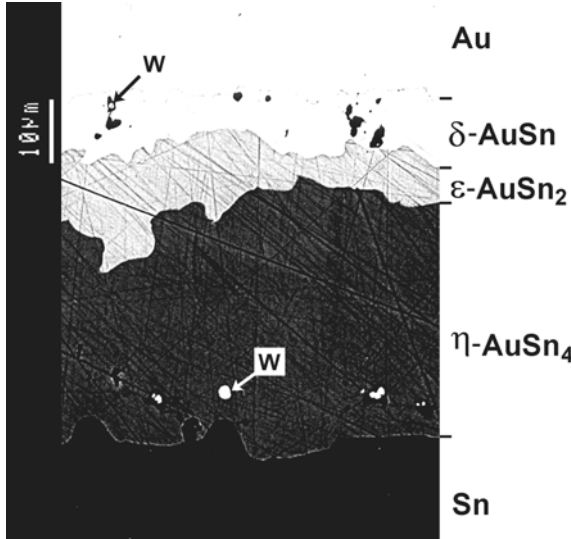
Fig. (6.3-1) BEI of the reaction zone in a Au/Sn couple after annealing in vacuum at 180 °C for 36 hrs. W-particles were used as Kirkendall markers. Only three product layers are visible after standard metallographic preparation using 0.25 μm diamond slurry for the final polishing.
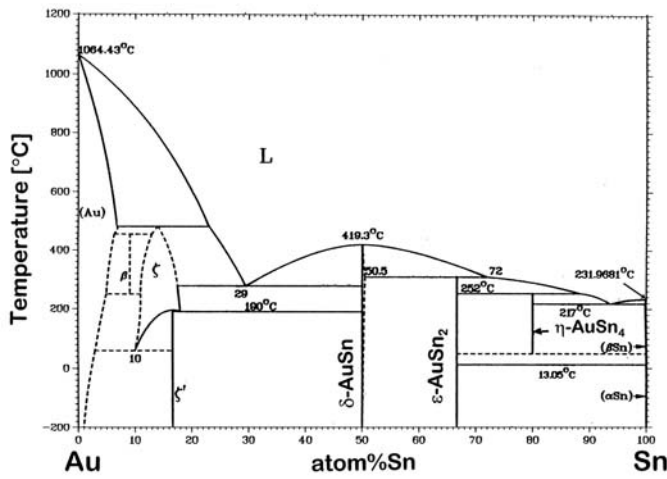
Fig. (6.3-2) Binary Au-Sn phase diagram [2] .
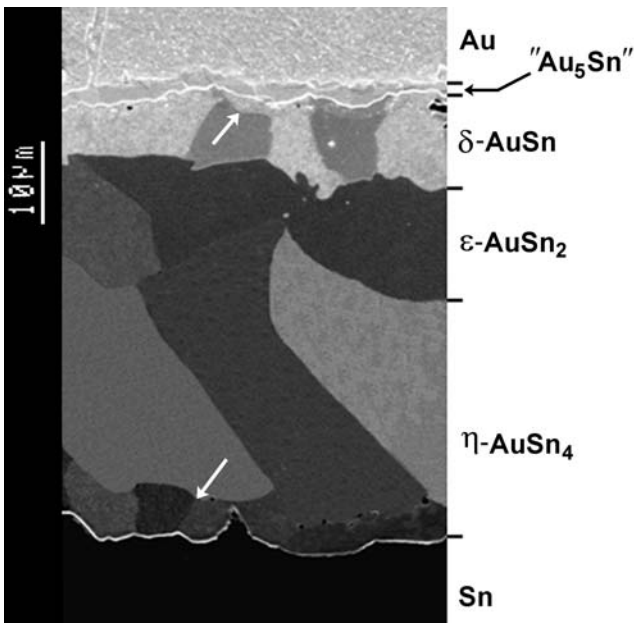
Fig. (6.3-3) BEI of a cross-section of the annealed Au/Sn couple (180 °C; 36 hrs) after polishing with SiO$_2$-suspension (OPS™) as a final finish. The layer of "Au$_5$Sn" is clearly visible.
The positions of the Kirkendall planes are indicated by arrows.

technical difficulties connected with the preparation of well-defined reproducible samples. Nevertheless, as explained before, the ratio of intrinsic fluxes of the diffusing species across the growing layer is related to the stoichiometric coefficients in the equations of the corresponding interfacial reactions. Thus, the question here is: "To what extent is it possible to rationalize diffusional growth of the line-compounds and the Kirkendall effect manifestations in the Au/Sn reaction couples using the alternative physico-chemical approach explained in Chap. 4?"

If for the sake of simplification, we neglect the presence of the "Au$_5$Sn"- layer, then the following reaction scheme can be used for the analysis:
Interface I **-** Sn/AuSn$_4$ on the AuSn$_4$-side:
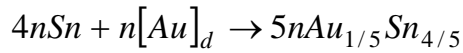
$$4nSn + n[Au]_d \rightarrow 5nAu_{1/5}Sn_{4/5}$$

Interface II-AuSn$_4$/AuSn$_2$ on the AuSn$_4$-side:
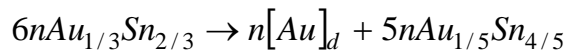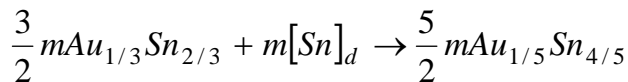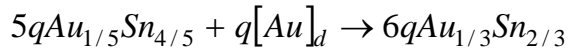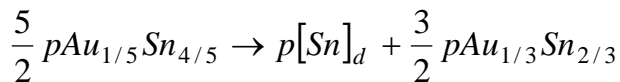
$$\frac{3}{2}mAu_{1/3}Sn_{2/3} + m[Sn]_d \rightarrow \frac{5}{2}mAu_{1/5}Sn_{4/5}$$

$$6nAu_{1/3}Sn_{2/3} \rightarrow n[Au]_d + 5nAu_{1/5}Sn_{4/5}$$

Interface II-AuSn$_4$/AuSn$_2$ on the AuSn$_2$-side:

$$\frac{5}{2}pAu_{1/5}Sn_{4/5} \rightarrow p[Sn]_d + \frac{3}{2}pAu_{1/3}Sn_{2/3}$$

$$5qAu_{1/5}Sn_{4/5} + q[Au]_d \rightarrow 6qAu_{1/3}Sn_{2/3}$$

Interface III-AuSn$_2$/AuSn on the AuSn$_2$-side:

$$2pAu_{1/2}Sn_{1/2} + p[Sn]_d \rightarrow 3pAu_{1/3}Sn_{2/3}$$

$$4qAu_{1/2}Sn_{1/2} \rightarrow q[Au]_d + 3qAu_{1/3}Sn_{2/3}$$

Interface III-AuSn$_2$/AuSn on the AuSn-side:

$$3rAu_{1/3}Sn_{2/3} \rightarrow r[Sn]_d + 2rAu_{1/2}Sn_{1/2}$$

$$3sAu_{1/3}Sn_{2/3} + s[Au]_d \rightarrow 4sAu_{1/2}Sn_{1/2}$$
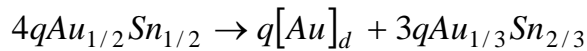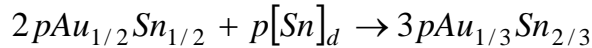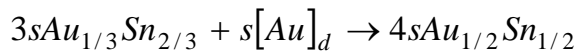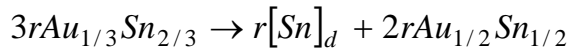
Interface IV- AuSn/Au on the AuSn -side:

$$rAu + r[Sn]_d \rightarrow 2rAu_{1/2}Sn_{1/2}$$
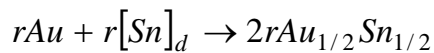
Apparently, the resultant thickness of the product layers depends upon the growth from and at the same time, consumption by the neighbouring layers. The total width of each reaction product ($a+b$, $c+d$ and $e+f$ in Fig. (Fig. 6.3-4)), however, always increases (parabolically) with time.
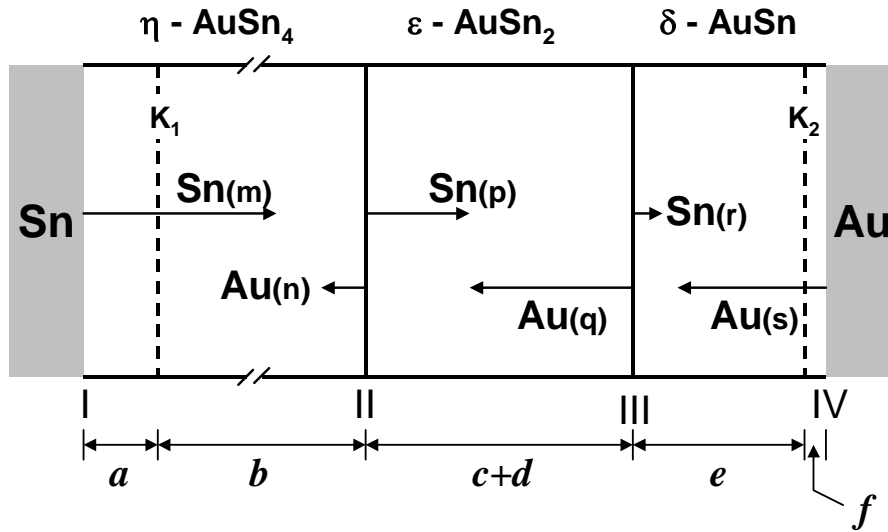
Fig. (6.3-4) Schematic illustration of the growth of diffusion layers in a binary Au/Sn couple

Before proceeding further, one important experimental finding has to be mentioned. Returning to Fig. (6.3-3), one can note a "duplex" grain morphology developed in the δ-AuSn and η-AuSn₄ product layers. This microstructural feature is now understood as a manifestation of the Kirkendall effect (see Chap. 4), and can be explained (qualitatively) by considering the different nucleation sites of the grains in the growing phase layer using chemical reaction equations as a starting point. The AuSn- as well as AuSn₄-intermetallic is growing from two sides with a different type of nucleation, and these differently nucleated grains meet at the Kirkendall plane. Therefore, the location of the (stable) Kirkendall plane(s) inside the multiphase diffusion zone can be identified by the boundary between the different grain morphologies within the microstructure of the polycrystalline reaction product(s). This "demarcation line" separating the sub-layers coincides with the position of the Kirkendall markers. This phenomenon was found to be independent of the presence of any inert particles (markers).

The δ-AuSn and η-AuSn₄ product layers in the Au/Sn couple can be considered as if each of them were composed of two domains bounded by the Kirkendall plane and the interphase interfaces. The thickness of the parts of the intermetallic layers growing on either side of the Kirkendall plane (a, b and e, f in Fig. (6.3-4)) can be expressed in terms of the coefficients m, n, p, q, r, s and molar volume of the phase involved ($V_m^{AuSn_4} = 14.99$ cm³/mole; $V_m^{AuSn} = 13.44$ cm³/mole [3]):

$$V_m^{AuSn_4} \times 5n = a$$

$$V_m^{AuSn_4} \times \left(\frac{5}{2}m + 5n - \frac{5}{2}p - 5q\right) = b$$

$$V_m^{AuSn} \times (2r + 4s - 2p - 4q) = e \qquad \text{(6.3-1)}$$

$$V_m^{AuSn} \times 2r = f$$

On the other hand, the "*uniform*" crystal morphology of the product layer of the ε-AuSn$_2$ is indicative for the absence of a Kirkendall plane (see Chap. 4). Although no (stable) Kirkendall plane exists in the AuSn$_2$, it is also possible to think of this product layer as if it consists of two parts with (unknown) thicknesses (c and d in Fig. ((6.3-4)) related to the stoichiometric coefficients in the pertinent reaction equations and the molar volume of the ε- phase ($V_m^{AuSn_2} = 14.38$ cm^3/mole [3]). It follows that

$$V_m^{AuSn_2} \times \left(\frac{3}{2}p + 6q - \frac{3}{2}m - 6n\right) = c$$

$$\text{(6.3-2)}$$

$$V_m^{AuSn_2} \times (3p + 3q - 3r - 3s) = d$$

Note that depending upon the relative rate of a diffusion-controlled formation (and consumption) of the AuSn$_2$ - phase on either side of the AuSn$_2$/AuSn - and AuSn$_4$/AuSn$_2$ - interfaces, one of the values of c and d can be negative.

Let us again turn our attention to the Au/Sn couple annealed at 180 °C for 36 hrs (Fig. (6.3-1)). The corresponding average values of a, b, e and f are 4.45, 32.6, 6.51 and 2 μm, respectively, and the width of the ε-AuSn$_2$-phase in the reaction zone (i.e. $c+d$) was measured as 8.9 μm. In order to examine the Kirkendall marker behaviour in this couple, two limiting cases are to be considered:

I) In the diffusion-controlled interaction, the rate of consumption of AuSn$_2$ on the AuSn-side of the AuSn$_2$/AuSn-inerface ($3r+3s$) resulting in the production of the AuSn-intermetallic is higher than its formation from the AuSn-phase ($3p+3q$). This means that $c \geq 8.9$ μm and $d \leq 0$. If we take $c = 8.9$ μm and $d = 0$, then the set of Eq. (6.3-1 and 6.3-2) yields (in mole/m^2) the following values for the stoichiometric coefficients $m = 2.47$, $n = 0.06$, $p = 0.32$, $q = 0.70$, $r = 0.074$ and $s = 0.094$. Accordingly, the ratio of

volume intrinsic fluxes, $\dfrac{|J_{Au}|}{|J_{Sn}|} = \dfrac{D_{Au}V_{Sn}}{D_{Sn}V_{Au}}$, in the binary intermetallic at 180 °C are found

to be $m/n = 0.024$ in η-AuSn$_4$, $s/r = 12.70$ in δ-AuSn and $q/p \geq 2.19$ in ε-AuSn$_2$.

One can see that the results for the η-AuSn$_4$ and δ-AuSn products are consistent with those obtained on the basis of standard analysis of the Kirkendall effect in the annealed Au/Sn-couple, which could not be otherwise, since both models describe the same phenomenological process in terms of purely phenomenological quantities. This, in fact, underlines the equivalence of the diffusion based and physico-chemical approaches used.

II) Another alternative can be suggested. That is $c \leq 0$ and $d \geq 8.9$ μm. This implies that the consumption of AuSn$_2$ on the AuSn$_4$-side of the AuSn$_4$/AuSn$_2$-interface ($\dfrac{3}{2}m + 6n$) is faster than the formation of this phase on another side of the reaction interface ($\dfrac{3}{2}p + 6q$). For this limiting case we found (in mole/m^2) that m = 2.47, n = 0.06, p = 0.73, q = 0.49, r = 0.074 and s = 0.094, and the ratio of volume intrinsic fluxes across the growing AuSn$_2$-layer was determined as $\dfrac{|J_{Au}|}{|J_{Sn}|} = \dfrac{D_{Au}V_{Sn}}{D_{Sn}V_{Au}} = \dfrac{q}{p} \leq 0.67$. Now, the values of the Kirkendall velocities in the product layers developed in the annealed Au/Sn couple can be obtained in a rather straightforward way

$$2tv = -2t(V_{Sn}J_{Sn} + V_{Au}J_{Au})$$ (6.3-3)

Further calculations can be simplified considerably, if we assume that partial molar volumes of diffusing species in each binary Au-Sn intermetallic are equal to the molar volume of this phase, i.e. $V_{Sn} = V_{Au} = V_m$. With these assumptions Eq. (6.3-3) takes on the following forms:

for the AuSn$_4$-layer: $V_m^{AuSn_4} \times (n - m) = 2tv_K^{AuSn_4} = x_K^{AuSn_4}$, and

for the AuSn-layer: $V_m^{AuSn} \times (s - r) = 2tv_K^{AuSn} = x_K^{AuSn}$.

For the annealed Au/Sn-couple (180 °C; 36 hrs), the co-ordinates of the Kirkendall plane in these products were found to be $x_K^{AuSn_4}$ = -36.13 μm and x_K^{AuSn} = 11.64 μm. The corresponding values of the Kirkendall velocities, computed through the last two

equations, are -1.28×10^{-10} m/s and 4.5×10^{-11} m/s in the AuSn$_4$- and AuSn-product layer, respectively.

III) An analogous procedure can be used to estimate a magnitude of the Kirkendall velocity in the AuSn$_2$-layer as well. For the first limiting case, one finds

$$2tv_K^{AuSn_2} \geq x_K^{AuSn_2} \geq V_m^{AuSn_2} \times (q - p) \geq 5.46 \ \mu m , \text{ and } v_K^{AuSn_2} \geq 2.13 \times 10^{-11} \ m/s .$$

Similarly, for the second limiting case:

$$2tv_K^{AuSn_2} \leq x_K^{AuSn_2} \leq V_m^{AuSn_2} \times (q - p) \leq -3.45 \ \mu m , \text{ and } v_K^{AuSn_2} \leq -1.3 \times 10^{-11} \ m/s .$$

Again, as in the previous case of the Cu/Sn couple, the position of the plane within the diffusion zone of the annealed couple where the Kirkendall markers were situated at time $t = 0$ (i.e. $x_o = 0$), was found by subjecting the corresponding composition profile to the Sauer-Freise treatment. Using the experimental results and assessments outlined in this section, the Kirkendall velocity diagram pertain to the Au/Sn diffusion couple, annealed at 180 °C for 36 hrs, was constructed (Fig. (6.1-5)). One can see that the line $2tv_K = x_K$ intersects the velocity plot twice in the domains of the reaction zone corresponding to the single-phased product layers of η-AuSn$_4$ and δ-AuSn intermetallics. This means that two (microstructurally stable) Kirkendall planes will emerge upon interdiffusion, one in the η- and one in the δ-phase layer, as was indeed observed experimentally (Fig. (6.3-1 and 6.3-2). The value of $2tv$ for the AuSn$_2$-phase lays somewhere in the shaded areas of Fig. (6.1-5).
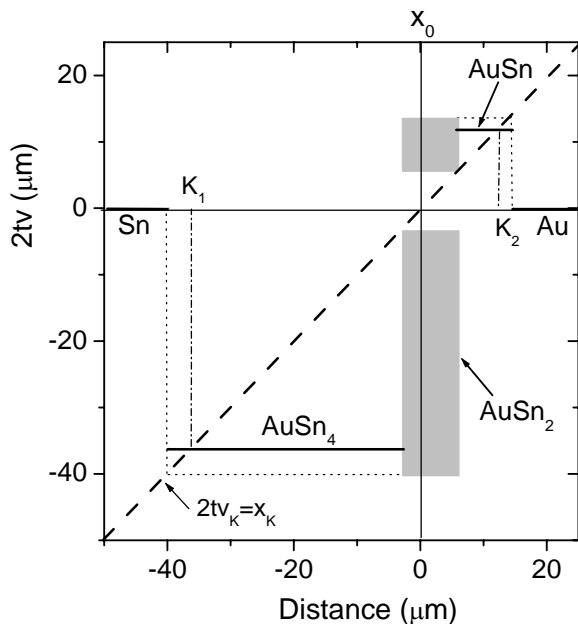
Fig. (6.3-5) The Kirkendall velocity diagram constructed for the Au/Sn diffusion couple annealed at 180 °C for 36 hrs. The straight-line $2tv_K = x_K$ intersects the velocity plot twice (at the positions K$_1$ and K$_2$), i.e. the Kirkendall plane bifurcates. The shaded areas indicate the possible values of the Kirkendall velocity in the ε-AuSn$_2$ product layer.
Note that the Kirkendall marker velocity in the AuSn$_2$-phase can not be higher than the velocity of the moving Sn/AuSn$_4$ and AuSn/Au interfaces.

6.4 Concluding remarks

The examples given in this paper show quite clearly that an understanding of the Kirkendall effect manifestations has great potential for providing insights into the finer nuances of multiphase diffusion.

The manifestations of the Kirkendall effect and its role in morphological evolution of the reaction zone associated with the nucleation and growth of the product intermetallic layers in Cu/Sn and Au/Sn binary systems could be explained in terms of an alternative theory considering the diffusion-controlled interactions at the interphase interfaces.

However, much remains to be learned about the Kirkendall effect manifestations accompanying multilayer growth in the Cu/Sn and Au/Sn systems. For example, the diffusion anisotropy of the Cu-Sn and Au-Sn intermetallics may render the analysis of the Kirkendall marker migration rather cumbersome, and the possible contribution of the grain boundaries in the overall diffusion transport in product layers at these low temperatures may add even more complexity to the phenomenological description.

Undoubtedly, results of the present study are of importance for a broad engineering community dealing with the reliability of electronic devices. The Kirkendall plane is a notoriously problematic microstructural feature in any joint, because of higher mechanical failure risk at this plane. Also, the realization that the Kirkendall plane can be multiple, which suggests that diffusion porosity may develop at more than one location inside the interconnect, now opens this field to exploration.

References

1. J. Kloeser, E. Zakel, F. Bechtold and H. Reichel, Reliability investigations of fluxless flip-chip interconnects on green tape ceramic substrates, IEEE A, **19** (1996) 24-32
2. Th. Massalski (Ed.), Binary Alloy Phase Diagrams, American Society for Metals, Ohio (1986)
3. P. Villars, L. Calvert, Pearson's Handbook of Crystallographic Data for Intermetallic Phases, American Society for Metals, Ohio (1985)

Appendix

Diffusion in a binary solid state system

A.1 The basic concepts

In metallurgy many physical processes are controlled by diffusion, such as homogenisation, non-martensitic transformation, precipitation, oxidation and sintering. Sir W. C. Roberts, in 1896, for the first time reported the systematic study of diffusion of gold in solid lead [1]. In almost all the structural applications containing heterogeneous materials systems diffusion is ubiquitous at elevated and even in many cases at ambient temperature, depending on the material systems. An understanding of this process is crucial in a wide variety of research fields, ranging from (relatively) bulk applications as in composite materials or coatings to very thin metallization films in microelectronics. Basically there are two approaches to study diffusion in solid state, the *atomistic approach*, where the nature of the diffusing species in atomic level is explicitly considered and the *continuum approach*, where the diffusing substance is treated as continuous medium, ignoring the nature of diffusion in atomic level. Advantage of the latter approach is that one can analyse and predict the micro and or macroscopic physico-chemical changes in applications without going to rather complicated atomistic model. Extensive research is going on to understand the atomistic models, however we shall refrain ourselves from going into the details of these interesting models where still many questions are to be addressed.

A.2 Fick's laws

Adolf Fick proposed the phenomenological diffusion theory [2]. If we consider the flux of particles (atoms, molecules, ions etc) in a one-dimensional system because of a concentration gradient, it can be expressed as,

$$J = -D\left(\frac{\partial C}{\partial x}\right)$$
(A.2-1)

where J (mole/m^2/s) is the flux, D (m^2/s) is the diffusion coefficient, C (mole/m^3) is the concentration and x (m) is the position parameter. The negative sign stems from the fact that diffusion occurs in the direction opposite to the increasing concentration gradient.

Fick's first law prevails only in the cases of steady states as shown in Fig. (A.2-1) where composition does not change with time. However, if composition changes with time at a particular position, as shown in Fig. (A.2-2), Fick's second law should be used, which was derived from the Fick's first law and law of mass conservation:

$$\frac{\partial C}{\partial t} = -\frac{\partial J}{\partial x} = \frac{\partial}{\partial x}\left(D\frac{\partial C}{\partial x}\right)$$

(A.2-2)

where t is time(s).
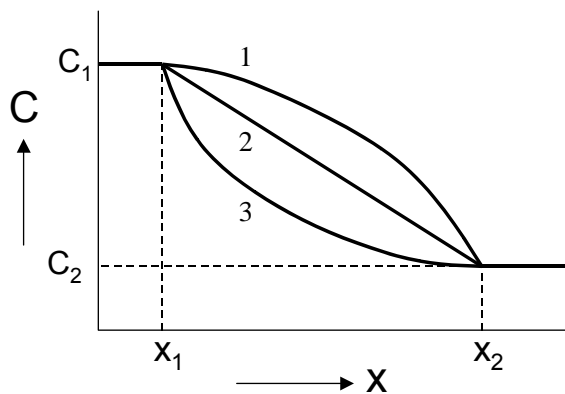
Fig. (A.2-1) Concentration profile of a system where concentration is always same (can be like 1, 2 or 3) with respect to position at any time.
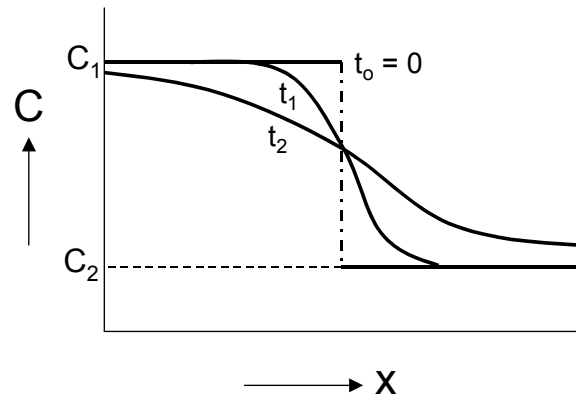
Fig. (A.2-2) Concentration profile of a system where concentration changes with respect to position with time ($t_2 > t_1 > t_o$).

If D is not a function of position (or composition) and the diffusion distance is short relative to dimensions of the initial inhomogeniety in an infinite systems, one can find the solution for $C(x,t)$ in terms of error functions. In "small" systems, where complete homogenisation is approached, one can treat the same by "separation of variables". For extensive treatments one can go through the classical book written by J. Crank [3].

A.3 Interdiffusion coefficient

From experiments in early 20th century, it was evident that the diffusion coefficient in solid-state is not constant, but is a function of *composition* and *temperature* [4, 5]. In structural applications very often two materials of different compositions are in contact with each other at a temperature when interdiffusion takes place through an interfacial product layer. The composition changes in a particular position because of the concentration gradient, and the interdiffusion coefficient, $\tilde{D}$ also changes along the sample with composition. The interdiffusion coefficient relates the interdiffusion flux $\tilde{J}_i$ with the concentration gradient by $\tilde{J}_i = -\tilde{D}\dfrac{\partial C_i}{\partial x}$; i = components A or B. The interdiffusion fluxes are defined in the laboratory-fixed frame of reference (see section A.8). The interdiffusion coefficient $\tilde{D}$ is, in general, a function of composition and, therefore, of x $\left(\tilde{D} = \tilde{D}(x)\right)$ and Fick's second law can be written as

$$\frac{\partial C}{\partial t} = \frac{\partial}{\partial x}\left(\tilde{D}\frac{\partial C}{\partial x}\right) = \frac{\partial \tilde{D}}{\partial x}\frac{\partial C}{\partial x} + \tilde{D}\frac{\partial^2 C}{\partial x^2} \qquad\qquad \text{(A.3-1)}$$

The term $\partial \tilde{D}/\partial x$ makes the equation inhomogeneous, and the solution in closed form is not possible.

However, instead of finding solution for *C(x,t)*, one can find the solution for $\tilde{D} = \tilde{D}(C)$ and this treatment is known as Matano-Boltzmann analysis.

A.4 Some standard and thermodynamical relations

Before proceeding further, we shall consider a few standard and thermodynamical relations for a binary system of species A and B, which will be used very frequently in the proceeding sections (some derivations can be found in Ref. [6]):

$$N_A + N_B = 1 \qquad\qquad \text{(A.4-1)}$$

where N_A and N_B are the mole fractions of A and B.

$$C_A = \frac{N_A}{V_m}; \qquad\qquad C_B = \frac{N_B}{V_m} \qquad\qquad \text{(A.4-2)}$$

where C_i is the concentration of species i and V_m is the molar volume.

$$N_A V_A + N_B V_B = V_m \qquad\qquad \text{(A.4-3)}$$

where V_i is the partial molar volume of the species i.

$$C_A + C_B = \frac{1}{V_m} \qquad\qquad\qquad \text{(A.4-4)}$$

$$C_A V_A + C_B V_B = 1 \qquad\qquad\qquad \text{(A.4-5)}$$

$$N_A dV_A + N_B dV_B = 0 \qquad\qquad\qquad \text{(A.4-6)}$$

$$C_A dV_A + C_B dV_B = 0 \qquad\qquad\qquad \text{(A.4-7)}$$

$$V_A dC_A + V_B dC_B = 0 \qquad\qquad\qquad \text{(A.4-8)}$$

$$dC_A = \left(\frac{V_B}{V_m^2}\right) dN_A; \qquad\qquad dC_B = \left(\frac{V_A}{V_m^2}\right) dN_B \qquad\qquad \text{(A.4-9)}$$

A.5 Matano-Boltzmann analysis for the interdiffusion coefficient (applied to systems where the total volume does not change with reaction/mixing):

The Matano-Boltzmann analysis is used frequently by researchers to study diffusion in the solid-state. By this method one can measure interdiffusion coefficients, $\tilde{D}$, at different compositions from the concentration profile measured by microprobe analysis. However, this method is restricted to systems where the *partial molar volumes of the components are constant*, i.e. *the total volume does not change with reaction and mixing* (see A.6). Consider the case, when two materials with initial compositions C_B^- and C_B^+ are coupled and annealed for reasonably short time, t, such that after annealing, still some part of the end-members is not affected by the diffusion process as shown in Fig. (A.5-1a). Boundary conditions can be written

$$C_B = C_B^- \qquad for \quad x \langle 0 \quad at \quad t = 0$$
$$C_B = C_B^+ \qquad for \quad x \rangle 0 \quad at \quad t = 0 \qquad\qquad \text{(A.5-1)}$$

where "-" and "+" represents the left- and right-hand end of the reaction couple. Boltzmann [7] introduced the variable

$$\lambda = \lambda(C_B) = x / t^{\frac{1}{2}} \qquad\qquad\qquad \text{(A.5-2)}$$

which means that C_B is a function of λ only. This relation states that all compositions in a diffusion zone move parabolically in time with respect to one fixed frame of reference.
By using the definition of λ,

$$\frac{\partial C_B}{\partial t} = \frac{\partial C_B}{\partial \lambda}\frac{\partial \lambda}{\partial t} = -\frac{1}{2}\frac{x}{t^{\frac{3}{2}}}\frac{\partial C_B}{\partial \lambda}$$

$$\frac{\partial C_B}{\partial x} = \frac{\partial C_B}{\partial \lambda}\frac{\partial \lambda}{\partial x} = \frac{1}{t^{\frac{1}{2}}}\frac{\partial C_B}{\partial \lambda}$$

(A.5-3)

Transforming Eq. (A.5-3) in Fick's second law (Eq. (A.2-2))

$$-\frac{x}{2t^{\frac{3}{2}}}\frac{\partial C_B}{\partial \lambda} = \frac{\partial}{\partial x}\left(\frac{\tilde{D}}{t^{\frac{1}{2}}}\frac{\partial C_B}{\partial \lambda}\right) = \frac{1}{t}\frac{\partial}{\partial \lambda}\left(\tilde{D}\frac{\partial C_B}{\partial \lambda}\right)$$

By using Eq. (A.5-2)

$$-\frac{\lambda}{2}\frac{\partial C_B}{\partial \lambda} = \frac{\partial}{\partial \lambda}\left(\tilde{D}\frac{\partial C_B}{\partial \lambda}\right)$$

(A.5-4)

This treatment is known as Boltzmann transformation and this transformation was used for the first time by Matano [8] to study interdiffusion in the solid-state.

Initial conditions at time $t = 0$ can be written as considering Eq. (A.5-2),

$$C = C_B^- \quad at \quad \lambda = -\infty$$

$$C = C_B^+ \quad at \quad \lambda = +\infty$$

(A.5-5)

Eq. (A.5-4) contains only total differentials and $\partial \lambda$ can be cancelled from both sides. Integrating between initial composition C_B^- to the concentration of interest to measure the interdiffusion coefficient, $\tilde{D}$, at C_B^* ($C_B^- < C_B^* < C_B^+$) leads to

$$-\frac{1}{2}\int_{C_B^-}^{C_B^*}\lambda dC_B = \tilde{D}\frac{dC_B}{d\lambda}\bigg|_{C_B^-}^{C_B^*}$$

(A.5-6)

The data is always measured at some fixed time so that t is constant. If we assume that after annealing the ends of the couple are not affected then $dC_B/dx = 0$ at C_B^- and C_B^+. Using Eq. (A.5-2) one can write,

$$-\frac{1}{2}\int_{C_B^-}^{C_B^*}x dC_B = \tilde{D}t\frac{dC_B}{dx}\bigg|_{C_B^-}^{C_B^*} = \tilde{D}t\left(\frac{dC_B}{dx}\right)_{C_B^*}$$

or,

$$\tilde{D}\left(C_B^*\right) = -\frac{1}{2t}\left(\frac{dx}{dC_B}\right)_{C_B^*}\int_{C_B^-}^{C_B^*}x dC_B$$

(A.5-7)

and

101

$$\int_{C_B^-}^{C_B^+} x \, dC_B = 0 \tag{A.5-8}$$

Eq. (A.5-8) defines the plane $x_M = 0$, the initial contact plane between the end-members, called the *Matano plane*.

The Matano plane position, x_M, can be determined from the concentration penetration curve of the system measured by X-ray microanalysis by equalising the area P and Q as shown in Fig. (A.5-1b).
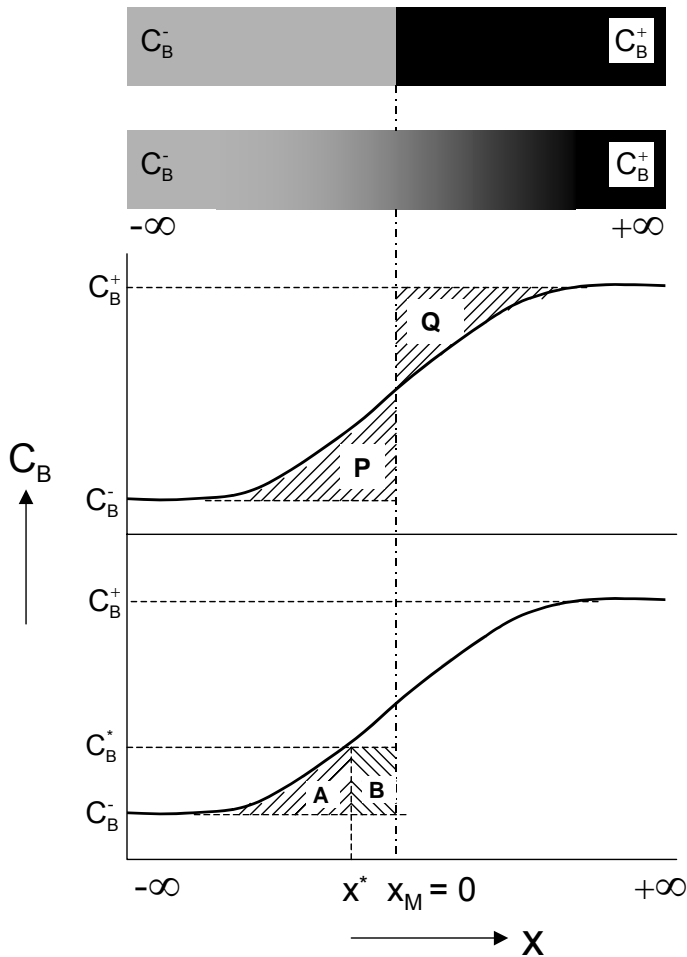
Fig. (A.5-1a) Diffusion couple with end member compositions C_B^- and C_B^+ before and after annealing for time t.

(1b) Matano plane $x_M = 0$ can be found by equalizing the areas P and Q.

(1c) The value of the integral in Eq. (A.5-7) is equal to the shaded area (A+B) as shown in Eq. (A.5-10).

After integrating by parts, Eq. (A.5-7) can be written as,

$$\tilde{D}(C_B^*) = -\frac{1}{2t}\left(\frac{\partial x}{\partial C_B}\right)_{C_B^*}\left[x^*(C_B^* - C_B^-) - \int_{-\infty}^{x^*}(C_B - C_B^-)dx\right] \tag{A.5-9}$$

From Fig. (A.5-1c), the interdiffusion coefficient can be expressed in terms of shaded area as,

$$\tilde{D}\left(C_B^*\right) = \frac{1}{2t}\left(\frac{\partial x}{\partial C_B}\right)_{C_B^*}\left[A + B\right] \qquad\qquad\text{(A.5-10)}$$

The main disadvantage of this analysis is that one has to find the position of the Matano plane, x_M. When the total volume does not change with reaction/mixing, this is easy to determine. However, when the total volume changes, determining the initial contact plane (denoted by x_o) is rather confusing (see section (A.6, A.19)).

A.6 Effect of change in total volume with reaction/mixing

Most of the real systems, in diffusion, are affected by a change in total volume. The effect could be very minor to considerable, depending on the deviation of molar volume from the ideal case. Let us consider an ideal system, as shown in Fig. (A.6-1a): the partial molar volumes V_A and V_B of the components A and B, respectively are always fixed, in both the cases, 1 (where $V_A = V_B = V_m$) or 2 (where $V_A \neq V_B$ but constant for all compositions). In this case the total volume does not change and there will be no difference in length in the diffusion couple sample after annealing for time, t. However, in almost all real systems the molar volume deviates from ideality (dashed line) as shown in Fig. (A.6-1b and -1c). In the case of Fig. (A.6-1b), there is a negative deviation from ideality and the total volume of the reaction/mixing product between end members N_B^- and N_B^+ will decrease, so that it will result into shrinkage of the diffusion couple specimen as shown in Fig. (A.6-1b). In the case of Fig. (A.6-1c), because of a positive deviation from ideality, the total volume will increase with reaction/mixing and there will be swelling of the specimen. In non-ideal cases, the partial molar volumes of the components can be found from the gradient in the V_m vs. N_B plot at the point of interest and by extending it to N_B *zero* and *one*. As shown in Fig. (A.6-1b) and (A.6-1c) the partial molar volumes of A and B at N_B^* are V_A^* and V_B^*, and are related to the molar volume at N_B^* by $V_m^* = N_A V_A^* + N_B V_B^*$.

In the ideal case, when there is no change in total volume (i.e. partial molar volumes of the components do not change), one can easily find out the initial contact plane (called Matano plane), x_M, following the procedure shown in Fig. (A.5-1b), so that Matano-Boltzmann method can be used to analyse for the interdiffusion coefficient. However, when total volume changes with reaction/mixing, the position of the initial contact plane (denoted by x_o) becomes vague as *one will find two different values*, depending on whether it is determined from -∞ or from +∞ side (see section A.19). For these cases

one should follow the method shown in the section A.9 to determine interdiffusion coefficients, when there is no need to define the initial contact plane.

(a)   (b)   (c)
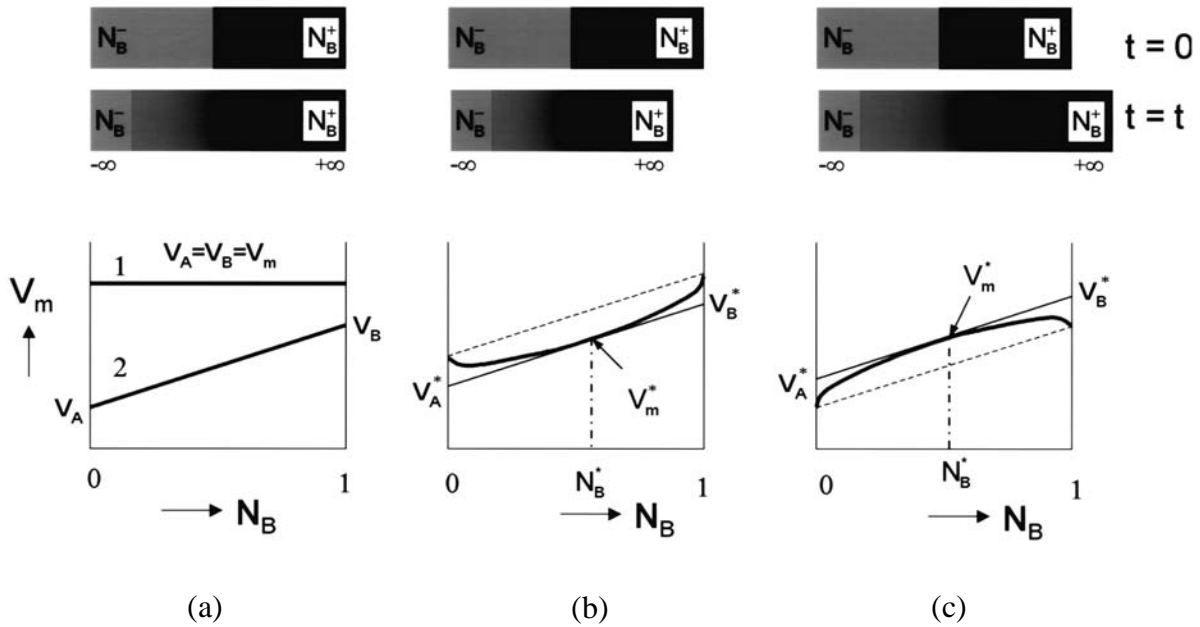
Fig. (A.6-1a) The ideal cases, like 1 or 2, when partial molar volumes of the components are always fixed and there will be no change in total volume in the diffusion couple after reaction/mixing.

(1b) when the molar volume deviates negatively from ideality (dotted line), the diffusion couple specimen shrinks, after annealing for time, t. The partial molar volumes of A and B at N_B^* are V_A^* and V_B^*.

(1c) when the molar volume deviates positively from ideal case (dotted line), diffusion couple specimen swells, after annealing for time, t. The partial molar volumes of the components at N_B^* are V_A^* and V_B^*.

A.7 Kirkendall effect

By the Matano-Boltzmann analysis one can quantify the interdiffusion coefficient, $\tilde{D}$, which is, in fact, a kind of average diffusivity of the elements, and it does not shed light on the diffusivities of the species, separately. In the early stage, it was common belief among researchers that diffusivities of the species are the same. In 1929 Pfiel [**9**] reported one peculiar phenomenon while studying oxidation of iron and steel:

"It had frequently been noticed that small particles of foreign matter (such as pieces of muffle) falling on the surface of oxidising iron were gradually buried. The scale grew up round these particles until they finally disappeared beneath the surface, but they could afterwards be found by breaking up the layer of scale".

These foreign particles were inert to the diffusing species, iron and oxygen and this observation reflected that iron diffuses through the oxide scale to the surface, where it reacts with oxygen to form oxide.

Hartley [10] was the first to use purposely foreign inert particles, titanium dioxide, in an organic acetone/cellulose-acetate system, to study the inequality of the diffusing species. Shortly after that Smigelkas and Kirkendall [11] used the same technique to examine the inequality of diffusivities of the species in the Cu-Zn system by introducing molybdenum as an inert marker. Researchers dealing with metallic systems at that time were not familiar with Hartley's work and the effect of inequality of diffusivities on the inert marker was named as the Kirkendall effect [12].

In the experiment by Smigelkas and Kirkendall, a rectangular bar (18×1.9 cm^2) of 70-30 wrought brass (70wt%Cu-30wt%Zn) was taken. This bar was ground and polished and then 130 μm diameter molybdenum wires, which are inert to the system, were placed on opposite sides of the surfaces. Then a copper layer of 2500 μm was deposited on that, as shown in Fig. (A.7-1). This couple was subjected to annealing at 785 °C. After annealing for a certain time one small piece was cross-sectioned to examine and the rest of the part was annealed further. Following this method, it was possible to get specimens at different annealing times. With annealing, α-brass grows in between and after etching, the distance between the markers was measured. If the diffusivities of copper and zinc are the same and there is no change in volume during diffusion/reaction, marker should not move and stay at the original position.

However, after measuring, it was clear that with increasing annealing time, the distance between markers decreases parabolically with time. Considering the change in the lattice parameter, it was found that only 1/5th of the displacement occurred because of molar volume change. This shift was explained by Kirkendall as [11]:

"The movement of the insoluble molybdenum wire was conclusive evidence that the alpha brass was being forced back as a whole (or attracted back) as a result of the diffusing out of the zinc atoms individually".

From this study two conclusions were drawn which had enormous impact at that time on solid-state diffusion:

1. *The rate of diffusion of zinc is much greater than that of copper in alpha brass, and*

2. *When zinc diffuses more rapidly then copper in alpha brass, the interface shifts to compensate at least partially for the diffusion rate.*
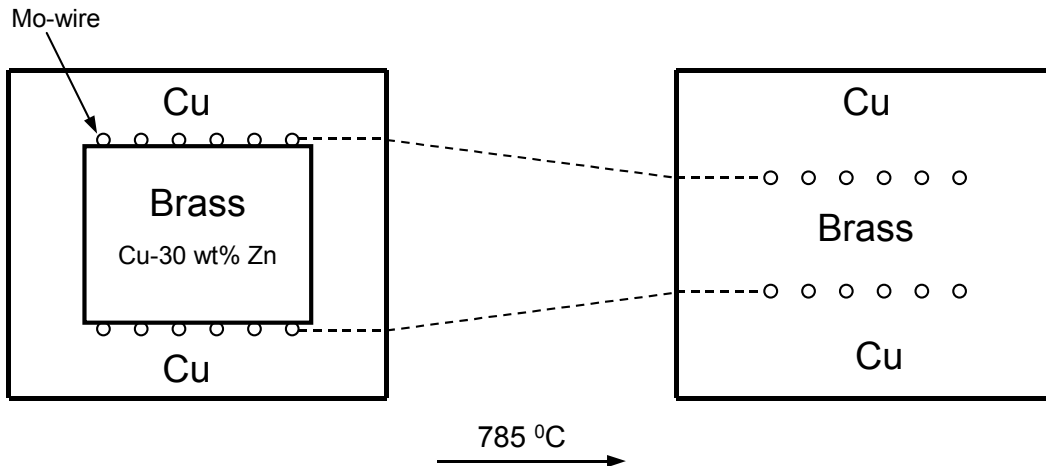
Fig. (A.7-1) Schematic representation of a cross-section of the diffusion couples prepared by Smigelkas and Kirkendall [11] before and after annealing at 785 °C. Molybdenum wires moved closer to each other with increasing time, t.

Till then, direct exchange or ring mechanisms were accepted as diffusion mechanism in the solid-state as shown in Fig. (A.7-2-a, -b). If any of these mechanisms would be true then diffusivities of the species should be the same. However, from the Kirkendall's experiment, it is evident that Zn diffuses faster than Cu, which results into the movement of the markers. When zinc diffuses away, all the sites are not occupied by the flow of Cu from opposite direction and because of that vacant sites are left unoccupied. In other sense, there should be a flow of vacancies opposite to the faster diffusing species Zn to compensate for the difference between the Zn and Cu flux. Vacancies will flow towards the brass side and excess Zn will diffuse towards the Cu-side. Ultimately, this results into shrinking in the brass side and swelling in the copper side so that markers move to the brass side. In some diffusion reactions pores can be found in the product phase (see for example Fig. (4.1-2b, 6.1-2 and 6.2-2). If there is not enough plastic relaxation during the process, vacancies will coalesce to form pores or voids in the reaction layer.

From this experiment, it was clear that diffusion occurs by a vacancy mechanism and after that the direct exchange and ring mechanisms were abandoned. At first this work was highly criticized but later this phenomenon was confirmed from experiments on many other systems [13]. Readers, interested on the historical developments are advised to read the article by Nakajima [14] and da Silva followed by comments from Kirkendall [15]. In fact, five years before Kirkendall's publication, Huntington and Seitz [16] already showed that diffusion occurs by the vacancy mechanism, not by direct exchange, but at that time this work was overlooked.
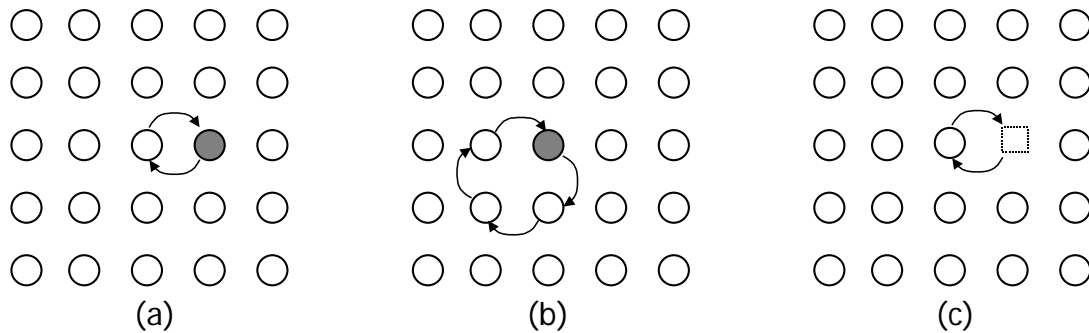
Fig. (A.7-2) Atomic diffusion mechanisms: a) direct exchange mechanism, b) ring mechanism and c) vacancy mechanism.

The impact of Kirkendall's work, at that time, can be realized from R. F. Mehl's [17] comment on his work,

"If verified, this "Kirkendall effect" would greatly modify not only the treatment of diffusion data but also the theory of mechanism of diffusion. It would, for example, be no longer possible to represent diffusion data in a substitutional solid solution by one coefficient, applying to both metal atoms since the separate coefficients are equal, but one would have to show two coefficients, one each for each of the two metal atoms."

A.8 Darken analysis: relation between interdiffusion and intrinsic diffusion coefficients

From Kirkendall's experiment it was clear that the diffusion process in solid solutions cannot be described by one diffusion coefficient, rather, one has to determine the diffusivity of both the species. This was treated mathematically by Darken [18]. Almost

at the same time, Hartley and Crank [19] studied the same subject and they named the diffusivities of species as *intrinsic diffusion coefficient*. Seitz [20] and Bardeen [21] studied the solid-state diffusion process more extensively.

Let us consider a binary diffusion couple of species A and B, of the compositions N_B^- and N_B^+, as shown in Fig. (A.8-1). Before annealing fiducial (inert) markers are introduced at the initial bonding interface and annealed at elevated temperature so that interdiffusion takes place. When interdiffusion starts, the markers will be trapped at a certain fixed composition and cannot escape at later stage so that they move along with that fixed composition. If the intrinsic diffusivity of B (D_B) is higher than the intrinsic diffusivity of A (D_A) at that marker plane (called Kirkendall plane), then the Kirkendall marker plane will move to the right hand side from the initial contact interface, $x_{M/o}$. Matano plane, x_M is the initial contact interface when there is no change in total volume and is fixed with respect to the ends of the diffusion couple. This initial contact plane is denoted by x_o when volume changes upon reaction/mixing (see A.19).

The intrinsic molar flux at the Kirkendall plane can be expressed by Fick's first law as,

$$J_A = -D_A \left(\frac{\partial C_A}{\partial x} \right)_K ; \qquad J_B = -D_B \left(\frac{\partial C_B}{\partial x} \right)_K \qquad \text{(A.8-1)}$$

This Kirkendall reference plane, x_K, is not fixed but moves relative to the laboratory frame of reference. If we consider that this Kirkendall plane moves from $x_{M/o} = 0$ with a velocity, v_K, then the relation between interdiffusion fluxes, $\tilde{J}_A$ and $\tilde{J}_B$ (measured with respect to $x_{M/o}$) and intrinsic diffusion fluxes, J_A and J_B (measured with respect to the Kirkendall frame of reference at the position x_K) can be written as,

$$\tilde{J}_A = J_A + v_K C_A ; \quad \tilde{J}_B = J_B + v_K C_B \qquad \text{(A.8-2)}$$

where $\tilde{J}_A$ and $\tilde{J}_B$ are related by (using Eq. (A.4-8))

$$\tilde{J}_A = -\tilde{D} \left(\frac{\partial C_A}{\partial x} \right) = \frac{V_B}{V_A} \tilde{D} \frac{\partial C_B}{\partial x} = -\tilde{J}_B \frac{V_B}{V_A} \qquad \text{(A.8-3)}$$

In terms of volume flux (volume flux = partial molar volume of component, $V_i \times$ molar flux),

$$J_A^{vol} = V_A \tilde{J}_A = V_A J_A + v_K V_A C_A ; \quad J_B^{vol} = V_B \tilde{J}_B = V_B J_B + v_K V_B C_B \qquad \text{(A.8-4)}$$

In an "infinite" diffusion couple (where ends of the couple are not touched by diffusion) from Eq. (A.8-3)

$$V_A \tilde{J}_A + V_B \tilde{J}_B = J_A^{vol} + J_B^{vol} = 0 \tag{A.8-5}$$

From Eq. (A.8-1, -4 and -5) it follows that,

$$-V_A D_A \left(\frac{\partial C_A}{\partial x}\right)_K + V_A C_A v_K - V_B D_B \left(\frac{\partial C_B}{\partial x}\right)_K + V_B C_B v_K = 0 \tag{A.8-6}$$

By using the standard thermodynamic relation as stated by Eq. (A.4-5 and -8)

$$v_K = V_B (D_B - D_A)\left(\frac{\partial C_B}{\partial x}\right)_K = \frac{V_A V_B}{V_m^2}(D_B - D_A)\left(\frac{\partial N_B}{\partial x}\right)_K = -(V_B J_B + V_A J_A)$$

$$\tag{A.8-7}$$
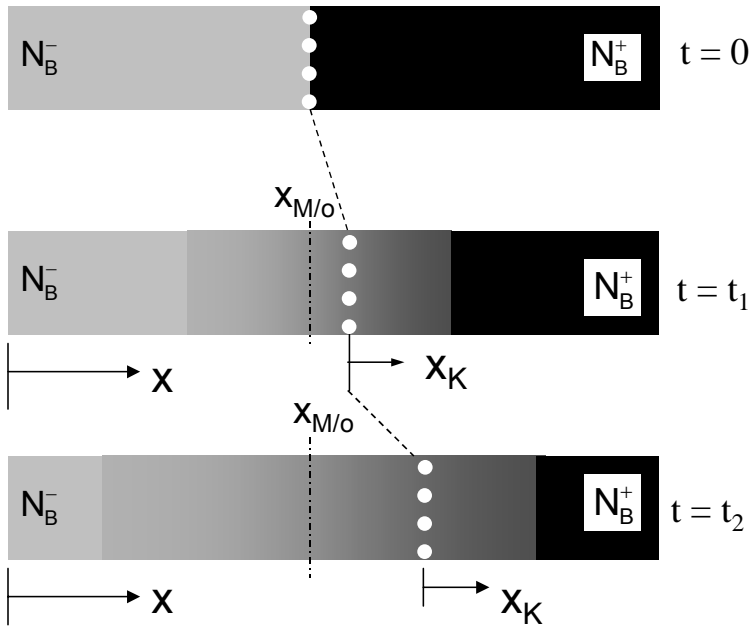
Fig. (A.8-1) Schematic representations of a diffusion couple with the end members N_B^- and N_B^+ demonstrating the Kirkendall effect. Inert markers (white spots) placed at initial contact interface before annealing are shifted with increasing annealing time ($t_2 > t_1$) to the right (from $x_{M/o}$) as the diffusion of the species B is higher than the species A. The Kirkendall frame of reference, x_K, moves with time, with respect to one end of the unreacted part of the specimen or with respect to $x_{M/o} = 0$.

Substituting Eq. (A.8-7) in Eq. (A.8-2) and comparing with Eqs. (A.4-5 and A.8-3) leads to

$$-\tilde{D}\frac{\partial C_B}{\partial x} = J_B + v_K C_B = -D_B \frac{\partial C_B}{\partial x} + C_B V_B (D_B - D_A)\frac{\partial C_B}{\partial x} =$$

$$-(1 - C_B V_B)D_B \frac{\partial C_B}{\partial x} - C_B V_B D_A \frac{\partial C_B}{\partial x} = -(C_A V_A D_B + C_B V_B D_A)\frac{\partial C_B}{\partial x}$$

$$\tilde{D} = V_A C_A D_B + V_B C_B D_A \tag{A.8-8}$$

In the special case when partial molar volumes of the components are equal and do not change with the composition so that $V_m = V_A = V_B$, Eq. (A.8-8) reduces to,

$$\tilde{D} = N_A D_B + N_B D_B \tag{A.8-9}$$

Eq. (A.8-9) is known as the Darken equation.

(Note: Interdiffusion coefficients can be measured at any composition in a concentration profile, however, intrinsic diffusivities can only be measured at compositions indicated by inert markers introduced in the couple prior to annealing).

A.9 Interdiffusion coefficient considering changes in total volume upon mixing/reaction

One can determine $\tilde{D}$ as a function of the composition by the Matano-Boltzmann analysis (see A.5) for a diffusion couple for the ideal cases where the total volume does not change. Ballufi [22] first derived the solution for the interdiffusion coefficient for systems involving a deviation in molar volumes from the ideal case and changes in the total volume upon mixing/reaction. Some time later, Sauer and Freise [23] generalized the Matano-Boltzmann analysis for the same conditions. Later Wagner [24] came to the same relation but in a different way and then Den Broeder [25] developed the same theory based on graphical interpretation. In the following sections Wagner's approach is demonstrated elaborately.

From Fick's first law (Eq.(A.2-1)) and through Eqs. (A.4-3) one can write,

$$\tilde{D}\frac{dC_B}{dx} = \tilde{D}\frac{V_A}{V_m^2}\frac{dN_B}{dx} = -\tilde{J}_B = -\frac{\left(N_B V_B + N_A V_A\right)}{V_m}\tilde{J}_B \qquad (A.9\text{-}1)$$

By using the condition in Eq. (A.8-3), Eq. (A.9-1) can be written as,

$$\tilde{D} = \frac{V_m\left(N_B\tilde{J}_A - N_A\tilde{J}_B\right)}{\partial N_B/\partial x} \qquad (A.9\text{-}2)$$

The time of the diffusion experiment is sufficiently short so that no changes in composition occur at either end of the couple, and therefore, the integrals at the ends vanish. Following Boltzmann (Eq. (A.5-2)) [7] the composition of the sample is a single valued function of the auxiliary variable

$$\lambda = \lambda(C) = \frac{x}{t^{\frac{1}{2}}} \qquad (A.9\text{-}3)$$

where x is the distance from the initial contact plane, x_o (see A.19), such that $x = x - x_o$ ($x_o = 0$). This equation states that any composition in a diffusion zone moves parabolically with time from x_o.

From Fick's second law, (Eq. (A.2-2)),

$$\frac{\partial}{\partial t}\left(\frac{N_A}{V_m}\right) = \frac{\partial C_A}{\partial t} = -\frac{\partial \tilde{J}_A}{\partial x} \tag{A.9-4a}$$

$$\frac{\partial}{\partial t}\left(\frac{N_B}{V_m}\right) = -\frac{\partial \tilde{J}_B}{\partial x} \tag{A.9-4b}$$

Sauer-Freise [22] introduced the auxiliary variable

$$Y = \frac{N_B - N_B^-}{N_B^+ - N_B^-} \tag{A.9-5}$$

from which one can write

$$N_A = \left(1 - N_B^+\right)Y + \left(1 - N_B^-\right)(1 - Y) \tag{A.9-6a}$$

$$N_B = N_B^+ Y + N_B^-(1 - Y) \tag{A.9-6b}$$

Substitution of Eq. (A.9-4, -6a, -6b) in (-4a and -4b) yields

$$\frac{\lambda}{2t}\left[\left(1 - N_B^+\right)\frac{d}{d\lambda}\left(\frac{Y}{V_m}\right) + \left(1 - N_B^-\right)\frac{d}{d\lambda}\left(\frac{1-Y}{V_m}\right)\right] = \frac{\partial \tilde{J}_A}{\partial x} \tag{A.9-7a}$$

$$\frac{\lambda}{2t}\left[N_B^+ \frac{d}{d\lambda}\left(\frac{Y}{V_m}\right) + N_B^- \frac{d}{d\lambda}\left(\frac{1-Y}{V_m}\right)\right] = \frac{\partial \tilde{J}_B}{\partial x} \tag{A.9-7b}$$

Multiplying through Eq. (A.9-7a) by N_B^- and Eq. (A.9-7b) by $\left(1 - N_B^-\right)$ and subtracting corresponding sides,

$$-\frac{\lambda}{2t}\left(N_B^+ - N_B^-\right)\frac{d}{d\lambda}\left(\frac{Y}{V_m}\right) = N_B^- \frac{\partial \tilde{J}_A}{\partial x} - \left(1 - N_B^-\right)\frac{\partial \tilde{J}_B}{\partial x} \tag{1.9-8a}$$

In the same way multiplying through Eq. (A.9-7a) by N_B^+ and Eq. (A.9-7b) by $\left(1 - N_B^+\right)$ and subtracting corresponding sides, leads to

$$\frac{\lambda}{2t}\left(N_B^+ - N_B^-\right)\frac{d}{d\lambda}\left(\frac{1-Y}{V_m}\right) = N_B^+ \frac{\partial \tilde{J}_A}{\partial x} - \left(1 - N_B^+\right)\frac{\partial \tilde{J}_B}{\partial x} \tag{A.9-8b}$$

From Eq. (A.9-3) one can write

$$d\lambda = \frac{dx}{t^{\frac{1}{2}}} \tag{A.9-9}$$

Next we multiply $d\lambda$ to the left hand side and $dx/t^{1/2}$ to the right hand side of the Eq. (A.9-8a) and then integrate for a certain fixed time, t, from $\lambda = -\infty$ to a particular

position of interest $\lambda = \lambda^*$ (corresponds to the mole fraction N_B^*). Following integration by parts of the left hand side of the equations we find,

$$\frac{1}{2t}\left(N_B^+ - N_B^-\right)\left[-\frac{\lambda^* Y^*}{V_m^*} + \int_{-\infty}^{\lambda^*}\frac{Y}{V_m}\,d\lambda\right] = \frac{1}{t^{\frac{1}{2}}}\left[N_B^-\tilde{J}_A^* - \left(1 - N_B^-\right)\tilde{J}_B^*\right] \qquad \text{(A.9-10a)}$$
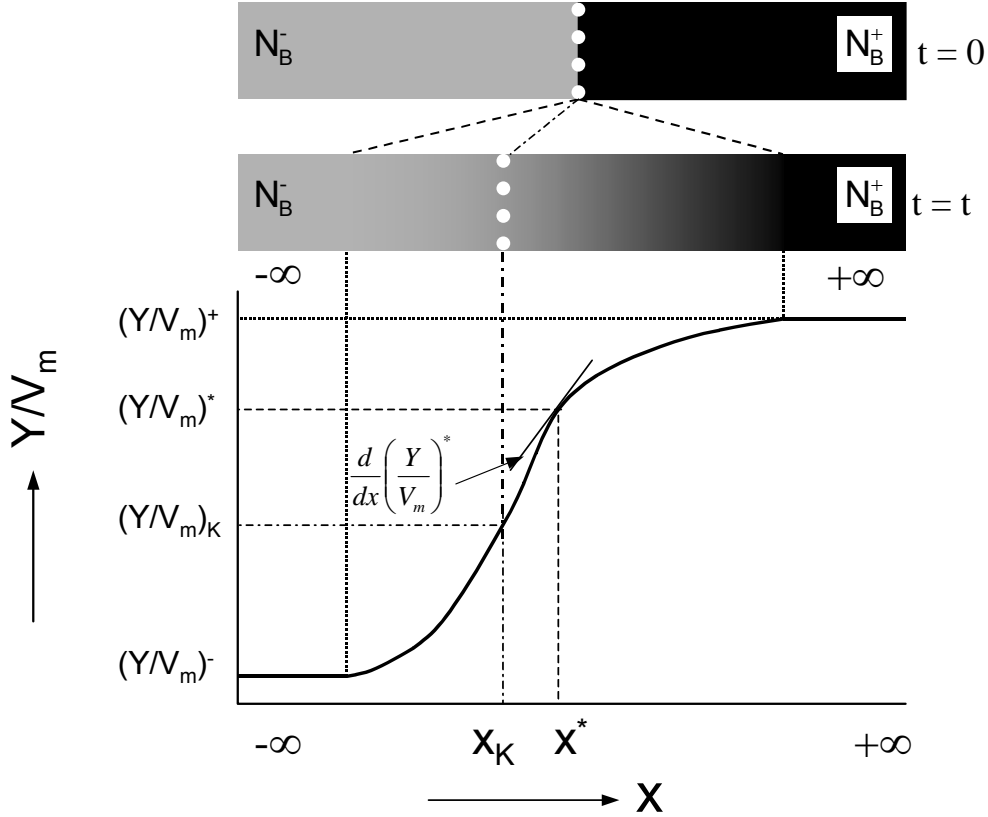
Fig. (A.9-1) Schematic representations of a diffusion couple, N_B^- and N_B^+, demonstrating diffusion after time, t. White spots represents the inert Kirkendall markers moving depending on the inequality of diffusing species A and B. The interdiffusion coefficient, $\tilde{D}$, can be determined at any position, let us say here at x^*, however, intrinsic diffusivities can only be measured at Kirkendall marker (plane) position, x_K.

Same way, from Eq. (A.9-8b) after multiplying $d\lambda$ to the left hand side and $dx/t^{1/2}$ to the right hand side and integrate from $\lambda = \lambda^*$ to $\lambda = +\infty$. Following integration by parts of the left hand side of the equations we find,

$$\frac{1}{2t}\left(N_B^+ - N_B^-\right)\left[-\frac{\lambda^*\left(1 - Y^*\right)}{V_m^*} - \int_{\lambda^*}^{+\infty}\frac{\left(1 - Y\right)}{V_m}\,d\lambda\right] = \frac{1}{t^{\frac{1}{2}}}\left[-N_B^+\tilde{J}_A^* + \left(1 - N_B^+\right)\tilde{J}_B^*\right]$$

$$\text{(A.9-10b)}$$

J_A^* and J_B^* are the fluxes at $\lambda = \lambda^*$. Multiplying through Eq. (A.9-10a) by $\left(1 - Y^*\right)$ and Eq. (A.9-10b) by Y^* and subtracting corresponding sides, one obtains

$$\frac{1}{2t}\left(N_B^+ - N_B^-\right)\left[\left(1 - Y^*\right)\int_{-\infty}^{\lambda^*}\frac{Y}{V_m}d\lambda + Y^*\int_{\lambda^*}^{+\infty}\frac{(1-Y)}{V_m}d\lambda\right] = \frac{1}{t^{\frac{1}{2}}}\left[N_B^*\tilde{J}_A^* - \left(1 - N_B^*\right)\tilde{J}_B^*\right]$$

(A.9-11)

Substituting Eq. (A.9-2) for $N_B = N_B^*$ in Eq. (A.9-11) and using $d\lambda = \dfrac{dx}{t^{\frac{1}{2}}}$ and solving for $\tilde{D}$, one obtains

$$\tilde{D}\left(N_B^*\right) = \frac{\left(N_B^+ - N_B^-\right)V_m^*}{2t\left(\partial N_B/\partial x\right)_{x=x^*}}\left[\left(1 - Y^*\right)\int_{-\infty}^{x^*}\frac{Y}{V_m}dx + Y^*\int_{x^*}^{-\infty}\frac{(1-Y)}{V_m}dx\right]$$

(A.9-12)

By differentiating Eq. (A.9-5) and substituting in Eq. (A.9-12) one can write,

$$\tilde{D}\left(Y^*\right) = \frac{1}{2t\dfrac{d\left(Y/V_m\right)^*}{dx}}\left[\left(1 - Y^*\right)\int_{-\infty}^{x^*}\frac{Y}{V_m}dx + Y^*\int_{x^*}^{\infty}\frac{(1-Y)}{V_m}dx\right]$$

(A.9-13)

Interdiffusion coefficients can be measured at any position in the diffusion zone. The advantage of this method is that, to measure interdiffusivities, it is not necessary to find out the position of x_o, which becomes cumbersome in real systems, where total volume changes with reaction/mixing. Here, V_m^* is the molar volume at Y^*. If the molar volume V_m is independent of composition changes, the factor V_m in front of the expression in brackets cancels against V_m in the denominator of the integrals. If the diffusion couple consists initially of pure components, i.e. $N_B^- = 0$ and $N_B^+ = 1$, the auxiliary variable Y is equal to the mole fraction, N_B.

Den Broeder [24] graphically treated and modified the Matano-Boltzmann equation (Eq. (A.5-9)) to find the solution for the interdiffusion coefficient as

$$\tilde{D}\left(C_B^*\right) = \frac{1}{2t}\left(\frac{\partial x}{\partial C_B}\right)_{C_B^*}\left[\left(1 - Y_{C_B}^*\right)\int_{-\infty}^{x^*}\left(C_B - C_B^-\right)dx + Y_{C_B}^*\int_{x^*}^{\infty}\left(C_B^+ - C_B\right)dx\right]$$

(A.9-14)

where $Y_{C_B} = \dfrac{C_B - C_B^-}{C_B^+ - C_B^-}$, C_B is the concentration of B and, C_B^- and C_B^+ are the concentrations at left- and right-hand unreacted part of the end members, respectively.

Note that the values calculated by Wagner's approach (Eq. (A.9-13)) and Den Broeder's approach (Eq. (A.9-14)) will be the same. The difference is in the way of treating the experimental data points. In Den Broeder's approach the interdiffusion coefficient is determined from the concentration profile, C_i vs. x (where i represents the species, i), where as in Wagner's approach it is calculated after converting the mole fraction, N_i to the Sauer-Freise auxiliary variable, Y (by Eq. (A.9-5)).

A.10 Intrinsic diffusion coefficients

Intrinsic diffusivities can be measured straightforwardly only at the Kirkendall plane position, x_K, marked by the markers as shown in Fig. (A.9-1), since this marker plane moves parabolically with time starting from $t = 0$ (contrary to markers put in other positions in the couple at $t = 0$). This is the only plane, which is immediately affected by the diffusion process at the start of the annealing and once the markers are trapped in a certain composition, they stay at that same composition for the entire annealing time and this plane acts as a reference to determine the intrinsic diffusivities. From Wagner analysis it is possible to derive the relation for the intrinsic diffusivities. Multiplying through Eq. (A.9-10a) by N_B^+ and (A.9-10b) by N_B^-, then adding them and after rearranging:

$$\frac{1}{2t}\left(N_B^+ - N_B^-\right)\left[-\lambda_K\left\{\frac{Y_K}{V_m^K}N_B^+ + \frac{(1-Y_K)}{V_m^K}N_B^-\right\} + \left\{N_B^+\int_{-\infty}^{\lambda_K}\frac{Y}{V_m}d\lambda - N_B^-\int_{\lambda_K}^{+\infty}\frac{(1-Y)}{V_m}d\lambda\right\}\right]$$

$$= \frac{1}{t^{\frac{1}{2}}}\left[-N_B^+\left(1-N_B^-\right)\tilde{J}_B^K + N_B^-\left(1-N_B^+\right)\tilde{J}_B^K\right]$$

(A.10-1)

where subscript and superscript "K" corresponds to the Kirkendall plane position. After rearranging Eq. (A.10-1)

$$\tilde{J}_B^K = \frac{t^{\frac{1}{2}}}{2t} \left[\lambda_K \frac{N_B^K}{V_m^K} - N_B^+ \int_{-\infty}^{\lambda_K} \frac{Y}{V_m} d\lambda + N_B^- \int_{\lambda_K}^{+\infty} \frac{(1-Y)}{V_m} d\lambda \right] \qquad (A.10\text{-}2)$$

Using Eq. (A.9-9) and rearranging again one can find

$$\tilde{J}_B^K = vc_B^K - \frac{1}{2t} \left[N_B^+ \int_{-\infty}^{x_K} \frac{Y}{V_m} dx - N_B^- \int_{x_K}^{\infty} \frac{(1-Y)}{V_m} dx \right] \qquad (A.10\text{-}3)$$

From Eq. (A.8-2) $\tilde{J}_B^K = -D_B \dfrac{\partial C_B}{\partial x} + vc_B^K \qquad (A.10\text{-}4)$

So from Eq. (A.10-3 and -4) we can write,

$$D_B = \frac{1}{2t} \left(\frac{\partial x}{\partial C_B} \right)_K \left[N_B^+ \int_{-\infty}^{x_K} \frac{Y}{V_m} dx - N_B^- \int_{x_K}^{+\infty} \frac{(1-Y)}{V_m} dx \right] \qquad (A.10\text{-}5a)$$

where $\dfrac{\partial C_B}{\partial x} = \dfrac{V_A}{V_m} \left(N_B^+ - N_B^- \right) \dfrac{d}{dx} \left(\dfrac{Y}{V_m} \right)$

In the same way, multiplying Eq. (A.9-10a) by $\left(1 - N_B^+\right)$ and (A.9-10b) by $\left(1 - N_B^-\right)$ and following the same procedure, one can determine the intrinsic diffusivity for component A.

$$D_A = \frac{1}{2t} \left(\frac{\partial x}{\partial C_A} \right)_K \left[N_A^+ \int_{-\infty}^{x_K} \frac{Y}{V_m} dx - N_A^- \int_{x_K}^{+\infty} \frac{(1-Y)}{V_m} dx \right] \qquad (A.10\text{-}5b)$$

From Eq. (A.10-5a and -5b) and Eq. (A.4-8), the ratio of diffusivities can be written as

$$\frac{D_B}{D_A} = \frac{V_B}{V_A} \left[\frac{N_B^+ \int_{-\infty}^{x_K} \frac{Y}{V_m} dx - N_B^- \int_{x_K}^{\infty} \frac{(1-Y)}{V_m} dx}{-N_A^+ \int_{-\infty}^{x_K} \frac{Y}{V_m} dx + N_A^- \int_{x_K}^{\infty} \frac{(1-Y)}{V_m} dx} \right] \qquad (A.10\text{-}6)$$

Heumann [26] and van Loo [27] derived relations for the intrinsic diffusivities in different way.

A.11 Integrated diffusion coefficient

The equations above cannot be used straightforward to calculate diffusion coefficients for compounds with a narrow homogeneity range, as it is not possible to measure the vanishingly small concentration gradient. Wagner [23] introduced a new variable, the

integrated diffusion coefficient $\tilde{D}_{int}$ to describe the diffusion in line compounds. Consider the presence of a line compound β with a very narrow homogeneity range of $N_B^{\beta 1}$ and $N_B^{\beta 2}$, such that $N_B^{\beta 1} \leq N_B^{\beta} \leq N_B^{\beta 2}$, in a system as shown in the schematic phase diagram Fig. (A.11-1a). Two end members N_B^- and N_B^+ are coupled at elevated temperature for time t and the resulting concentration profile is shown in Fig. (A.11-1b). The total thickness of β is $\Delta x_\beta \left(= x_{\beta 1} - x_{\beta 1}\right)$. The integrated diffusion coefficient can be expressed from Eqs. (A.9-5 and -14) for β as,

$$\tilde{D}_{int}^{\beta} = \int_{N_B^{\beta 1}}^{N_B^{\beta 2}} \tilde{D} dN_B = \frac{\left(N_B^{\beta} - N_B^-\right)\left(N_B^+ - N_B^{\beta}\right)}{N_B^+ - N_B^-} \frac{\Delta x^2}{2t}$$

$$+ \frac{\Delta x}{2t}\left[\frac{N_B^+ - N_B^{\beta}}{N_B^+ - N_B^-} \times \int_{-\infty}^{x^{\beta 1}} \frac{V_m^{\beta}}{V_m}\left(N_B - N_B^-\right)dx + \frac{N_B^{\beta} - N_B^-}{N_B^+ - N_B^-} \times \int_{x^{\beta 2}}^{\infty} \frac{V_m^{\beta}}{V_m}\left(N_B^+ - N_B\right)dx\right]$$

$$(A.11-1)$$

$\tilde{D}_{int}^{\beta}$ can be related to the average interdiffusion coefficient

$$\tilde{D}_{av}^{\beta} = \frac{\tilde{D}_{int}^{\beta}}{N_B^{\beta 2} - N_B^{\beta 1}} = \frac{1}{N_B^{\beta 2} - N_B^{\beta 1}} \int_{N_B^{\beta 1}}^{N_B^{\beta 2}} \tilde{D} dN_B$$

which cannot be measured because of the unknown value of $\left(N_B^{\beta 2} - N_B^{\beta 1}\right)$.
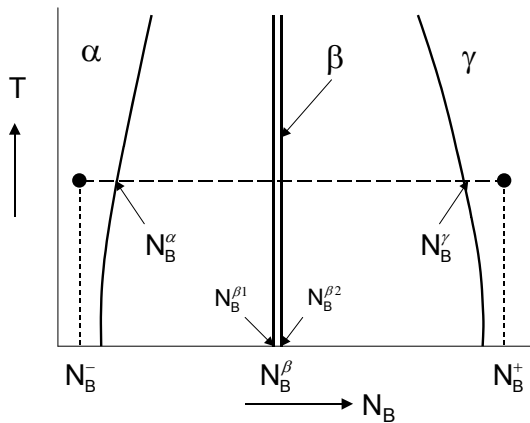
Fig. (A.11-1a) Schematic example of a phase diagram, where only one line compound β exists.
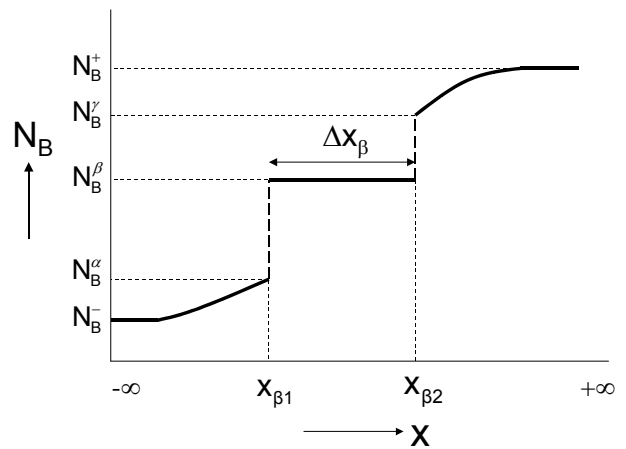
Fig. (A.11-1b) Schematic representation of a composition profile of a diffusion couple N_B^- and N_B^+, corresponding to Fig. (A.11-1a) after annealing time t.

In the case of a diffusion system where several line compounds exist and where no solubility in the end members of the components occur as shown in Fig. (A.11-2a and -2b), Eq. (A.11-1) can be written as,

$$\tilde{D}_{\text{int}}^{\beta} = \frac{\left(N_B^{\beta} - N_B^{-}\right)\left(N_B^{+} - N_B^{\beta}\right)}{N_B^{+} - N_B^{-}} \frac{\Delta x_{\beta}^{2}}{2t} + \frac{\Delta x_{\beta}}{2t} \text{ x}$$

$$\left[\frac{\left(N_B^{+} - N_B^{\beta}\right)\sum_{\nu=2}^{\nu=\beta-1} \frac{V_m^{\beta}}{V_m^{\nu}}\left(N_B^{\nu} - N_B^{-}\right)\Delta x_{\nu} + \left(N_B^{\beta} - N_B^{-}\right)\sum_{\nu=\beta+1}^{\nu=n-1} \frac{V_m^{\beta}}{V_m^{\nu}}\left(N^{+} - N^{\nu}\right)\Delta x_{\nu}}{N_B^{+} - N_B^{-}}\right]$$

(A.11-2)

From Fig. (A.11-2b), Eq. (A.11-2) can be expressed as,

$$\tilde{D}_{\text{int}}^{\beta} = \frac{ab}{a+b} \frac{\Delta x_{\beta}^{2}}{2t} + \frac{\Delta x_{\beta}}{2t}\left[\frac{b\left(\frac{V_m^{\beta}}{V_m^{\varepsilon}}P + \frac{V_m^{\beta}}{V_m^{\alpha}}Q\right) + a\left(\frac{V_m^{\beta}}{V_m^{\gamma}}R + \frac{V_m^{\beta}}{V_m^{\delta}}S\right)}{a+b}\right]$$

(A.11-3)
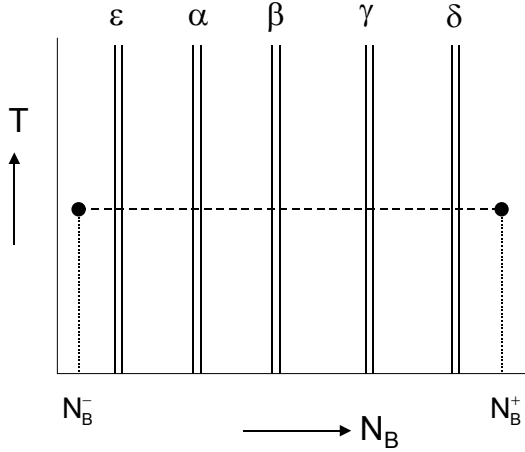
Fig. (A.11-2a) Schematic representation of a phase diagram having several line compounds.
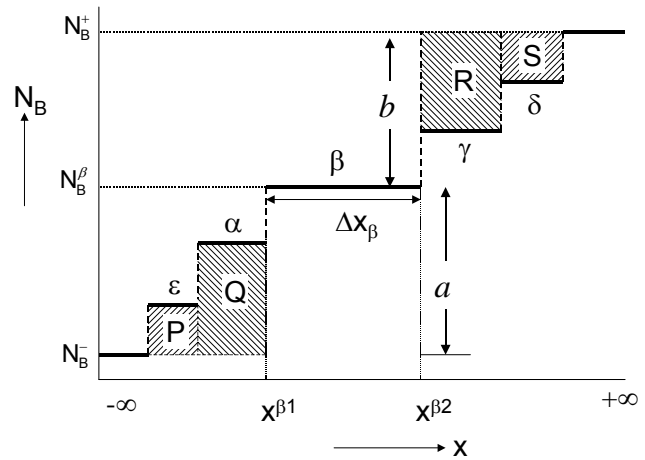
Fig. (A.11-2b) Schematic composition profile of a diffusion couple, after annealing time *t*. Compositions correspond to the phase diagram shown in Fig. (A.11-2a).
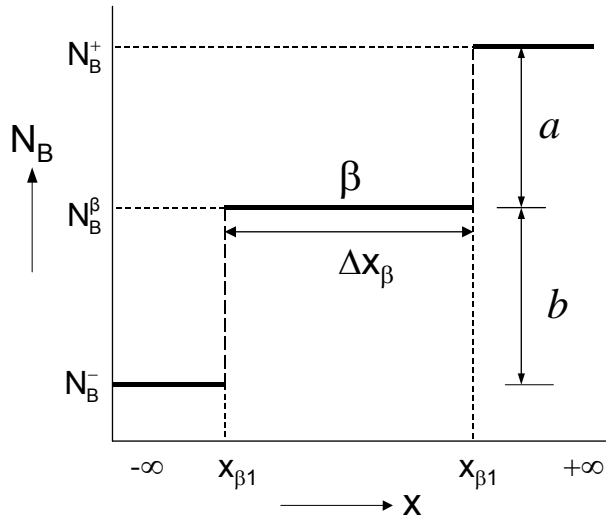
Fig. (A.11-3) Schematic representation of a composition profile of a diffusion couple containing only one line compound

In the special case that only one intermetallic compound, β, exists between two end members, N_B^- and N_B^+, as shown in Fig. (A.11-3), then Eq. (A.11-3) reduces to,

$$\tilde{D}_{int}^{\beta} = \frac{ab}{a+b}\frac{\Delta x_{\beta}^2}{2t} = \frac{ab}{a+b}k_p \qquad (A.11-4)$$

where k_p is the parabolic growth constant (see Eq. (A.17-3)). In the case of a diffusion couple with pure end members, A and B i.e. $N_B^- = 0$ and $N_B^+ = 1$, then, $a + b = 1$ and Eq. (A.11-4) further reduces to,

$$\tilde{D}_{int}^{\beta} = ab\frac{\Delta x_{\beta}^2}{2t} = abk_p \qquad (A.11-5)$$

A.12 Intrinsic diffusion coefficients for line compounds

In the case of a line compound one cannot measure the intrinsic diffusion coefficients of elements, because of the vanishingly small concentration gradient at the Kirkendall plane position in a compound with a very narrow homogeneity range. However, one can measure the ratio of the intrinsic diffusivities by Eq. (A.10-6), as there is no need to measure the slope. In the case of a diffusion couple as shown in Fig. (A.12-1), if the Kirkendall marker plane is situated at x_K, the ratio of intrinsic diffusivities can be written by using Eq. (A.9-5) and (A.10-6) as,

$$\frac{D_B}{D_A} = \frac{V_B}{V_A}\left[\frac{N_B^+\Phi - N_B^-\Psi}{-N_A^+\Phi + N_A^-\Psi}\right] \qquad (A.12-1)$$

where

$$\Phi = \left(\int_{-\infty}^{x_{\beta 1}} \frac{\left(N_B - N_B^-\right)}{V_m} dx + \frac{\left(N_B^\beta - N_B^-\right)}{V_m^\beta} \Delta x_1 \right); \quad \Psi = \left(\int_{x_{\beta 2}}^{+\infty} \frac{\left(N_B^+ - N_B\right)}{V_m} dx + \frac{\left(N_B^+ - N_B^\beta\right)}{V_m^\beta} \Delta x_2 \right)$$

In the case of Fig. (A.12-2), when no solubility exists in the end members, all the compounds have a narrow homogeneity range and the Kirkendall plane is located in β-phase at x_K, then Φ and Ψ in Eq. (A.12-1) can be written as,

$$\Phi = \left(\sum_{v=2}^{\beta-1} \frac{\left(N_B^v - N_B^-\right)}{V_m^v} \Delta x^v + \frac{\left(N_B^\beta - N_B^-\right)}{V_m^\beta} \Delta x_1 \right); \quad \Psi = \left(\sum_{v=\beta+1}^{n-1} \frac{\left(N_B^+ - N_B^v\right)}{V_m^v} \Delta x^v + \frac{\left(N_B^+ - N_B^\beta\right)}{V_m^\beta} \Delta x_2 \right)$$

or,

$$\Phi = \left(\frac{P}{V_m^\varepsilon} + \frac{Q}{V_m^\alpha} + \frac{A}{V_m^\beta} \right); \quad \Psi = \left(\frac{S}{V_m^\delta} + \frac{R}{V_m^\gamma} + \frac{B}{V_m^\beta} \right)$$

In the special case when there is only one layer, β, growing between two end members, and the Kirkendall plane position x_K is present in that phase, as shown in Fig. (A.12-3), the equations reduce to,

$$\Phi = \frac{\left(N_B^\beta - N_B^-\right)}{V_m^\beta} \Delta x_1 = \frac{A}{V_m^\beta}; \quad \Psi = \frac{\left(N_B^+ - N_B^\beta\right)}{V_m^\beta} \Delta x_2 = \frac{B}{V_m^\beta}$$
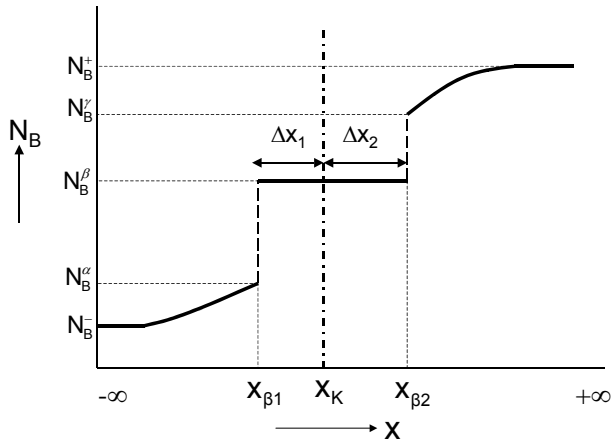
Fig. (A.12-1) Schematic composition profile for the case when only one line compound β grows between the end members α and γ. The Kirkendall marker plane is in the β phase at position x_K.
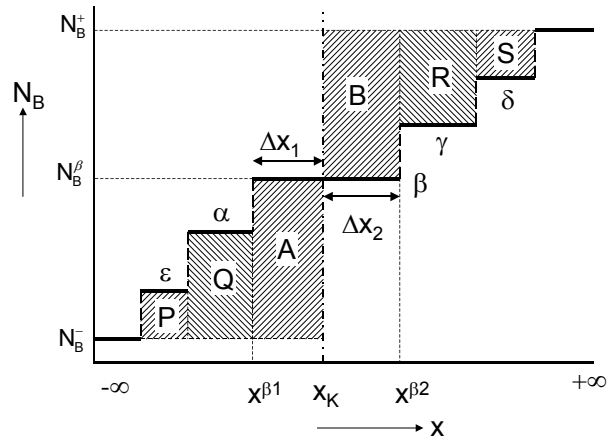
Fig. (A.12-2) Schematic composition profile for the case when several line compounds exist. The Kirkendall marker plane is in the β phase at position x_K.
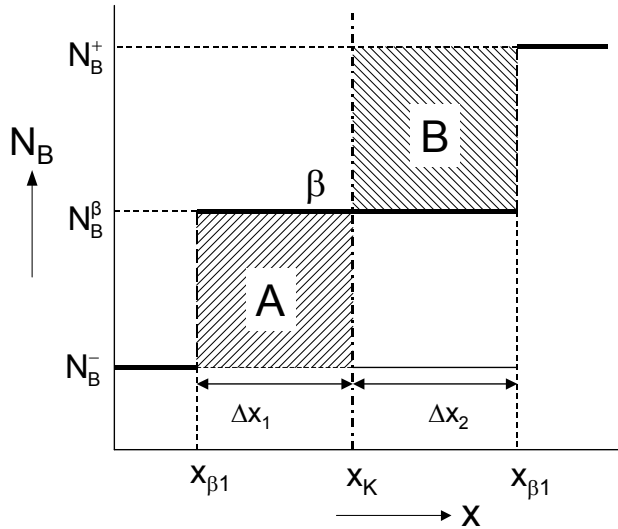
Fig. (A.12-3) Schematic composition profile of a diffusion couple when only one line compound exists. The Kirkendall marker plane is inside the β phase at position x_K.

In the case of pure end members, $N_B^- = 0$ and $N_B^+ = 1$, Eq. (A.12-1) reduces to

$$\frac{D_B}{D_A} = \frac{V_B}{V_A}\left[\frac{N_B^+\Phi}{N_A^-\Psi}\right] = \frac{V_B}{V_A}\left[\frac{\Phi}{\Psi}\right]$$

(A.12-2)

and if there is only one compound between two pure end member then,

$$\Phi = \frac{N_B^\beta}{V_m^\beta}\Delta x_1 \;\; ; \;\; \Psi = \frac{1-N_B^\beta}{V_m^\beta}\Delta x_2 \;\; \text{and Eq. (A.12-2) further reduces to}$$

$$\frac{D_B}{D_A} = \frac{V_B}{V_A}\left[\frac{N_B^\beta}{\left(1-N_B^\beta\right)}\frac{\Delta x_1}{\Delta x_2}\right]$$

(A.12-3)

It should be reminded, that the value V_B/V_A is difficult to determine in line compounds. Therefore, one actually finds from experiments the ratio $\dfrac{V_A D_B}{V_B D_A}$, which is also a material constant.

A.13 Tracer diffusion coefficients

Another way to study and get knowledge of diffusion in a pure material or in alloys is through the use of tagged atoms of radioisotopes. For instance, to measure the tracer diffusivity of species B in a binary alloy of A_xB_{1-x}, a thin layer of tracer B^* is deposited on a flat surface as shown in Fig. (A.13-1a). After annealing at a certain temperature, T for a certain time t (such that the deposited layer before annealing is thin compared to $\sqrt{Dt}$), the distribution of B^* can be written after solving Fick's second law (Eq. (A.2-2)) as [3],

$$C_B^*(x,t) = \frac{N_B^*}{\sqrt{\pi D_B^* t}} \exp\left(-\frac{x^2}{4D_B^* t}\right) \qquad \text{(A.13-1)}$$

where C_B^* is the concentration of B* at a distance, x, from the surface. N_B^* is the number of moles of tracer atoms deposited per unit area.

Radioisotopes should have sufficient half-life, not too short or too long, in order to measure their concentration by the emission of β or γ rays. They are chemically the same as species B, with only one or two neutron mass difference. After certain annealing time the specimen is cross-sectioned at different distances x (as shown by dotted lines in Fig (A.13-1b)) to measure isotope concentrations. Then after plotting $\ln C_B^*$ to x, D_B^* (which is practically identical to D_B) can be measured from the slope $-\dfrac{1}{4D_B^* t}$, as shown in Fig. (A.13-1c).
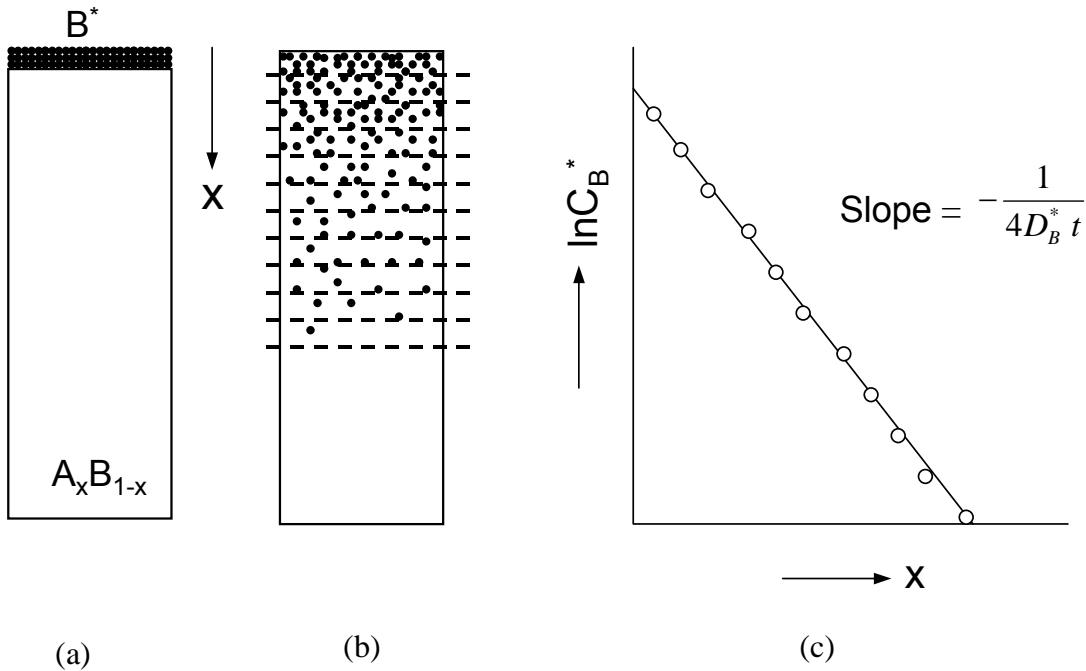
Fig. (A.13-1) a) Tracer B* is deposited as a very thin layer on the alloy A_xB_{1-x}, b) the specimen is cross sectioned at different distances after annealing at temperature T for time, t to measure the tracer concentrations, c) the concentration of tracer C_B^* is plotted vs. distance x. The tracer diffusivity of B can be measured from the slope of the curve according to Eq. (A.13-1).

A.14 Phenomenological equations: Darken's analysis for the relation between interdiffusivity, intrinsic diffusivities and tracer diffusivities

Mathematical formulations as shown in previous chapters are theoretically sound. However, to gain more insight into the conditions of the treatment and the phenomenological process one has to understand it through a thermodynamical point of view. Basic conditions of the previous equations are that the system is under isothermal and isobaric conditions; that no high external force is present (which might cause plastic deformation of the sample or, possibly, pressure dependent diffusion coefficients) and time dependent effects are absent. This holds specifically for the recrystallisation processes, when small grains found during the early stage of the diffusion process might grow. This might cause a gradual transition from grain boundary diffusion to the much slower bulk diffusion. We consider here bulk diffusion throughout the whole process.

If further the diffusion process occurs under the condition of local equilibrium, then

$$J_A = -L_A \frac{d\mu_A}{dx} \; ; \qquad J_B = -L_B \frac{d\mu_B}{dx} \tag{A.14-1}$$

where μ_i is the thermodynamic (or chemical) potential for component i, L_i is the phenomenological coefficient, independent of $d\mu_i/dx$ and only dependent on the composition.

If we consider the force, F due to the chemical potential, and v_B is the velocity of species B, then the mobility of B can be written as, $M_B = v_B/F$. The flux can be written as (considering the force for the diffusion is the chemical potential gradient)

$$J_B = C_B v_B = M_B F C_B = -M_B C_B \frac{d\mu_B}{dx} = -L_B \frac{d\mu_B}{dx} = -D_B \frac{dC_B}{dx}$$

So, the phenomenological constant $L_B = M_B C_B$ and

$$D_B = M_B C_B \frac{d\mu_B}{dC_B} \tag{A.14-2}$$

From Eq. (A.4-2, -9 and A.14-2) can be written as,

$$D_B = \frac{V_m}{V_A} M_B N_B \frac{d\mu_B}{dN_B} = \frac{V_m}{V_A} M_B \frac{d\mu_B}{d \ln N_B} \tag{A.14-3}$$

We know that,

$$\mu_B = \mu_B^o (T, P) + RT \ln a_B = \mu_B^o (T, P) + RT (\ln N_B + \ln \gamma_B) \tag{A.14-4}$$

where the activity of B is $a_B = \gamma_B N_B$, γ_B is the activity coefficient of B, R is the gas constant and μ_B is the chemical potential of B.

From Eqs. (A.14-3 and -4),

$$D_B = \frac{V_m}{V_A} M_B RT \frac{d \ln a_B}{dN_B} = \frac{V_m}{V_A} M_B RT \left(1 + \frac{d \ln \gamma_B}{d \ln N_B}\right) \tag{A.14-5}$$

In case of the diffusion of an infinitely thin layer of radioactive tracer of B in an alloy of A-B as shown in section A.13, the volume terms as well as the non-ideality term in Eq. (A.14-5) vanish and we can write

$$D_B^* = M_B^* RT \tag{A.14-6}$$

which is known as the Nernst-Einstein relation.

By transforming, Eq. (A.14-6) in Eq. (A.14-5),

$$D_B = D_B^* \frac{V_m}{V_A} \frac{d \ln a_B}{d \ln N_B} = D_B^* \frac{V_m}{V_A} \left(1 + \frac{d \ln \gamma_B}{d \ln N_B}\right) \tag{A.14-7a}$$

In the same way, for species A,

$$D_A = D_A^* \frac{V_m}{V_B} \frac{d \ln a_A}{d \ln N_A} = D_A^* \frac{V_m}{V_B} \left(1 + \frac{d \ln \gamma_A}{d \ln N_A}\right) \tag{A.14-7b}$$

Combining Eq. (A.8-8) and (A.14-7) and using the Gibbs-Duhem equation $\dfrac{d \ln a_A}{d \ln N_A} = \dfrac{d \ln a_B}{d \ln N_B}$, we can write for the interdiffusion coefficient,

$$\tilde{D} = \left(N_A D_B^* + N_B D_A^*\right)\left(\frac{d \ln a_B}{d \ln N_B}\right) \tag{A.14-8}$$

This relation was first proposed by Darken [18]

The ratio of diffusivities in terms of tracer diffusivities can be expressed by,

$$\frac{D_A}{D_B} = \frac{V_A}{V_B} \frac{D_A^*}{D_B^*} \tag{A.14-9}$$

From Eq.s (A.14-9 and A.10-6) it follows that

$$\frac{D_B^*}{D_A^*} = \left| \frac{N_B^+ \displaystyle\int_{-\infty}^{x_K} \frac{Y}{V_m} dx - N_B^- \displaystyle\int_{x_K}^{\infty} \frac{(1-Y)}{V_m} dx}{-N_A^+ \displaystyle\int_{-\infty}^{x_K} \frac{Y}{V_m} dx + N_A^- \displaystyle\int_{x_K}^{\infty} \frac{(1-Y)}{V_m} dx} \right| \tag{A.14-10}$$

which is directly measurable by the classical diffusion couple method.

A.15 Relation between integrated and tracer diffusion coefficients

Consider a diffusion couple of alloys A and B (between end members N_B^- and N_B^+) where one phase with a narrow homogeneity range (line compound), β, is forming as shown in Fig. (A.15-1). It is apparent that layer β is formed at the interface II by the dissociation of species B and by the reaction of N_B^+ with species A, which dissociated at interface I and then diffused through the product layer. In the same way, at interface I, β is formed by the dissociation of species, A from the end-member alloy N_B^- and by the reaction with the diffused species B released from interface II.
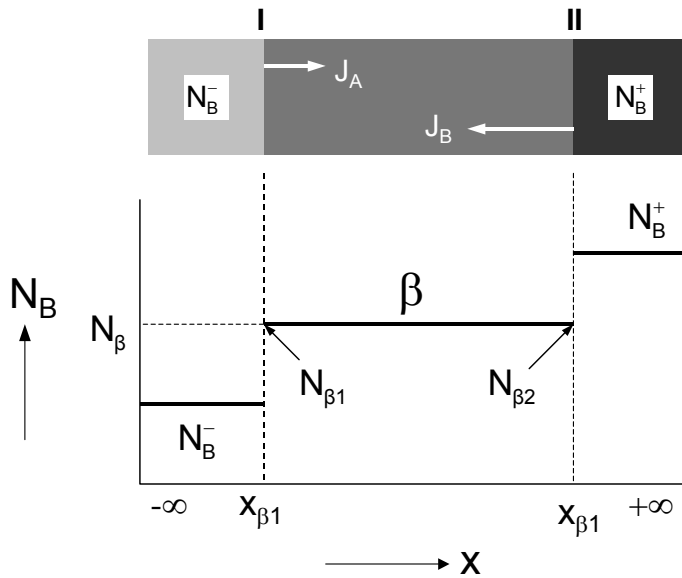
Fig. (A.15-1) Diffusion couple between end members N_B^- and N_B^+. Compound N_β with very narrow homogeneity range formed by diffusion/reaction. Movement of flux of species A and B are shown.

By definition the integrated diffusion coefficients of phase, β (Eq. A.11-1) is equal to

$$\tilde{D}_{\text{int}} = \int_{N_{\beta_1}}^{N_{\beta_2}} \tilde{D} dN_B \tag{A.15-1}$$

where N_{β_1} and N_{β_2} are the composition of β phase at interface I and II such that $N_{\beta_1} \le N_\beta \le N_{\beta_2}$.

Using Eq. (A.14-8) and Eq. (A.15-1) can be written as

$$\tilde{D}_{\text{int}} = \int_I^{II} \left(N_A D_B^* + N_B D_A^* \right) N_B \, \partial \ln a_B = \left(N_A D_B^* + N_B D_A^* \right) N_B \left[\ln a_B^{II} - \ln a_B^I \right]$$

$$\tag{A.15-2}$$

Here, the energy per mole of B for dissociation in interface II can be represented by the Gibbs energy, $\Delta G^o = -RT \ln a_B^{II}$ (where $\mu_B = \mu_B^o + RT \ln a_B$) and the energy per mole of B for the reaction at interface I to form β can be written by $\Delta G^o = RT \ln a_B^I$. So the total energy to form β by diffusion (one mole of) B (by dissociation and reaction) can be written as $\Delta_r G_B^o = -RT \left(\ln a_B^{II} - \ln a_B^I \right)$. So that Eq. (A.15-2) can be written as,

$$\tilde{D}_{int} = -\left(N_A D_B^* + N_B D_A^* \right) \frac{N_B \Delta_r G_B^o}{RT} \qquad \text{(A.15-3)}$$

It should be noted that $N_B \Delta_r G_B^o$ is equal to $N_A \Delta_r G_A^o$, where $\Delta_r G_A^o$ is the Gibbs energy for the net reaction per mole of species A moving from interface I to interface II.
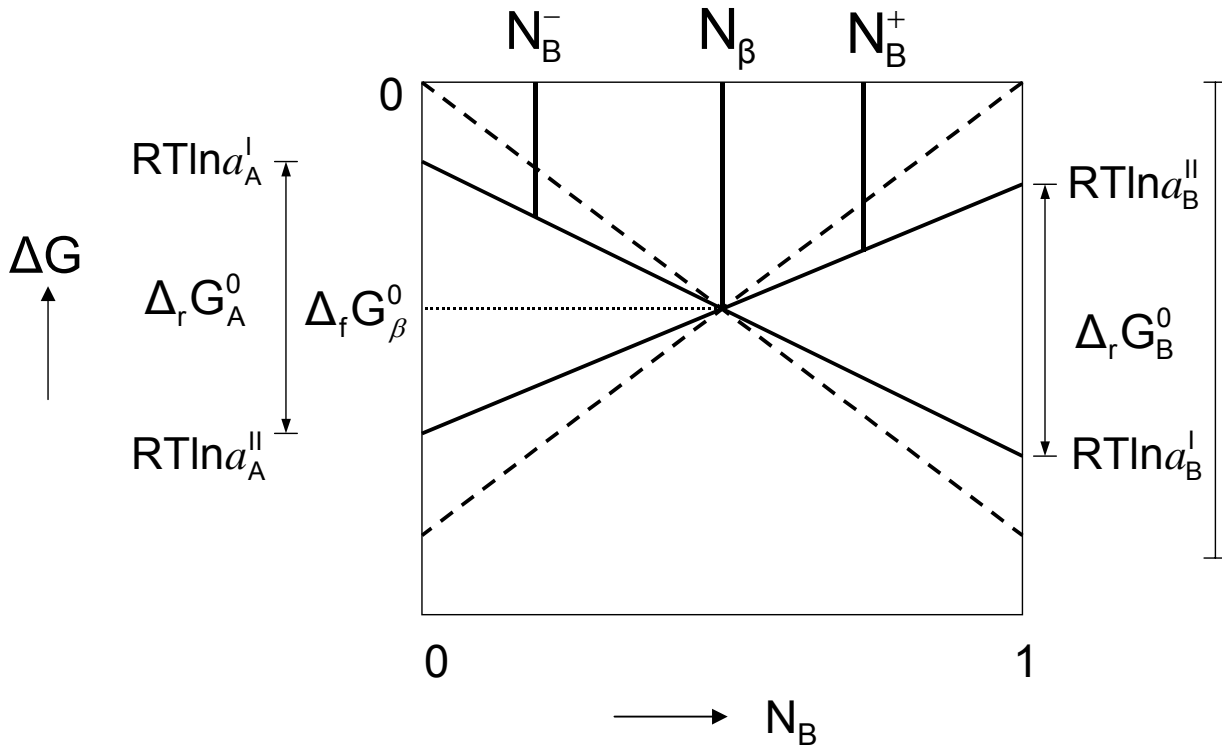
Fig. (A.15-2) Stability diagram for A-B system with three line compounds, N_B^-, N_β and N_B^+; $\Delta_r G_i^0$ is the Gibbs energy for the net reaction per mole of species given in Eq. (A.15-3). In the case of pure end members A-B, the energy of formation for the β-phase can be expressed (as explained by dashed lines) by $\Delta_f G_\beta^0$.

In the case β phase is forming between pure end members A and B ($N_B^- = 0$ and $N_B^+ = 1$, respectively) Eq. (A.15-3) can be written as

$$\tilde{D}_{\text{int}} = -\left(N_A D_B^* + N_B D_A^*\right)\frac{\Delta_f G_\beta^0}{RT} \qquad\qquad (A.15\text{-}4)$$

where $\Delta_f G_\beta^0$ is the Gibbs energy of formation per mole of particles for the β-phase. In this condition if β-phase has the composition of $A_x B_{1-x}$ then, $\Delta_f G_\beta^0 = (1-x)\Delta_r G_B^0 = x\Delta_r G_A^0$.

The change in energy can better be understood from Fig. (A.15-2).

The Kirkendall marker velocity as expressed by Eq. (A.8-7) can be written in terms of the tracer diffusion coefficients of the species with the help of Eq. (A.14-7) and (A.4-9) by

$$v_K = V_B\left(\frac{V_m}{V_A}D_B^* - \frac{V_m}{V_B}D_A^*\right)\Theta\frac{\partial C_B}{\partial x} = \frac{1}{V_m}\left(V_B D_B^* - V_A D_A^*\right)\Theta\frac{\partial N_B}{\partial x} \qquad (A.15\text{-}5)$$

where Θ is the thermodynamic factor $\dfrac{\partial \ln a_A}{\partial \ln N_A} = \dfrac{\partial \ln a_B}{\partial \ln N_B}$.

In the case when $V_A = V_B = V_m$ Eq. (A.15-5) reduces to

$$v_K = \left(D_B^* - D_A^*\right)\Theta\frac{\partial N_B}{\partial x} \qquad\qquad (A.15\text{-}6)$$

A.16 Vacancy wind effect and Manning's correction

Darken's treatment correlates interdiffusion, intrinsic diffusion and tracer diffusion coefficients of the species with the aid of thermodynamic factor (Eq. (A.14-7 and -8)). As explained, in a binary system the intrinsic diffusivities of the species are different. When diffusion is controlled by vacancy mechanism, the net flow of matter in one direction will be balanced by a net flow of vacancies in the opposite direction. Manning [28, 29] showed how this vacancy flux can affect the intrinsic diffusion and proposed the incorporation of a *correction factor* to the equations, which relates the intrinsic and interdiffusion coefficients with tracer diffusion coefficients. Manning explained that the net flux of vacancies will create a vacancy wind effect. This effect will enhance the intrinsic diffusion coefficients of the faster species whereas it will decrease the diffusion rate of a slower species. In this way it also affects to the interdiffusion coefficients and will result into increased Kirkendall marker velocity.

Assuming there is no supersaturation, binding of vacancies and no clustering in the alloy, Manning modified the Eqs. (1.14-7a and -7b) using a random alloy model. He showed that in a binary diffusion couple the intrinsic diffusion coefficients can be written as

$$D_A = \frac{V_m}{V_B} D_A^* \Theta (1 + W_A)$$
(A.16-1a)

$$D_B = \frac{V_m}{V_A} D_B^* \Theta (1 - W_B)$$
(A.16-1b)

where the vacancy wind factor $W_i = \dfrac{2N_i \left(D_A^* - D_B^*\right)}{M_o \left(N_A D_A^* + N_B D_B^*\right)}$, M_o is a constant, which

depends on the crystal structure of the system, N_i is the mole fraction of species i and Θ is the thermodynamic factor $\partial \ln a_A / \partial \ln N_A = \partial \ln a_B / \partial \ln N_B$. From Eq. (A.16-1) the relation for interdiffusion coefficient (Eq. (1.8-8)) was modified to

$$\tilde{D} = \left(N_A D_B^* + N_B D_A^*\right) \Theta\, W_{AB}$$
(A.16-2)

where $W_{AB} = 1 + \dfrac{2N_A N_B \left(D_A^* - D_B^*\right)^2}{M_o \left(N_A D_B^* + N_B D_A^*\right)\left(N_A D_A^* + N_B D_B^*\right)}$

In the same way the Kirkendall marker velocity (Eq. (A.8-7 or A.15-5)) after some mathematics was modified to

$$v_K = V_B \left(\frac{V_m}{V_A} D_B^* - \frac{V_m}{V_B} D_A^*\right) \alpha\, \Theta\, \frac{\partial C_B}{\partial x} = \frac{1}{V_m} \left(V_B D_B^* - V_A D_A^*\right) \alpha\, \Theta\, \frac{\partial N_B}{\partial x}$$

(A.16-3)

where $\alpha = 1/f$ and f is the correlation factor for self diffusion.

In the ideal case when $V_A = V_B = V_m$ Eq. (A.16-3) reduces to

$$v_K = \left(D_B^* - D_A^*\right) \alpha\, \Theta\, \frac{\partial N_B}{\partial x}$$
(A.16-4)

Values of M_o and α for face centered cubic, body centered cubic, simple cubic and diamond structure are 7.15, 5.33, 3.77, 2 and 1.280, 1.375, 1.531, 2 respectively.

Later Manning [30] and Dayananda [31] extended this approach to consider the vacancy wind effect to multicomponent systems.

Many experiments have been conducted to compare the experimental results on intrinsic diffusion coefficients and those calculated by Manning's method from tracer

diffusion coefficients. The outcome is ambiguous. Schmatz et. al. [32] and Irio et. al. [33] found that the Manning's correction led to a better match between the ratio of self-diffusivities calculated from the Kirkendall effect and the ratio determined by radiotracer measurements. However there was significant disagreement in the absolute values of the self-diffusivities between those experimentally determined and those calculated by Manning's approach. Kohn et. al. [34] also found discrepancies between experimental and calculated values. Meyer [35] and Dallwitz [36] calculated the Kirkendall marker shift and found good agreement between experimentally determined results and the values predicted by Manning's model. Carlson [37] found that the vacancy wind effect is an important parameter for intrinsic diffusion fluxes and determined the values at different compositions for the Ti-V system. Although the model for vacancy wind effect was developed for random solid solutions, Sohn and Dayananda [38] used the same model to calculate the vacancy wind effect in β'-FeAl phase. In this study the vacancy wind effect is calculated in β-NiAl and γ'-Ni$_3$Al phases as discussed in Chap. 5.

A.17 Growth kinetics, Kirkendall marker velocity and velocity curve construction

Following the Boltzmann variable (Eq. (A.5-2)) $\lambda = \lambda \, (C) = x/t^{1/2}$ and from experiments, it is well known that in a diffusion controlled growth, all compositions in a diffusion layer will move parabolically in time in the laboratory frame of reference from $x_{M/o}$ (where x_M and x_o are the initial contact interface, for the conditions as explained in A.8 and A.19).

In the case of line compounds or the phases with narrow homogeneity range, phase layers will have an almost fixed composition and will grow with that fixed composition. In this case phase boundaries will move parabolically in time from the $x_{M/o}$ and the layer thickness also will grow parabolically such that

$$\Delta x^2 = d^2 = 2k_p t \qquad\qquad (A.17\text{-}1)$$

where Δx or d are the layer thickness of the phases or the total layer thickness of a diffusion grown system; k_p is called the parabolic growth constant.

Kirkendall markers placed at the initial contact interface will be trapped to a certain composition and move parabolically in time with that composition right from beginning of the diffusion process and act as a reference plane to calculate intrinsic diffusivities at that composition.

If we consider x_K and $x_{M/o}$ as the Kirkendall marker plane position at times, $t = t$ and $t = 0$, respectively, then the Boltzmann variable corresponding to the Kirkendall marker composition can be written as

$$\lambda_K = \lambda(C_K) = \frac{x_K - x_{M/o}}{t^{\frac{1}{2}}} = \frac{x_K}{t^{\frac{1}{2}}} \tag{A.17-2}$$

where initial contact interface $x_{M/o} = 0$.

By differentiating with respect to t and replacing λ_K, one can find the Kirkendall velocity,

$$v_K = \frac{dx_K}{dt} = \frac{d\left(\lambda_K t^{\frac{1}{2}}\right)}{dt} = \frac{\lambda_K}{2t^{\frac{1}{2}}} = \frac{x_K}{2t} \tag{A.17-3}$$

Following Eq. (A.8-7), the velocity of any particular composition in a diffusion zone or Kirkendall marker composition also can be found from the knowledge of intrinsic diffusion coefficients by

$$v = V_B (D_B - D_A) \frac{\partial C_B}{\partial x} \tag{A.17-4}$$

If one has the knowledge on tracer diffusivities, thermodynamic factor and partial molar volumes of the species, the velocity can be found by Eq. (A.15-5).

As mentioned earlier, the intrinsic diffusivities are materials constant. One can determine intrinsic diffusivities at different compositions from incremental couple experiments (i.e. by using different end member compositions in different couples). Because of the different end member compositions, Kirkendall markers placed at the initial contact plane will be trapped at different compositions. Then the velocity curve for any diffusion couple over the whole composition range can be constructed using intrinsic diffusivities calculated from several couples over the homogeneity range of a phase with the help of concentration gradient at that composition in the particular couple.

One can find the *numbers, location and the nature of the Kirkendall plane(s)* from the intersection of the straight line $2tv_K = x_K$ (Eq. (A.17-2)) and a plot of $2tv$ vs. x determined through Eq. (A.17-4) (by multiplying $2t$ in both sides) (see Chap. 1).

However, in the case of a line compound (or in a phase with narrow homogeneity range) one cannot measure the vanishingly small concentration gradient required to plot

velocity curve by Eq. (A.17-4). This equation can be modified to make suitable for line compounds.

Using Eq. (A.4-9) and Eq. (A.17-4) it can be written as

$$v = \frac{V_A V_B}{V_m^2} (D_B - D_A) \frac{\partial N_B}{\partial x} \qquad (A.17\text{-}5)$$

Eq. (A.8-8) with the help of Eq. (A.4-2) can be rearranged as,

$$\tilde{D} V_m = N_A V_A D_B + N_B V_B D_A \qquad (A.17\text{-}6)$$

Integrating Eq. (A.17-5) for a line compound, lets say β-phase, as shown in Fig. (A.11-3), with a very narrow composition range $N_B^{\beta 2} - N_B^{\beta 1}$ (where $N_B^{\beta 1} \leq N_B^{\beta} \leq N_B^{\beta 2}$) with a thickness $\Delta x_{\beta} = \left(x^{\beta 1} - x^{\beta 2} \right)$ grown after annealing for time, t, one can write

$$\int_{x^{\beta 1}}^{x^{\beta 2}} v dx = \int_{N_B^{\beta 1}}^{N_B^{\beta 2}} \frac{V_A V_B}{V_m^2} (D_B - D_A) \partial N_B \qquad (A.17\text{-}7)$$

From the fact that velocity of a line compound is constant at each composition in that phase and the intrinsic diffusivities are materials constants, the Eqs. (A.17-6 and A.17-7) can further be written as

$$v \Delta x_{\beta} = \frac{V_A V_B}{V_m^2} \frac{(D_B - D_A)}{N_A V_A D_B + N_B V_B D_A} \int_{N_B^{\beta 1}}^{N_B^{\beta 2}} \tilde{D} \, dN_B \qquad (A.17\text{-}8)$$

From the definition of integrated diffusion coefficient (Eq. (A.11-1)) and rearranging Eq. (A.17-8), the velocity can be written as

$$v = \frac{V_A}{V_m} \frac{\dfrac{D_B}{D_A} - 1}{\left(\dfrac{V_A D_B}{V_B D_A} \right) N_A + N_B} \frac{\tilde{D}_{int}}{\Delta x_{\beta}} \qquad (A.17\text{-}9)$$

In the case of a multilayered multiphase system containing phases with line compounds or narrow homogeneity range, one can find the velocity curve (line) for each phase separately and *2tv* vs. *x* for the whole system through Eq. (A.17-9) will lead to a stepwise plot.

To construct the velocity plot by Eq. (A.17-4) for the phases with wide homogeneity range and Eq. (A.17-9) for line compounds, one needs to determine first the diffusion

parameters. However, sometimes it could be easier to find the Kirkendall marker velocity directly, without going to details of the diffusion parameters or even without determining the concentration gradient.

If we denote the integrals of the Eqs. (A.10-5a) and (A.10-5b), in the relation for intrinsic diffusion coefficients as $\phi = \int_{-\infty}^{x_K} \frac{Y}{V_m} dx$ and $\psi = \int_{x_K}^{+\infty} \frac{1-Y}{V_m} dx$, and then replacing D_B and D_A in Eq. (A.17-4), it follows that

$$v = \frac{1}{2t} \left[\left(V_B N_B^+ + V_A N_A^+ \right) \phi - \left(V_B N_B^- + V_A N_A^- \right) \psi \right] \qquad \text{(A.17-10)}$$

"-" and "+" represents for the $-\infty$ and $+\infty$ side of the diffusion couple. In the special case when both the end members are from pure materials then in a composition profile plotted with respect to composition of the element B, then $N_B^- = 0$, $N_A^- = 1$, $N_B^+ = 1$, $N_A^+ = 0$ and Eq. (A.17-10) reduces to

$$v = \frac{1}{2t} \left[V_B \phi - V_A \psi \right] \qquad \text{(A.17-11)}$$

Note the main advantage of this relation is that one can use it for phases with a wide homogeneity range as well as for line compounds directly from a composition profile after converting to a Y/V_m vs. x plot. In the case of a diffusion layer consists of line compounds, as shown in Fig. (A.12-2 and -3), Φ and Ψ in Eq. (A.12-1) are related as $\phi = \Phi / \left(N_B^+ - N_B^- \right)$ and $\psi = \Psi / \left(N_B^+ - N_B^- \right)$.

A.18 Molar volume and partial molar volumes

Important prerequisite to calculate diffusion parameters are molar volume and partial molar volumes. By definition, the molar volume, V_m of a phase can be determined from

$$V_m = \frac{V_{cell}}{n_a} N_{Avo} \qquad \text{(A.18-1)}$$

where V_{cell} is the volume of the unit cell (m^3) determined with the help of lattice parameter data available in literature, N_{Avo} is the Avogadro number (6.022×10^{23} mole^{-1}) and n_a is the number of atoms in the unit cell.

When virtually no structural vacancies are present in a unit cell the number of atoms, n_a in the last equation can be replaced by the number of lattice sites, n_s in a unit cell. On the other hand, when constitutional vacancies are created in the structure, then $n_a = n_s - n_V$, with n_V being the number of vacancies present in the unit cell.

Consider, for example, the β-NiAl phase as shown in the phase diagram (Fig. (3.1-1)). The deviation from stoichiometry can be accomplished in principle by two different mechanisms, either by the formation of anti-structure defects or, as in the case of the Al-rich NiAl intermetallics, by the occurrence of structural vacancies on the Ni-sublattice, so called triple-defects. The concentration of the constitutionally generated vacancies can be appreciable.

The molar volume can be calculated from the available data on the lattice parameter of cubic β-NiAl phase (Fig. (A.18-1)) and vacancy concentrations (Fig. (A.18-2)) as shown in Fig. (A.18-3). The presence of antisite atoms does not affect the number of atoms present in the unit cell.
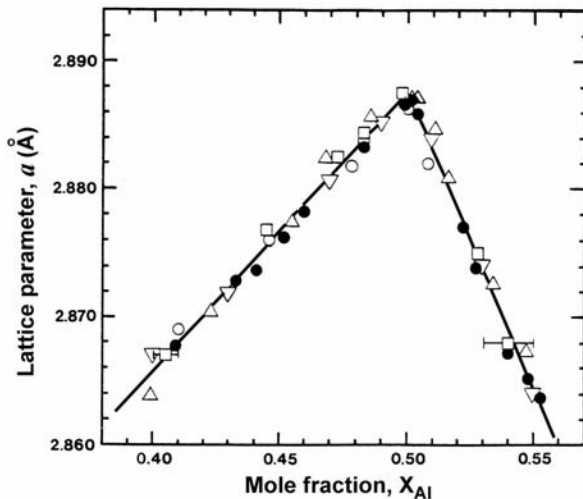
Fig. (A.18-1) Variation of lattice parameter as a function of mole fraction in β- NiAl phase [39].
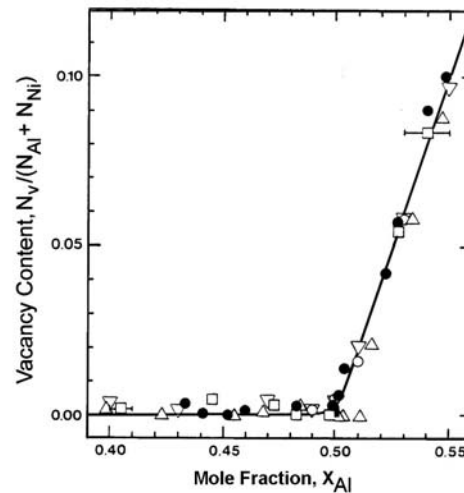
Fig. (A.18-2) Variation of vacancy fraction, $N_V/(N_{Ni}+N_{Al})$ in the NiAl phase as a function of the mole fraction in β-NiAl phase [39].

The values of the partial molar volumes of the components in NiAl were determined from the extensions of the plot in Fig. (A.18-3) at $X_{Al} = 1$ and $X_{Al} = 0$, respectively. For off-stoichiometric compositions it was found that $V_{Ni} = 1.08 \times 10^{-6}$, $V_{Al} = 13.4 \times 10^{-6}$ m^3/mole in the Al-rich domain, and $V_{Ni} = 6.44 \times 10^{-6}$, $V_{Al} = 8.05 \times 10^{-6}$ m^3/mole in the

Ni-rich part of the homogeneity range. Note that small absolute changes in the molar volume near the "equiatomic" composition have a dramatic effect on the vales of the partial molar volume of the components in β-NiAl phase.

However, in most cases, the details of the lattice parameter and/or vacancy concentration, over the whole homogeneity range of the phases are not available. In that case, we generally can use the molar volume calculated at stoichiometric compositions from available data in reference as the average molar volume of the phase. There are two options regarding the partial molar volume of the components in a phase. One can assume, $V_A = V_B = V_m$ and use the molar volume of the phases as the partial molar volume of the components in that phase. In our study we have taken this assumption in the case of line compounds on the conjecture that the molar volume does not change with composition in that phase. In the case of a system containing phases with wide homogeneity range, we have considered the molar volumes of the pure components as the partial molar volumes of the elements (i.e. by assuming $V_A \neq V_B$, but constant following Fig (A.6-1a)) in a phase.
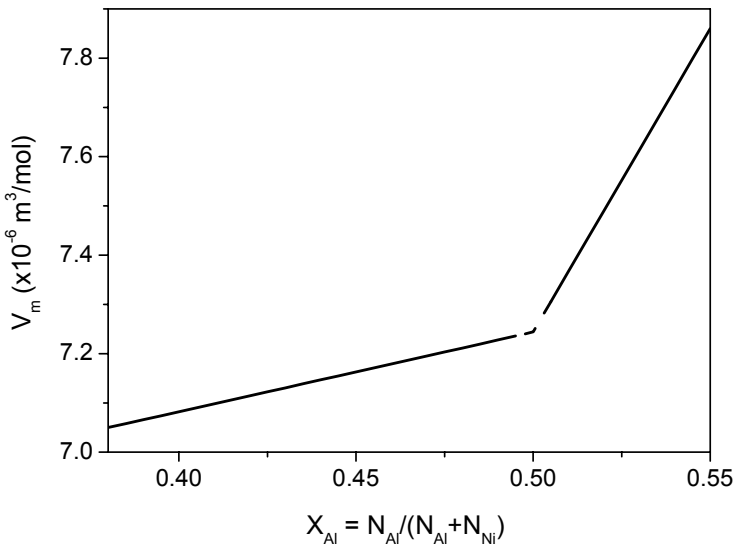
Fig. (A.18-3) Variation of the molar volume, V_m within the homogeneity range of the β- NiAl phase

A.19 Initial contact plane, x_o in the case of change in total volume with reaction/mixing

To determine interdiffusion coefficients by the Matano-Boltzmann analysis (A.5), it is necessary to find the initial contact plane, x_o. If the total volume does not change, one can find the position graphically through the Eq. (A.5-8). If, however, the total volume

does change, one might wonder whether the same procedure can be followed using Y/V_m or $(1-Y)/V_m$ vs. x plot, as given in Eqs. (A.19-1 and A.19-2).

The initial contact plane positions are found at $x_o^{-\infty}$ and $x_o^{+\infty}$ as shown in Figs. (A.19-1 and A.19-2) by equalizing the areas A and B.

$$\int_{l^{-\infty}}^{x_o^{+\infty}} \frac{Y}{V_m}\,dx + \int_{x_o^{+\infty}}^{l^{+\infty}} \left(\frac{1}{V_m^+} - \frac{Y}{V_m}\right)dx = 0 \tag{A.19-1}$$

$$\int_{l^{-\infty}}^{x_o^{-\infty}} \left(\frac{1}{V_m^-} - \frac{(1-Y)}{V_m}\right)dx + \int_{x_o^{-\infty}}^{l^{+\infty}} \frac{(1-Y)}{V_m}\,dx = 0 \tag{A.19-2}$$

where $l^{+\infty}$ and $l^{-\infty}$ are the coordinates at the right- and left-hand unreacted part of end-members.

From the fact that A and B (in Fig. (A.19-1) and (A.19-2)) are equal, we can write

$$A+C = B+C \tag{A.19-3}$$

Fig. (A.19-1) Schematic representation of the Y/V_m vs. x plot. The position of initial contact plane, $x_o^{+\infty}$ was found by equalizing the area A and B.
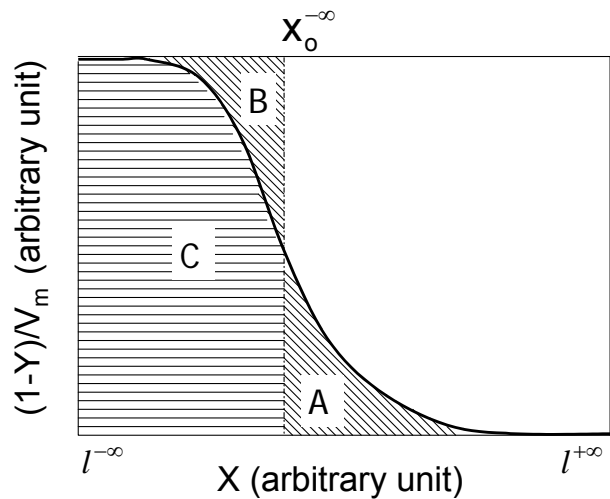
Fig. (A.19-2) Schematic representation of the $(1-Y)/V_m$ vs. x plot. The position of initial contact plane, $x_o^{-\infty}$ was found by equalizing the area A and B.

Considering Fig. (A.19-1), after rearranging Eq. (19-3) can be written as

134

$$l^{+\infty} - x_o^{+\infty} = V_m^+ \int\limits_{l^{-\infty}}^{l^{+\infty}} \frac{Y}{V_m} dx \tag{A.19-4}$$

So by this integration of Y/V_m vs. x one finds the initial contact position, $x_o^{+\infty}$ fixed with respect to the right-hand end of the couple.

In the same way from Eq. (A.19-3) and Fig. (A.19-2) after rearranging we can write

$$x_o^{-\infty} - l^{-\infty} = V_m^- \int\limits_{l^{-\infty}}^{l^{+\infty}} \frac{(1-Y)}{V_m} dx \tag{A.19-5}$$

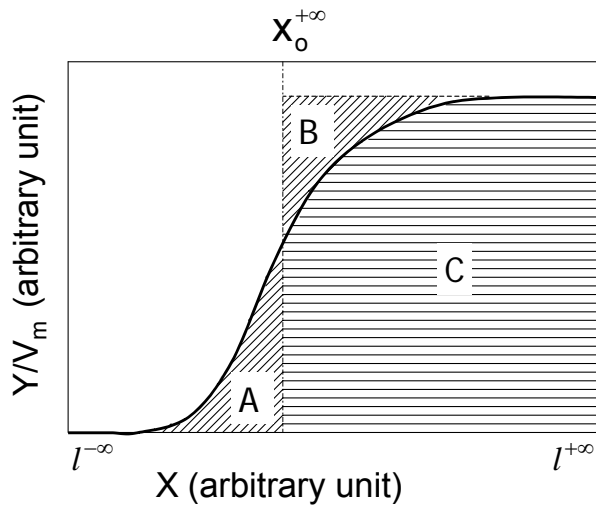and we find the initial contact position $x_o^{-\infty}$ fixed with respect to the left-hand end of the couple.

The molar volume in a system can be written as:

$$V_m = V_m^- + \left(V_m^+ - V_m^-\right)Y \pm \Delta V \tag{A.19-6}$$

where V_m is the molar volume, V_m^- and V_m^+ are the molar volumes at the left- and right hand unreacted end of the diffusion couple where $V_m^+ \rangle V_m^-$. The term $\pm \Delta V$ gives the deviation of molar volume from the ideality.

Adding Eq. (19-4 and -5) and rearranging leads to

$$l^{+\infty} - l^{-\infty} - x_o^{+\infty} + x_o^{-\infty} = \left(V_m^+ - V_m^-\right)\int\limits_{l^{-\infty}}^{l^{+\infty}} \frac{Y}{V_m} dx + \int\limits_{l^{-\infty}}^{l^{+\infty}} \frac{V_m^-}{V_m} dx \tag{A.19-7}$$

With the help of Eq. (A.19-6), Eq. (A.19-7) can be written as

$$x_o^{+\infty} - x_o^{-\infty} = \pm \int\limits_{l^{-\infty}}^{l^{+\infty}} \frac{\Delta V}{V_m} dx \tag{A.19-8}$$

In the ideal condition, if the partial molar volumes are constant, $x_o^{+\infty}$ and $x_o^{-\infty}$ will be found at same location since $\pm V$ will be equal to *zero*. However, when there is a deviation of molar volume from the ideality, the locations of $x_o^{+\infty}$ and $x_o^{-\infty}$ will be different. This difference will be equal to the integral in Eq. (A.19-8), which is in fact equal to the expansion or shrinkage Δx of the couple, depending on the positive or negative deviation of the molar volume from ideality, respectively.

The problem is: which is the position of x_o of the original contact plane between the end-members? It cannot, of course, depend on the choice of the reference point $l^{-\infty}$ or $l^{+\infty}$.

This problem might better be understood from examples on hypothetical systems. Let us consider two compounds in A-B system, α ($A_{0.75}B_{0.25}$) and γ ($A_{0.25}B_{0.75}$), which react to produce 2 moles of β ($A_{0.4}B_{0.6}$). If we consider the molar volumes of α and δ as being 1 and 2 units, respectively, then in the ideal condition when the partial molar volumes of the species are constant, the molar volumes of β will be 1.7 units.

In terms of reaction equations we can write:

$$0.6A_{0.75}B_{0.25}(\alpha) + 1.4A_{0.25}B_{0.75}(\gamma) = A_{0.4}B_{0.6}(\beta) \qquad \text{(A.19-9)}$$
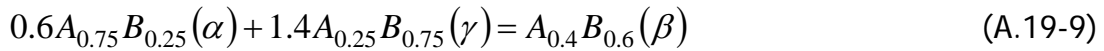
In terms of volume balance:

$$0.6 \times 1(\alpha) + 1.4 \times 2(\gamma) = 2 \times 1.7(\beta) \qquad \text{(A.19-10)}$$

From the volume balance it is clear that 0.6 units of α will react with 2.8 units of γ to produce 3.4 units of β, which means that there is no change in total volume after reaction.

Next, we consider a positive deviation of molar volume from the ideality by choosing for the molar volume of β 1.85 units. Then the volume balance for Eq. (A.19-9) will be

$$0.6 \times 1(\alpha) + 1.4 \times 2(\gamma) = 2 \times 1.85(\beta) \qquad \text{(A.19-11)}$$

which means that from total 3.4 units of reactants a total of 3.7 units of product will be formed, i.e. there will be expansion by $\Delta x = 0.3$ units as shown in Fig. (A19-3a and -3b).

(a)   (b)

Fig. (A.19-3) Schematic illustration of the effect of a positive deviation of the molar volume from the ideality after interaction for the ideal and non-ideal cases: a) fixing from left-hand side, and b) fixing from right-hand side.

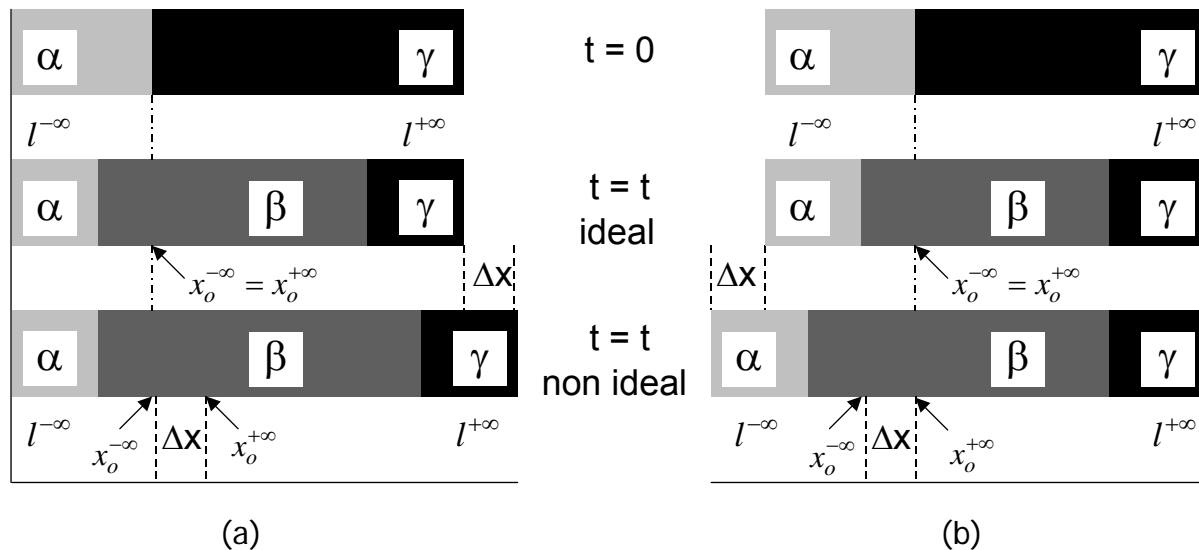In the ideal case, the initial contact planes, $x_o^{-\infty}$ (determined from the $(1-Y)/V_m$ vs. x plot) and $x_o^{+\infty}$ (determined from the Y/V_m vs. x plot) are found to be at the same location of 0.6 units from α/β interface as shown in Fig. (A.19-3a and -3b). In the non-ideal case, the locations of $x_o^{-\infty}$ and $x_o^{+\infty}$ are found to be at 0.6 and 0.9 units, respectively from α/β interface and the difference in the locations between these two planes ($x_o^{+\infty} - x_o^{-\infty}$) is, in fact, exactly equal to the expansion of the diffusion couple, Δx after interaction as shown in Fig. (A.19-3a and -3b). In the case of a positive deviation of the molar volume from ideality $x_o^{+\infty} > x_o^{-\infty}$, whereas in the case of negative deviation of molar volume from ideality $x_o^{+\infty} < x_o^{-\infty}$, if we take the position of α/β interface as x = 0.

So the "real" position of x_o is somewhere in between the values of $x_o^{+\infty}$ and $x_o^{-\infty}$. In the case of homogeneous expansion or contraction, one can calculate its position from the equation $x_o = x_o^{-\infty} \bigg/ \left(1 - \dfrac{\Delta x}{d}\right)$, where Δx is the expansion/shrinkage of the couple and d is the total layer width. In the example given above, this leads to a value of 0.65 units from the α/β interface. By assuming homogeneous expansion/shrinkage, we consider that the ratio of partial molar volumes of the species, V_B/V_A is constant over the entire diffusion zone. In real situations considering this assumption is more or less realistic if one line-compound grows in a diffusion couple, but might fail in more complex systems. On the other hand it should be mentioned that we are dealing with a second-order effect: the expansion/shrinkage of a couple is mostly below a few percent of the layer thickness. Therefore, the possible error in the position of x_o is mostly within the limits of error.

Sauer-Freise [23], Wagner [24], Den Broeder [25] and van Loo [27] circumvented the problem and derived the relations for interdiffusion and intrinsic diffusion coefficients, where finding the position of x_o is not necessary for calculations. However, in these equations, the values of V_A and V_B required for calculations are often unknown. Besides, to construct the velocity diagram, one still needs to calculate the position of initial contact plane.

In fact through the Sauer-Freise treatment adopted by Wagner as explained in A.9 one can find the initial contact plane. If inert markers are used before interaction, one can

calculate the value of $2tv_K$ at the Kirkendall marker position after interaction provided that the values of V_A and V_B are known. This gives the displacement of Kirkendall marker plane from the initial contact plane and it is possible to find the accurate position the initial contact plane from the known position of the Kirkendall marker plane position.

It is possible to show that the expression for the ratio of diffusivities (Eq. (A.10-6)) at the Kirkendall plane in β-phase can be given by

$$\frac{D_B}{D_A} = \frac{\left[N_B^{\gamma} \int\limits_{-\infty}^{x_K} \frac{Y}{V_m} dx - N_B^{\alpha} \int\limits_{x_K}^{+\infty} \frac{(1-Y)}{V_m} dx \right]\left[-\left(1 - N_B^{\gamma}\right)\int\limits_{-\infty}^{x_0} \frac{Y}{V_m} dx + \left(1 - N_B^{\alpha}\right)\int\limits_{x_0}^{+\infty} \frac{(1-Y)}{V_m} dx \right]}{\left[-\left(1 - N_B^{\gamma}\right)\int\limits_{-\infty}^{x_K} \frac{Y}{V_m} dx + \left(1 - N_B^{\alpha}\right)\int\limits_{x_K}^{+\infty} \frac{(1-Y)}{V_m} dx \right]\left[N_B^{\gamma} \int\limits_{-\infty}^{x_o} \frac{Y}{V_m} dx - N_B^{\alpha} \int\limits_{x_0}^{+\infty} \frac{(1-Y)}{V_m} dx \right]}$$

$$(A.19-12)$$

Here, no values of V_A and V_B are needed; the expression is valid for the cases where $V_A = V_B$, $V_A \neq V_B$ but constant and for the case where homogeneous expansion or shrinkage occurs. In fact, comparison between Eqs. (A.10-6 and A.19-12) shows the relation between the value of V_A/V_B and the position of the initial contact plane x_o in the laboratory frame of reference.

A.20 Diffusion based approach to predict the thickness of the layers, Kirkendall marker position and marker velocity

We shall illustrate this approach by using examples of the interaction in the Co-Si system. The experimental data required for the calculation can be found from Table (4.1-1) (Chap. 4).

Lets consider the case when Co and Si are coupled at 1100 °C for 100 hours. According to phase diagram (Fig. (4.1-1)) three phases, Co_2Si, $CoSi_2$ and $CoSi_2$, with narrow homogeneity range should develop and grow during interdiffusion. A schematic diagram in Fig. (A.20-1) shows the diffusion zone developed after annealing for time t at 1100 °C and the thickness of the layers are assumed to be u, v and w μm for Co_2Si, $CoSi_2$ and $CoSi_2$, respectively. First we consider that in all the phases Kirkendall marker planes are present, so that they divide each layer into two parts, $u = u_1 + u_2$, $v = v_1 + v_2$ and $w = w_1 + w_2$.

Calculation of the thickness of the layers:

First, from the relation for integrated diffusion coefficients, $\tilde{D}_{\text{int}}$ we can calculate the thickness of the layers using the schematic composition profile shown in Fig. (A.20-1). Data required for molar volumes are listed in Table (4.1-1). Three equations can be written for the integrated diffusion coefficients of three phases developed following Eq. (A.11-2) as,

$$\tilde{D}_{\text{int}}^{Co_2Si} = \frac{1}{t}\left(0.11u^2 + 0.084\,uv + 0.05\,uw\right) \times 10^{-12} \; m^2 \, / \, s$$

$$\tilde{D}_{\text{int}}^{CoSi} = \frac{1}{t}\left(0.125\,u^2 + 0.084\,uv + 0.071\,uw\right) \times 10^{-12} \; m^2 \, / \, s \qquad \text{(A.20-1)}$$

$$\tilde{D}_{\text{int}}^{CoSi_2} = \frac{1}{t}\left(0.11u^2 + 0.066\,uv + 0.098\,uw\right) \times 10^{-12} \; m^2 \, / \, s$$

From Table (4.1-1), we know the experimentally determined values of the integrated diffusion coefficients for different phases and we can find the thickness of the layers by solving the three equations in Eq. (A.20-1) for an annealing time of 100 hrs. The thickness of the layers are found as $u = \Delta x_{Co_2Si} = 131$ μm, $v = \Delta x_{CoSi} = 321$ μm and $w = \Delta x_{CoSi} = 6.8$ μm.
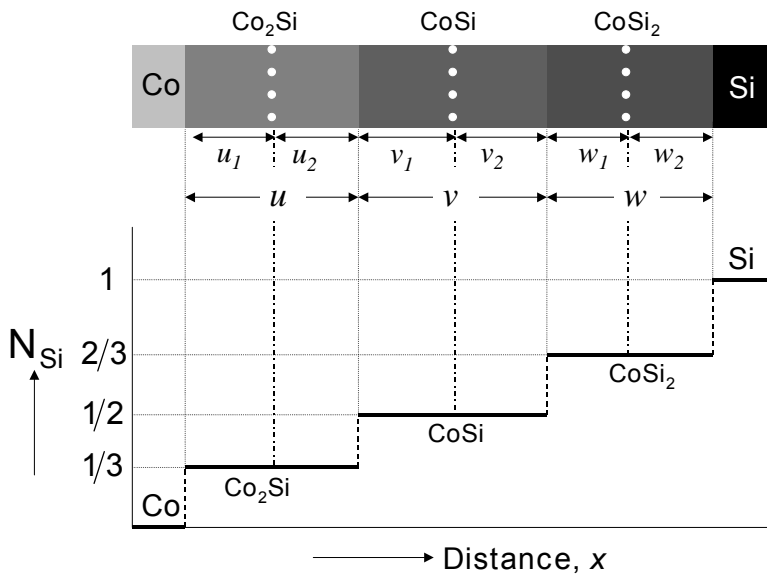
Fig. (A.20-1) Schematic diagram of the diffusion layers grown in a diffusion couple Co/Si after annealing at 1100 °C for 100 hrs. The white dots represent the inert markers in assumed positions of the Kirkendall marker planes.

Kirkendall marker positions:

Kirkendall marker position(s) can be found from the ratio of diffusivities of the phases at Kirkendall marker positions. Let us consider the layer for Co_2Si-phase. The ratio of diffusivities D_{Si}/D_{Co} in this phase can be written with the help of Eq. (A.12-1) as

$$\frac{V_{Co}D_{Si}}{V_{Si}D_{Co}} = \frac{\frac{1}{3}u_1}{\left(1-\frac{1}{3}\right)u_2 + \left(\frac{6.56}{6.60}\right)\left(1-\frac{1}{2}\right)v + \frac{6.56}{7.75}\left(1-\frac{2}{3}\right)w} \qquad (A.20\text{-}2)$$
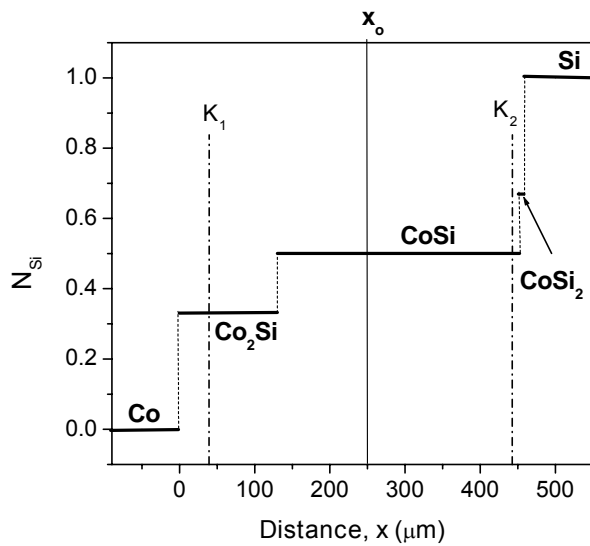
Fig. (A.20-2a) The calculated profile of the diffusion couple of Co/Si at 1100 °C after annealing for 100 hrs along with details of the Kirkendall marker position and the initial contact plane, x_o.
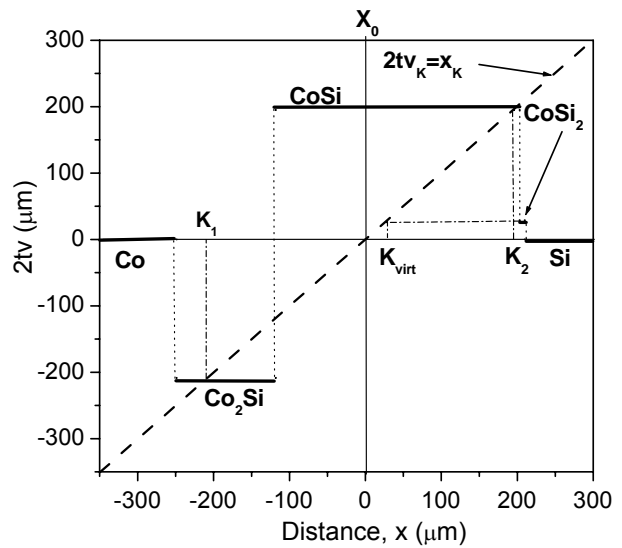
Fig. (A.20-2b) The Kirkendall velocity diagram calculated for the diffusion couple Co/Si for the annealing time of 100 hrs at 1100 °C. Note the presence of two Kirkendall planes. A virtual Kirkendall plane position, K_{virt}, is shown for the phase $CoSi_2$.

We know from Table (4.1-1) the ratio of diffusivities in the Co_2Si phase and the thickness of the layers as $u = u_1 + u_2 = 131$ μm, $v = 321$ μm and $w = 6.8$ μm (see above). Solving Eq. (A.20-2), we find the value of $u_1 = 40$ μm and $u_2 = 91$ μm which gives the location of the Kirkendall plane in this phase.

In the same way, from the ratio of diffusivities at assumed marker planes in the CoSi and $CoSi_2$ phases, we find $v_1 = 313.8$ μm, $v_2 = 7.6$ μm, $w_1 = -209$ μm and $w_2 = 215.8$

μm. The negative value of w_I reflects that there will be no Kirkendall marker plane in the CoSi$_2$-phase (for further clarification, see Chap. 4.1).

Initial contact plane, x_o and velocity diagram construction:

The initial contact plane, x_o to plot the velocity diagram can be found from the Sauer-Freise treatment as explained in the section A.19. This position was found to be at 250 μm from the Co/Co$_2$Si interface. The details of the calculated positions are shown in Fig. (A.20-2a). From the initial contact plane position, x_o, Kirkendall plane positions, x_K ($= x_K - x_o$) were found to be at -210 and 195 μm in the Co$_2$Si and CoSi phases, respectively.
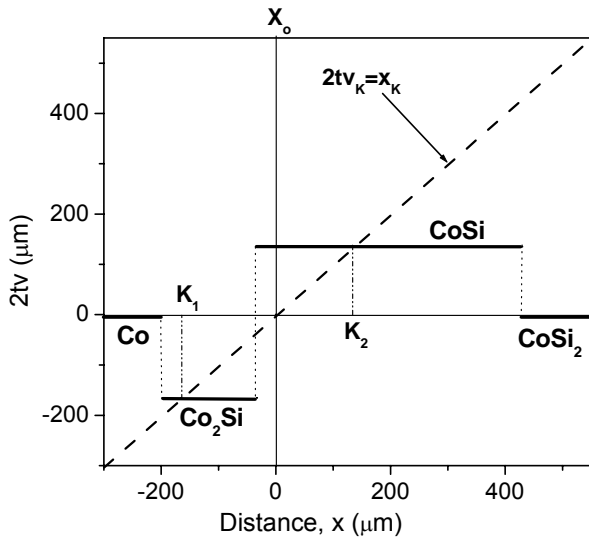
Fig. (A.20-3a) The Kirkendall velocity diagram calculated for the diffusion couple Co/CoSi$_2$ for the annealing time of 100 hrs at 1100 °C. Note the presence of Kirkendall plane in both the phases.
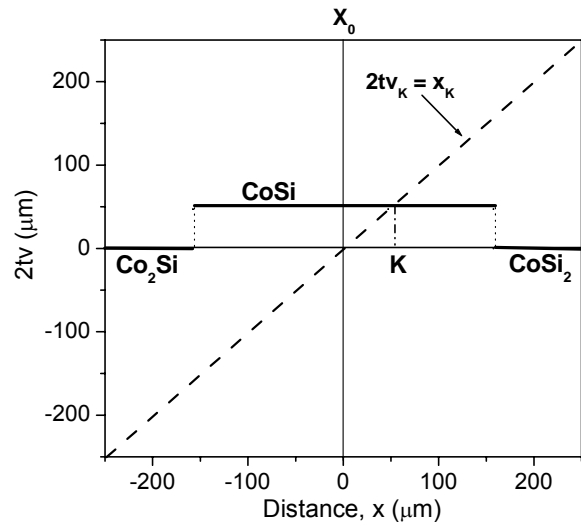
Fig. (A.20-3b) The Kirkendall velocity diagram calculated for the diffusion couple Co$_2$Si/CoSi$_2$ for the annealing time of 25 hrs at 1100 °C.

Another way of finding the velocity of the phases (and the Kirkendall marker plane in those phases) is from Eq. (A.17-9) with the help of data available on the integrated diffusion coefficients, thickness of the layers and the ratio of intrinsic diffusivities of the species as listed in Table (4.1-1). The values for V_{Si} and V_{Co} are taken equal to the molar volume of the relevant phase: $V_{Si} = V_{Co} = V_m$. The values are calculated -2.9×10^{-10}, 2.7×10^{-10} and 0.4×10^{-10} m/s for the phases Co$_2$Si, CoSi and CoSi$_2$, respectively. Now, we can construct the velocity diagram by plotting *2tv* vs. *x* from the velocity data calculated by Eq. (A.17-9), which gives a stepwise plot and by the straight-line $2tv_K = x_K$, from the Kirkendall marker position found as shown in Fig. (A.21-2b). Note that the straight line, $2tv_K = x_K$ intersects the velocity diagram only twice, in the

phases of Co_2Si and $CoSi$, which reflects the presence of two Kirkendall planes in the system. The virtual Kirkendall plane, K_{virt} [40] for the $CoSi_2$ can be found from the intersection of the extension of the velocity line for that phase and the line $2tv_K = x_K$.

Same way one can calculate the details of the other couples, such as for $Co/CoSi_2$ and $Co_2Si/CoSi_2$. In the $Co/CoSi_2$ diffusion couple two phases, Co_2Si and $CoSi$ will grow, whereas in the $Co_2Si/CoSi_2$ couple only one phase $CoSi$ will grow, according to the phase diagram. The calculated values for all the diffusion couples are listed in Table (4.1-2). The velocity curves constructed are shown in Fig. (A.20-3a and 3b). The positions of the Kirkendall planes were found to be in good agreement with the experimental results as shown in Fig. (4.1-2, -3 and -4), after taken care of the pores present in the layers.

A. 21 Some special notes

i) According to the phase rule, ($F = C-P+2$, where F is the degree of freedom, C is the number of components and P is the number of phases) the presence two-phase regions are forbidden, in a binary diffusion couple, having three degrees of freedom: pressure, temperature and composition. However, in many cases the phase interfaces of the layers are found wavy resulting from the anisotropy in the crystal orientations having different rates of diffusion.

ii) In the derivation of the equations we assumed that at the interface two adjacent phases are in thermodynamic equilibrium. In practice this requirement is fulfilled if the annealing time is sufficiently long. It is verified by the parabolic time dependence of the penetration plot.

According to the parabolic law of diffusion, all the compositions in a diffusion zone move parabolically in time in the laboratory fixed frame of reference (initial contact plane). Before proceeding to calculate diffusion parameters one should make experiments for at least two different annealing times with the same end-member compositions and plot $c_i \, vs. x/t^{1/2}$ to check whether the plots coincide. One can also make diffusion couples for different annealing times and for different combinations of end-members and then calculate the interdiffusion coefficients. The interdiffusion coefficient is a material constant and the value at a particular composition and annealing temperature should be the same.

In the case of a system with line compounds, one should conduct experiments for different annealing times and plot Δx^2 vs. t. All data points should fall in a straight line according to Eq. (A.17-3).

iii) Vacancy diffusion can operate through the lattice (called volume diffusion), grain boundary or dislocations (called pipe diffusion). At high homologous temperature (T/T_m, T_m is the melting point) lattice diffusion is more favourable whereas at low homologous temperature short circuit can take place, i.e. the diffusion rate through grain boundaries or dislocations is higher. Both the activation energy, Q and frequency factor, D_o in Arrhenius equation $D = D_o exp(-Q/RT)$ for the short circuit diffusion is less than the lattice diffusion and one gets the deviation in the slope when the diffusion coefficient is plotted versus temperature, because of changing on the diffusion mechanism as shown in Fig. (A.21-1). R is the gas constant (8.31 J/mole.K) and T is the temperature in Kelvin.

iv) The bonding face may sometimes be covered by a very thin layer of, for example, an oxide film. If the oxide film acts as a diffusion barrier, one may find an incubation time before the diffusion takes place. This problem was found in a Ti-Al system [41].

v) Small amounts of impurities e.g. carbon and phosphorus may affect the diffusion behaviour. With the presence of impurities, the system may change to ternary system and boundaries of the layers need no longer be straight. Besides, different compounds may also form in the layer [42]. The impurities may also affect the diffusion process by interacting with vacancies or by segregation to dislocations and grain boundaries.
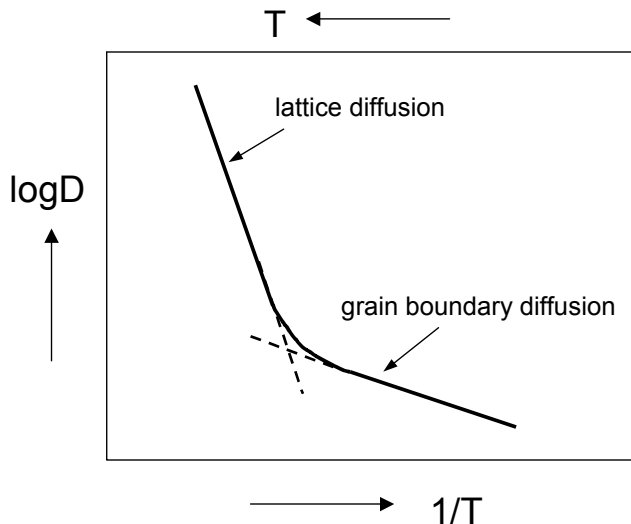

Fig. (A.21-1) Schematic diagram of $\log D$ vs. $1/T$ for polycrystal sample is showing domination of volume (lattice) diffusion at high temperatures and of grain boundary diffusion at low temperatures.

vi) The reaction between elements to form a new compound may be the rate-limiting step, specially in thin-film condition, but after reaching a certain thickness the diffusion process eventually becomes rate limiting. This is extensively discussed in Ref. [43, 44]. In fact, in bulk diffusion couples at high temperatures, no clearly proven case of reaction limited growth is known to the author although an insufficient number of data points and the spread in the plot of Δx^2 vs. t can make it difficult to find the exact relation between the layer thickness and time.

vii) Sometimes the extension of the curve Δx^2 vs. t to time, $t = 0$, shows a positive value of Δx, instead of *zero*. That may happen by fast grain boundary diffusion in the initial stage, because of the presence of small grains. However, in later stage, when by recrystallisation large grains are formed with increasing annealing time, the growth will be parabolic.

The same behaviour also can be found because of the growth of the layers during the heating stage.

viii) Sometimes one or more phases seem to be missing in the diffusion zone. In thin-film experiments or after short annealing times this can occur and may be the result of a competition between the linear and parabolic stage during growth [43]. After long annealing times in a bulk diffusion couple it may happen because of the very high difference in the growth rate (i.e. interdiffusion or integrated diffusion coefficient) of the phases. In fact, layers could be present as very thin layers and not easy to detect. In the Au-Sn diffusion couple, the phase Au_5Sn was thought to be missing according to literature (as discussed in Chap. 6.3). After careful etching, we found the presence of this layer, which was not visible without an etching treatment.

Another reason for the absence of some phases can occur because of a very high Kirkendall effect. Especially when several phases are involved, great difference may occur in the diffusion rate of the components. It may cause supersaturation of vacancies near a phase boundary. Vacancies will then accumulate to form large number of pores, which ultimately may result into a gap at interface. In that case supply of the diffusion component stops and phases already developed adjacent to the gap will be consumed and vanish. The cracks arising from other sources, like volume effects or a difference in the coefficient of thermal expansion can cause the same effect.

ix) A non-equilibrium phase may nucleate [45] in a diffusion couple because of surface energy contributions [44], especially in thin-film condition.

x) There are some examples when the use of external pressure changes the kinetics of the layer growth as well as interface concentrations [46]. Large pressures lead to interface concentration values, which are identical with equilibrium bulk phases given by the phase diagram. According to our own knowledge an external pressure of typically ~5 MPa is enough to make a good contact between end members. We never found differences between compositions of two phases measured in equilibrated two-phase alloys and those at the phase interfaces in long annealed diffusion couples.

References

1. W.C. Roberts-Austen, On the diffusion of metals, Phil. Trans. Roy. Soc. **A187** (1896) 383-415
2. A. Fick, Uber diffusion, Progg. Ann. **94** (1855) 59
3. J. Crank, The mathematics of diffusion, Oxford University Press, 1956
4. G.v. Hevesy and W. Seith-Freiburg, Diffusion in metallen, Z. Electrochem **37** (1931) 528-31
5. G. Grube and A. Jedele, Diffusion und korrosion von kupfer-nickel-Legierungen, Z. Elechtrochem. **38** (1932) 799-807
6. L.E. Trimble, D. Finn and A. Cosgarea, Jr., A mathematical analysis of diffusion coefficients in binary systems, Acta Met. **13** (1965) 501-07
7. L. Boltzmann, Zur integration der diffusionsgleichung bei variabeln diffusions-coefficienten, Ann. Physik. **53** (1894) 959-64
8. C. Matano, On the relation between the diffusion-coefficients and concentrations of solid metals (the nickel-copper system), Jap. J. Phys. **8** (1933) 109-13
9. L.B. Pfeil, The oxidation of iron and steel at high temperatures, J. Iron Steel **119** (1929) 501-47
10. G.S. Hartley, Diffusion and swelling of high polymers, Part I: The swelling and solution of a high polymer solid considered as diffusion process, Trans. Faraday Soc. **46** (1946) 6-11
11. A.D. Smigelkas and E.O. Kirkendall, Zinc diffusion in alpha brass, Trans. AIME **171** (1947) 130-34.
12. L.S. Darken and R.W. Gurry, Physical chemistry of metals, McGraw Hill Book Company, 1953.
13. L.C.C. da Silva and R.F. Mehl, Interface and marker movements in diffusion in solid solutions of metals, Trans. AIME **191** (1951) 155-73
14. H. Nakajima, The discovery and acceptance of the Kirkendall effect: The result of a short research career, JOM **49** (1997) 15-19
15. L.C.C. da Silva, A reflection on R.F. Mehl and the Kirkendall effect, JOM **50** (1998) 6-7
16. H.B. Huntington and F. Seitz, Mechanism for self diffusion in metallic copper, Phys. Rev. **61** (1942) 315-25
17. R.F. Mehl, Discussion following Ref. [11], Trans. AIME **171** (1947) 135-42
18. L.S. Darken, Diffusion, mobility and their interrelation through free energy in binary metallic systems, Trans. Met. Soc. AIME **175** (1948) 184-201
19. G.S. Hartley and J. Crank, Some fundamental definitions and concepts in diffusion process, Trans. Faraday Soc. **45** (1949) 801-8
20. F. Seitz, On the theory of vacancy diffusion in alloys, Phys. Rev. **15** (1948) 1513-23
21. J. Bardeen, Diffusion in binary alloys, Phys. Rev. **1** (1949) 1403-5
22. R.W. Ballufi, On the determination of diffusion coefficients in chemical diffusion, Acta Met. **8** (1960) 871-73

23. F. Sauer and V. Freise, Diffusion in binären gemischen mit volumenänderung, Z. Electrochem. **66** (1962) 353-63
24. C. Wagner, The evaluation of data obtained with diffusion couples of binary single-phase and multiplayer systems, Acta Met. **17** (1969) 99-107
25. F.J.A. den Broeder, A general simplification and improvement of the Matano-Boltzmannn method in the determination of the interdiffusion coefficients in binary systems, Scripta Met. **3** (1969) 321-26
26. T. Heumann, Zur berechnung von diffusionkoeffizienten bei ein und mehrphasiger diffusion in festen legierungen, Z. Phys. Chem. 201 (1952)168-89
27. F.J.J. van Loo, On the determination of diffusion coefficients in a binary metal system, Acta Met. **18** (1970) 1107-11
28. J.R. Manning, Diffusion in a chemical concentration gradient, Phys. Rev. **124** (1961) 470-82
29. J.R. Manning, Diffusion and the Kirkendall shift in binary alloys, Acta Met. **15** (1967) 817-26
30. J. R. Manning, Cross terms in the Thermodynamic diffusion equations for multicomponent alloys, Met. Trans. **1** (1969) 499-505
31. M.A. Dayananda, Atomic mobilities and vacancy wind effects in multicomponent alloys, Met. Trans. **2** (1971) 334-35
32. D.J. Schmatz, H.A. Domain and H.I. Aaronson, Test of the Manning vacancy-flux correction in α Cu-Zn, J. Appl. Phys. **37** (1966) 1741-43
33. N.R. Iorio, M.A. Dayananda and R.E. Grace, Intrinsic diffusion and vacancy wind effects in Ag-Cd alloys, Met. Trans. **4** (1973) 1339-46
34. A. Kohn, J. Levasseur, J. Philibert and M. Wanin, Essai de verification experimentale des theories de l'effect Kirkendall dans systemes fer-nickel et fer-cobalt, Acta Met. **18** (1970) 163-73.
35. R.O. Meyer, Pressure and vacancy-flow effects on the Kirkendall shift in silver-gold alloys, Phys. Rev. **181** (1969) 1086-94
36. M.J. Dallwitz, The vacancy-flow effect in silver-gold alloys, Acta Met. **20** (1972) 1229-34
37. P.T. Carlson, Interdiffusion and intrinsic diffusion in binary vanadium-titanium solid solutions at 1350 °C, Met. Trans. A **7A** (1975) 199-208
38. Y.H. Sohn and M.A. Dayananda, Interdiffusion, intrinsic diffusion and vacancy wind effect in Fe-Al alloys at 1000 °C, Scripta Mat. **40** (1999) 79-84
39. Y.A. Chang and J.P. Neumann, Thermodynamics and defect structure of intermetallic phases with the B2 (CsCl) structure, Prog. Solid State Chem. **14** (1982) 221-301
40. F.J.J. van Loo, B. Pieraggi and R.A. Rapp, Interface migration and the Kirkendall effect in diffusion driven phase transformations, Acta Mat. Metall. **38** (1990) 1769-79
41. F.J.J. van Loo, Diffusion in the Titanium-Aluminium system, PhD Thesis, 1971
42. C.P. Heijwegen and G.D. Rieck, Influence of carbon on the interdiffusion of Mo and Ni, Metall. Trans. **4** (1973) 2159-67
43. V.I. Dybkov, Reaction diffusion in heterogeneous binary systems, J. Mater. Sci. **21** (1986) 3078
44. F.M. d'Heurle, Nucleation of a new phase from the interaction of two adjacent phases: some silicides, J. Mater. Res. **3** (1988) 167-95
45. B. Lustmann and R.F. Mehl, Trans. Met. Soc. AIME, **147** (1942) 369-95
46. Y. Adda and J. Philibert, Atom movements and mass transport in solids, Les Éditions de Physique, Les Ulis (1991)

Further study
1. L.S. Darken and R.W. Gurry, Physical chemistry of metals, McGraw Hill Book Company, 1953.
2. J. Crank, The mathematics of diffusion, Oxford University Press, 1956.
3. P. G. Shewmon, Diffusion in solids, McGraw-Hill Book Company, USA, 1963.
4. J.S. Kirkaldy, D.J. Young, Diffusion in the condensed state, The Institute of Metals, 1987.
5. Y. Adda and J. Philibert, Atom movements and mass transport in solids, Les Éditions de Physique, Les Ulis, 1991.
6. A.R. Alnatt, A.B. Lidiard, Atomic transport in solids, Cambridge University Press, 1993.
7. M.E. Glicksman, Diffusion in solids, John Wiley & Sons, Inc., NewYork, 2000.

Summary

Diffusional growth of intermetallic compounds and elucidation of the Kirkendall effect accompanying solid-state reactions are subjects of considerable complexity, having broad applicability in materials science and engineering.

The migration of inert Kirkendall markers as a result of unequal mobilities of the components during solid-state interdiffusion in a binary system can be rationalized using the Kirkendall velocity diagram. In a diffusion-controlled interaction the Kirkendall plane (identified by inert particles placed at the initial contact surface of a reaction couple), need not be unique. Multiple planes can be developed but, on the other hand, the Kirkendall plane after interaction can be unstable, i.e. markers can get dispersed into the diffusion zone and no unique location of the Kirkendall plane can be defined.

An experimental verification of the phenomenological approach to rationalize possible bifurcation of the Kirkendall plane inside one single diffusion-grown compound layer is presented. A reaction couple, in which a single layer of β-NiAl intermetallic is growing during interdiffusion from its adjacent phases, is used as a model system. The corresponding Kirkendall velocity diagram was constructed on the basis of inter- and intrinsic diffusion coefficients data obtained with the diffusion couple technique. The agreement between the predicted and experimentally determined positions of the marker planes was found to be well within the range of uncertainty of the experimental results, which demonstrates the validity of the model.

Research into the Ni-Al system was further extended in order to determine the Ni and Al tracer diffusivities in the β-NiAl and γ'-Ni$_3$Al phases. Because of lack of suitable Al isotopes, measurements of Al tracer diffusivities in these phases were not possible directly by the tracer method. In this study the classical diffusion couple technique is used to determine tracer diffusivities of both species in these two phases.

For the first time, in a Ti/TiAl$_3$ diffusion couple trifurcation of the Kirkendall plane was found and this was rationalized by using velocity diagram construction.

It is observed that the position of a stable Kirkendall plane is characterized not only by the presence of inert markers, but also by a different grain morphology at both sides of this plane. A physico-chemical approach is developed which elucidates the role of the Kirkendall effect in the morphogenesis of interdiffusion systems. The occurrence of one or more Kirkendall planes, characterized by morphology changes in the reaction layer, turns out to be related to the different sites where the product grains originate at both sides of each Kirkendall plane. The model is demonstrated using the experimental results in the Co-Si system, in which only line compounds occur. It is shown that the predictions using the physico-chemical approach are in good agreement with the experimentally found positions of the Kirkendall plane(s). The presence or absence of inert markers at the Kirkendall planes provides insight into the initial stages of reaction phase formation.

The application of the phenomenological model was also used in Cu/Sn and Au/Sn systems to predict/analyze the characteristic features of a diffusion-grown zone consisting of line compounds, which are of great importance for electronics industry. The applicability of this model was further validated on the growth of intermetallic compounds in Ag-Zn and Ti-Al systems where phases develop with a wide homogeneity range.

Samenvatting

De groei van intermetallische verbindingen door diffusie en het optreden van het daarmee gepaard gaande Kirkendall effect zijn complexe onderwerpen die van groot belang zijn in de wetenschap en technologie van Materialen.

De verplaatsing van inerte Kirkendall markers, die het gevolg is van ongelijke diffusiestromen tijdens interdiffusie in vaste stoffen, kan worden verklaard via het Kirkendall snelheidsdiagram. Daaruit blijkt dat de positie van het Kirkendall vlak (gedefinieerd als het oorspronkelijke grensvlak tussen de twee vaste stoffen dat gemarkeerd wordt door inerte deeltjes daarin aangebracht vóór het diffusieproces) niet uniek is. Meerdere Kirkendall vlakken kunnen zich ontwikkelen gedurende het diffusieproces, maar het oorspronkelijke vlak kan ook een diffuus gebied vormen van markers: het Kirkendall vlak is instabiel.

In dit proefschrift wordt een experimentele bevestiging van het optreden van bifurcatie van het Kirkendall vlak (opsplitsen in twee vlakken) gegeven in een binair systeem waarin één diffusielaag van een intermetallische verbinding wordt gevormd. De groei van β-NiAl tussen de aangrenzende Ni-Al verbindingen wordt als model gehanteerd. Het Kirkendall snelheidsdiagram werd geconstrueerd op basis van interdiffusie- en intrinsieke diffusiecoëfficiënten die bepaald werden via de diffusiekoppeltechniek. De geldigheid van het ontwikkelde model werd aangetoond door de goede overeenstemming tussen de experimentele en voorspelde resultaten.

De research in het Ni-Al systeem werd vervolgd door voor de β-NiAl en γ'-Ni$_3$Al fasen de tracer diffusiecoëfficiënten te bepalen van Ni en Al op een indirecte manier via de diffusiekoppeltechniek. Op een directe manier is dit onmogelijk door het ontbreken van een geschikte isotoop van Al.

Voor de eerste keer werd trifurcatie experimenteel waargenomen in een Ti-Al

diffusiekoppel: de oorspronkelijk in het grensvlak aangebrachte markers werden teruggevonden in drie vlakken in de diffusiezone. Dit fenomeen kon weer verklaard worden via het Kirkendall snelheidsdiagram.

Het blijkt dat een stabiel Kirkendall vlak niet alleen gekarakteriseerd wordt door de aanwezigheid van inerte markers, maar ook door een verschillende korrelmorfologie aan weerszijden van dit vlak. Er werd een fysisch-chemisch model ontwikkeld waaruit de rol van het Kirkendall effect op de morfologie van de interdiffusiezone helder wordt. De vorming van één of meerdere Kirkendall vlakken blijkt samen te hangen met de verschillende plaatsen waar nieuw gevormde kristallieten nucleëren. Het model wordt verduidelijkt aan de hand van het Co-Si systeem, waarin een aantal zuiver stoechiometrische verbindingen voorkomen. De voorspellingen gedaan op basis van de fysisch-chemische methode betreffende de posities van de Kirkendall vlakken komen goed overeen met de experimentele waarden. De aan- of afwezigheid van inerte markers in een Kirkendall vlak verschaft inzicht in het beginstadium van het diffusieproces, met name over de gelijktijdige of sequentiële groei van de verschillende intermetallische verbindingen.

De experimentele bevestiging van onze modellen op de Cu-Sn en Au-Sn systemen werd uitgevoerd vanwege het grote belang van deze systemen in de elektronische industrie, met name in verband met microsoldeerverbindingen. Ten slotte werden onze modellen ook toegepast op systemen zoals Ag-Zn en Ti-Al waarin fasen voorkomen met een breed homogeniteitsgebied. Ook daarin werden onze voorspellingen experimenteel bevestigd.

Acknowledgements

In the title page, although only my name is present, but, in fact, this dissertation would not have been possible without the expert guidance of my esteemed supervisors especially Prof. Frans J.J. van Loo and Dr. A.A. Kodentsov. Frans is not a man of many words, however, his oral and written comments have always been extremely perceptive and appropriate. On the other hand, Sasha (Kodentsov) always had lot to say and kept on overwhelming me with his over excitement and sometimes unusual (as at least seemed to me) way of response to the problems. They both were enthusiastic about work and responded much faster than I could have expected. Nevertheless Sasha helped me out of his way on many matters which were not related to research to make things easier for me here. Although it is difficult to express my gratitude in words, my special thanks to both of you for all your concern.

With deep gratitude and pleasure, I like to thank my promoter Prof. G. de With (Bert) for his help. I appreciate his extra support to his students and judging matters without getting influenced by the comments from others, although they were not negative.

I greatly acknowledge the motivation, help and support I got from my parents and brothers throughout my career. I also thank my sisters in law (bodo and chhoto khepi) who stood besides me always.

I thank my wife Bhavna, for all her support and motivation and also for designing very nice cover page. I acknowledge my parents, brother and sister in law for support and their concern for me.

I acknowledge the financial support for the project RIPOSTE and for fruitful discussions with the project members.

I am very much thankful to Huub van der Palen for his incessant help in the laboratory. His technical expertise was invaluable and helped me to conduct experiments without much trouble.

I thank my housemate Vinayak and friend Gabriel (who is afraid of growing mushroom in the neck) for the fun we had during endless discussions/arguments on many useless topics with striking comments.

I would like to thank my officemate Victor for his help on many occasions and for sharing his experiences in life which were an unknown arena for me!

I thank Prof. Herbert Ipser and Prof. Ülo Ugaste for taking part in Ph.D. commission and reading my thesis. I also thank Herbert for arranging my stay in University of Vienna, where I enjoyed a lot. I acknowledge COST ACTION 531 for providing financial support.

I acknowledge Christoph, Karthik, Dr. Hans, Dr. Klaus, Prof. Mikula, Peter for giving good company in Vienna.

I would also like to thank many other friends, former and present colleagues, Mark, Pascal, Ola, Boris, Nathalie, Chary, Geil, Hans, Bert, Niek, Marco, Neils, Maru, Emilio, Okan, Amir, Linda, Christa, Imanda, Daniela, Francasca, Tamara, Talal, Olavio, for their timely help and good company which made my stay comfortable here.

I acknowledge my childhood friends, Subrata, Pratap, Bhaskar, Asim, Hero, Bisu, Prasenjit, Sajal, Shamit and many others.

List of publications

The present work:

1. A. Paul, A.A. Kodentsov, F.J.J. van Loo, Bifurcation and trifurcation of a Kirkendall plane during multiphase interdiffusion, submitted to Defects and Diffusion forum, 2004.
2. Aloke Paul, Alexander A. Kodentsov, Frans J.J. van Loo, Intermetallic growth and Kirkendall effect manifestations in Cu/Sn and Au/Sn diffusion couples, Z. Metallkunde, In Press, 2004.
3. A. Paul, A.A. Kodentsov and F.J.J. van Loo, Bifurcation of the Kirkendall plane during interdiffusion in the intermetallic compound β-NiAl, Acta Materialia, **52** (2004) 4041-48.
4. A. Paul, M.J.H. van Dal, A.A. Kodentsov and F.J.J. van Loo, On the behaviour of Kirkendall markers in solid-state diffusion, Archive of Metallurgy and Materials, **49** (2004) 259-76.
5. Alexander A. Kodentsov, Aloke Paul, Frans J.J. van Loo, Bifurcation of the Kirkendall plane and patterning in reactive diffusion, Z. Metallkunde, **95** (2004) 58-60.
6. A. Paul, M.J.H. van Dal, A.A. Kodentsov and F.J.J. van Loo, The Kirkendall Effect in Multiphase Diffusion, Acta Materialia, **52** (2004) 623-630.
7. A. Paul, A.A. Kodentsov, G. de With, F.J.J. van Loo, Formation of AB_2-intermetallics in the Au-Sb-Bi system, Intermetallics, **11** (2003) 1195-1203.
8. C. Cserháti, A. Paul, A.A. Kodentsov, M.J.H. van Dal, F.J.J. van Loo, Intrinsic Diffusion in Ni_3Al System, Intermetallics, **11** (2003) 291-297.
9. A. Paul, M.J.H. van Dal, A.A. Kodentsov and F.J.J. van Loo, The Kirkendall Effect in Multiphase Interdiffusion, Defects and Diffusion Forum, **216-217** (2003) 65-72.

Others:

1. U. Ramamurty and A. Paul, Variability in Mechanical Properties of a Metal Foam, Acta Materialia, **52** (2004) 869-76.
2. A. Paul and U. Ramamurty, Strain rate sensitivity of a closed-cell aluminium foam, Materials Science and Engineering A, **281A**, (2000) 1-7.
3. A. Paul, T. Seshacharyulu and U. Ramamurty, Tensile strength of a closed-cell Al foam in the presence of notches and holes, Scripta Materialia, **40** (1999) 809-814.
4. Christoph Luef, Aloke Paul, Hans Flandorfer, Alexander Kodentsov and Herbert Ipser, Enthalpies of mixing of metallic systems relevant for lead free soldering: Ag-Pd and Ag-Pd-Sn, Submitted to Journal of Alloys and Compunds, 2004.

Unpublished research (to be submitted):

1. A.A. Kodentsov, A. Paul and F.J.J. van Loo, The Kirkendall effect in solid-state diffusion, to be submitted to Critical Reviews in Solid State and Material Sciences (invited review article).
2. A. Paul, A.A. Kodentsov and F.J.J. van Loo, On the determination of initial contact plane in a binary diffusion couple.
3. A. Paul, A.A. Kodentsov and F.J.J. van Loo, Diffusion in the β-NiAl phase.
4. A. Paul, C. Luef, A.A. Kodentsov, H. Flandorfer, H. Ipser and F.J.J. van Loo, Solid-state diffusion controlled interaction in the Cu(Ni)/Sn system.
5. A. Paul, A.A. Kodentsov and F.J.J. van Loo, Application of physico-chemical approach in a binary diffusion couple with saturated end-members (two-phase alloy).
6. U. Ramamurty and A. Paul, Notched Strength under tensile and compressive loading of a closed cell Al foam.

Curriculum Vitae

Aloke Paul was born on 4th of October 1973 in Durgapur, India. After finishing schooling, he was selected for Bachelor of Engineering (B.E.) degree through a state wise competitive examination and joined National Institute of Technology (former name REC), Durgapur in the Department of Metallurgical Engineering. In this course the title of the thesis project was "Study of the effect of surface coating on isothermal oxidation behaviour of low carbon steel". In 1996, he obtained his bachelor degree and was further selected for Master of Engineering (M.E.) through a national competitive examination and joined in the Metallurgical Department, Indian Institute of Science, Bangalore, India. During this course the title of the project was "Biobeneficiation of iron ore minerals", which led to the thesis. After receiving Master degree in 1998, he joined as research associate in Nanyang Technological University, Singapore. There he worked on the project of "Mechanical properties of a closed cell aluminium foam". In 2001, he started his Ph.D. project in the Laboratory of Materials and Interface Chemistry (former name Solid State and Materials Chemistry), Eindhoven University of Technology, The Netherlands (and in collaboration with PHILIPS, Eindhoven) under supervision of Dr. A.A. Kodentsov, Prof.dr. G. de With and Prof.dr. Frans J.J. van Loo, which resulted into this thesis.